Identification and characterization of cystinuria modulating genes: L-Ergothioneine as a potential treatment for preventing cystine lithiasis

Clara Mayayo Vallverdú

Programa de Doctorat en Biomedicina

Identification and characterization of cystinuria modulating genes: L-Ergothioneine as a potential treatment for preventing cystine lithiasis

Memòria de tesi doctoral presentada per
Clara Mayayo Vallverdú
per optar al grau de doctora per la Universitat de Barcelona

Tesi realitzada en el laboratori de Genètica Molecular Humana de l'Institut d'Investigació Biomèdica de Bellvitge (IDIBELL) sota la direcció de la Dra. Virginia Nunes Martínez i la co-direcció del Dr. Miguel López de Heredia Alonso

Els directors **La doctoranda**

Virginia Nunes Miguel López de Heredia Clara Mayayo

Barcelona, Setembre 2021

AGRAÏMENTS (ACKNOWLEDGMENTS)

Vaig prometre'm escriure aquest apartat amb temps per retornar com cal l'estima rebuda durant aquests anys, però com no, aquí estic escrivint-los *last-minute*. Així potser evitarà que m'allargui massa...

Virginia, gracias por acogerme *in extremis* para hacer el TFM y proponerme pedir la beca lanzadera para quedarme trabajando con vosotros. Qué alegría el día que nos la concedieron y que penuria con las posteriores tentativas realizadas para conseguir la beca definitiva… Pero… ¡lo hemos conseguido! Gracias por luchar por mi continuidad año tras año, tener siempre la puerta del despacho entreabierta para poder abordarte en cualquier momento y por la libertad, autonomía y confianza en mi trabajo.

Miguel, gracias por enseñarme todas tus manías para trabajar con la máxima meticulosidad, des de pipetear una recta patrón perfecta a diseñar de forma optimizada las bases de datos para facilitar el posterior análisis. También por dedicarle todo el tiempo necesario a mis constantes visitas a tu mesa para diseñar y discutir los experimentos. En estos últimos dos años la comunicación a distancia ha sido más intermitente y difícil, pero gracias de nuevo para acabar encontrando siempre un huequito para mí.

Esther, intentaré fer un *abstact* dels meus agraïments cap a tu que ens coneixem... Encara recordo el primer dia que em vas ensenyar a fer una necròpsia de cap a peus. A part dels guants suats i deixar-me les ulleres fora per evitar que se m'entelessin degut al que m'imposaves (a mi i a tot@s), les hores van passar volant i vaig sortir fascinada i plena, sensació semblant al sortir del primer dia de pràctiques als alumnes de genètica. I això ha fet que hagi arribat fins aquí. Mil gràcies per ensenyar-me tot el que sé de ratolins i *estabu*! Aquests dos últims anys no podria haver tingut millor companyia per treballar *mano a mano*... gràcies per la teva ajuda incondicional, cuidar-me tant, donar-me empenta o parar-me els peus quan ho necessitava, i per creure i confiar en mi (tant dins com fora del lab). Has sigut el meu pilar. La connexió tant especial que tenim a nivell personal també ho ha fet tot molt més fàcil. Espero que els rotllos que t'he arribat a fotre en dinars, cafès, necros, poyatas, ordinadors, passadissos, metros... sobre les experiències Mayayo et serveixin per fer més *portable* l'adolescència dels Montalvo-Prat, a qui sempre tindré una estima molt especial.

No m'oblido de tots els que heu format part de Z en algun moment d'aquesta experiència. Laura, gracias por enseñarme a genotipar ratones y pacientes, hacer tampones y tener localizado cualquier reactivo, muestra, kit… dentro del caos del laboratorio. Mirian, empezamos juntas la experiencia en Z y creo que no he reído tanto cómo en esa época… espero mantener siempre nuestros reencuentros en Barcelona, Ibiza, Heidelberg o dónde sea. Isa, juntes ens vam endinsar al món dels WB i això uneix... quina llàstima que ja no visquis a Barcelona per mantenir les nostres quedades, però tenim pendent el viatge a Mallorca que va truncar la pandèmia. Ferran, la teva ment brillant em va posar en *jaque* més d'un cop durant la teva estada d'estiu al lab... no deixis mai d'avisar-me quan tornes de Londres, m'encanta retrobar-nos per posar-nos al dia i fer crítica de com va el món, amb el nostre humor irònic i passió pel *cotilleo*. A la resta d'estudiants que heu anat passant per Z, gràcies per aportar aire fresc, deixar-me explotar les meves ganes d'ensenyar i fer-me conscient de les manies acumulades en aquest anys de doctorat.

I més enllà de Z, agrair al departament de Genètica l'acollida i acompanyament durant aquests anys. Als X-ALD per adoptar-me tant dins com fora el lab... Leire, gracias por siempre estar dispuesta a resolver mis dudas sobre materiales, métodos, burocracia y core facilities del IDIBELL, y por desahogarnos juntas de nuestras *data shit*. Laura, ara has agafat tu el relleu de la Leire, gràcies per aportar la teva vitalitat, xerrameca i ànima *cotilla* al despatx de predocs (algun dia et tornaré a cantar *l'Amazing Grace* a ple pulmó). I gràcies a la Cris per la seva amabilitat, al Juanjo per les seves *batallitas* i a l'Edgard per ser el millor presi de la comi de festes. Als *worms*, Xènia, Carmen, Dimitri i David, per ser l'ànima etílica-festiva de genètica i les vostres propostes constants de flama... quan es pugui hem de tornar a l'Apolo per rememorar els sopars de Nadal. I als IPs Mercè, Sara i Julian per generar un ambient tant agradable, i al Javi i l'Antònia per la seva ajuda i suport en qualsevol moment.

Tampoc m'oblido de tots els col·laboradors que m'heu ensenyat, ajudat i posat les coses tant fàcils per construir i fer créixer aquesta tesi: els aminoàcids d'en Rafa Artuch, la quantificació de GSH d'en Fede Pallardó, els anàlisis i màster classes bioinformàtiques d'en José Luís Mosquera, l'O2k d'en Pablo Garcia-Roves, l'espectrofotòmetre de la Glòria Garrabou, l'ull de nefròleg d'en Miquel Hueso, els consells de cristal·lògraf d'en papa Pini... mil milers de gràcies!!

Però durant aquests anys no tot ha sigut vida de lab...

Als *Enamorats*, per ser la millor fusió de colles del món! Al nucli del Fort Pius: Pini, Berta, Eloy, Gabri, Hug, Sillero, Àlvarez... és molt fort que ja fa 16 anys que ens coneixem, que ens continuïn fent gràcia les mateixes bromes i que ens tinguem incondicionalment pels bons i pels mals moments. I les incorporacions de les *Sororitat vs patriarcat*: Carla, Eli, Miriam, Mompra, Paloma, Silvia i Vargas, gràcies per ser la millor font de desconnexió setmanal, *birreo* i *perreo*. Però també gràcies per els infinits debats que m'han format en feminisme, dret, política, ecologia, habitatge..., conèixer món junts i estimar-nos tant.

I com oblidar que el començament del doctorat va anar acompanyat del projecte d'independència. Carla i Carlos, vosaltres vau viure el meu dia a dia durant 3 anys i mig. Que ràpid van passar i que malament ho vaig passar el dia en que us havia de dir que deixava el pis (piCet) per les mil i una circumstàncies vitals. Carlos, quin perill els dos començant el doctorat al idi i vivint junts... m'encantava desfogar-me i despotricar del món científic amb tu, però també escarxofar-nos al sofà i poder parlar de tot. Carla, gràcies per no tenir ni idea de ciència, per ser una font d'energia inesgotable, per tenir les coses tant clares i per entendre'm tant.

I Carla *again,* gràcies per fer el targetasu casi a cegues dels bitllets d'avió a Argentina, *El diario d'un chevrolet* no existiria sense la teva determinació. Més enllà de les aventures i els personatges que vam conèixer anant a visitar la Mompra, que liessis a la Renau perquè també vingués, i que la convivència de les 4 fos tant genial no te preu. La relació entre totes cada cop és més forta i m'encanta saber que sempre teniu un sí incondicional per apuntar-vos a tots els plans. Mompreta, cuida'm a la Carla ara que viureu juntes i ni se'us acudeixi enfadar-vos!! Ah, i mai deixis d'enviar-me els teus *podcasts* personals amiwi!!

Clara Renau, després de coincidir intermitentment en els anys sense pena ni glòria, el viatge a Argentina ens va donar l'oportunitat de conèixer-nos a fons i començar a descobrir les infinites coses que tenim en comú i el semblant que funcionen els nostres cervellets. Gràcies a tu vaig

retrobar-me amb el futbol. Com vaig gaudir dels dijous de partits amb Belles Glòries!!! Llàstima que els meus creuats diguessin prou... Però per sort teníem un pla B i vam començar a quedar per cantar juntes i... va arribar el confinament. I amb el confinament, Clares Confinades!! Quin plaer fer música amb tu a distància, però encara més juntes al teu buc d'assaig i ja ni et dic en els concertets que hem pogut fer en directe. Gràcies per posar sempre les coses tant fàcils i llançar-te a tocar amb entusiasme qualsevol proposta musical que et faci... et prometo que algun dia compondrem el *hit* de la nostra fòbia social irracional a anar a comprar al mercat.

I un record especial a les de la uni, Agnès, Anna, Isshak, Júlia, Mar i Mirna. Ens teniu abandonades a la Mar i a mi a Barcelona, menys mal que no ens importa anar-vos fent vistes allà on sigueu. Mar, hem portat vides paral·leles des de que vam acabar la uni cosa que ha fet que ens uníssim encara més... i m'encanta saber que en breus les paral·lels es creuaran de nou per començar el màster juntes. Gràcies pel suport d'aquests últims mesos i per ser tant bona amiga i companya de viatge. I Alberto, vam trobar en el *lindy-hop* un *hobby* que ens va permetre veure'ns més sovint. Llàstima que la meva *patapalo* ara em té fora de combat, però sempre ens quedaran les nostres birretes per compartir la visió similar que tenim de les coses, cantar i ensenyar-nos música que ens toca la fibra.

Guapires, Anna, Clara, Jandro, Júlia, Laura, Laureta, Maria, Mariona, Mercè, Paula, Sara i Vic, ens hem vist néixer i créixer els uns als altres, compartint estius, Nadals, SS i findes al bell mig de la Conca de Barberà. La nostra relació està al *limbo* entre l'amistat i la família, i això fa que la complicitat entre nosaltres sigui gegant. Em fa molt feliç veure que passen els anys i, tot i que les vides es compliquen, arriba el primer finde d'agost i el món s'atura per retrobar-nos i començar la Festa Major de Pira. Gràcies per fer-me viure aquest agost de clausura a través de les vostres festes, bogeries i vivències... l'any que ve prepareu-vos! Poder sopar amb vosaltres cada nit després de passar-me el dia escrivint ha fet que no em tornés boja.

Natàlia, per on començo... has format part d'aquest doctorat de principi a fi i hem aconseguit superar totes les turbulències amb èxit! Gràcies per saber llegir les meves necessitats en cada moment i no consentir-les sempre, per adaptar-te a la meva agenda de els dimarts gòspel, dijous futbol, findes plens de plans i poca disponibilitat..., per ser la meva fan, *reviwer* i crítica, per tenir les coses tant clares, pels mil projectes vitals, per no deixar-me mai de sorprendre, per fer-me riure i plorar (amb el que em costa), per revolucionar-me la vida i per quedar-t'hi a viure. Però sobretot, per sempre dir-me les veritats, aquelles veritats que punxen, però que em demostren tot el que m'arribes a conèixer i estimar, em fan créixer i ser millor persona. S'acaba una etapa i tinc moltes ganes de començar la següent juntes!! També agrair a la teva família l'acollida i estima que sempre em mostren quan vaig a Vic, em sento com a casa! I a *Can Cacauet* volum XI, aquest pis de doctorands que acabarà sent de doctores! Mireia i Leire, gràcies per aguantar-nos totes les *monyanes* a la Natàlia i a mi, per fer la convivència tant fàcil i per els dijous al vespre de *birreo* a la terrassa.

Finalment, toca agrair el suport de la família. A les meves germanes, és un orgull i una sort tenir-vos com a pilars de la meva vida. Júlia, no hauria pogut tenir millor referent en el qual emmirallar-me des de ben petita... sempre has anat 2 (o 200) passes per davant i la teva "extroversió" i determinació a l'hora de prendre decisions em fascinen. Ara ja fa uns anys que UK ens ha separat físicament, però d'aquesta edat "adulta" em quedo amb el fet que la meva ídol s'ha convertit en

la meva fan i aquesta reciprocitat és increïble. Maria, quantes coses he aprés de tu... tot i tenir 6 anys menys, aquesta distància fa molt temps que s'ha esfumat i m'has fet de germana gran, estilista, *rrpp*... La teva ment súper oberta i lluita política-social m'han fet reflexionar i ser més conscient de tot. Tens una aura, una sensibilitat i un humor que fan que estant amb tu les coses es vegin més fàcils i estic convençuda que això farà que tot et vagi genial. Laura (Laureta), és impossible no veure l'iguals que arribem a ser... *xortxes*, desastres, anant sempre a última hora, aturadetes en certs moments i loquis en altres, viciades a qualsevol cosa, esportistes (de pilota), no sabem dir que no a res (i menys a una festa), empàtiques de cap a peus... Això sí, ets la meva versió millorada accentuant totes les virtuts i fins i tot, el que no son virtuts, i això et fa molt especial. Papa, quina sort que encara que sigui des del camp de la Història també convisquis amb tesis doctorals. Entendre, apreciar i valorar el món precari en el qual entrava, i el fet d'explicar-me a cada pas el que s'esperava de mi m'ha ajudat molt. Espero recuperar la freqüència de sopars amb tu i la Roser, a qui li agraeixo que sempre estigui pendent de tot. Mama, quina sort que tu no entenguessis aquest món i que sempre m'hagi acompanyat la teva visió crítica d'exigir-nos el millor de nosaltres en cada cosa que fem (un 9,5 només? Jajaj). Mil gràcies per cuidar-me tant incondicionalment en tot moment i per fer-me qui soc ara. Admiro enormement la teva capacitat d'adaptació i acceptació a les situacions vitals que t'hem fet viure cada una de les germanes. Ara ja sembles una més de nosaltres (menys quan toca renyar-nos per parar-nos els peus) i els atacs de plorar de riure que tenim quan estem les 5 juntes em donen vida. Padrina, la teva fortalesa, caràcter i humor irònic amb 90 anys son una passada... gràcies per preguntar-me cada setmana que havia descobert aquella setmana.

Vaig prometre'm, també, no oblidar el procés de recuperació de l'operació de menisc i creuat d'ara fa un any... Gràcies mama per acollir-me a casa de nou quan no podia ni dutxar-me sola i tenir infermera particular per les cures i punxades d'heparina, a les germanetes per la companyia, a la Natàlia per la paciència que no té, a tots els que em vau venir a veure al bar de la cantonada de casa i al servei de Rehabilitació de l'Hospital Esperança, els conductors d'ambulància i companys de *rehab* que vau fer que els 3 mesos de *parón* vital per cuidar-me passessin de la millor manera possible i amb optimisme! Així que, com diria Ovidi Montllor,

"Un pensament però, per aquells que estaran junts a tots i tots junts. Per aquells que ara estan tan lluny però tan a prop, tan a dins de nosaltres, per aquells que fan possible l'esperança de viure"

TABLE OF CONTENTS

LIST OF FIGURES

LIST OF TABLES

ACRONYMS & ABBREVIATIONS

4F2hc	Surface antigen 4F2 heavy chain
AA	Amino acid
Ab	Antibody
AGT1	Aspartate and glutamate transporter 1
asc-1	System asc amino acid transporter-1
asc-2	System asc amino acid transporter-2
ATP	Adenosine triphosphate
$b^{0,+}$AT	System $b^{0,+}$ amino acid transporter
BBM	Brush border membrane
BIOPS	Biopsy Preservative Solution
BLM	Basolateral membrane
BSA	Bovine serum albumin
BW	Body weight
CaOx	Calcium oxalate
CBS	Cystathionine β-Synthase
CDME	L-cystine dimethylester
cDNA	complementary DNA
CME	L-cystine methylester
CS	Citrate synthase
CssC	Cystine
Ct	Threshold cycle
DEG	Differential expressed genes
DIC	Mitochondrial dicarboxylate carrier
dKO	Double knockout mouse
dNTP	Deoxynucleotide triphosphate
DTT	Dithiothreitol
EDS	Energy dispersive spectroscopy
EDTA	Ethylenediaminetetraacetic acid
EFSA	European Food Safety Authority
ENU	N-ethyl-N-nitrosourea
ESWL	Extracorporeal shockwave lithotripsy
ETC	Electron transport chain
FCCP	Carbonyl cyanide-p-trifluoromethoxyphenylhydrazone
FDA	Food and Drug Administration
GCL	Glutamate cysteine ligase
GCLC	Glutamate cysteine ligase catalytic subunit
GCLM	Glutamate cysteine ligase modifier subunit
GFR	Glomerular filtration rate
GGT	γ-Glutamyltransferase
GOI	Gene of interest
GPx	Glutathione peroxidase
GRAS	Generally recognized as safe
GS	Glutathione synthase
GSH	Glutathione
GSSG	Glutathione disulfide

GST	Glutathione S-Transferase
HAT	Heteromeric amino acid transporter
HED	Human Equivalent Dose
iNOS	inducible Nitric Oxide Synthase
KO	Knock out
LAT1	System L amino acid transporter 1
LAT2	System L amino acid transporter 2
L-Erg	L-Ergothioneine
MLPA	Multiplex ligation-dependent probe amplification
Mrp	Multidrug resistant proteins
mtDNA	Mitochondrial DNA
NAD^+	Nicotinamide adenine dinucleotide
NaDC	Sodium-dicarboxylate 2 exchanger
NEM	N-ethylmaleimide
NSF	Non stone former
O2k	Oroboros-2k
OAT	Organic anion transporter
OCT	Organic cation transporter
OCTN	Organic cation and zwitterion transporter
OCTN1	Organic cation transporter novel, type 1
OGC	2-oxoglutarate carrier
ORP	Oxidation-reduction potential
OXPHOS	Oxidative phosphorylation
PBS	Phosphate buffer saline
PCA	Principal component analysis
PCNL	Percutaneous nephrolithotomy
PCR	Polymerase chain reaction
PEPT2	Peptide transporter 2
PFA	Paraformaldehyde
qPCR	Quantitative polymerase chain reaction
RIN	RNA integrity number
ROI	Region of interest
ROS	Reactive oxygen species
rpm	Revolutions per minute
RT	Room temperature
rt-PCR	retro-transcriptase polymerase chain reaction
SEM	Standard error of the mean
SEM	Scanning electron microscopy
SF	Stone former
SLC	Solute carrier
SOD	Superoxide dismutase
SPF	Specific pathogen-free
TCA	Tricarboxylic acid
TEA	Tetraethylammonium
UPL	Universal Probe Library
URS	Ureteroscopy
UV	Ultra-violet

VNO	Virginia Nunes oligonucleotide database
WB	Western Blot
WT	Wild type
xCT	systemic xc- amino acid transporter
y^+LAT1	system y^+L amino acid transporter 1
y^+LAT2	system y^+L amino acid transporter 2

SUMMARY

Cystinuria, with a worldwide prevalence estimated at 1:7000, is a rare inherited disease characterized by urine hyperexcretion of cystine and dibasic amino acids. Its clinical manifestation is cystine lithiasis in the urinary system due to the low solubility of cystine at physiological urine pH which causes its precipitation and, as a consequence, stone formation. Cystine stones account for 1-2 % of adult and 6-8 % of pediatric urinary tract lithiasis and, the high recurrence rate of stone episodes involving repeted urologic interventions, results in chronic kidney disease in most patients. Cystinuria is caused by genetic defects in *SLC3A1* and *SLC7A9* genes, which encode the heavy (rBAT) and the light ($b^{0,+}$AT) subunits of the renal amino acid transport system $b^{0,+}$, respectively. However, a high phenotype variability is observed in cystinuric patients as even brothers with the same mutation show different onset of stone episodes, recurrence and treatment response. There is no effective treatment for cystinuria and current therapeutic approaches are conservative measures (hydration therapy, diet recommendations and urine alkalinization), and when stones appear, thiol drugs as D-penicillamine are prescribed, although present multiple side-effects. Both the lack of genotype-phenotype correlation in cystinuric patients and the absence of an effective treatment induce the search and characterization of cystinuria modulating genes to propose novel therapeutic strategies, which are addressed in this thesis. First, as AGT1 (*SLC7A13*) was recently described as the second kidney cystine transporter, its involvement on amino acid reabsorption and cystine lithiasis was assessed in cystinuria mouse models and in cystinuric patients (Chapter I). Cystinuric mice that expressed AGT1 showed higher levels of cystine reabsorption and a lower rate of stone formation during the whole 6-month follow-up, indicating its protective effect against cystine lithiasis. However, in cystinuric patients, no cystinuria causative or modulating effect could be associated to AGT1 after screening *SLC7A13* gene in 9 cystinuric patients with only one or any mutation detected in *SLC3A1* and *SLC7A9* genes. Then, an RNA-seq analysis was performed to identify differentially expressed genes in the kidneys of the *Slc7a9*$^{-/-}$ mouse model (Chapter II). The pathway enrichment analysis of differentially expressed genes of both male and female mice unveiled an impairment of the oxidative phosphorylation system. To validate this finding, the oxidative phosphorylation system and the Tricarboxylic acid cycle function were studied in the kidneys of the *Slc7a9*$^{-/-}$ mice. A citrate intracellular depletion, a reduced NAD^+/NADH ratio, a lower complex IV enzymatic activity and a decreased mitochondrial maximal respiration capacity was observed in *Slc7a9*$^{-/-}$ mice, revealing a mitochondrial dysfunction in cystinuria. Finally, as in a previous group's work *Slc22a4* (encoding OCTN1) was found downregulated in *Slc7a9*$^{-/-}$ stone former mice compared to non-stone former ones, the therapeutical potential in cystine lithiasis of the main molecule transported by OCTN1, L-Ergothioneine (L-Erg), was evaluated (Chapter III). The preventive (before any stone event) and long-term administration (6 months) of L-Erg (16 mg/kg/day) induced a reduction of above 50 % in the number of stone former mice and delayed the lithiasis onset in the *Slc7a9*$^{-/-}$ treated group by increasing cystine solubility in urine. L-Erg effect in cystine lithiasis was showed to be dependent on its internalization and derived metabolism as no effect was observed when treating *Slc7a9*$^{-/-}$*Slc22a4*$^{-/-}$ mice. In addition, the therapeutic intervention restored the mitochondrial dysfunction in the kidneys described in chapter II and ameliorated the oxidative defect related to cystinuria. In summary, no evidence of a cystinuria causative or modulating effect could be associated to AGT1 in our cohort of patients, but in the *Slc7a9*$^{-/-}$ mouse model the presence of AGT1 was associated to a lower rate of stone formation, a kidney mitochondrial dysfunction related to cystinuria has been described for the first time and L-Erg has been shown to be a potential treatment for preventing cystine lithiasis.

RESUMEN

La cistinuria es una enfermedad rara caracterizada por la hiperexcreción de cistina y aminoácidos dibásicos. A nivel clínico, los pacientes presentan episodios recurrentes de litiasis en el sistema urinario debido a la baja solubilidad de la cistina en orina que induce su precipitación y la posterior formación del cálculo. Los cálculos de cistina representan el 1-2 % de las litiasis detectadas en adultos y el 6-8 % en pacientes pediátricos. La alta recidiva de episodios litiásicos y las consecuentes intervenciones quirúrgicas derivan en muchos casos en daño renal crónico. La cistinuria está causada por un defecto en el sistema de transporte $b^{0,+}$ debido a mutaciones en los dos genes que codifican su subunidad pesada rBAT (*SLC3A1*), y ligera $b^{0,+}$AT (*SLC7A9*). En los pacientes cistinúricos se observa una alta variabilidad en el transcurso de la enfermedad, e incluso hermanos con la misma alteración genética presentan diferencias en la edad de aparición del primer cálculo, la recidiva en que los padecen y su respuesta al tratamiento. A día de hoy, no existe un tratamiento efectivo para la cistinuria. La primera línea de tratamiento consiste en una terapia conservadora para prevenir la aparición del cálculo (ingesta de líquidos, recomendaciones dietéticas y alcalinización de la orina) y, cuando se detecta un cálculo, se prescriben compuestos quelantes como la D-penicilamina, aunque presentan múltiples efectos secundarios. En esta tesis, la falta de correlación genotipo-fenotipo en los pacientes y la necesidad de encontrar un tratamiento efectivo, han inducido la búsqueda y caracterización de genes moduladores de la cistinuria y la investigación de una nueva opción terapéutica. En primer lugar, la reciente descripción de AGT1 (*SLC7A13*) como segundo transportador renal de cistina promovió el estudio de su implicación en la reabsorción de aminoácidos y en la formación de cálculos de cistina en modelos murinos y en pacientes cistinúricos (Capítulo I). En los ratones cistinúricos que presentan AGT1, se observó una mayor capacidad de reabsorción de cistina y una reducción en la tasa de aparición de litiasis durante 6 meses de seguimiento. Sin embargo, al secuenciar el gen *SLC7A13* en 9 pacientes con sólo una o sin mutaciones en los genes *SLC3A1* y *SLC7A9* no se encontró evidencia de la implicación de AGT1 en la cistinuria. En segundo lugar, se realizó un análisis transcriptómico con el fin de detectar genes diferencialmente expresados en los riñones del modelo murino *Slc7a9*$^{-/-}$ (Capítulo II). Al analizar las vías que englobaban los genes diferencialmente expresados detectados, se descubrió un defecto en la fosforilación oxidativa. Con el propósito de validar esta alteración genética, se estudió el estado de la fosforilación oxidativa y el ciclo de los ácidos tricarboxilicos en los riñones del ratón *Slc7a9*$^{-/-}$. Los resultados hallados fueron una depleción de los niveles de citrato intracelular, una reducción en la ratio NAD^+/NADH, una menor actividad enzimática del complejo IV y un descenso de la capacidad respiratoria máxima, evidenciando la disfunción mitocondrial en cistinuria. Por último, dando continuidad a resultados previos obtenidos en el grupo que manifestaron la diferencia de expresión génica del transportador OCTN1 (*Slc22a4*) entre ratones formadores y no formadores de cálculos de cistina, se estudió el potencial terapéutico de su principal substrato, la L-Ergotioneina (L-Erg) (Capítulo III). La administración de L-Erg (16 mg/kg/día) a modo preventivo y crónico en el modelo *Slc7a9*$^{-/-}$ redujo por más del 50 % el número de ratones con litiasis a los 7 meses y, atrasó la aparición de estos. El efecto producido por la L-Erg fue debido a un incremento de la solubilidad de cistina en orina y dependiente de su internalización y metabolización, debido a que al tratar el modelo *Slc7a9*$^{-/-}$ *Slc22a4*$^{-/-}$ los resultados obtenidos no se reprodujeron. En el riñón, la intervención terapéutica conllevó una mejora de la función mitocondrial y del estado oxidativo. En resumen, en nuestra cohorte de pacientes no hemos encontramos evidencia del efecto causal o modulador de *SLC7A13* en la cistinuria, pero en el modelo *Slc7a9*$^{-/-}$ hemos podido relacionar la presencia de AGT1 con una menor formación de cálculos de cistina, hemos descrito la disfunción mitocondrial en cistinuria y hemos demostrado el potencial terapéutico de la L-Erg en la prevención de la litiasis de cistina.

INTRODUCTION

1. INTRODUCCTION

1.1. THE URINARY SYSTEM

The excretory system removes the waste products of metabolism from body fluids helping to maintain internal homeostasis. Its main part is the urinary system, although other organs such as the skin, the lungs and the liver also participate in the excretion process. The urine is the final waste product of the urinary system and it is produced in the kidneys, transported via the ureters to the bladder (where it can be stored for hours) and excreted via the urethra.

1.1.1. The kidneys

The kidneys are the central organ of the urinary system as they generate the urine. In addition, they are involved in other body processes such as blood pH and pressure regulation, fluid and electrolytes balance, erythropoietin and calcitriol production, and the reabsorption of important metabolites. Anatomically, they are described as bean-shaped organs divided in three internal regions: the renal cortex (glomeruli and convoluted tubules), the renal medulla (renal papilla) and the renal pelvis (calyces), and are connected through the ureter, the renal artery and vein, the lymphatic vessels and the nerves by their concave medial border (the *hilum*) (**Figure 1**).

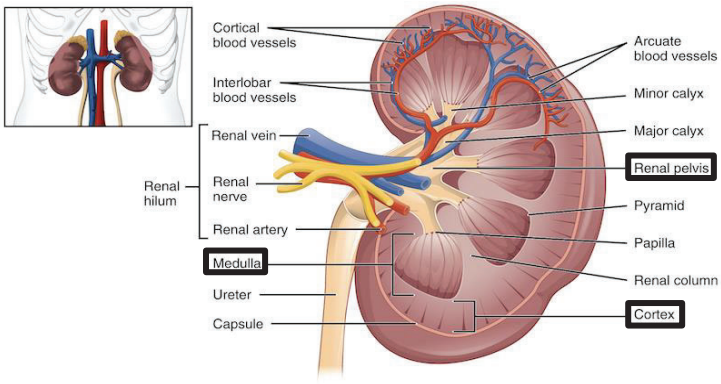

Figure 1. Kidney internal structure

Taken from sunshineclinic.org

The functional unit of the kidney is the nephron, which is constituted by the glomerulus, the Bowman's capsule, the proximal convoluted tubule, the loop of Henle, the distal convoluted tubule, the collecting ducts and the blood supply network. Functionally, nephrons can be divided in two parts: the renal corpuscle (glomeruli and Bowman's capsule) responsible for blood filtration, and the renal tubule, which reabsorb and secrete metabolites (**Figure 2**).

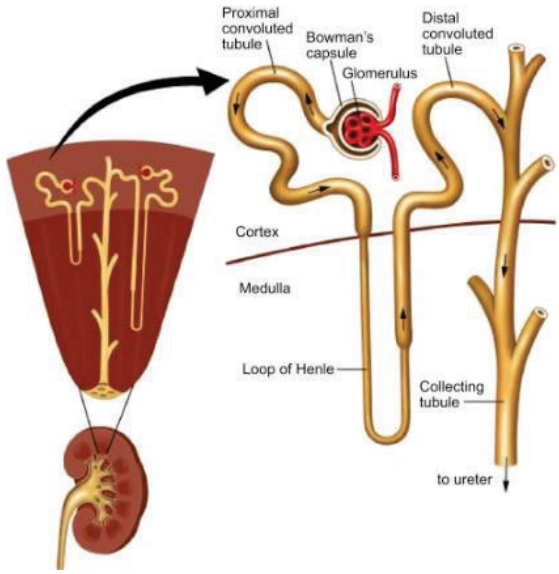

Figure 2. Diagram of a nephron

Taken from Matta & Massa, 2017.

1.1.1.1. Glomerular filtration

The blood coming through the renal artery flows into the glomeruli via the efferent arteriole, it is filtrated in the glomerular capillaries and exits the glomeruli through the afferent arteriole. In the glomerular capillaries, the hydrostatic pressure drives the filtrate to multiple filtration layers before achieving the Bowmans's capsule, which receives the filtrate and conduces it to the proximal tubule. In healthy circumstances, the filtrate is similar to blood plasma, but it contains almost no proteins nor cell components. The glomerular filtration rate (GFR) corresponds to the filtrate formed in one minute and is, on average, 125 mL per minute in humans. This means that around

180 L of plasma are filtered daily although only 2 L of urine are excreted. Thus, 99 % of the filtrate is reabsorbed by renal tubules.

1.1.1.2. Tubular reabsorption

Tubular reabsorption is a selective process by which water, inorganic ions, amino acids and other essential molecules from the glomerular filtrate are returned to the circulatory system. In addition, secretion of unwanted substances directly from the bloodstream to the filtrate can also occur in the tubules. Different mechanisms of reabsorption are observed in the tubules such as passive diffusion due to concentration gradient, active transport, pinocytosis or receptor-mediated endocytosis.

Renal tubules are divided into four differentiated segments:

- The proximal tubules, which initiate the reabsorption of most nutrients (as glucose, amino acids and vitamins), electrolytes (60 % of sodium, chloride and potassium, and 90 % of bicarbonate) and water (60 %). To optimize the surface area of reabsorption, the apical membranes of proximal tubule epithelial cells present a brush-border structure, covered in microvilli. In addition, cells of this segment contain high amounts of mitochondria to ensure energy supply to active transport systems and detoxification processes (Wang et al., 2010). Proximal tubules are divided in three segments (S1, S2 and S3) based on differences in cell ultrastructure.
- The loop of Henle, which mainly recovers water, sodium and chloride from the urine. It is divided in three parts: the thin descending limb that reabsorbs water by osmosis; the thin ascending limb that reabsorbs sodium, potassium and chloride; and the thick ascending limb which can further remove sodium and chloride if necessary.
- The distal tubule, which reabsorbs solutes, especially sodium, chloride and calcium, and secretes potassium. It is the shortest segment of the nephron and its reabsorption is regulated by hormones.

- The collecting ducts (and its final part named Bellini Ducts), which are formed by the union of several distal tubules. Its main role is the reabsorption of water regulated by anti-diuretic hormone and aquaporins.

1.1.2. Amino acid transporters

Amino acids are essential for all cells and organisms as are needed for protein and molecule synthesis, as intermediates for cell metabolism and as signaling molecules. An accurate amino acid transport through all body compartments is crucial to maintain organism homeostasis and physiology. As no specific transporters for each amino acid exist, more than 60 amino acid transporters have been described so far with specialized functions in different tissues and organs. They are classified into 11 solute carriers (SLC) families based on sequence identity and are summarized in **Table 1** and reviewed in Kandasamy et al 2018 (Kandasamy et al., 2018).

1.1.2.1. Renal amino acid transporters

Glomerular filtrate contains amino acids that need to be reabsorbed in the tubules. Thus, the apical membrane of epithelial tubular cells holds specialized transporters to avoid amino acid loss in the urine (**Figure 3**). Under physiological conditions, 450 mmols of amino acids enter daily to the lumen of tubules, but more than 99 % of them are reabsorbed (Silbernagl, 1988). As mentioned before, most filtered amino acids are reabsorbed in the brush border membrane (BBM) of proximal tubules, specifically in the early segments (S1 and S2) where most transporters are located. There are few exceptions as B^0AT3 and EAAT3 which are also located in the S2-S3 segments, and AGT1/rBAT, which is located in the S3 (Makrides et al., 2014; Nagamori et al., 2016; Shayakul et al., 1997).

In addition, amino acids can be recovered as oligopeptides and peptides, which are reabsorbed in the tubule by four different mechanisms: endocytosis accomplished by intracellular lysosomal degradation, by specific transporters (as PEPT2), by luminal hydrolysis of peptides followed by free amino acid reabsorption, or by peritubular uptake (Silbernagl, 1988).

Table 1. Amino acid transporters

Gene	Protein	Substrate(s)	Gene	Protein	Substrate(s)
SLC1A1	EAAT3	D,E,C	***SLC15A3***	PHT2	H
SLC1A2	EAAT2	D,E	***SLC15A4***	PHT1	H
SLC1A3	EAAT1	D,E	***SLC16A10***	MCT10/TAT1	W,Y,F
SLC1A4	ASCT1	A,S	***SLC17A6***	VGLUT2	E
SLC1A5	ASCT2	D,Q,C	***SLC17A7***	VGLUT1	E
SLC1A6	EAAT4	D,E	***SLC17A8***	VGLUT3	E
SLC1A7	EAAT5	D,E	***SLC25A2***	ORC2	K,R,H,O,Cit
SLC3A1	rBAT	*	***SLC25A12***	AGC-1/ Aralar1	D,E
SLC3A2	4F2hc	*	***SLC25A13***	AGC-2/ Aralar2	D,E
SLC6A5	GlyT2	G	***SLC25A15***	ORNT1/ORC1	K,R,H,O,Cit
SLC6A7	PROT	P	***SLC25A18***	GC-2	E
SLC6A9	GlyT1	G	***SLC25A22***	GC-1	E
SLC6A14	$ATB^{0,+}$	Neutral and cationic AA	***SLC25A38***	SLC25A38	G
SLC6A15	B^0AT2	P,L,V,I,M	***SLC32A1***	VIAAT	G,GABA
SLC6A17	B^0AT3/ NNT4	L,M,P,C,A,Q,S,H,G	***SLC36A1***	PAT1	G,P,A
SLC6A18	B^0AT3/XT 2	G,A	***SLC36A2***	PAT2	G,P,A
SLC6A19	B^0AT1	Neutral and cationic AA	***SLC36A4***	PAT4	P,W
SLC6A20	SIT1/ IMINO	P	***SLC38A1***	SNAT1	G,A,N,C,Q,H,M
SLC7A1	CAT-1	K,R,O	***SLC38A2***	SNAT2	G,P,A,S,C,Q,N,H, M
SLC7A2	CAT-2	K,R,O	***SLC38A3***	SNAT3	Q,N,H
SLC7A3	CAT-3	K,R,O	***SLC38A4***	SNAT4	G,A,S,C,Q,N,M
SLC7A5	LAT1	H,M,L,I,V,F,Y,W	***SLC38A5***	SNAT5	Q,N,H,A
SLC7A6	y^+LAT2	K,R,Q,H,M,L,V	***SLC38A7***	SNAT7	Q
SLC7A7	y^+LAT1	K,R,Q,H,M,L,A,C	***SLC38A8***	SNAT8	Q,A
SLC7A8	LAT2	Neutral AA except P	***SLC38A9***	SLC38A9	R,L
SLC7A9	$b^{0,+}AT$	R,K,O,CssC	***SLC38A10***	SLC38A10	Q,A
SLC7A10	Asc-1	G,A,S,C,T	***SLC43A1***	LAT3	L,I,M,F,V
SLC7A11	xCT	D,E,CssC	***SLC43A2***	LAT4	L,I,M,F,V
SLC7A12	Asc-2	G,A,S,C,T	***SLC66A1***	PQLC2	R,K,H,O
SLC7A13	AGT1	D,E,CssC	***SLC66A4***	CTNS	CssC
SLC7A14	SLC7A14	Cationic AA			

*Adapted from Kandasamy et al., 2018. *Heavy subunit of a heteromeric transporter (1.1.2.2).*

Finally, the basolateral membrane (BLM) also contains transporters that transfer the amino acids recovered by apical transporters from the lumen to the bloodstream. Additionally, amino acids from the bloodstream can be internalized by basolateral transporters (**Figure 3**).

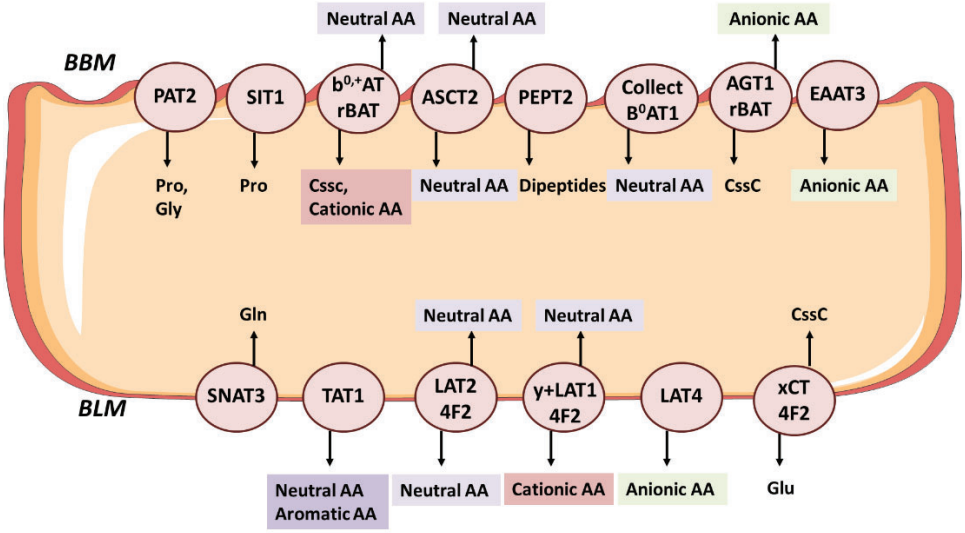

Figure 3. Principal renal amino acid transporters

At the BBM, PAT2 and SIT1 uptake small amino acids from the lumen. Cationic amino acids and cystine are exchanged for neutral amino acids by $b^{0,+}$AT/rBAT. Cystine is also reabsorbed by AGT1/rBAT in exchange for anionic amino acids, which are internalized by EAAT3. Neutral amino acids are uptaken by the antiporter ASCT2 and the transporter B^0AT1, which is expressed together with collectrin. In addition, dipeptides are internalized by PEPT2 and hydrolyzed in the intracellular space. At the BLM, TAT1 effluxes neutral and aromatic amino acids, LAT2/4F2 exchanges neutral amino acids, y^+LAT1 exchanges cationic by neutral amino acid and LAT4 effluxes anionic amino acids. SNAT3 is described to reabsorb glutamine and xCT, to exchange glutamate for cystine. AA = amino acids, BBM = brush border membrane and BLM = basolateral membrane. Adapted from Verrey et al., 2009.

1.1.2.2. Heteromeric amino acid transporters

Among SLCs, heteromeric amino acid transporters (HATs) have unique structural features as they are composed of two subunits: a heavy and a light chain covalently bound by a disulfide bond (Mastroberardino et al., 1998; Palacín & Kanai, 2004). Heavy chains mediate the trafficking of the complex to the membrane and are essential for

the stabilization and maturation of the heterodimer whereas light chains confer substrate specificity (Bröer & Wagner, 2002). To date, two heavy subunits have been identified: rBAT and 4F2hc, encoded by *SLC3A1* and *SLC3A2* genes, respectively. In addition, ten light chains have been described: LAT1, y^+LAT2, y^+LAT1, LAT2, $b^{0,+}$AT, asc1, xCT, asc2, AGT1 and arpAT, all from the SLC7 family and encoded by *SLC7A5* to *SLC7A13* and *SLC7A15* genes, respectively. LAT1, y^+LAT2, y^+LAT1, LAT2, asc1 and xCT are associated with 4F2hc, and $b^{0,+}$AT and AGT1 with rBAT (Fotiadis et al., 2013; Nagamori et al., 2016). The other two light subunits, asc2 and arpAT have been only characterized in mice and interact with a yet unknown heavy subunit (**Table 2**).

Table 2. Heteromeric amino acid transporters and their substrates

Heavy subunit (Gene)	**Light subunit**	**Gene**	**AA substrates**
rBAT (*SLC3A1*)	$b^{0,+}$AT	*SLC7A9*	R, K, O, cystine
	AGT1	*SLC7A13*	D, E, cystine
4F2hc (*SLC3A2*)	y^+LAT1	*SLC7A7*	K, R, Q, H, M, L
	y^+LAT2	*SLC7A6*	K, R, Q, H, M, L, A, C
	LAT1	*SLC7A5*	H, M, L, I, V, F, Y, W
	LAT2	*SLC7A8*	AA^o except P
	Asc1	*SLC7A10*	G, A, S, C, T
	xCT	*SLC7A11*	E, cystine$^-$
Unknown	Asc2	*SLC7A12*	G, A, S, C, T
	arpAT	*SLC7A15*	-

Heavy subunits belong to SLC3 family and lights subunits, to SLC7. AA = amino acids, AA^o = neutral amino acids. Adapted from Palacín et al., 2011.

$b^{0,+}$AT and rBAT association is of particular relevance for this work as they form the $b^{0,+}$ system, which is a Na^+-independent transporter that mediates the uptake of cystine and dibasic amino acids in exchange for intracellular neutral amino acids (Chillarón et al., 1996; Pfeiffer et al., 1999). In fact, they form a heterotetrameric protein complex composed of two $b^{0,+}$AT and two rBAT subunits (**Figure 4**). rBAT is a type II membrane N-glycoprotein with an intracellular N-terminus, a transmembrane domain and an

extracellular C-terminus that ensures that $b^{0,+}$AT reaches the membrane. $b^{0,+}$AT is a transmembrane protein composed of 12 transmembrane segments and intracellular N and C-terminus, responsible for amino acids exchange. At the extracellular second loop, $b^{0,+}$AT has a conserved cysteine residue that form the disulfide bond with another cysteine residue of rBAT (Palacín et al., 2011; Yan et al., 2020).

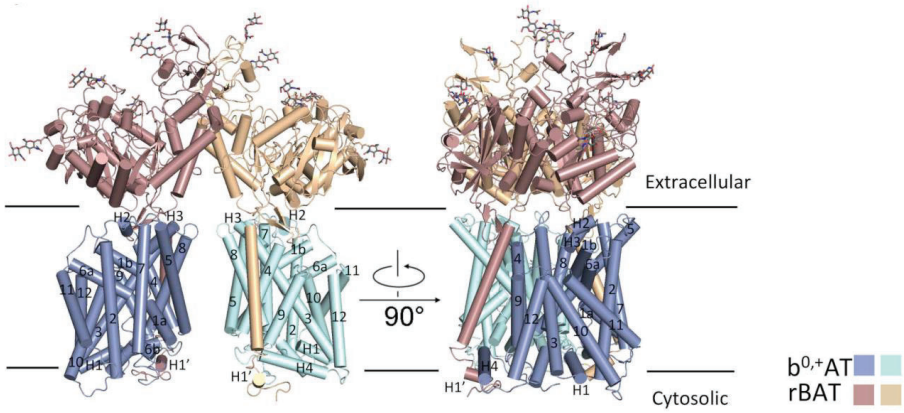

Figure 4. The heteromeric rBAT/$b^{0,+}$AT amino acid transporter

Two $b^{0,+}$AT-rBAT heterodimers form the functional heterotetramer through rBAT proteins interaction. Taken from (Yan et al., 2020).

$b^{0,+}$AT/rBAT heterotetramers are mainly expressed in the BBM of epithelial cells of kidneys and intestine (Pickel et al., 1993). More precisely, $b^{0,+}$AT/rBAT complexes are located in the S1-S2 of the kidney proximal tubules, where are responsible for 90 % of cystine reabsorption (Bauch et al., 2003; Pfeiffer et al., 1999). However, rBAT protein is also detected in the S3 segment where oligomerizes with AGT1 (Nagamori et al., 2016).

1.1.2.3. Aminoacidurias

More than 20 pathological conditions have been associated to amino acid transporter malfunction (reviewed in Yahyaoui and Pérez-Frías 2020). Of them, aminoacidurias are a group of diseases caused by metabolic or transport defects that induce an abnormally excretion of amino acids in the urine. Most aminoacidurias are inherited as are a consequence of gene mutations. The implementation of chromatography

methods to quantify amino acid levels in urine allowed to be diagnosed in childhood. Phenotypically, aminoacidurias present a wide range of symptoms depending on which amino acid(s) is(are) hyperexcreted. Most important aminoacidurias are summarized in the **Table 3** and due to the relevance for this work, cystinuria is further described in its own chapter (1.2).

Table 3. Principal aminoacidurias

Disease	ORPHAcode	Gene	Protein	Cause	Prevalence	Inheritance	Symptoms
Cystinosis	213	*CTNS*	Cystinosin	Defect in cystine lysosomal transport	1/100000	Autosomal recessive	Fanconi syndrome, polyuria, polydipsia, growth retardation…
Cystinuria	214	*SLC3A1, SLC7A9*	rBAT, $b^{0,+}$AT	Defect in cystine, lysine, arginine and ornithine renal transport	14/100000	Autosomal recessive, partially dominant	Cystine lithiasis
Dicarboxylic aminoaciduria	2195	*SLC1A1*	EAAC1	Defect in renal, intestinal and neural glutamate and aspartate absorption	2.8/100000	Autosomal recessive	Hypoglycemia, intellectual disability and obsessive-compulsive tendencies
Hartnup disease	234500	*SLC6A19*	B^0AT1	Abnormal renal and intestinal absorption of nonpolar amino acids, in particular tryptophan	4/100000	Autosomal recessive	Dermatitis, intermittent cerebellar ataxia and psychosis-like symptoms
Iminoglycinuria	42062	*SLC36A2* and *SLC36A1, SLC6A19-20?*	PAT2 ¿PAT1?	Abnormal renal reabsorption of glycine, proline and hydroxyproline	6.68/100000	Autosomal recessive	Relative benign disorder associated with encephalopathy, mental retardation, deafness, blindness, kidney stone and gyrate atrophy
Lysinuric protein intolerance	470	*SLC7A7*	y^+LAT1	Poor renal and intestinal absorption of cationic amino acids	1.7/100000	Autosomal recessive	Urea cycle dysfunction that leads to hyperammonemia that can induce coma, brain damage and death

1.2. CYSTINURIA

1.2.1. History of cystinuria

In 1810, Wollaston described for the first time a cystine stone (Wollaston, 1810). He observed a compact, semitransparent and with a slight tinge of yellow stone composed of an unusual substance (**Figure 5**). Wollastone called it cystic oxide because the calculi were taken from the bladder (from the greek *Kystis*) and thought it contained oxygen, as by destructive distillation it yielded carbonate of ammonia. In 1817, Marcet described the case of a men who died with symptoms of renal calculi and, in the postmortem study, he found "cystic oxide" calculi in his kidney (Marcet, 1817). In addition, this man had two brothers that also suffer from kidney and urethra "cystic oxide" calculi. Thus, Marcet placed the origin of the "cystic oxide" calculi formation in the kidney and suggested a familial component in this disease.

Figure 5. The first cystine stone described by Wollaston in 1810

In 1830, Berzelius demonstrated that the unusual substance was not an oxide but an amine and rename it as cystine (Berzelius, 1833). During the middle 19th century, several studies revealed the presence of sulfur in cystine calculi and the empirical formula was finally stablished ($C_6H_{12}N_2S_2O_4$) (Jones, 1840). Urinary analysis of stone former patients showed that cystine was hyperexcreted (Toel, 1855) leading to naming the disease as cystinuria. In 1908, Garrod included cystinuria as one of the four Inborn Errors of Metabolism (Garrod, 1908). However, this was not completely correct as cystinuria is a consequence of a transport defect, not an enzyme defect.

Until 1951, the additional hyperexcretion of lysine, arginine and ornithine in cystinuria patients was not demonstrated (Dent & Rose, 1949; Stein, 1951). Urinary aminogram alterations together with normal plasma aminogram lead Dent and Rose to formulate the hypothesis that cystinuria was a renal disease caused by a defect in the common reabsorption mechanism of cystine, lysine, arginine and ornithine (Dent & Rose, 1949). In 1961, Milne investigated the amino acid intestinal absorption in cystinuria patients and conclude that the defect was not severe enough to cause any clinical disability or malnutrition as the absorption of cystinuria related amino acids is almost complete at range of ingestion (Milne et al., 1961).

Yet in the 1950s, Harris published several papers related to the heredity of cystinuria and, after examining the amino acid content of urine from patients and their relatives, postulated the cystinuria pattern of inheritance (Harris et al., 1955). In 1966, Rosenberg classified cystinuria patients according to the urinary excretion pattern of their parents (obligate heterozygous): cystinuria type I patients

corresponded to those whose parents present a normal urinary pattern, and non-type I (type II or III), to those whose parents have cystine mild or severe hyperexcretion (Rosenberg et al., 1966).

Three decades later, throughout the 1990s, the two cystinuria causing genes *SLC3A1* and *SLC7A9* were identified. In 1992-93, three cDNAs encoding a cystine, lysine, arginine and ornithine transporter were cloned from rat (Tate et al., 1992; Wells & Hediger, 1992), rabbit (Bertran et al., 1992) and human (Furriols et al., 1993). The codifying sequence of these cDNAs, *SLC3A1*, was studied in cystinuria patients and mutations in this gene showed to be responsible for type I cystinuria (Calonge et al., 1994). Then, the gene responsible for cystinuria type no-I was mapped by linkage analysis to 19q12-13.1 (Bisceglia et al., 1997; Wartenfeld et al., 1997) and the *SLC7A9* gene was finally identified (Feliubadaló et al., 1999). *SLC3A1* and *SLC7A9* genes encode rBAT and $b^{0,+}$AT proteins, respectively, that together form the heteromeric complex $b^{0,+}$AT/rBAT responsible for cystine, lysine, arginine and ornithine reabsorption in the apical membrane of intestine and renal proximal tubules.

1.2.2. Genetics and Classification

Genetic variants in *SLC3A1* (2p21) and *SLC7A9* (19q12) are known to cause cystinuria, but its inheritance pattern is complex. *SLC3A1* mutations are inherited as an autosomal recessive disease, but mutations in *SLC7A9* gene present an autosomal dominant with incomplete penetrance pattern (Font-Llitjós et al., 2005). More than 240 mutations have been identified so far in the *SLC3A1* gene, and 159 in the *SLC7A9* (Sahota et al., 2020). Among *SLC3A1* mutations, p.Met467Thr is the most frequent observed (30% of known alleles), followed by p.Thr216Met (13%) and the duplication dupE5-E9 (11%) (Eggermann et al., 2012; Font-Llitjós et al., 2005). *SLC3A1* huge deletions can affect part of the neighboring gene *PREPL* causing hypotonia-cystinuria syndrome (OMIM #606407), characterized by cystinuria, hypotonia, mild intellectual disability and growth hormone deficiency (Jaeken et al., 2006). *SLC7A9* most frequent mutations are p.Gly105Arg (20%) and p.Arg333Trp (11%) (Eggermann et al., 2012; Font-Llitjós et al., 2005). Ethnic influence is observed in certain mutation frequencies, as an example, in Spanish patients the duplication c.614dupA accounts for 29% of *SLC7A9* alleles studied (Eggermann et al., 2012; Li et al., 2020). However, about 10 % of cystinuria patients remain genetically uncharacterized (for one or both alleles) leading a door open for the involvement of other genes in cystinuria (Chillarón et al., 2010; Olschok et al., 2018; Sahota et al., 2020).

As mentioned before, prior to genetic analysis, cystinuria patients were classified according to the urinary excretion pattern of their parents (obligate heterozygous). Cystinuria type I patients corresponded to those whose parents presented a normal urinary pattern, and non-type I (type II or III), to those whose parents had mild or severe cystine hyperexcretion (**Table 4**) (Rosenberg et al., 1966). When the genes responsible to cause cystinuria were identified, the International Cystinuria Consortium proposed a new cystinuria classification based on the genetics of the disease (Dello Strologo et al., 2002). Accordingly, cystinuria type A corresponds to patients carrying mutations in *SLC3A1* gene, type

B cystinuria to patients with mutations in *SLC7A9* gene and cystinuria type AB, to patients with mutations in both genes (**Table 4**) (Dello Strologo et al., 2002). Almost all type I patients correspond to cystinuria type A whereas almost all non-type I, to type B cystinuria (**Table 4**). However, although digenic inheritance has been demonstrated in a cystinuria type AB mouse model (Espino et al., 2015), type AB patients diagnosed so far do no present lithiasis; in fact, only those who are AAB or BBA have stone episodes (Font-Llitjós et al., 2005; Wong et al., 2015).

Table 4. Genetic and clinical classification of cystinuria

Genetic classification	**Type A**	**Type B**		**Type AB**
Frequency	45%	53%		2%
Gene locus	Chromosome2 (*SLC3A1*)	Chromosome 9 (*SLC7A9*)		Chromosomes 2 & 9 (*SLC3A1*/*SLC7A9*)
Subunit affected	rBAT (heavy subunit)	$b^{0,+}$AT (light subunit)		rBAT and $b^{0,+}$AT
Phenotypical classification	Type I	Type non-I		
		Type II	Type III	
Urinary excretion of cystine in heterozygotes (µmol/g Cre)	Normal	Elevated	Mild	Normal
	0-100	**990-1740**	**100-600**	**0-100**

Cre = Creatinine. Adapted from Krombach et al., 2011.

1.2.3. Clinical features

Cystinuria is the most common primary inherited aminoaciduria with an estimated global incidence of 1:7000, which ranges from 1:2000 in the United Kingdom to 1:100000 in Sweden (Bostroem & Hambraeus, 1964; Chillarón et al., 2010; Kum et al., 2019). However, this incidence could be underestimated as non-stone former cystinuria patients might never been diagnosed (Thomas et al., 2014). Cystine urolithiasis accounts for 1-2 % of adult and 6-8 % of pediatric urinary tract calculi (Erbagci et al., 2003; Leusmann et al., 1990; Milliner et al., 1993).

Cystinuria is characterized by a defect in cystine and dibasic amino acid (lysine, arginine and ornithine) transport which affects their reabsorption in both intestine and renal proximal tubules (Dent & Rose, 1949; Milne et al., 1961; Stein, 1951). At intestinal level, no clinical effect is observed as, although cystinuria related amino acids cannot be freely absorbed, whole proteins, oligopeptides and peptides can (Asatoor et al., 1974; Milne et al., 1961). In addition, plasma levels of these amino acids are slightly lower in cystinuria patients but are not described as pathological (Dent et al., 1954; Mårtensson et al., 1990; Morin et al., 1971). However, the renal reabsorption defect leads to a hyperexcretion of cystine, lysine, arginine and ornithine (Dent & Rose, 1949; Stein, 1951). The only pathological clinical manifestation described so far is cystine lithiasis in the urinary system due to the low solubility of

cystine at physiological urine pH that induces its precipitation and, consequently, stone formation (Königsberger et al., 2000).

About 94 % of patients develop cystine stones during their lifetime and, of them, 75 % develop bilateral stones (Eggermann et al., 2012; Knoll et al., 2005). The recurrence rate of stone episodes is higher than 60 %, which can be lowered with an optimal clinical management (Claes & Jackson, 2012; Moore et al., 2019). However, on average, untreated patients present a new stone episode every 1-2 years and undergo a surgical procedure to remove them every 3 years (Barbey et al., 2000). Recurrent renal stone episodes that cause obstructive uropathy and the needed of repeted urologic interventions results in chronic kidney disease (CKD) in most patients (57.6 % CKD stage 2 and 17.8 %, stage 3) (Kum et al., 2019; Thomas et al., 2014). Thus, only 25 % of cystinuria patients preserve normal renal function (Kum et al., 2019; Prot-Bertoye et al., 2015). In addition, the risk of CKD in cystinuria is higher than in other types of kidney stones (Prot-Bertoye et al., 2015).

Cystinuria has a phenotypical heterogenicity as patients may present their first stone episode at an early age as well as in the later adulthood, or may not present symptoms other than aminoaciduria throughout their lives (Stephens, 1989). Cystine stone onset ocurrs during childhood-adolescence in 75 % of patients, 25 % in the first ten years of life and a further 50 % between the first and second decade of life (Dello Strologo et al., 2002; Stephens, 1989). No gender differences have been observed on the age of stone onset, but male patients present a more sever affection than females (even in siblings sharing the same mutation) (Dello Strologo et al., 2002). This could be explained by anatomical differences as male urinary tract is more susceptible to obstructions.

1.2.4. Diagnosis

As cystinuria is a rare disease, diagnosis is often missed or delayed, and an early diagnose is essential for renal function prevention in patients (Moore et al., 2019). Cystinuria diagnosis is usually achieved by analyzing the stone composition as cystine can be identified by a positive nitroprusside cyanide stone test or by infrared spectroscopy and X-ray diffraction (cystine stones are lightly opaque due to sulfur content) (Knoll et al., 2005; Moussa et al., 2020; Nakagawa & Coe, 1999). Other diagnostic approaches are the determination of urinary amino acid excretion pattern in a 24h urine sample, the microscopic examination of crystals in urine and the genetic analysis of *SLC7A9* and *SLC3A1* genes (Eggermann et al., 2012; Knoll et al., 2005; Moussa et al., 2020). Young patients with recurrent or bilateral stones, or with siblings affected by stone disease should always be screened for cystinuria (Hovgaard et al., 2015; Thomas et al., 2014). Although genetic testing is not performed routinely, it should be used for genetic counselling and for detecting cystinuria in the first years of life as the diagnostic based on amino acid hyperexcretion is limited by the huge variability observed at young ages due to tubular immaturity (Servais et al., 2021).

1.2.5. Therapeutical approaches

With a stone episode onset often within the first two decades of life, recurrence rates of 60% or greater, together with the lack of an effective treatment, cystinuria patients require an intensive follow-up to preserve their renal function. Conservative measures are focused on preventing stone formation (hydration, diet recommendations and urine alkalinization) and when fail, pharmacological treatment using thiol drugs is applied to dissolve cystine stones. Current therapeutical approaches are described below.

1.2.5.1. Conservative measures

- **Hydration**: increasing daily fluid intake to rise diuresis could help to maintain cystine urine concentration bellow its saturation point (250 mg/L at pH 7) (Chillarón et al., 2010; Pak & Fuller, 1983). This means that if, on average, 1-1.5 g of cystine are excreted per day in cystinuria patients, at least 4 L of liquid should be drunk. The amount of liquid consumption can be adjusted according to each patient's excretion. In addition, it is important to drink before bedtime, at least once during the night, and upon awakening (Servais et al., 2021).
- **Diet**: there are two main dietary recommendations although its effect has not been demonstrated in clinical trials. On one hand, restriction of dietary sodium intake to 6 g/day (less than 2 g/day of salt) is thought to reduce cystine excretion but in recent diet studies no relation was observed (Siener et al., 2021). On the other hand, restriction in animal protein consumption is also recommended as reduces the intake of cystine and its precursor methionine, and increase urine pH (Rodman et al., 1984; Woodard et al., 2019). In addition, ingestion of vegetables containing citrate and malate could increase urine pH (Siener et al., 2021).
- **Alkalinization**: urine pH is a crucial determinant of cystine solubility, and thus, of stone formation. Cystine solubility increase as increase the pH: 1 mmol/L at pH 7 to 2 mmol/L at pH above 7.5 (Pak & Fuller, 1983). The most recommended alkalinizing agent is potassium citrate (60-80 mEq/day in adults) as it increases the pH without increasing sodium intake (Fjellsted et al., 2001).

1.2.5.2. Pharmacological approaches

Pharmacological treatment is focused on avoiding cystine formation using cysteine binding/thiol drugs. The two main thiol-containing agents used are **D-penicillamine** (Halperin et al., 1981) and **tiopronin** (α-mercaptopropionylglycine) (Pak et al., 1986) which prevent stone formation and dissolve already formed stones. As cystine molecules are two cysteines bound by a disulfide bond, these drugs induce the reduction of the disulfide bond and form cystine-drug products, which are up to 50-fold more soluble in the urine. Both agents are effective reducing free cystine in urine, but present severe side effects as alterations in taste perception, proteinuria, stomach pain, immune-mediated diseases or muco-cutaneous lesions. At the beginning of its prescription, up to 80 % of patients showed those side

effects which lead to decrease medication adherence of thiol-binding drugs (Pak et al., 1986). However, gradual escalation to the optimal dose has been related to lower to 20-30 % side effects (Deberardinis et al., 2008; Prot-Bertoye et al., 2019). For these reasons, the duration of D-penicillamine and tiopronin treatment should be evaluated for each patient and should be prescribed to those with a high recurrence rate despite good adherence to the other cystinuria therapeutical approaches.

Captopril is another thiol-binding drug which form captopril-cysteine dimers that are 200 times more soluble than cystine (Perazella & Buller, 1993). In addition, captopril is an angiotensin-converting enzyme that could improve blood pressure and protect renal function. Although it has been demonstrated that prevents cystine stone formation in retrospective studies, prospective long-term studies fail to prove it. Thus, nowadays, captopril is not recommended for cystinuria (Pearle et al., 2014; Servais et al., 2021).

1.2.5.3. New therapeutic options

New thiol-containing drugs, tolvaptan, inhibitors of crystal growth and antioxidant compounds are going to be introduced in this part although they are still under development.

Bucillamine is a thiol drug currently used in Japan and South Korean to treat rheumatoid arthritis which has a low toxicity profile. In fact, is not a thiol-compound but a di-thiol one which could allow to administrate lower dosages. Bucillamine phase two clinical trial in patients with cystinuria is currently underway in the United States (ClinicalTrials.gov Identifier: NCT02942420).

Tolvaptan is a vasopressin 2 receptor antagonist approved by the Food and Drug Administration (FDA) to treat hereditary polycystic kidney disease. It is being studied for cystinuria for its diuretic effect. In a study using a mouse model of cystinuria it was demonstrated that, tolvaptan, induces liquid intake, increases urinary volume and delays stone growth (Bai et al., 2021). Then, a pilot study of short-term safety, tolerability and impact of urinary stone risk was carried in 4 young cystinuria patients (two doses, daily for 4 days) (Nelson et al., 2020). A significant increase in diuresis with the consequently reduction in cystine urinary concentration was achieved without several side effects (only extreme thirst). However, further studies should be performed to study long-term effects and the influence on stone formation.

Inhibitors of crystal growth, compounds that due to their structural semblance to cystine molecules are attached to crystal surfaces perturbing crystal growth, are also being studied.

- **L-cystine dimethylester** (CDME) or **L-cystine methylester** (CME) mimic L-cystine but with the carboxylate groups substituted by esterified methyl groups (Lee et al., 2015). CDME showed greater results lowering the growth rate of cystine crystals *in vitro* (Lee et al., 2015). *In vivo* studies were also performed feeding a cystinuria mouse model with 10 mg/kg of CDME daily for 4 weeks and showed a significant decrease in stone weight and size in the treated

group, although an increase in the number of stones was observed (Lee et al., 2015). No adverse side effects were observed after oral administration of CDME although previous studies in where CDME was parentally administered showed a potential toxicity (Lee et al., 2015; Rech et al., 2007; Wilmer et al., 2007). Clinical trials in humans are needed to study if CDME has side effects and to demonstrate its potential as stone growth inhibitor in humans.

- **L-cystine diamides** are also being evaluated for their potential inhibitor capacity of cystine crystallization. First approaches were computational but then, *in vitro* and animal model studies confirm its effectiveness in preventing the stone formation better than CDME (Hu et al., 2016; Yang et al., 2018). However, as in the CDME, clinical trials in humans are needed to study its bioavailability, discard side-effects and confirm its potential as stone growth inhibitor.
- **Selenium** has been proved to reduce calcium oxalate (CaOx) renal stone formation by binding to crystal surface (Sakly et al., 2003) and its being hypothesized that could bind to cysteine inhibiting cystine crystals growth (Chrzan et al., 2015). A clinical study in a 48-patient cohort receiving selenium (200 mg/daily) for 6 weeks showed to reduce their cystine crystal volume (Mohammadi et al., 2018).

In the last few years, **antioxidant molecules** are being investigated as a potential treatment for cystinuria as showed cystine crystal/stone growth inhibitor properties, although the mechanism by which they act remains unknown. **α-Lipoic acid** is the most promising antioxidant drug as showed to prevent cystine stone formation by increasing cystine solubility in urine in a cystinuria mouse model (Zee et al., 2017). A phase two clinical trial involving 50 participants (ClinicalTrials.gov Identifier: NCT02910531) is estimated to be completed by the end of 2022. A preliminary study supplementing conventional potassium citrate with regular doses of α-Lipoic acid in 2 pediatric patients showed an improvement in cystine solubility and supersaturation parameters (Cil & Perwad, 2020). **Salvianolic acid B**, an antioxidant constituent of the medical herb *Salvia miltiorrhiza* (Danshen), showed to reduce cystine crystals deposition in a HK-2 cell cultures and in kidneys and bladders of cystinuria mouse model related to a decrease in oxidative stress levels (Yifan et al., 2019). **Selenium**, described above as a potential crystal growth inhibitor, also has antioxidant and anti-inflammatory properties that are hypothesized to be an additional factor for its crystalluria preventive effect (Mohammadi et al., 2018).

Finally, **gene therapy** approaches are being investigated in mouse models to treat cystinuria, although results are not currently available (Bai et al., 2019).

1.2.5.4. Urological interventions

When stone formation cannot be avoided and stones achieve more than 7 mm in diameter, they should be removed by ureteroscopy (URS), percutaneous nephrolithotomy (PCNL) or extracorporeal shockwave lithotripsy (ESWL). Ureteral stones are easier to pass spontaneously, but if after 4 weeks of

the stone detection is not excreted, surgical treatment must be considered. For renal stones, complete clearance is basic to avoid (early) recurrence. Periodic evaluations every year are necessary to detect stones in an early stage and prevent surgical interventions that, due to the recurrence, could lead to kidney damage.

1.2.6. Animal models for cystinuria

Cystinuria naturally occurs in cats, dogs, ferrets, caracals and wolves, but they are species not suited for laboratory studies. The discovery of *SLC3A1* and *SLC7A9* as genes responsible for causing cystinuria allowed the generation of mouse models to better understand its pathophysiology and provided a powerful tool to test potential treatments. Thus, in 2003, the first cystinuria type A and type B mouse models were developed by disrupting *Slc3a1* and *Slc7a9* genes, respectively (Feliubadaló et al., 2003; Peters et al., 2003). To date, 9 different cystinuria mouse models have been generated and will be introduced as being essential for this thesis (**Table 5**).

Pebbles (Peters et al., 2003), the first cystinuria type A mouse model, was generated in Ingenium Pharmaceuticals by genome-wide mutagenesis induced by N-ethyl-N-nitrosourea (ENU) treatment. A mutant mouse line with elevated urinary concentration of cystine, lysine, arginine and ornithine together with an urolithiasis phenotype was identify. The causative mutation is a missense mutation in the *Slc3a1* gene that leads to the amino acid change p.D140G in the extracellular domain of rBAT protein. There is no detectable effect on the *Slc3a1* mRNA expression, but rBAT protein is not expressed in the BBM of proximal tubules, indicating an affection in protein stability and localization. All male mutants developed bladder and/or kidney calculi during the first year of life but, at this age, stones were observed in only 23 % of females.

Stones (Feliubadaló et al., 2003), the first cystinuria type B mouse model, was generated in Dr. Nunes' group disrupting *Slc7a9* gene by homologous recombination that replaced 6.1 kb of the *Slc7a9* genomic sequence (including exons 3 to 9) with a neomycin resistant gene cassette. In this mouse model, $b^{0,+}$AT protein expression is completely abolished but the rBAT protein is still detected in the BBM of proximal tubules. Phenotypically, homozygous mice present severe hyperexcretion of cystine, lysine, arginine and ornithine and heterozygous mice, a moderate hyperexcretion, mimicking human cystinuria type B. At 12 months of age, cystine crystalluria was observed in 82 % of homozygous mice and cystine lithiasis in the urinary bladder in 42 % of them. In this model, no sex differences were observed as about 42 % of males and females present cystine stones. *Stones* have been used in several studies to understand the molecular mechanism of cystinuria type B and have been validated as good model for antilithiasic pharmacological studies (Font-Llitjós et al., 2007).

In 2014, a new cystinuria type A mouse model arose due to a spontaneous mutation in 129S2/SvPasCrl mice (Livrozet et al., 2014). The c.1232G>A point mutation in the *Slc3a1* gene lead to the p.E383K amino acid exchange in the rBAT protein and cause its absence in the BBM of proximal tubules (although

mRNA expression is preserved). Phenotypically, 129S2/SvPasCrl mutant mice presented cystinuria related amino acids hyperexcretion and 80 % of male mice developed cystines stones in the bladder by the firsts four months of life. Cystine crystals were observed in both male and female but cystine stones were found mainly in males (as was described in the other cystinuria type A model). An increase in early mortality was observed in this model which correlated to the presence of bilateral obstruction and hydronephrosis.

Recently, a novel cystinuria type A mouse model has been generated by homologous recombination in embryonic stem cells replacing a *Slc3a1* genomic region of 5.7 kb, which include the exon 1 (Zee et al., 2017). All *Slc3a1*$^{-/-}$ male mice presented cystine hyperexcretion and developed stones within 6 weeks of age. No data of female mice is available.

To study the digenic inherence pattern of cystinuria, a type AB mouse model was generated by crossing cystinuria type A (*Pebbles*) and type B (*Stones*) mouse models (Espino et al., 2015). The expression protein analysis of the BBMs revealed that the double heterozygous mice (*Slc7a9*$^{+/-}$*Slc3a1*$^{+/-}$) have around 40% lower levels of $b^{0,+}$AT/rBAT heterodimers when comparing to wild-type ones (WT). Mild cystine hyperexcretion in all mice and 4 % of calculi formation rate at 8 months of age were observed in double heterozygous (*Slc7a9*$^{+/-}$*Slc3a1*$^{+/-}$), demonstrating the possible digenic inherence of cystinuria. In addition, double homozygous mice (*Slc7a9*$^{-/-}$*Slc3a1*$^{-/-}$) showed an increased prevalence and severity of lithiasic phenotype when comparing with single ones.

Finally, novel cystinuria type A and type B models have been generating by the CRISPR/Cas9 technique.

For type A, the genome editing approach target *Slc3a1* exon 2 and *Tyr* exon 1 to obtain an albino cystinuria type A mice (Beckermann et al., 2020). Two mutant mice, c.527_531delTTGAG;insA and c.526insTT, were obtained and both showed cystine hyperexcretion and urinary cystine crystals. Male mice exhibit a higher rate of stone formation overtime compared to females. At 40 weeks of age, the stone formation rate of c.527_531delTTGAG;insA male mice was 80 %, but no stone events were observed in females. In mice carrying the c.526insTT mutation, 90 % and 20% of males and females developed stones, respectively.

For cystinuria type B, sgRNAs targeting intron 2-3 and 12-13 of the *Slc7a9* gene were used resulting in a 12 kb of the *Slc7a9* gene deletion (Bai et al., 2021). Phenotypically, 90 % of homozygous male mice presented cystine stones at two months of age and 100 % at six months. However, in females, no stone events were observed at six months of age.

As it was used for this thesis work, the knockout (KO) mice of the L-Ergothioneine transporter (*Slc22a4,* OCTN1) needs to be introduced. *Slc22a4*$^{-/-}$ mice were generated by homologous recombination replacing *Slc22a4* exon 1 by a neomycin resistance gene cassette (Kato et al., 2010). A blood metabolome analysis to identified OCTN1 substrates revealed the absence of L-Erg among 112

metabolites. Then, L-Erg deficiency was further observed in all tissue samples in *Slc22a4*$^{-/-}$ mice. In addition, after oral administration of [^{3}H]-Ergothioneine, *Slc22a4*$^{-/-}$ mice could not retained this metabolite in the body and its urinary excretion was increased compared to WT mice.

Recently in our group, *Slc22a4*$^{-/-}$ and *Slc7a9*$^{-/-}$ (*Stones*) mice were crossed to obtain a double mutant mouse model. At 40 weeks of age, double mutant male mice showed a 15 % increase in stone formation rate compared to *Slc7a9*$^{-/-}$ male mice. However, although double mutant females presented an early stone onset, at 40 weeks of age no significant differences in the stone formation were observed (Lopez de Heredia et al., 2021).

Table 5. Cystinuria mouse models currently available

Gene	Protein	Cystinuria type	Mutation	Generation procedure
Slc3a1	rBAT	A	p.D140G	N-ethyl-N-nitrosourea
			p.E383K	Spontaneous mutation
			Deletion of exon 1	Homologous recombination
			c.527_531delTTGAG;insA	CRISPR/Cas9
			c.526insTT	CRISPR/Cas9
Slc7a9	$b^{0,+}$AT	B	Deletion of exons 3-9	Homologous recombination
			Deletion of exons 3-12	CRISPR/Cas9
Slc3a1/Slc7a9	rBAT/$b^{0,+}$AT	AB	p.D140G/ deletion of exons 3-9	Mouse breading
Slc7a9/Slc22a4	$b^{0,+}$AT/OCTN1	B	Deletion of exons 3-9/ Deletion of exon 1	Mouse breading

1.2.7. Modulators of cystine lithiasis

Although the discovery of cystinuria causing genes allowed to settle the molecular basis of cystinuria and to define a new patient classification, neither the genetic nor the previous established classification can be associated to the clinical course in these patients. The hyperexcretion of cystine is the main condition for cystine stone formation, and although the severity of *SLC3A1* and *SLC7A9* mutations correlates with the level of amino acids hyperexcretion, it does not correlate to cystine lithiasis onset and recurrence (Dello Strologo et al., 2002; Font et al., 2001). Moreover, a high phenotype variability is observed as even patients with the same mutation show different onset of stone episodes or stone recurrence rates. In addition, mutation analyses allow to detect genetic variants in most patients but there are still a 10 % that remain genetically uncharacterized for one or both cystinuria causing alleles (Dello Strologo et al., 2002; Olschok et al., 2018). Thus, the lack of genotype-phenotype correlation in

cystinuria patients and the remaining 10 % of uncharacterized patients justifies the search of cystine lithiasis modulating genes and compounds.

1.2.7.1. Genetic background, sex and diet

As described above (1.2.6), cystinuria mouse models present different onset and severity of its lithiasic phenotype. This could be explained as they were generated by distinct procedures that resulted in a variety of specific mutations in either *Slc3a1* or *Slc7a9* genes. However, previous results of our group revealed the impact of mice background on stone formation when the lithiasic phenotype of cystinuria type B model was compared between mice in pure C57Bl6/J and mixed C57Bl6/J-129 and C57Bl6/J-C3H backgrounds (Espino, 2012). Although similar levels of cystine hyperexcretion were observed, stone formation rate was more than two times higher in mixed backgrounds than in the pure one, suggesting the existence of cystinuria modifier genes in the different strains.

Another factor that induces differences in stone formation is sex. Surprisingly, most female mouse models present lower cystine stone formation rate (although cystine hyperexcretion is also detected) than its males counterparts (Livrozet et al., 2014; Peters et al., 2003). Similarly, in humans, male patients present a more severely affection and higher stone recurrence rates than females, although no differences in cystine excretion levels are observed (Dello Strologo et al., 2002). Thus, it suggests that there is/are some factor(s) that regulates cystine crystal aggregation differently in males and females in addition of anatomical differences.

Finally, diet composition could affect stone development. Dietary restriction of sodium and animal protein intake are recommended to cystinuria patients to prevent stone formation, although no strong evidence could be obtained in clinical studies. However, a study using a cystinuria mouse model showed that an increase in the amount of cystine in the chow, from 0.31 % to 0.36 %, accelerated dramatically the stone onset and increased the rate of stone formation (Woodard et al., 2019). Thus, cystine (or its precursors) dietary uptake could modulate stone formation in cystinuric patients. In addition, a study in healthy subjects showed that a balanced mixed-diet or a lacto-ovo-vegetarian diet reduced the urinary cystine concentration by increasing urine pH (Siener et al., 2021). This finding suggests that there are dietary components that could affect urinary pH and therefore modulate cystine lithiasis.

1.2.7.2. AGT1

For several years $b^{0,+}$AT was believe to be the only light chain that heterodimerized with rBAT in the apical membrane, being responsible for 90 % of cystine reabsorption under physiological conditions. However, the differential distribution of $b^{0,+}$AT and rBAT along proximal tubule segments suggested that rBAT had an unknow partner in the S3 segment where $b^{0,+}$AT is not expressed. In 2016, AGT1, encoded by *SLC7A13,* was described as a second cystine renal transporter (Nagamori et al., 2016). AGT1

heterodimerizes with rBAT in the renal apical membrane S3 segment of proximal tubules where mediates efflux of anionic amino acids in exchange for cystine. In addition, AGT1 colocalize with EAAT3, which prevents the urinary loss of aspartate and glutamate released by AGT1/rBAT. Cystine reabsorption by AGT1/rBAT (≈ 10 %) may not be relevant under physiological conditions, but it may have an important role in cystinuria. In fact, cystinuria double KO mice (*Slc7a9*$^{-/-}$*Slc3a1*$^{-/-}$) showed an increased prevalence and severity of the lithiasic phenotype compared to both single KO mice (Espino et al., 2015). However, the only published study screening the *SLC7A13* gene in a cohort of 17 patients with no detected mutations in *SLC3A1* and *SLC7A9* genes showed no evidence of an AGT1 role in cystinuria (Olschok et al., 2018).

1.2.7.3. OCTN1

Previous analysis of whole genome microsatellites and mRNA expression comparing *Slc7a9*$^{-/-}$ non-stone and stone former mice in Dr. Nunes' group, lead to identify *Slc22a4* as a possible modulating gene of cystine lithiasis. Thus, in her thesis, Dr. Espino described that *Slc22a4* mRNA expression was reduced by 50 % in lithiasic mice when comparing to non-lithiasic ones (Espino, 2012). This gene encodes for an organic cation and zwitterion transporter, OCTN1, highly expressed in the kidney BBM.

OCTN1 belongs to the SLC22 family which comprises organic cation transporters (OCT), organic cation and zwitterion transporters (OCTN) and organic anion transporters (OAT) (reviewed in Koepsell 2020). They are polyspecific transporters as recognize a broad range of molecules and are responsible for drug intestinal absorption, and its hepatic and renal excretion. These transporters share a conservative structure as consist of intracellular N-terminus, 12 transmembrane domains, one extracellular loop between the first and the second transmembrane domain, one intracellular loop between the sixth and the seventh domain, and an intracellular C-terminus.

In 1997, Tamai *et al* cloned for the first time the human *SLC22A4* cDNA (Tamai et al., 1997). Then, they expressed OCTN1 in HEK293 cells to study its transport activity and observed that OCTN1 could transport [^{3}H]Tetraethylammonium (TEA), a model of organic cation. As OCTN1 presented higher activity at neutral or alkaline pH than in acidic one, it was defined as a pH-dependent transporter. Further studies in mice suggested that OCTN1 had higher affinity for L-carnitine than TEA (Tamai et al., 2000). In addition, they observed that OCTN1 was widely distributed across mammal tissues and it was mainly expressed in kidney (Tamai et al., 2000). However, it was in 2005 when Gründemann *et al* demonstrated, by testing several substrates in HEK293 cells expressing human OCTN1, that they key substrate of OCTN1 was L-Ergothioneine (L-Erg) (Gründemann et al., 2005). As L-Erg transport by OCTN1 results to be 100 times more efficient than that of TEA or carnitine, and OCTN2 did not transport L-Erg at all, Gründemann *et al* proposed a functional name for OCTN1: Ergothioneine Transporter (ETT). The relevance of OCTN1 in L-Erg transport was further demonstrated as a blood metabolome analysis of *Slc22a4*$^{-/-}$ mice revealed the absence of L-Erg (among 112 metabolites) followed by the observation

that L-Erg was no detected in any tissue sample analyzed from *Slc22a4*$^{-/-}$ mice (Kato et al., 2010). Apart from L-Erg, TEA and L-carnitine, OCTN1 could be involved in the transport of other compounds as nucleosides (Drenberg et al., 2017), acetylcholine (Pochini et al., 2016) and metformin (Noritaka Nakamichi et al., 2013). However, its preference for L-Erg has been recently reaffirmed (Tucker et al., 2019).

As mention before, OCTN1 is widely distributed across tissues and highly expressed at the apical membrane of intestine, kidney, and erythrocytes (Gründemann et al., 2005). OCTN1 is responsible for the uptake of L-Erg from diet (intestine), from blood to tissues, and to reabsorb it from the urine. Thus, OCTN1 is crucial to uptake, distribute and retain L-Erg in the body, reinforced by *Slc22a4*$^{-/-}$ mice showing a L-Erg deficiency in all tissues and higher urinary excretions rates (Kato et al., 2010). However, the physiological role behind such regulation has not yet been established as *Slc22a4*$^{-/-}$ mice is viable, shows normal growth and does not present any abnormal phenotype in any organ (Kato et al., 2010), neither in zebrafish (Pfeiffer et al., 2015) nor in *C. elegans* models (Cheah et al., 2013). Nevertheless, OCTN1 malfunction and lower levels of L-Erg have been related to diverse disorders as Chron's disease, rheumatoid arthritis, Parkinson disease, interstitial fibrosis, ischemia or CKD (**Table 6**).

Table 6. Review of L-Ergothioneine studies related to diseases

Injury/ Pathology	Model	Organ/ tissue	Dose	Provided	L-Erg action	L-Erg effect observed	References
UV irradiation	Cell cultured	Fibroblast	10-500 µM for 9 days		Scavenging of O_2^- and O_2	Lower levels of induced ROS and reduced protein and lipid oxidative damage	Markova et al., 2009; Obayashi et al., 2005
Methylglyoxal -Induced Injuries	Cell cultured		2 µM		Inhibition of NF-κβ transcription pathway	Protection against hyperglycemic damage	Song et al., 2017
High glucose endothelial senescence	Cell cultured		0.01-1 mM		Upregulation of SIRT1 and SIRT6, downregulation of NF-κβ	Protection against glucose induced endothelial senescence	D'onofrio et al., 2016
UVA irradiation (15J/cm^3)	Immortalized human skin keratinocyte cell line	Skin	125-500 nM		NRF2 pathway activation	Reduced UVA-induced ROS, inhibition of apoptosis, avoided DNA fragmentation and alleviated mitochondrial dysfunction	Hseu et al., 2015
B-amyloid induced toxicity	*C. elegans*	Whole worm	0 to 5 mM	Diluted in agar		Reduced β-amyloid accumulation, prolonged lifespan and improved worm mobility	Cheah et al., 2019
Memory	Mice	Hippocampus	1-50 mg/kg for two weeks	Oral		Enhanced object recognition memory promoting neuronal maturation in hippocampus	Nakamichi et al., 2021

Injury/ Pathology	Model	Organ/ tissue	Dose	Provided	L-Erg action	L-Erg effect	References
Neuronal injured induced by β-amyloid	Mice	Brain	0.5-2 mg/kg for 16 + 39 days	Oral		Prevented β-amyloid accumulation and lipid peroxidation in hippocampus, maintained GSH/GSSG ratio and improved learning and memory abilities	Yang et al., 2012
Depression	Mice	Brain	120 mg/g of diet	Oral		Promoted neuronal differentiation and exerted an antidepressant effect	Nakamichi et al., 2016
Diabetic nephropathy	Mice	Kidney	Knocking OCTN1		Increases moesin expression	Exacerbated interstitial fibrosis	Makiishi et al., 2021
Chronic kidney disease	Mice	kidney	Knocking OCTN1			Increased fibrosis and oxidative stress markers in kidney	Shinozaki et al., 2017
Liver fibrosis	Mice & cell culture	Liver	High content diet	Oral	Reduction of NOX4 and LI90 expression	Reduced liver fibrosis	Tang et al., 2016
Ischemia-reperfusion in liver	Rats	Liver	1.2 mg/kg/d	Oral	HSP70 over-expression	Lowered liver injury and induced a better survival rate	Bedirli et al., 2004
Preeclampsia	Rats	Plasma	25 mg/kg/day	Oral	Reduction of mitochondrial H_2O_2	Improved mitochondrial dysfunction and oxidative stress associated to preeclampsia	Morillon et al., 2020
Lung injury	Rats	Lung	15 or 150 mg/kg	Parental		Decreased lung injury and inflammation in cytokine insufflate rats	Repine&Elkins, 2011
Oxaliplatin-induced peripheral neuropathy	Rats	Dorsal root ganglion (DRG) neurons	15 mg/kg	Oral	Competing with oxaliplatin for OCTN1 transport	Inhibited oxaliplatin accumulation in DRG neurons and in their mitochondria, and reduced oxidative stress	Nishida et al., 2018

Injury/ Pathology	Model	Organ/ tissue	Dose	Provided	L-Erg action	L-Erg effect	References
Diabetic embryopathy in pregnant	Rats	Offspring/litter	1.147 mg/kg	Oral	Inhibition of glucose-mediated free radicals	Reduced embryo malformations	Guijarro et al., 2002
Type-2 diabetes	Rats	Kidney	35 mg/kg	Oral	NRF2 activation, downregulation of NF-κβ and TGF-β1	Improved renal function and glucose homeostasis, reducing renal inflammation and hypertriglyceridemia	Dare et al., 2021
Neuronal differentiation	Neural progenitor cells (NPC)	Brain	500 μM			Promoted NPC differentiation but suppressed proliferation by reducing oxidative stress	Ishimoto et al., 2014
Aging	Human	Blood and plasma	basal levels			Blood levels of L-Erg decreased with age and correlated with mild cognitive impairment	Cheah et al., 2016
Cardiovascular disease	Human	Blood and plasma	basal levels			The most predictive molecule for low risk of cardiovascular disease	Smith et al., 2019
Chronic kidney disease	Human	Blood	Basal levels of CKD patients			Reduced levels of L-Erg were detected in CKD patients that were restored after kidney transplantation	Shinozaki et al., 2017
Chron's Disease	Human	Blood	Basal levels of Chron's Disease patients			Lower levels of L-Erg were detected in Chron's Disease patients	Kato et al., 2010
Early Cardiovascular disease	Human aortic endothelial cells	Endothelium	0.1-0.3 mM			Reduced VCAM-1, ICAM-1 and E-selectin expression. Reduced adhesion molecular expression	Martin, 2010

1.2.7.3.1. L-Ergothioneine

In 1908, Charles Tanret described for the first time the L-Erg molecule, but it was after the discovery of its specific transporter, in 2005, when it started to be a focus of research interest. It is a natural metabolite of L-histidine synthesized by cyanobacteria (Pfeiffer et al., 2011), mycobacteria (Genghof, 1964) and non-yeast-fungi (Kornberg & Krebs, 1957) that animals must absorb from dietary sources as mushrooms, beans or red meet. Although animals cannot synthesize L-Erg, the presence of a specific transporter in most animal tissues that ensures its absorption and retention in the body, its long half-life (Kawano et al., 1982) and its ability to accumulate in injured tissues (reviewed in Halliwell, Cheah, and Drum 2016), suggest that L-Erg has an important physiological role.

L-Erg is synthesized from histidine by three steps: trimethylation of the NH_2 group of histidine to form hercynine; which reacts with cysteine to form hercynylcysteine sulfoxide; that is finally converted to L-Erg (Kornberg & Krebs, 1957) (**Figure 6B**). In some organisms, an additional intermediate step in the L-Erg synthesis can occur metabolizing hercynine to γ-glutamylhercynylcysteine sulfoxide, prior to hercynylcysteine sulfoxide synthesis (**Figure 6A**) (Seebeck, 2010). Then, in addition to hercynine, L-Erg could derive in other metabolic products as S-Methyl-L-Ergothioneine and L-Ergothioneine sulfonate (Gross et al., 2004; Servillo et al., 2017; Tang et al., 2018). Although animals cannot synthesized L-Erg, all precursors and products mentioned above have been detected in mouse and human tissues and body fluids suggesting that L-Erg is metabolized in animals (Cheah et al., 2017; Tang et al., 2018).

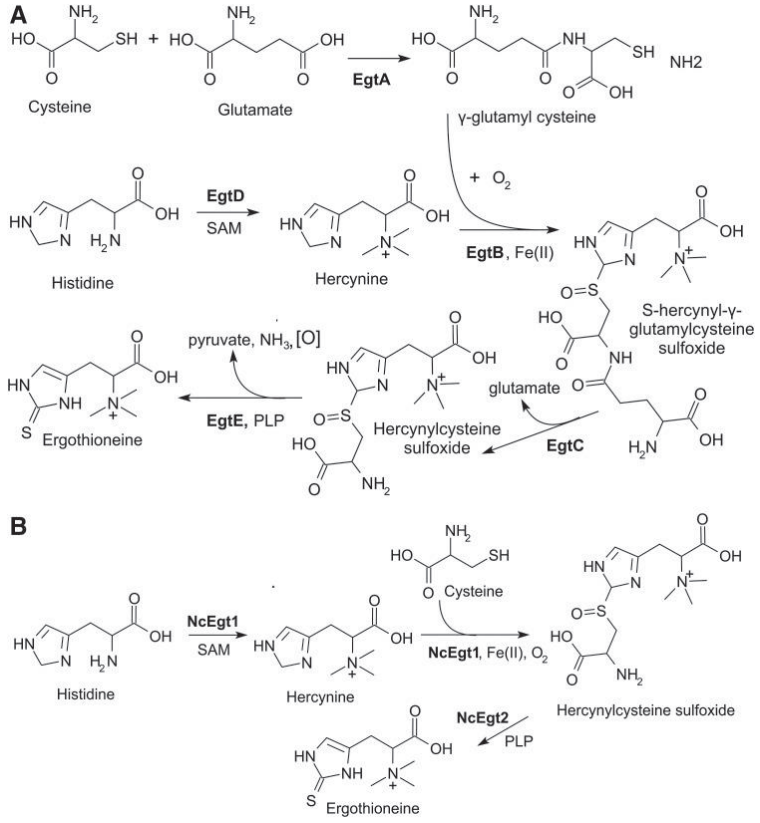

Figure 6. L-Ergothioneine synthesis

*L-Erg biosynthesis steps in **(A)** mycobacteria and **(B)** fungi. Taken from Cumming et al., 2018.*

L-Erg is a molecule with antioxidative and anti-inflammatory effects which role associated to pathologies has been described in several organs and tissues (**Table 6**). It is more stable than other antioxidants as, although it could exist as a tautomer between its thiol and thione forms, at physiological pH is predominantly a thione (Heath & Toennies, 1958; Motohashi et al., 1976). So, it does not suffer auto-oxidation as easily as other thiol antioxidants as Glutathione (GSH) (Heath & Toennies, 1958). L-Erg acts as antioxidant scavenging reactive oxygen and nitrogen species (as hydroxyl radicals (Akanmu et al., 1991), singlet oxygen (Stoffels et al., 2017) and peroxynitrite

(Aruoma et al., 1997)) and chelating divalent metal cations as copper (Akanmu et al., 1991) and zinc (Hanlox, 1971), which can also induce oxidative damage.

In Dr. Espino's thesis, L-Erg was hypothesized to be a therapeutical agent for cystine lithiasis as the expression of its specific transporter OCTN1 is reduced by 50 % in lithiasic mice when comparing to non-lithiasic ones (Espino, 2012). In the present thesis, L-Erg has been administered to cystinuria mouse models to confirm this hypothesis. Several beneficial properties support the use of L-Erg as a potential therapeutical agent for cystinuria:

a) L-Erg has a **specific transporter** (OCTN1) highly expressed in the BBM of proximal tubules.
b) L-Erg is a **natural** molecule.
c) L-Erg is **safe**: toxicology studies in rats administering a single dose of 2000 mg/kg/day or continuous high doses of 700 mg/kg/day for 13 weeks showed no side-effects even in fertility, gestation or in litter/offsprings (Forster et al., 2015). These results lead to establish a no-observed-adverse-effect level (NOAEL) of L-Erg of 800 mg/kg per day for adults (Turck et al. 2016). In humans, the only published study observed no adverse effects after the administration of 25 mg/day of L-Erg for 7 days (Cheah et al., 2017). Moreover, the FDA recognized L-Erg as "generally recognized as safe" (GRAS) and the European Food Safety Authority (EFSA) approved L-Erg supplementation in young children, and pregnant and breastfeeding adults (FDA, 2017; Turck et al., 2017).
d) When L-Erg is administered, it is **retained** in the body and **accumulated** in tissues, above all in liver, whole blood and **kidney** (Tang et al., 2018).
e) L-Erg is a **thiol/thione molecule** that could bind cysteine preventing cystine formation.
f) L-Erg is an **antioxidant** molecule and, in the last years, antioxidant molecules showed cystine growth inhibitor properties in studies using mouse models and even α-Lipoic acid is in clinical trial phase II (Cil & Perwad, 2020).

1.2.8. Urolithiasis and Oxidative Stress

It is well known that oxidative stress is implicated in many clinical disorders such as cancer, neurodegeneration, obesity or cardiovascular diseases (Cross et al., 1987; Liguori et al., 2018). Actually, oxidative damage has been described in most tissues affecting its lipid and protein properties, and inducing mutations in both nuclear and mitochondrial DNA (Cross et al., 1987; Richter et al., 1988). The kidneys are vulnerable to oxidative stress as they have high metabolic needs to filter and reabsorb blood waste products, and to maintain fluid and electrolyte balance, acid-base homeostasis and blood pressure. Particularly, proximal tubule cells are the most energy demanding as are responsible for reabsorbing the 80 % of the blood filtrate (Bhargava & Schnellmann, 2017; Zhuo & Li, 2013). Most evidences associating oxidative stress and kidney disease are related to acute injury or CKD (Ling & Kuo, 2018; Palipoch, 2013), but, oxidative damage has been described in other renal pathologies as glomerulonephritis, cystinosis, polycystic disease and urolithiasis (Andries et al., 2019; Budisavljevic et al., 2003; Ceban et al., 2016; Vaisbich et al., 2011).

In the case of urolithiasis, it has been described that oxidative stress damage is caused by crystal interaction with renal tubular epithelial cells (Hirose et al., 2010; Khan, 1995; Khaskhali et al., 2009). Most studies have been performed in calcium CaOx stones, as are the most frequent type of kidney stones (Alelign & Petros, 2018). Cellular injury induces reactive oxygen species (ROS) generation and an inflammatory response that retains crystals promoting its aggregation and allowing stone formation (Ceban et al., 2016; Wilson et al., 2018). In addition, studies on urolithiasis patients describe that most stone formers had an oxidative defect as showed a decrease in Superoxide Dismutase (SOD), Glutathione S-Transferase (GST) and Glutahione Peroxidase (GPx) activity; lower levels of GSH; and an accumulation of lipid peroxidation (Ceban et al., 2016; Huang et al., 2003; Tungsanga et al., 2005). Moreover, studies in cell cultures and mouse models showed a mitochondrial dysfunction related to CaOx stones as lower activities of tricarboxylic acid (TCA) cycle and electron transport chain (ETC) enzymes were observed (Patel et al., 2018; Veena et al., 2008).

In cystinuria there is no evidence of crystal retention by epithelial cells and stones appear to be formed freely in the lumen solution (Evan et al., 2006). Cystine is described to crystallize in the Bellini Ducts, where water is reabsorbed, as histological analysis of stone former patients showed an inflamed and fibrotic tissue plugged with deposits of cystine crystals (Evan et al., 2006). In contrast to CaOx lithiasis, cystine plugs are formed due to supersaturation and are easily released as are not strongly attached to tissue (Coe et al., 2010; Evan et al., 2006). However, renal epithelial cell damage is produced in cystinuria as proteomic profiles of urines of patients showed increased levels of proteins of inflammatory, wound healing and oxidative stress pathways (Bourderioux et al., 2015; Kovacevic et al., 2015, 2019). Moreover, there is also an increasing evidence of an oxidative status defect in cystinuria, with patients showing a reduce activity of SOD, GPx and inducible Nitric Oxide Synthase (iNOS) enzymes, and an accumulation of lipid peroxidation in blood samples (Al-Shehabat et al., 2017; Yifan et al., 2019). In addition, a decrease in GSH levels was observed in leukocytes of cystinuric patients (Mårtensson et al., 1990). Moreover, studies using cystinuria mouse models detected a lower activity of SOD and GPx enzymes and an increase in lipid peroxidation in kidney samples (Yifan et al., 2019). Also, lower levels of GSH, of both reduced and oxidized forms, were observed in cystinuric mice livers (Woodard et al., 2019). Finally, the evidence of the relation between oxidative stress and cystinuria is reinforced by the promising results obtained after treating cystinuria mouse models with antioxidant molecules (Cil & Perwad, 2020; Mohammadi et al., 2018; Yifan et al., 2019; Zee et al., 2017).

1.2.8.1. GSH synthesis

GSH is considered the most important antioxidant molecule of animals and one of its three components is cysteine. GSH is synthesized in the cytosol of most cells by two ATP consuming enzymatic steps that catalyze the ligation of three peptides: glutamate, cysteine and glycine. The first step is performed by the enzyme glutamate cysteine ligase (GCL) that catalyze the union of glutamate and cysteine resulting in γ-glutamyl-L-cysteine. Then, glycine is added by the glutathione synthase (GS) enzyme to

obtaining the final product: γ-L-glutamyl-L-cysteinyl-glycine. Under physiological conditions, GSH synthesis is limited by two factors: cysteine availability and GCL activity (Jackson, 1969).

1.2.8.1.1. Cysteine as a limiting precursor

Cysteine sources are dietary intake, protein degradation and its synthesis from methionine via the transsulfuration pathway (**Figure 7**). The transsulfuration pathway takes place manly in liver as cysteine is needed for GSH synthesis. However, this pathway is also active in kidney as kidney homocysteine metabolism is essential to maintain physiological homocysteine levels and the enzyme activity of the whole pathway has been detected in different kidney sections (House et al., 1997; Ishii et al., 2004; Li et al., 2006). In addition, changes in the expression of the Cystathionine β-Synthase (CBS) enzyme in the kidneys are related to other pathological conditions as fibrosis after urolateral obstruction or renal ischemia-reperfusion (Jung et al., 2013; Prathapasinghe et al., 2008). Cystinuria patients present slightly lower plasma levels of cystine although are not described as pathological (Asatoor et al., 1974; Mårtensson et al., 1990; Milne et al., 1961). However, the impact of these slightly lower levels in the transsulfuration pathway and in GSH synthesis has not been deeply studied. There is only one study that analyzed GSH content in leukocytes of cystinuria patients in which reduced levels of the antioxidant molecule were detected (Mårtensson et al., 1990). Concerning cystinuria mouse models, although both *Slc7a9*$^{-/-}$ and *Slc3a1*$^{-/-}$ mice showed significantly lower cystine plasma levels (Feliubadaló et al., 2003; Woodard et al., 2019), GSH content has only been studied in the livers of *Slc3a1*$^{-/-}$ mice, which showed a decreased in the total GSH pool as lower levels of both oxidized and reduced forms were observed (Woodard et al., 2019).

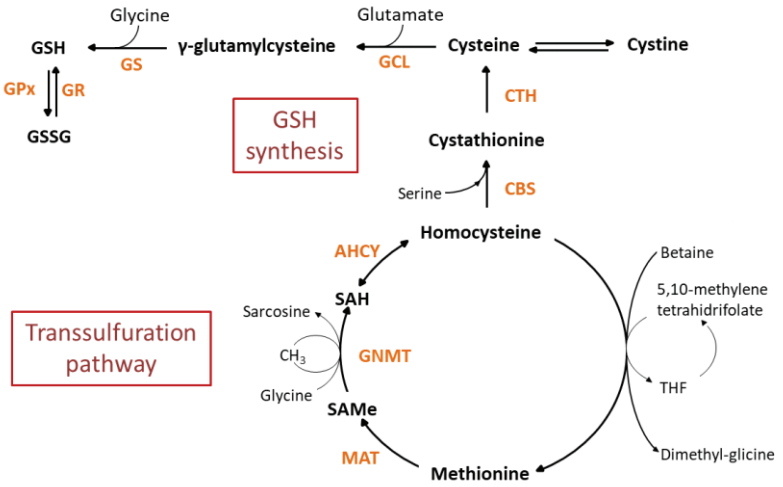

Figure 7. Transsulfuration pathway and GSH synthesis

Representation of the transsulfuration pathway, which results in the generation of cysteine from methionine, and the GSH synthesis steps. MAT = Methionine Adenosyltransferase, GNMT = Glycine N-Methyltransferase, AHCY = Adenosylhomocysteinase, CBS = Cystathionine β-synthase, CTH = Cystathionine γ-lyase, GCL = Glutamate cysteine ligase, GS = Glutathione synthase, GR = Glutathione reductase, GPx = Glutathione peroxidase.

1.2.8.1.2. GCL as a limiting enzyme

GCL is the rate-limiting enzyme for GSH synthesis as its intracellular concentration is particularly low comparing to GS enzyme (Dalton et al., 2004). In addition, only the GCL enzyme is exposed to feedback inhibition by GSH, the final product of this pathway (Richman & Meister, 1975). GCL is a heterodimer composed by two subunits: GCLC, that is the catalytic or heavy subunit, and GCLM, the modifier or light subunit. It has been demonstrated that GCLC itself possess all the catalytic activity of the enzyme and it is affected by the feedback inhibition of GSH (Huang, Chang, et al., 1993b). However, although being enzymatically inactive, GCLM increases the enzyme efficiency by lowering the K_m of GCLC for glutamate and increasing the K_i for GSH (Chen et al., 2005; Huang et al., 1993). As the GCLC K_m for cysteine is similar to its intracellular concentration (Bannai & Tateishi, 1986), cysteine is a limitant precursor of GSH and variations on cysteine intracellular content could affect GSH synthesis.

1.2.8.2. GSH regulation in the kidney

As mentioned above, the kidneys are susceptible to oxidative stress due to their energy consuming functions, mainly in proximal tubules, as are responsible for reabsorbing and detoxifying most part of the blood filtrate and uses a high rate of aerobic metabolism (and have poor glycolytic capacity) (Weinberg et al., 2000). It is well known that the liver is the main producer and exporter of GSH to provide other organs, and proximal tubule cells are the primary site of plasma GSH extraction (Anderson & Meister, 1980; Hahn et al., 1978). The reason of it is that GSH turnover occurs predominantly in proximal tubules as their cells possess the highest γ-glutamyltransferase (GGT) enzyme activity (Hinchman & Ballatori, 1990). GGT is the only enzyme that can initiate GSH degradation cleaving the γ-glutamyl bond that binds glutamate and cysteine. GGT is an ectoenzyme and, in the kidneys, it is located in the BBM of proximal tubule cells (Hanigan & Frierson, 1996). Thus, the efflux of GSH to the luminal content of proximal tubules is essential for its turnover. Under physiological conditions, low levels of GSH are detected in urine as GGT cleaves GSH in γ-glutamyl- and cysteinylglycine, and BBM dipeptidases (Dpep1) liberate cyst(e)ine and glycine (**Figure 8**). Thus, the cysteinylglycine dipeptide, γ-glutamyl-amino acids and/or the freely amino acids are reabsorbed by proximal tubule amino acid transporters (**Figure 8**). However, deficiencies in the GGT enzyme are shown to produce glutathionuria (and glutathionemia) in both mouse models and patients (Harding et al., 1997; Schulman et al., 1975).

This process by which the kidneys extracts most of the plasma GSH that has been released by the liver is called interorgan metabolism (Anderson et al., 1980; Griffith & Meister, 1979). The purpose of interorgan metabolism is thought to be GSH turnover in the BBMs of kidneys to regenerate GSH amino acid constituents which can be redistributed to different organs to be used for protein synthesis or to resynthesized GSH (Griffith & Meister, 1979; Mcintyre, 1980). Thus, GSH also serve as a major reserve and transporter of cysteine in its reduced form, as cysteine in the extracellular space is autoxidized to cystine (Mcintyre, 1980).

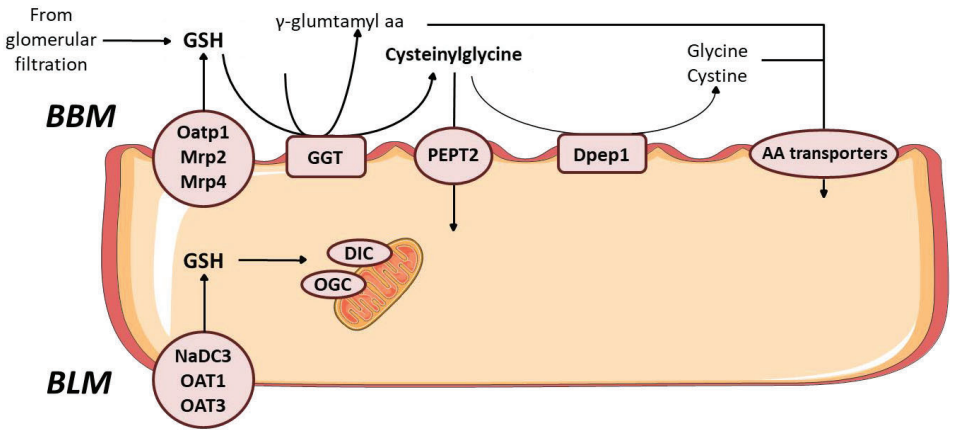

Figure 8. Schematic representation of GSH metabolism in the kidney

GSH is internalized from the blood supply by transporters placed at the BLM. Then, BBM transporters mediates GSH efflux to the luminal fluid where it is cleaved by GGT enzyme. Cysteinylglycine can be internalized by PEPT2 transporter or further hydrolyzed to glycine and cystine by Dpep1, and then freely amino acids are reabsorbed by BBM transporters. As mitochondria cannot synthetized GSH, it is internalized by DIC and OGC transporters. AA = amino acids, BBM = brush border membrane and BLM = basolateral membrane.

In summary, in kidney cells coexist pathways of synthesis, degradation, uptake and efflux of GSH (**Figure 8**). The uptake takes place at BLM where, although does not exist a specific GSH transporter, the sodium-dicarboxylate 2 exchanger (NaDC3, *SLC13A3*) (Schorbach et al., 2013) and the organic anion transporters (OAT1/3, *SLC22A6-8*) (Lash et al., 2007) have been described to uptake GSH in proximal tubule cells. However, there is controversy about the OAT1/3 role (Hagos et al., 2013). Concerning the GSH efflux in the BBMs, it is suggested to be mediated by the organic anion transporting polypeptide (OATP1A1, *SLC21A1*) (Li et al., 1998) and the multidrug resistant proteins 2 and 4 (Mrp2/4, *ABCC2/4)* (Lou et al., 2003; Rius et al., 2006), although further studies are needed to demonstrate it. Finally, as GSH cannot be synthesized in the mitochondria, the mitochondrial dicarboxylate carrier (DIC, *SLC25A10*) and the 2-oxoglutarate carrier (OGC, *SLC25A11*) have been described to uptake GSH in the mitochondrial matrix to maintain mitochondrial GSH pool (Chen et al., 2000).

1.2.8.3. Mitochondrial function and urolithiasis

The kidney is the second organ (after the heart) with more mitochondria per cell, in particular, proximal tubule cells are the ones with higher mitochondria density as they require high amounts of energy for transport and detoxifying functions (Wang et al., 2010). Mitochondria are intracellular organelles responsible for vital processes as energy metabolism, apoptosis and preservation of cellular calcium and redox homeostasis.

The key role of mitochondria is energy production. Adenosine triphosphate (ATP) is the main energy molecule of our cells, and its production takes place in the mitochondrial inner membrane through oxidative phosphorylation (OXPHOS). First, glycolysis, fatty acid oxidation and TCA pathways reduce the coenzymes nicotinamide adenine dinucleotide (NAD^+) and flavin adenine dinucleotide (FADH) to NADH and $FADH_2$, respectively, transferring them the electrons produced by the oxidation of its substrates. Then, these coenzymes transfer the electrons to the electron transport chain (ETC). The components of the ETC are NADH dehydrogenase (Complex I), succinate dehydrogenase (Complex II), cytochrome c reductase (Complex III), cytochrome c oxidase (Complex IV) and ATP synthase. Electrons from coenzymes flow from one complex to another which pump protons to the intermembrane space that will be used by ATP synthase to produce ATP phosphorylating ADP.

However, Complex I and Complex III can reduce O_2 generating ROS (Sugioka et al., 1988; Turrens et al., 1985). Under physiological conditions, mitochondrial ROS production can be controlled by antioxidant defenses as SOD and GPx (Handy et al., 2009; Narrea et al., 2007). But, under pathological conditions, an overproduction of ROS can occur which cannot be handled by antioxidant enzymes. This situation causes mitochondrial dysfunction, damaging mitochondrial DNA (mtDNA) and inducing mitochondrial protein modifications.

Mitochondria organelles contain their own DNA (mtDNA) that encode 37 genes corresponding to 13 subunits of the ETC, 2 ribosomal RNAs (rRNAs) and 22 transfer

RNAs (tRNAs). Thus, except Complex II which subunits are only encoded by nuclear DNA, almost all components of the ETC have essential structural subunits encoded by both DNAs. Nevertheless, mitochondria depend on nuclear DNA as it encodes more than 95 % of mitochondrial proteins that are then imported into the mitochondria, including the mitochondrial transcription and replication machinery.

There is growing evidence in the role of mitochondrial dysfunction in the stone formation process, manly in CaOx stones as are the most frequent and studied type. Different mechanisms have been proposed about the involvement of mitochondrial dysfunction in stone disease (Reviewed in Plotnikov et al., 2020). CaOx crystals interact with renal epithelial cells and can be internalized by endocytosis, and both extracellular membrane damage and the increase in the intracellular levels of calcium produce oxidative stress and ROS generation (Lieske et al., 2000; Veena et al., 2006). ROS overproduction induces mitochondrial dysfunction that causes a) apoptosis and lipid peroxidation leading to cell membrane injury that serve as a deposit of CaOx crystals (Fong-Ngern et al., 2017), b) apoptosis and cell death leading to release apoptotic bodies, cell debris and subcellular organelles that serve as a materials for the stone nidus formation promoting crystal nucleation and aggregation (as mitochondrial components have been found in CaOx stone matrix) (Govindaraj & Selvam, 2001; Hirose et al., 2012), and c) the secretion of proinflammatory cytokines and the followed inflammatory response promoting Randall's plaque formation (Khan, 2014; Poon et al., 2018). In the particular case of cystinuria, although an impairment in endosomal transport was observed in the urine of patients (Kovacevic et al., 2019), cellular endocytosis of cystine crystals has not been reported. However, it has been observed epithelial cell injury and cellular debris in the lumen of crystallizing areas of patients (Evan et al., 2006). In addition, proteomic profiles of urines of patients showed increased levels of proteins of inflammatory, wound healing, fibrosis and oxidative stress pathways highlighting the damage on tubular epithelial cells (Bourderioux et al., 2015; Kovacevic et al., 2015, 2019). However, direct evidence of mitochondrial dysfunction has not been described in cystinuria, so further studies are needed.

OBJECTIVES

2. OBJECTIVES

The aim of this study is to identify and evaluate cystinuria modulating factors using mouse models to better understand interpatient variability, to propose new therapeutic agents for cystinuria, and to contribute to the knowledge of the molecular consequences of the disease. This general aim was achieved by fulfilling the following specific objectives:

1) To study the involvement of AGT1, the second cystine transporter described in the brush border membrane of kidneys, in cystinuria by:
    i) Evaluating amino acids reabsorption and cystine lithiasis rate in mice lacking AGT1 expression (*Slc3a1*$^{-/-}$ and female *Slc7a9*$^{-/-}$).
    ii) Searching for variants in *SLC7A13* in cystinuria patients and assessing its amino acid excretion levels.
2) To identify new cystinuria modulating factors by:
    i) Analyzing kidney gene expression of the *Slc7a9*$^{-/-}$ cystinuria mouse model by RNA-seq.
3) To study L-Ergothioneine, the main substrate of OCTN1, as a therapeutical target for cystinuria by:
    i) Evaluating the therapeutic potential of L-Ergothioneine in *Slc7a9*$^{-/-}$ and *Slc7a9*$^{-/-}$*Slc22a4*$^{-/-}$ mouse models.
    ii) Studying L-Ergothioneine mechanism of action.

METHODS

3. METHODS

3.1. MICE PROCEDURES

3.1.1. General management

3.1.1.1. IDIBELL Animal Facility

The IDIBELL Animal Facility is a specific pathogen-free (SPF) installation that handles immunocompromised and genetically modified strains of animals. Animals are maintained under health and environment-controlled conditions to ensure research quality and reproducibility. It is an Animal Facility accredited by the Association for Assessment and Accreditation of Laboratory Animal Care (AAALAC), B9900010. All methods employed in this thesis were approved by the Animal Experimentation Ethics Committee of IDIBELL and by the corresponding regional authority according to EU directive 2010/63/EU.

Mice were kept in a temperature and humidity-controlled room with 12-hour light-dark cycle. Cages, placed in ventilated racks, contained 3 to 5 mice with *ad libitum* access to food (standard chow: VRF1 P, Special Diets Services, UK, code: 801900) and drinking water. Male and female mice were separated after weaning and maintained in different cages, except for reproductive proposes. Once a week, cages were cleaned, and food and water refilled or replaced.

3.1.1.2. Mice colonies

Two cystinuria mouse models were used in this thesis: *Slc7a9*$^{-/-}$ and *Slc3a1*^{D140G}. In addition, the *Slc22a4*$^{-/-}$ mouse model (as *Slc22a4* codify the main transporter of L-Erg) and the double KO *Slc7a9*$^{-/-}$*Slc22a4*$^{-/-}$ were also employed. The **Table 7** further describes the models used:

Table 7. Mouse models used in this thesis

Gene affected	Protein affected	Background	Disease/alteration
***Slc7a9*$^{-/-}$**	$b^{0,+}$AT	C57BL/6J	Cystinuria type B
***Slc3a1*^{D140G}**	rBAT	C57BL/6J	Cystinuria type A
***Slc7a9*$^{-/-}$*Slc22a4*$^{-/-}$**	$b^{0,+}$AT/OCTN1	C57BL/6J	Cystinuria type B & no L-Erg transporter

3.1.1.3. Mice genotyping

All mice used were genotyped twice: at weaning (21 days old) to determine its genotype and at the beginning/end of the experiment, to confirm it. For genotyping, DNA was extracted from 5 mm distal-tail biopsies using a NaOH digestion method. First, 100 µL of 50 mM NaOH was added to a tube containing the tail biopsy and left with continuous shaking at 99ºC for 20-30 min. Then, to neutralize the reaction, 10 µL of 1 M Tris Buffer were added. After 10 min of centrifugation at 13,000 rpm and RT, supernatants were carefully collected and transferred to a new tube. DNA was quantified using a NanoDrop ND-1000 (Thermo Scientific) and samples were diluted to obtain a final concentration of 50-60 ng/µL, adequate for PCR reaction protocols.

The Thermo Scientific DreamTaq Green PCR Master Mix (2X), which already contains DreamTaq Green buffer, $MgCl_2$, dNTPs and a DNA polymerase, was used to amplify sample sequences. Thus, the PCR Master Mix was prepared according to **Table 8** and 9 µL were added to 1 µL of DNA of each sample (50-60 ng/µL). All PCRs were run in duplicates and with positive (samples of known WT, heterozygous and KO genotype) and negative (water) controls. PCR thermal cycles were optimized for each mouse model according to its primer sequences (**Table 9 and 10**).

Table 8. PCR Master Mix

Reagent	Volume (µL)
Ultrapure H_2O	3
Dream Taq Green DNA polymerase (2X)	5
Primers (5 µM)	0.5

***Table 9. PCR thermal cycles of Slc7a9$^{-/-}$ and Slc22a4$^{-/-}$ (left), and Slc3a1^{D140G} (right)* sequences**

Slc7a9$^{-/-}$* and *Slc22a4$^{-/-}$			***Slc3a1^{D140G}***		
Cycles	**Temperature**	**Time**	**Cycles**	**Temperature**	**Time**
1	95ºC	5 min	1	95ºC	5 min
35	95ºC	30 sec	11	95ºC	30 sec
	60ºC	30 sec		69ºC (-1ºC per cycle)	30 sec
	72ºC	30 sec		72ºC	40 sec
1	72ºC	7 min	22	95ºC	30 sec
1	4ºC	for ever		58ºC	30 sec
				72ºC	40 sec
			1	72ºC	7 min
			1	4ºC	for ever

PCR amplified products were resolved in a freshly prepared 2 % agarose gel containing 1X SYBR™ Safe DNA Gel Stain. Gels were run with 1X TAE (Tris-Acetate-EDTA from PanReac AppliChem) buffer at 100 V for 20-25 min and visualized under UV light using a Molecular Imager® Gel Doc™ XR System (Bio-Rad). For fragments' size identification, 1 Kb Thermo Scientific™ GeneRuler™ DNA ladder was running with the samples.

Table 10. PCR primers

***Slc7a9*$^{-/-}$**			**Amplicon size (bp)**
VNO #619	Common	GCATTCGCCACAGGCTCTTC	
VNO #620	WT	CTGTGTTGGCCAGCACAGAC	452
VNO #621	KO	CGCAGCGCATCGCCTTCTAT	311
***Slc3a1*^{D140G}**			
VNO #1565	Common	CACCCTGGAATGTGCTTACA	
VNO #1568	WT	GACAAGGATGGGAATGGATA	120
VNO #1569	KO	GACAAGGATGGGAATGGATG	120
***Slc22a4*$^{-/-}$**			
VNO #1391	Common	GGGTGTGGTCCAGAGGACT	
VNO #1392	KO	TAGTTGCCAGCCATCTGTTG	255
VNO #1393	WT	GACTGACATACCATTGAAGC	313

Amplicon size reported relates to the size of the genome fragment delimited by each primer and the corresponding common primer. bp= base pairs

3.1.2. Experimental procedures

3.1.2.1. L-Ergothioneine administration

L-Erg was provided by Tetrahedron (www.tetrahedron.fr) and was orally administrated supplemented to drinking water to provide a dose of 16 or 200 mg/kg/day. The lower working dose was settled according to previous studies in our lab which demonstrated that, after 1 month of 13.5 mg/kg/day L-Erg treatment, the amount of L-Erg detected in the urine increased 175 times (unpublished data). Its Human Equivalent Dose (HED) correspond to 66 mg/day for a 60 kg adult (Nair & Jacob, 2016). The second dose was tested as a high-dose treatment which HED correspond to 1 g/day for a 60 kg adult. The experimental design of L-Erg treatments is summarized in **Figure 9**.

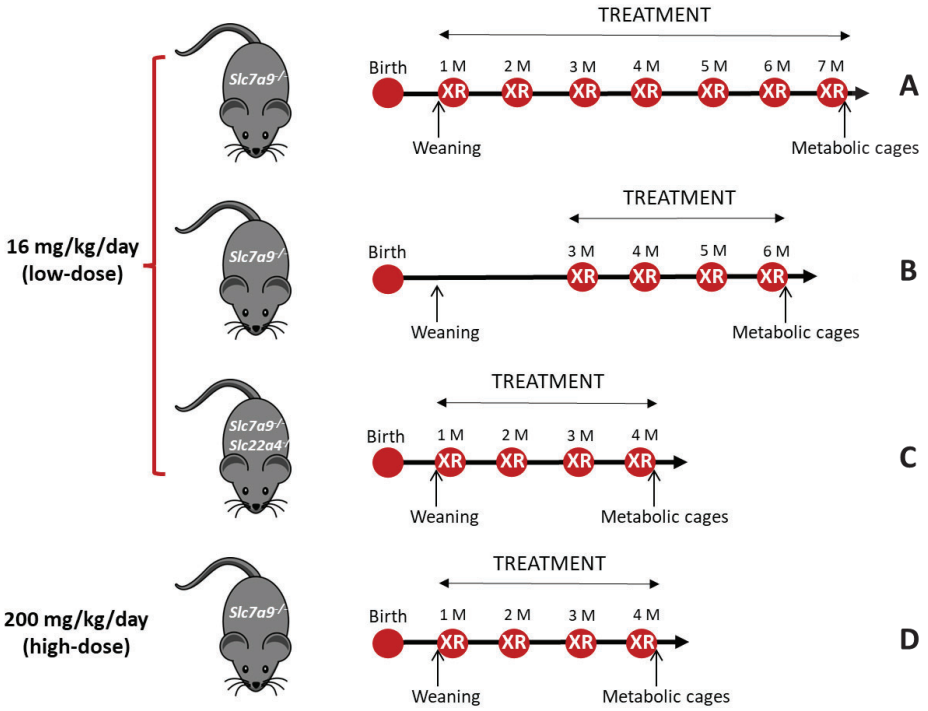

Figure 9. Experimental design of L-Erg administration and treatment follow-up

*Experimental design of low-dose L-Erg effect on **(A)** cystine stone formation in Slc7a9$^{-/-}$ mice, (**B**) cystine stone progression in Slc7a9$^{-/-}$ mice, (**C**) cystine stone formation in Slc7a9$^{-/-}$Slc22a4$^{-/-}$ mice and (**D**) high-dose L-Erg effect on cystine stone formation in Slc7a9$^{-/-}$ mice. XR = X-ray image acquisition, M =month of age.*

3.1.2.1.1. L-Ergothioneine effect on cystine stone formation

To evaluate the effect of L-Erg treatment on the cystine stone formation process *in vivo*, two different doses (16 and 200 mg/kg/day) were tested in *Slc7a9$^{-/-}$* mice and one (16 mg/kg/day) in *Slc7a9$^{-/-}$Slc22a4$^{-/-}$* mice. Mice were randomly assigned to treated or control group, since weaning and up to 4-7 months. As mice weight significantly increases from weaning to 7-months of age and to have a better control of the L-Erg dose administrated, L-Erg concentration in the drinking water of treated mice was adjusted per cage according to its mouse weight and water intake means. During the first month, L-Erg dose was adjusted twice per week and, afterwards, weekly. Water

intake and mouse weight of control group was also monitored to evaluate if L-Erg administration could induce changes in metabolic parameters during mice development or due to its chronic exposure. Stone onset and progression was determined monthly by X-ray imaging (see protocol below in 3.1.2.2).

- L-Erg (16 mg/kg/day) treatment in the *Slc7a9*$^{-/-}$ mouse model (**Figure 9A**): mice were randomly assigned to treated (n=40, 20 males and 20 females) or to control groups (n=40, 20 males and 20 females). Mice were followed-up for 6 months to test 16 mg/kg/day L-Erg dose as a preventive and chronical treatment for cystinuria.
- L-Erg (16 mg/kg/day) treatment in the *Slc7a9*$^{-/-}$*Slc22a4*$^{-/-}$ mouse model (**Figure 9C**): mice were randomly assigned to treated (n=22, 13 males and 9 females) or to control groups (n=22, 13 males and 9 females). Mice were followed-up for 4 months to determine if L-Erg effect requires its intracellular metabolism.
- L-Erg (200 mg/kg/day) treatment in the *Slc7a9*$^{-/-}$ mouse model (**Figure 9D**): *Slc7a9*$^{-/-}$ mice were randomly assigned to treated (n=55, 30 males and 25 females) or to control groups (n=55, 30 males and 25 females). Mice were followed-up for 4 months, as the main L-Erg effect was observed within the first 3 months of age, to test if L-Erg effect was dose-dependent.

The high number of mice used in *Slc7a9*$^{-/-}$ experiments was justified as the rate of lithiasic mice observed in the *Slc7a9*$^{-/-}$ mouse model is currently about 15 and 20 % at 4 and 6 months of age, respectively. In *Slc7a9*$^{-/-}$*Slc22a4*$^{-/-}$ mice, the rate of lithiasic mice observed is about 35 % at 4 months of age. Thus, all experiments were designed to obtain on average 8 lithiasic mice in the control group.

3.1.2.1.2. L-Ergothioneine effect on cystine stone progression

In order to determine L-Erg treatment effect on cystine stone growth rate *in vivo,* *Slc7a9*$^{-/-}$ lithiasic mice of 3 to 4-months old were randomly assigned to treated (n=16; 8 males and 8 females) or to control groups (n=13; 4 males and 9 females) (**Figure**

9B). The drinking water of the treated group was supplemented with 60 mg/L of L-Erg to administer a dose of 16 mg/kg/day. Stone progression was determined monthly by X-ray imaging (see protocol below in 3.1.2.2).

3.1.2.2. Cystine calculi detection by X-ray in vivo imaging

Cystine stones can be identified by X-ray imaging allowing to detect stone onset and follow-up its progression *in vivo*. X-ray images were taken using an IVIS Lumina XR Series III (Caliper LifeScience – Vertex Technics), an instrument design for small animal *in vivo* imaging. First, mice were anesthetized using isoflurane to better immobilize them. Then, mice were placed in the IVIS in a latero-lateral position, to avoid interferences from the spinal cord, and legs were fixed fully extended to keep away femur bounds from the bladder. In all images taken, a calibration curve of stones with already known weights was place next to the mice (**Figure 10**).

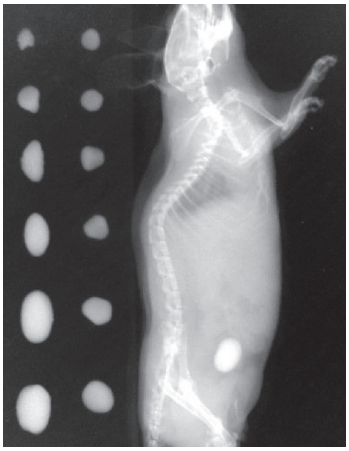

Figure 10. X-ray image of lithiasic mice

At the left part of the image, the calibration curve with different stone sizes is observed.

X-ray images were analyzed using Living Image® Software that allows calculating total density count of each region of interest (ROI). So, after drawing the perimeter of the calibration curve and the mice stones, the weight of the stone of interest could be extrapolated. Then, stone growth rate (Δweight/Δtime) was calculated from monthly images of lithiasic mice.

3.1.2.3. Metabolic cages

Metabolic cages are special individual cages with grid floors designed to separately collect urine and feces (**Figure 11**). In addition, water and food intake of each mouse can be easily monitored.

Figure 11. Mice metabolic cage

In this work, metabolic cages were used mostly to collect mice urine at the beginning (when possible) and at the end of the experiments, but also to control metabolic parameters: water and food intake, and mouse weight. Mice were housed individually for 4 days, considering the first day as an adaptation period and therefore the urine collect was discarded. Thus, metabolic data and urine samples collection was performed with intervals of regular 24 hours from the last three days at metabolic cages. To avoid urine evaporation and to ensure its preservation, 100 µL of mineral oil and 10 µL of sodium azide (10 mM) were added to the urine collector.

3.1.2.4. Tissue extraction

Necropsies were performed in a separate room and using sterile surgical material. Mice were sacrificed by cardiac puncture for blood-plasma-red blood cells collection and to allow a cleaner extraction of the other tissues. Mice were anesthetized using inhaled isoflurane and, to prevent blood coagulation during the extraction, syringes (ICO plus 3, 0.5x16 mm) were covered by EDTA (0.5 M). Once deeply asleep, a syringe was inserted under the sternum and directed toward mice left thoracic cavity drawing an angle of 20 degrees from the midline. When the heart is reached, the blood flows into the syringe by each heartbeat (helped with manual aspiration) and approximately 1 mL of blood per mouse can be collected. Then, blood was placed into Microvette

EDTA-tubes (Sarstedt), left 10 min at RT and followed by 3,000 rpm centrifuge for 10 min at 4ºC. Plasma and red blood cells were collected and store separately.

Mice died from exsanguination during cardiac puncture procedure, but cervical dislocation was also performed to ensure its death. Then, the abdominal cavity was opened to extract kidneys, liver and bladder. Kidneys and livers were directly frozen in liquid nitrogen to further store them at -80ºC. Bladders were opened to collect the contained stones, which were dried, weighted and stored at RT in the lab.

For the mitochondrial respirometry experiments, fresh tissues were needed, so, after kidney extraction they were placed in BIOPS buffer. Further protocol is described below in 3.8.1.

3.2. URINE PROCEDURES

3.2.1. Urine handle

Every 24 h urine was collected from metabolic cages. Then, urines were centrifuged at 1,500xg for 10 min at RT to remove any debris. Supernatants were transferred to new tubes measuring the urine volume excreted by each mouse. Second- and third-day urines were prestored at -20ºC awaiting to be mixed with the fourth-day urine. Mixed urines were stored at -80ºC until further analysis.

3.2.2. pH and ORP determination

pH and ORP (oxidation-reduction potential) measurements were determined in 24 h fresh urine samples using the 52 09 pH electrode (CRISON) and the 52 65 ORP platinum electrode (CRISON) for microsamples, respectively. First, a calibration step was performed before starting with sample measurements. During calibration and measurements, both calibration buffers and samples were slightly stirred to homogenize the solution. A minimum volume of 150 µL was needed to pH and ORP determination as electrodes had to be submerged to cover its diaphragm. After each measurement, electrodes were rinsed with distilled water and dried with a soft tissue.

3.2.3. Cystine precipitation assay

Cystine precipitation assay was performed as described in (Zee et al., 2017). Briefly, to evaluate if L-Erg influences cystine precipitation both *in vitro* and *in vivo*, *Slc7a9*$^{-/-}$ and L-Erg treated *Slc7a9*$^{-/-}$ urines were used. 400 µL of a supersaturated L-cystine solution (4 mM) was added to 100 µL of water (blank), 100 µL of a pool of *Slc7a9*$^{-/-}$ mice urine, 100 µL of a pool of *Slc7a9*$^{-/-}$ mice urine containing L-Erg 240 µM or 100 µL of a pool of *Slc7a9*$^{-/-}$ L-Erg treated mice urine (3-4 replicates per condition) (**Figure 12**). L-Erg 240 µM corresponds to the L-Erg urine concentration detected in mice after 1-month L-Erg 16 mg/kg/day treatment. Then, samples were vortexed to be homogenized and left at 4ºC for 72 h to allow cystine precipitation. After that, samples were centrifuged at 4,000 rpm and RT for 20 min and supernatant was discarded. The precipitate was dissolved in 1 mL of ultrapure H_2O and cystine concentration was obtained by UPLC-MS/MS in Dr. Rafael Artuch's laboratory, at Hospital Sant Joan de Déu, as decribed in Casado et al., 2018.

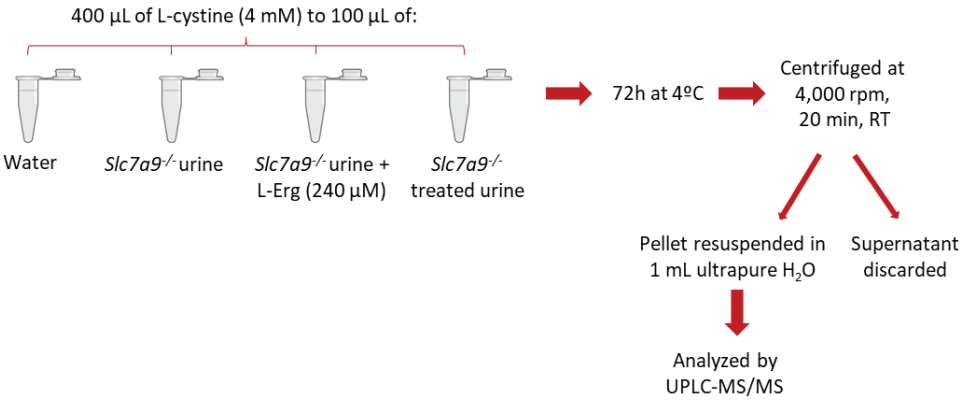

Figure 12. Experimental design of L-Erg effect on urine cystine precipitation

3.3. COMPOUND ANALYSIS IN BIOLOGICAL SAMPLES

Compounds refer to amino acids, organic acids and transsulfuration pathway components and biological samples analyzed were kidney and liver dialyzed extracts and urine. To obtain kidney and liver dialyzed extracts the same protocol was used. First, whole kidneys and livers were grinded using a pre-cooled mortar and pestle. Then, 100 mg of powdered tissue were homogenized in 400 µL of PBS-NEM buffer (10 mM). To induce protein precipitation, 4 % final concentration PCA was added and samples were centrifuged at 10,000 rpm for 15 min at 4ºC. Supernatants were transferred to a new tube and separated in aliquots of 100 µL for further analysis. Pellets were resuspended in 100 µL of NaOH (1 M) and used to determine total protein sample content by BCA Protein Assay Kit (ThermoScientific), following manufacturer procedures. Briefly, protein quantification was performed using a 96-well flat bottom plates and using increasing concentrations of BSA (ranging between 0 to 20 mg/mL) to set a calibration curve. The absorbance was read at 562 nm in the Titertek Multiskan Plus MK11 plate reader (LABSYSTEMS). Samples were tested in duplicates and its median concentration was calculated.

3.3.1. Amino acid and organic acid analysis

Amino acid and organic acid content were determined in kidney supernatant and urine samples by UPLC-MS/MS in Dr. Rafael Artuch's laboratory, at Hospital Sant Joan de Déu, as decribed in Casado et al., 2018. Intracellular metabolites were normalized by grams of tissue total protein content, and urine metabolites, by 24 h urine and mice body weight in grams (24h·BW) or mmol creatinine.

3.3.2. Transsulfuration pathway metabolite analysis

Metabolites of the transsulfuration pathway were analyzed by UPLC-MS/MS in Dr. Federico Pallardó's laboratory, at University of Valencia, as published in Escobar et al., 2016. These metabolites were analyzed in kidney and liver dialyzed extracts and were normalized by grams of tissue total protein content. In addition, GSH and GSSG content were measured in urine and normalized by creatinine.

3.4. GENE EXPRESSION ANALYSIS

3.4.1. RNA extraction

Total RNA was extracted from mice kidney and liver using Direct-Zol RNA mini prep kit (ZymoResearch). Tissues were grinded using a pre-cooled mortar and pestle, and 50 (for liver) or 100 (for kidney) mg were used to obtain total RNA. First, 600 µL of TRIzol™ Reagent were added to tissue samples and were immediately homogenized using a Polytron. Then, 120 µL of chloroform were added and samples were mixed carefully by inverting the tubes. After a 12,000xg centrifuge for 15 min at 4ºC, three phases could be observed and the aqueous transparent phase was transferred to a new tube. 300 µL of ethanol 70 % were added and, after mixing by pipetting, samples were transferred to a column placed in a 2 mL collection tube. A RT centrifuge at 12,000xg for 30 seconds was performed and the flow-through was discarded. From now on and until the elution step, all centrifugation steps had the same parameters (RT, 30 seconds, 12,000xg) and its flow-through was discarded. Then, 400 µL of Pre-wash buffer was added to the column and followed by a centrifugation step. A 15 min DNase treatment was done by adding to each column 80 µL of the DNase mix (75 µL of digestion buffer + 5 µL of DNase enzyme per sample). After that time, three washing steps followed by centrifugation were performed: the first one adding 400 µL of RNA pre-wash buffer and the two others, adding 700 µL of RNA wash buffer. Finally, to elute the RNA, a RNase-free tube was placed under the column before adding 50 µL of RNase-free water. After a centrifugation step, the flow-throw was kept as contained the RNA extracted.

3.4.2. RNA quantification

Two methods were used to quantify RNA as different additional data could be obtained from each one.

RNA concentration was measured spectrophotometrically using a NanoDrop® ND-1000 (Thermo Fisher Scientific). Apart from obtaining RNA quantity determining the absorbance at 260nm, RNA purity was assessed by analyzing 260/280 and 260/230

absorbance ratios. Ratios raging between 1.9-2.0 and 2.0-2.2, respectively, were assumed as pure.

However, as NanoDrop® quantifies any nucleic acid particle, the Qubit™ RNA BR Assay (Thermo Fisher Scientific) kit was used as a specific method to quantify RNA molecules. This assay is based on a fluorometric detection that, thanks to a specific RNA reagent, allows a selective measure for RNA over DNA and free nucleotides. Moreover, using the Qubit™ dsDNA Assay kit (Thermo Fisher Scientific), dsDNA quantification can be also specifically achieved to check DNA presence in the sample. Both kits use the same procedure which consisted of mixing, per sample, 4 µL of RNA or dsDNA specific colorimetric reagent with 196 µL of buffer solution. Then, 1 µL of each RNA extract was added to the mix followed by a 5 second vortex and 2 min incubation at RT. Finally, RNA and dsDNA concentration were determined using the Qubit® 2.0 Fluorometer (Thermo Fisher Scientific).

3.4.3. RNA quality assessment

RNA sample integrity was assessed by the Agilent 2100 Bionalyzer which is based on the lab-on-a-chip technology. Up to 12 samples could be loaded in each chip which microchannels contained a fluorescence dye. Dye molecules were attached to RNA strands and samples were electrophoretically separated and detected via laser induced fluorescence. The software output generates a gel-like and an electropherogram image and calculates sample concentration and the ribosomal ratio (as RNA degradation induces a decrease in the 18S to 28S ribosomal ratio). In addition, an RNA integrity number (RIN) between 1-10 (lowest to highest quality) is displayed for each sample considering the entire electrophoretic pattern.

To analyze RNA quality of kidney RNAseq samples, 1 µL of RNA (diluted to 300 ng/µL) was needed. The kit used was RNA 6000 Nano kit (Agilent) following manufacturer's instructions and the experiment was performed by the support of the Centres Científics i Tecnològics de la Universitat de Barcelona (CCiTUB). Only samples with RINs above 8 were sent to analyze.

3.4.4. Transcriptome analysis

21 RNA samples (6 WT male, 6 WT female, 6 *Slc7a9*$^{-/-}$ male and 3 *Slc7a9*$^{-/-}$ female) extracted from 4-month-old mouse kidneys were sent to the Sidra Institute (Doha) for the RNA-seq experiment where library construction, RNA sequencing, quality control for paired end reads, quantitation and gene annotation was performed. Differential expression analysis was accomplished in collaboration with Dr. Jose Luis Mosquera Mayo from the IDIBELL Bioinformatic Unit.

3.4.4.1. Preprocessing

Features with less than 10 counts across all samples were removed from the analysis. This led to a total of 26,390 genes. The Variance Stabilizing Transformation (VST) featured in DESeq2 package (v1.24.0) was applied to normalize the counts matrix (Love et al., 2014). A Principal Component Analysis (PCA) and a correlation heatmap based on a hierarchical clustering analysis were conducted to explore characteristic patterns of samples and identify potential undesired effects. The hierarchical clustering analysis was parameterized with the average method and the Pearson correlation coefficient-based dissimilarity. The robustness of the clusters identified by means of hierarchical clustering were assessed with pvclust package (v2.2.0) (Suzuki & Shimodaira, 2006). For this purpose, bootstrapping was implemented with 1000 replications. A p-value per cluster was obtained indicating how strong the cluster was supported by the data.

3.4.4.2. Differential expression analysis

Differential expression analysis was conducted using the DESeq2 package (v1.24.0). This method fits a generalized linear model (GLM) of the negative binomial distribution to estimate *log2 FoldChange* between comparison groups. Then it performs a Wald test to test the null hypothesis that there is no differential expression between the two groups of samples, in this particular case, no difference between *Slc7a9*$^{-/-}$ and WT female mice, and between *Slc7a9*$^{-/-}$ and WT male mice. Thus, the GLM was set with two main effects corresponding to genotype and sex. That is, for each gene the model considered was:

$$g_i \sim Genotype + Sex$$

where g_i is the ith-gene expression. Obtained *log2 FoldChange* values were shrunken using the apeglm shrinkage estimator package (v1.6.0) (Zhu et al., 2019). Raw p-values were adjusted for multiple testing using the Benjamini and Hochberg False Discovery Rate (FDR) (Benjamini & Hochberg, 1995). Any gene with an adjusted p-value lower than 0.05 and a |*log2 FoldChange*| higher than 0.4 in both male and female were considered to be differentially expressed.

3.4.4.3. Functional enrichment analysis

The Database for Annotation, Visualization and Integrated Discovery (DAVID) (v6.8) was used to identify enriched biological concepts and pathways (Huang et al., 2009). The list of differentially expressed genes (DEGs) found in both male and female mice was provided to the online tool and results are reported using the KEGG pathway database and ranked by adjusted p-values.

3.4.5. RT-qPCR gene expression analysis

3.4.5.1. Primer pairs and probes design

Gene expression experiments were designed using the Universal Probe Library (UPL) system developed by Roche. This system is based on 165 short (8-9 nucleotides) hydrolysis probes substituted with Locked Nucleic Acids that allows to analyze over five million transcripts of any sequenced organism. To make this system compatible with qPCR procedures, probes are labeled at the 5' end with fluorescein (FAM) and with a dark quencher at the 3'. When an organism and gene ID are provided to the online Assay Design Software (available on https://lifescience.roche.com/en_es/brands/universal-probe-library.html#assay-design-center), a list of target-specific primer sequences and its corresponding probes are display. Then, you can choose your best option based on gene analysis special requirements (isoform discrimination, sequence specific sites, intron-spanning assays…) and primers were ordered from Thermo Fisher Scientific. Primer pairs and

their corresponding UPL probes used in this work are described in **Table 11**, alphabetically ordered by gene symbol.

Table 11. List of UPL probes and its respective primers used in this thesis

Gene	Reference sequence	Primer pairs	UPL probe	Amplicon size (nucleotides)
Cs	NM_026444.4	ggcatgccagtgcttctt catgttgctgcttgaaggtc	68	96
Gclc	NM_010295.2	aggctctctgcaccatcact gaaagaagagggactttgatgc	6	111
Gclm	NM_008129.4	tgactcacaatgacccgaaa gctcttcacgatgaccgagt	66	134
Gss	NM_008180.2	tgtccaataaccccagcaag atcagtagcaccaccgcatt	81	88
Gsr	NM_010344.4	actatgacaacatccctactgtgg cccatacttatgaacagcttcgt	83	89
Gpx1	NM_008160.6	gtttcccgtgcaatcagttc caggtcggacgtacttgagg	2	81
Nfe2l2	NM_010902.4	catgatggacttggagttgc cctccaaaggatgtcaatcaa	3	95
Pdha1	NM_008810.3	gtcacttgtgtgatggtcagg gtggtccgtagggtttatgc	40	68
Pcx	NM_001162946.1	tccgtgtccgaggtgtaaa caggaactgctggttgttga	4	68
Sdhb	NM_023374.3	actggtggaacggagacaag cctctgtgaagtcgtctctgg	42	90
Actb	NM_007393.3	cctcaccctcccaaaagc gtggactcagggcatga	101	67

3.4.5.2. RT-qPCR protocol

Two steps were performed to transcribe 1 µg of total RNA into cDNA using the Transcription First Strand cDNA Synthesis kit (Roche). In the first step, RNA samples were diluted to get 1 µg of RNA in 11 µL of water, mixed with 2 µL of random hexamer primers (600 pmol/ µL) and heated to 65ºC for 10 min to denature RNA secondary structures. Then, the RT Master Mix was prepared according to **Table 12** and 7 µL were added to each sample. The RT reactions, in a final volume of 20 µL, were performed in a GeneAmp PCR System 9700 thermal cycler (applied Biosystems) and comprises a 10

min incubation at 25ºC followed by 60 min at 50ºC and a final 5 min step at 85ºC to inactive the RT enzyme (**Table 13**).

Table 12. RT Master Mix

Reagent	Volume (µL)
RT-Reaction buffer (5X)	4
RNase inhibitor (40 U/µL)	0.5
dNTP mix (10 mM)	2
RT enzyme (20 U/µL)	0.5

Table 13. RT thermal cycles

Temperature	Time
25ºC	10 min
50ºC	60 min
85ºC	5 min

cDNA dilutions ranging from 1:5 to 1:10 were used to analyze gene expression in kidney and liver tissues. For each gene of interest (GOI), a reaction Master Mix was prepared according to **Table 14**. 384-wells plates were set up adding 9 µL of the mixes of each GOI and then, 1 µL of diluted cDNA. Each sample was tested in triplicates for each gene and *actb* was established as a reference gene. Three types of controls were included in each plate and for each gene: a sample mix positive control (pool of RNA sample reaction), cDNA negative control (pool of RNA samples but lacking RT enzyme reaction) and qPCR negative control (samples substituted by 1 µL of water). Once the plates were set up, they were covered with a sealing foil to prevent sample evaporation and centrifuged for 2 min at 1,500xg and RT. qPCR reaction was run on a LightCycler 480 Real-Time PCR System (Roche). The thermal cycle protocol used is described in **Table 15**.

Table 14. qPCR Master Mix

Reagent	Volume (µL)
Primer mix (20 µM)	0.2
UPL probe mix (10 µM)	0.5
Probes Master (2X)	5
Ultrapure H_2O	3.6

Table 15. qPCR thermal cycle protocol

Analysis mode	Cycles	Segments	Ramp rate/slope (ºC/s)	Temp (ºC)	Time	Acquisition Mode
Pre-incubation						
None	1		4.8	95	10 min	None
Amplification						
Quantification	45	Denaturation	4.8	95	10 sec	None
		Annealing	2.5	60	30 sec	None
		Extension	4.8	72	1 sec	Single
Melting Curve Analysis						
Color Compensation	1	Denaturation	4.8	95	10 sec	None
		Annealing	2.5	50	30 sec	None
		Melting		70		Continuous
Cooling						
None	1		2.5	40	30 sec	None

Once the reaction was over, triplicates were analyzed using the LightCycler 480 Software. Then, data were exported to an excel file and a relative quantification was carried out using Delta-Delta Ct ($2^{-\Delta\Delta Ct}$) method (Livak & Schmittgen, 2001) with *Actb* as endogenous control and WT mice as a reference group.

3.5. PROTEIN PROCEDURES

3.5.1. Protein extraction

For this work, protein extracts were obtained from kidney. Two types of protein preparation protocols were combined (when needed) to analyze apical brush border membranes (BBM) and cytoplasmic protein expression from the same mice kidney. Thus, the BBM protocol described in Biber et al., 2007 was optimized by combining it with the TCA-Acetone protocol published in Méchin et al., 2007.

Before starting the protocol, two buffers had to be prepared: Buffer A (50 mM D-Mannitol (98 %, Merck) –250 mM sucrose (99.5 %, Merck) – 2 mM Tris-HCl at pH 7.1) and Buffer B (10 mM $CaCl_2$ (Merck) and 20 mM NEM (Sigma-Aldrich) in Buffer A). Buffers and samples were kept on ice during all the procedure.

Frozen kidneys were homogenized in 2.5 mL of Buffer A containing 25 µL of protease inhibitor cocktail (100 X) (Merck) using a motor driven homogenizer Glas-Col 099C K54 (Cole-Parmer®). When tissues were completely disrupted and no lumps could be observed, the homogenate was transferred to a 15 mL falcon and mixed with 2.5 mL of Buffer B containing 25 µL of protease inhibitors (100 X). To further mix the samples, falcons were placed for 15 min in an orbital mixer at 4ºC. Then, a 3,000xg centrifugation for 15 min at 4ºC was performed to remove any debris. Supernatants were transferred to ultracentrifuge tubes, which were calibrated by pairs and placed on a Sorvall ultracentrifuge for 1 h at 45,000xg and at 4ºC. F21S-8x50Y was the rotor used which has capacity for 8 samples at a time. After the ultracentrifuge step, cytoplasmic and BBM protein extraction procedures were separated: supernatants were employed to obtain cytoplasmic protein extraction (a) and, pellets, to obtain BBM protein extraction (b).

a) Supernatants were transferred to another ultracentrifuge tube. Total protein precipitation was induced by adding TCA (to a final sample concentration of 10 %) to the tubes and leaving them 1 h at 4ºC. After that time, samples were centrifuged at 16,000xg and 4ºC for 15 min on a Sorvall ultracentrifuge. Then,

supernatants were discarded and pellets were washed twice with 1.5 mL of cold acetone. To completely remove the acetone, samples were centrifuged at 16,000xg and 4ºC for 10 min. Supernatants were discarded and pellets were resuspended with 500 µL of Buffer A containing 5 µL of protease inhibitors (100 X) using a 2.5 mL Dounce Tissue Grinder. Once samples were completely homogenized, they were transferred into another tube and passed through a 25 G needle syringe 10 times to disrupt any lump and completely homogenize the sample.

b) Pellets from the first ultracentrifuge were resuspended with 5 mL of Buffer B containing 50 µL of protease inhibitors (1000X) and ultracentrifuged again at the same conditions (1 h, 45,000xg and 4ºC). Supernatants were discarded and pellets were resuspended with 100 µL of Buffer A and 10 µL of protease inhibitors (1000X), transferred to another tube and passed through a 25 G needle syringe 10 times to disrupt any lump and completely homogenize the sample.

Both cytoplasmic and BBM protein preparations were kept on ice to be quantified using the Pierce BCA Protein Assay kit (as described in 3.3) before its storage at -80ºC.

3.5.2. Western Blot protocol

As no protein has been described to be a good housekeeping protein in BBM extractions, to allow target proteins normalization the Bio-Rad's Stain-free technology was used in this work. This technology uses a proprietary trihalo compound to enhance tryptophan fluorescence when exposed to UV light. So, it makes proteins fluorescent *in situ* in the gel after a short photoactivation, allowing protein visualization in both gels and membranes. Thus, sample protein expression was normalized by its total protein lane transferred.

30 to 50 µg of protein extracts mixed with 4X Laemmli Sample Buffer (Bio-Rad), DTT (1M) (Bio-Rad) (if required) and water up to no more than 50 µL, were loaded into 4-15 % Stain-free Precast Protein Gels (Bio-Rad). Gels run for 90 min at 120 V in a running

buffer containing Tris (25 mM), Glycine (195 mM) and SDS (0.1 %). Precision Plus Protein™ All Blue Standards (Bio-Rad) was used as a protein weight ladder. After electrophoresis, Stain-free gels were activated by 45 seconds of UV light exposure in the ChemiDoc™ Touch (Bio-Rad). Resolved proteins were transferred into 0.2 µm nitrocellulose membranes using a Trans-Blot® Turbo™ transfer system (Bio-Rad) at 2.5 mA and 25 V for 7 minutes. After a blocking step of 45 min at RT with the Intercept™ blocking buffer (Li-Cor), membranes were incubated overnight at 4ºC with corresponding primary antibodies (**Table 16**) diluted in blocking buffer and 1X PBS-Tween (0.1 %) (1:1 proportion). The following day, primary antibodies were recovered and membranes were washed three times with 1X PBS-Tween (0.1 %). Then, membranes were incubated for 1 h at RT with fluorescent-labeled secondary antibodies (Li-cor) (**Table 17**), also diluted in blocking buffer and 1X PBS-Tween (0.1 %).

Membranes were developed in an infrared laser-based Odyssey® Classic (Li-Cor) which allows the detection of two proteins at once if primary antibodies derived from different host species and different fluorescent-labeled secondary antibodies are used. After membrane scanning, fluorescent bands were quantified using the Odyssey software. Additionally, total protein transfer to membranes was detected using a ChemiDoc™ Touch (Bio-Rad) and quantified using Image Lab™ Software. Then, fluorescent bands were normalized by total protein content.

Table 16. Primary antibodies used in this thesis

Recognized protein	Source	Dilution	Reference
AGT1	Rabbit	1:250	Gift from Dr. Kanai
GCLC	Rabbit	1:1000	Thermo Scientific (PA5-19702)
GGT1	Rabbit	1:500	GeneTex (GTX101198)
NRF2	Rabbit	1:1000	Abcam (ab31163)
rBAT	Rabbit	1:500	Gift from Dr. Palacín

Table 17. Secondary antibodies used in this thesis

Secondary antibody	Fluorophore	Visualized	Dilution	Reference
Donkey (polyclonal) Anti Rabbit IgG (H+L)	IRDue 680LT	Red	1:10,000	Li-Cor #926-68023
Donkey Anti Rabbit IgG (H+L)	IRDye 800CW	Green	1:10,000	Li-Cor #926-32220

3.6. NAD⁺/NADH DETERMINATION

NAD^+ and NADH were determined in mice kidneys using the EnzyChrome™ NAD^+/NADH assay kit (BioAssay Systems) which is based on a lactate dehydrogenase cycling reaction: the formed NADH will reduce a formazan (MTT) reagent. Then, the intensity of the reduced product color measured at 565 nm is proportional to the NAD^+ or NADH concentration in the sample.

For sample preparation, kidneys were grinded using a pre-cooled mortar and pestle. Then, 15 mg of frozen tissue were homogenized using a 2.5 mL Dounce Tissue Grinder in 100 µL of NAD^+ or 100 µL of NADH Extraction buffer for NAD^+ and NADH determination, respectively. To further normalize by total protein content, 10 µL of each extract was kept in another tube. Extracts were heated at 60ºC for 5 min and then, 20 µL of the Assay buffer and 100 µL of the opposite Extraction buffer was added to neutralize the extracts. Samples were centrifuged at 14,000 rpm and RT for 5 min and supernatants obtained were transferred to another tube and diluted 1:10 for NAD^+ and 1:2 for NADH quantification. 40 µL of each sample and standards were mixed with 80 µL of the Working Reagent (60 µL Assay buffer, 1 µL Enzyme A, 1 µL Enzyme B, 14 µL Lactate and 14 µL MTT) in each well of a flat bottom plate, by duplicate. Quickly, absorbance at t_0 was measured at 565 nm and re-read after 15 min incubation at RT.

NAD^+ and NADH concentration were calculated as follows:

$$[NAD\ or\ NADH] = \frac{\Delta \text{OD sample} - \Delta \text{OD blank}}{Slope\ of\ Standard\ curve\ x\ Total\ protein\ content}\ X\ dilution\ factor$$

3.7. MITOCHONDRIAL RESPIRATORY CHAIN ENZYMATIC ACTIVITIES

3.7.1. Tissue homogenization

Frozen kidneys were thawed on ice-cold mannitol (200 µL every 50 mg of tissue), cut in tiny pieces using small scissors and homogenized with a teflon plunger motor driven. Samples and materials were kept cold during the whole protocol. Ten down strokes at 850 rpm were performed per sample and homogenates were transferred to a 1.5 mL tube with a Pasteur pipette. Samples were centrifuged 20 min at 650xg and at 4ºC and supernatants were transferred to a new tube and pellets were resuspended in 200 µL of mannitol and homogenized again. The two supernatants obtained per sample were pooled and kept on ice. Then, total protein quantification was performed using the BCA protein assay (as described in 3.3). Five aliquots of 100 µL of each sample were diluted to 2 mg/mL with mannitol and stored to -80ºC until the analysis.

3.7.2. Enzyme activity assessment

3.7.2.1. Complex II activity

The spectrophotometer was configured at 600 nm and 37ºC. The reaction mix was freshly prepared for each carousel of 5 samples plus the internal quality control as described in **Table 18**. 976 µL of the reaction mix and 10 µL of kidney homogenates (2 mg/mL) were added to each cuvette, mixed and incubate at 37ºC for 5 min in the spectrophotometer. Then the baseline was read for 3 minutes. After that time, the reaction was trigger by adding 4 µL of 25 mM decylubiquinone and the decrease in absorbance was recorded for 3 min. Finally, complex II activity was calculated as the difference of activity with decylubiquinone and the baseline, normalized by citrate synthase activity and expressed as nmol/min·mg protein.

Table 18. Complex II reaction mix

Component	Volume per sample (µL)
500 mM KP pH 7.5	50
200 mM succinate	100
5 mM DCPIP	10
10 mM KCN	100
50 mg/mL BSA	40
Ultrapure H_2O	676

KP = potassium phosphate, DCPIP = 2,6-Dichloroindophenol, KCN = potassium cyanide, BSA = bovine serum albumin.

3.7.2.2. Complex IV activity

The spectrophotometer was configured at 550 nm and 37ºC and a cytochrome c reduced solution (0.1 mM) was freshly prepared as a reaction mix by adding 100 µL of a total reduced 100 % solution (saturated by dithionite) to a 12-13 mL of 100 µM cytochrome c in 50 mM KP buffer. Then, 980 µL were added to each cuvette and incubated at 37ºC for 5 min in the spectrophotometer. Meanwhile, kidney homogenates (2 mg/mL) were diluted taking 22 µL of sample and 66 µL of mannitol buffer. After the 5 min incubation, 20 µL of the diluted samples were added to the reaction mix and the decrease in absorbance was followed for 3 min. Finally, complex IV activity was calculated as normalized by citrate synthase activity and expressed as nmol/min·mg protein.

3.7.2.3. Citrate synthase activity

The spectrophotometer was configured at 412 nm and 37ºC. The reaction mix was freshly prepared for each carousel of 5 samples plus the internal quality control as described in **Table 19**. 930 µL of the reaction mix and 10 µL of kidney homogenates (2 mg/mL) were added to each cuvette, mixed and incubate at 37ºC for 5 min in the spectrophotometer. Then the baseline was read for 4 minutes. After that time, the

reaction was trigger by adding 50 µL of 10 mM oxalacetate and the increase in absorbance was recorded for 4 min. Finally, citrate synthase activity was calculated in as the difference of activity with oxalacetate and the baseline, and expressed as nmol/min·mg protein.

Table 19. Citrate synthase reaction mix

Component	Volume per sample (µL)
5 mM DTNB	20
10 mM acetyl-CoA	30
10 % Triton X-100	10
1 M Tris-HCl	100
Ultrapure H_2O	770

DTNB = 5,5'-Dithiobis(2-nitrobenzoic acid).

3.8. MITOCHONDRIAL RESPIROMETRY

Oroboros-2k (O2k) respirometer (Oroboros® Instrument Gmbh Corp, Austria) was used to measure oxygen consumption in saponin permeabilized renal biopsies, following the substrate-uncoupler-inhibitor titration (SUIT) protocol published in Cantó & Garcia-Roves, 2015.

3.8.1. Sample preparation

Kidneys were extracted from mice after cardiac puncture. Then, kidneys were cut in small transversal segments and were put into a tube on ice containing Biopsy Preservative Solution (BIOPS) at pH 7.1 (**Table 20**) to transport them to the Garcia-Roves Laboratory at University of Barcelona, where is placed the O2k respirometer. Once there, kidney transversal segments were transferred to a well containing 2 mL of fresh ice-cold BIOPS and cut into small pieces (1 mm^3). Small pieces were transferred into a new well containing 2 mL of ice-cold saponin solution (0.05 mg saponin/mL

BIOPS) and left stirring for 30 min at 4ºC to allow tissue permeabilization. After that time, kidney pieces were washed for 5 min under agitation on ice in another well containing 2 mL of MiR05 at pH 7.1 (**Table 21**) buffer. Carefully, 1.5-1.8 mg of dried kidney were introduced in the O2k chamber to achieve 0.75-0.9 mg/mL tissue concentration.

Table 20. BIOPS composition

Component	Final Concentration	Amount for 1 L
CaK_2EGTA	2.77 mM	27.7 mL
K_2EGTA	7.23 mM	72.3 mL
Na_2ATP	5.77 mM	3141 g
$MgCl_2 \cdot 6\ H_2O$	6.56 mM	1.334 g
Taurine	20 mM	2.502 g
Na_2Phosphocreatine	15 mM	4.097 g
Imidazole	20 mM	1.362 g
DTT	0.5 mM	0.077 g
MES	50 mM	9.76 g

Table 21. MiR05 composition

Component	Final Concentration	Amount for 1 L
EGTA	0.5 mM	0,190 g
$MgCl_2$ x 6 H_2O	3 mM	0.610 g
K-lactobionate	60 mM	120 mL
Taurine	20 mM	2.502 g
KH_2PO_4	10 mM	1.361 g
HEPES	20 mM	4.77 g
Sucrose	110 mM	37.65 g
BSA	1 g/L	1 g

3.8.2. SUIT protocol

Once oxygen consumption line was stable, each reagent was added using Hamilton syringes and leaving a signal stabilization period between each titration. First, the LEAK state of uncoupled respiration was assessed adding malate (2 mM) and pyruvate (20 mM). Then, ADP (5 mM) and $MgCl_2$ were added to quantify OXPHOS state. To check the integrity of the outer mitochondrial membrane, cytochrome C (10 mM) was added. If no effect is observed after cytochrome addition, measurements can continue. Then NADH-dependent complex I respiration was evaluated adding glutamate (20 mM). To measure complex II together with complex I respiration (OXPHOS CI+CII), succinate (10 mM) was added. Maximal uncouple respiration was determined by followed titration of FCCP (0.01 µM) which induces non-physiologic uncoupling of the mitochondrial internal state (ETS CI+CII). To inhibit complex I and measure the maximal respiration of complex II (ETS CII) rotenone (0.5 mM) was added. Finally, the residual oxygen consumption (ROX state) was quantified adding antimycin A (2.5 µM) (which inhibits complex III) and this value was subtracted from previous values recorded. In addition, all values were mass normalized.

3.9. ELECTRON MICROSCOPY

Cystine stones removed during the necropsy from mice bladder were left to dried at 60ºC for two hours. Stones were manually split in two parts to analyze both the outer surface and the internal layers of the stone, which allows to observe the stages of stone formation. Stone fragments were fixed with silicone, in its corresponding spatial orientation, to the 1 cm in diameter support element. No sample coating was needed as analysis were performed under low vacuum. Crystal morphology was assessed using a Scanning Electron Microscopy (SEM) Quanta 200 3D (FEI Company™). In addition, the SEM was coupled with energy-dispersive spectroscopy (EDS) (Thermo Fisher UltraDry, 30 mm^2) allowing the simultaneously analysis of stone elemental composition. Stone images were acquired with magnification ranging from100 to 1000 and image resolution of 512 x 340. Nine sections per each stone were analyzed (3 sections per 3 magnifications). The images and spectra presented in the corresponding

results section are a representation of data acquired and all images present a scale bar with indicated length.

3.10. HUMAN PROTOCOLS

Patients recruited in this thesis were clinically diagnosed of cystinuria (most at Fundació Puigvert or Hospital Universitari de Bellvitge). 8 presented one or two unexplained cystinuria causing alleles and 18 were genetically studied for the first time in this work. Informed consent was obtained from all participants or their legal guardian. Clinical data, blood and urine were collected when possible.

3.10.1. Human genotyping

3.10.1.1. DNA extraction

Patients' DNA was extracted from fresh blood using the Wizard® Genomic DNA Purification Kit (Promega) following manufacturer conditions. Briefly, 10 mL of fresh blood was mixed with 30 mL of Cell Lysis Solution and incubated for 10 min at RT. Samples were centrifuged at 2,000xg and RT for 10 min and the supernatants were discarded. From now on, all protocol centrifugation steps had the same parameters: 2,000xg for 10 min at RT. Then, 10 mL of Nuclei Lysis Solution and 3.3 mL of Protein Precipitation Solution were added to sample pellets and a centrifuge was performed. The supernatants obtained were transferred to a new tube and 10 mL of isopropanol were added. After mixing the samples by inversion, the DNA could be observed, and samples were centrifuged. Supernatants were discarded and 10 mL of 70 % ethanol were added to the pellets and samples were centrifuged again. Supernatant was aspirated to be discarded and tubes were left open to air dry the pellet. Finally, 800 µL of DNA Rehydration Solution were added and samples were incubated overnight at 4ºC.

Two methods were used to quantify DNA as different additional data could be obtained from each one: spectrophotometrically using a NanoDrop® ND-1000 (Thermo Scientific) and fluorometrically using the Qubit dsDNA Assay kit (Described above in 3.4.2).

3.10.1.2. Genotyping

3.10.1.2.1. PCR and Sanger Sequencing

A PCR followed by a Sanger Sequencing Analysis was performed to detect variants in *SLC3A1*, *SLC7A9* and *SLC7A13* genes. **Table 22** shows the optimized reaction mixes and thermal cycles of the DREAMTaq and, **Table 23**, the primer sequences used to amplify each exon of genes of interest.

The PCR amplification product was purified using the NucleoSpin® Gel and PCR clean-up kit from Macherey-Nagel. Briefly, 1 volume of sample was mixed with 2 volumes of Buffer NT1, loaded into a column and centrifuged at 11,000xg and RT for 1 min. The flow-through was discarded and 2 washing steps were performed adding 700 µL of Buffer NT3 to the column followed by a centrifuge at 11,000xg and RT for 1 min. To ensure the total removal of the washing Buffer NT3, the columns were placed for 5 min at 60ºC. Finally, to elute the purified DNA, 22 µL of the elution Buffer NE were added to the column and the flow-throw was kept in a 1.5 mL tube.

Purified products were sent to be analyzed by the company StabVida (Portugal) and the sequences obtained were assembled and studied with the Sequencher software (v5.4) to determine each sample genotype. As a reference sequence NG_008233.1 (*SLC3A1*), NG_001126335.2 (*SLC7A9*) and NC_000008.10 were used.

Table 22. PCR master mix and thermal cycles for patients' samples

PCR Master Mix		**PCR thermal cycles**		
Reagent	**Volume (µL)**	**Cycles**	**Temperature**	**Time**
Ultrapure H_2O	6.4	1	95ºC	5 min
Dream Taq Green DNA polymerase (2X)	10,5	35	95ºC	30 sec
Primers (10 µM)	1.05		60ºC	30 sec
			72ºC	60 sec
		1	72ºC	20 min
		1	15ºC	for ever

Table 23. Primers used to genotype patient samples

SLC3A1	**Exon**	**Sequence**
VNO #1092	E1-F	CTTTCTTCCTTGGCTGGACT
VNO #1093	E1-R	CTGAACAACCCAGGCATAAT
VNO #1094	E2-F	TACAGGCGTGAACCACTACA
VNO #1095	E2-R	ATCTTGCCCACTTTCCATTC
VNO #1096	E3-F	GCCTGGCCTGTCATATGTTAT
VNO #1097	E3-R	GGGTTTTACTAAATCAGTTCAATCA
VNO #1098	E4-F	TGTCCATTTCTGTGAAACACC
VNO #1099	E4-R	TCAAATAATTAAAGACTTGATTTTGC
VNO #1100	E5-F	TGCCAAGTTGTTAACAGTCAAA
VNO #1101	E5-R	TCAGGCTGAGAAAGAAAACAC
VNO #1102	E6-F	GAGCCCTTTGAAGAGGTTGT
VNO #1103	E6-R	CCTCCTACAGTGCTGGGTTT
VNO #1104	E7-F	ATGCTATCCTTCCCTTAGCC
VNO #1105	E7-R	CATTTTAGAGATAACTGGACAGCA
VNO #1106	E8-F	TTGCTACGTTGTGAACTTTCTG
VNO #1107	E8-9	CATGATTTTCAGCAATGCAA
VNO #1658	E9-F	GGGTGAAACTGGTTTATGTACCG
VNO #1659	E9-R	ACTTCACTTCACTTGGTAGATTTGT
VNO #1028	E10-F	GGATCGAGTGTTTTGGGTAAAT
VNO #1029	E10-R	CCAAGCAGCATGCTGTACAT
SLC7A9	**Exon**	**Sequence**
VNO #870	E1-F	CATTTCTAGGGTTGGACCGTG
VNO #832	E1-R	GGCCAGGAGAGCCATGAG
VNO #833	E2-F	ATGACTGACTTTGACTCTGGG
VNO #834	E2-R	TCTTCTGCCGTGTCACTAGGG
VNO #835	E3-F	CGCCCTCTTCCTTCCTCC
VNO #978	E3-R	TAGCAGCTGCCTGGCGTG
VNO #1662	E4-F	ACCCTGCCAGTATCCCTCTT
VNO #1663	E4-R	CAGAGACTCACTGGGGAGGA
VNO #783	E5/6-F	TCCCGTGGAGATACACTCA
VNO #840	E5/6-R	TGGAGTTAAAGTCACCTGGAG
VNO #841	E7-F	AGTCAAGGTGTGTGACGCTTG
VNO #842	E7-R	AGGAGAAGAGAAATCAGGCTG
VNO #785	E8-F	CTGAACGTGGGTCTCCGTG
VNO #786	E8-9	ACCTCCAGTGCTGACACCTG
VNO #1660	E9-F	ACCTCCTCACTCACTCTGCC
VNO #1661	E9-R	TCATAGCAAGGAATAAGGGCATCT
VNO #845	E10-F	GGAGCACAAGTCCTCAGTGG
VNO #846	E10-R	GCCTTGAAGATAGGCTGGTAG
VNO #787	E11-F	TTCGGTCTTCTGTGACATGAG
VNO #977	E11-R	GTCAGATTGGAACTAGAAGGCA
VNO #847	E12-F	ATGATTGAAATTGGAGGAGGG
VNO #848	E12-R	TGGAGTCAGGACAGGTGAGG
VNO #849	E13-F	CCTCACCCACAACAACTCC
VNO #850	E13-R	AAATTCAGCTGACTTGGCTAC

SLC7A13	Exon	Sequence
VNO #1408	1A-R	GACAGAGCAGCTGGGAAAAAAAGG
VNO #1409	1A-F	CGAAAATGGAACAGGAAGGACAGAA
VNO #1406	1B-R	CCAGGCTGGCATGATCTGATTC
VNO #1407	1B-F	TTTGGCTCCACGGTTGCTTT
VNO #1404	2-R	TCATTCCCTTTGGCCCTCTGT
VNO #1405	2-F	TGACCACCACACAACCTATCCACA
VNO #1402	3-R	CTCATGTGTTTCACAGTAACTGAGTA
VNO #1403	3-F	TTTTGTTTTTCTGCAGATGCTGTAG
VNO #1400	4A-R	CATGCGAAGCAGAGCTTTTAGC
VNO #1401	4A-F	TGCAGGTATCATTCATGGATGTTC
VNO #1398	4B-R	AAGTGCTACATTCTGGAAGGGAAAA
VNO #1399	4B-F	TAATATTTGCCTCCCTGATGTGTCT

Large exons were divided in two parts, A and B. F = Forward and R = Reverse.

3.10.1.2.2. MLPA

To further genetically characterize cystinuria patients, a Multiplex ligation-dependent probe amplification (MLPA) assay of *SLC3A1*, *PREPL* and *SLC7A9* coding exons was performed using specific probemixes for cystinuria (SALSA® MLPA® probemix P426-A1 Cystinuria). MLPA fluorescence-labeled probemixes target specific genomic sequences and hybridize with them conferring to each sequence a unique length. Then, sequences were separated by capillary electrophoresis and the fluorescence peaks obtained were proportional to copy numbers of each genomic region.

Briefly, 5 µL of DNA sample (20 ng/µL) or TE (no-DNA control) were heated at 98ºC for 5 min to denature the DNA. Tubes were cooled down to RT and 3 µL of hybridization master mix (**Table 24**) were added to each tube. After 1 min incubation at 95ºC, samples were left 16 h at 60ºC to allow hybridization. The following day, probes ligation was performed adding to each tube 32 µL of ligase master mix and incubating the samples 15 min at 54ºC. To inactivate the ligase enzyme samples were heated 5 min at 98ºC. Then, samples were cooled at RT and 10 µL of the polymerase master mix were added to each tube. Finally, a PCR was performed as described in **Table 25.**

Table 24. MLPA Master Mix reactions

Hybridization Master Mix		Ligase Master Mix		Polymerase Master Mix	
Reagent	**Volume (µL)**	**Reagent**	**Volume (µL)**	**Reagent**	**Volume (µL)**
MLPA buffer	1.5	Ultrapure H_2O	25	Ultrapure H_2O	7.2
Probemix	1.5	Ligase buffer A	3	SALSA PCR primer mix	2
		Ligase buffer B	3	SALSA polymerase	0.5
		Ligase-65 enzyme	1		

Table 25. PCR thermal cycles

Cycles	Temperature	Time
	95ºC	30 sec
35	60ºC	30 sec
	72ºC	60 sec
1	72ºC	20 min
1	15ºC	for ever

To separated DNA fragments obtained by length, 1.5 µL of the PCR product was mixed with 10 µL of formamide and 0.6 µL of LIZ 500, and then loaded onto an ABI Prism Genetic Analyzer 3130XL. Data analysis was performed using the GeneMapper™ Software. Peak heights were normalized by peak heights of reference probes. Then, the height of each peak is divided by the mean of all sample peaks of the same region of interest and the value obtained should be in one of the following fractions:

- **0**: homozygous deletion.
- **0,4 – 0,65**: heterozygous deletion.
- **0,8 – 1,20**: 2 copies of the region of interest.

- **1,3 – 1,64**: 3 copies of the region of interest.
- **1.75 – 2.15**: 4 copies of the region of interest.

3.11. STATISTICAL ANALYSIS

All data are expressed as mean ± standard error of the mean (SEM) for each group. Normal distribution was tested with D'Agostino & Pearson omnibus normality test. Then, Mann-Whitney or t-test were used accordingly. Statistical significance was considered when p-value ≤ 0.05, although p-values under 0.1 were also taken into consideration to further discuss its biological impact. Data analyses and figure design were performed with RStudio, version 3.6.0. Most frequently used R packages were openxlsx, dplyr, ggpubr, stringr, tidyr, devtools, ggplot2 and VennDiagram.

RESULTS

4. RESULTS

4.1. CHAPTER I: Study of AGT1 involvement in cystine, aspartate and glutamate reabsorption and in cystinuria.

In 2016, AGT1 was described as the second cystine transporter and the missing partner of rBAT in the S3 segment of proximal tubules (Nagamori et al., 2016). AGT1, encoded by *SLC7A13*, is a light chain that also heterodimerizes with the heavy chain rBAT in the apical membrane where mediates the efflux of anionic amino acids (aspartate and glutamate) in exchange for cystine (Nagamori et al., 2016). The evidence of a new transporter involved in cystine reabsorption in proximal tubules induced the study of its contribution in amino acid reabsorption and its possible role in cystinuria, both in mouse models and in patients.

4.1.1. AGT1 contribution to amino acid reabsorption and cystinuria in mice

Although the *Slc7a13*$^{-/-}$ mouse model is not available in our lab, two different approaches were used to study AGT1 involvement in amino acid reabsorption and cystinuria in mice. First, as female mice showed no expression of AGT1 in kidney (Nagamori et al., 2016), sex differences in amino acid excretion were assessed in WT and *Slc7a9*$^{-/-}$ mice (**Figure 13A-B**). Then, *Slc7a9*$^{-/-}$ and *Slc3a1*^{D140G} amino acid excretion were compared as *Slc3a1*^{D140G} mice has impaired both $b^{0,+}$AT/rBAT and AGT1/rBAT transporters (**Figure 13C**). All data presented in this section are from 3-month-old mice.

Protein expression analysis by Western Blot confirmed the lack of AGT1/rBAT transporter expression in females but showed no differences between stone and non-stone former *Slc7a9*$^{-/-}$ male mice, neither using an antibody against AGT1 nor against rBAT (**Figure 14A**). As not always protein function correlates with its expression, amino acid excretion patterns were assessed in all conditions. Both WT and *Slc7a9*$^{-/-}$ female mice showed, as expected, lower excretion of aspartate and glutamate when compared

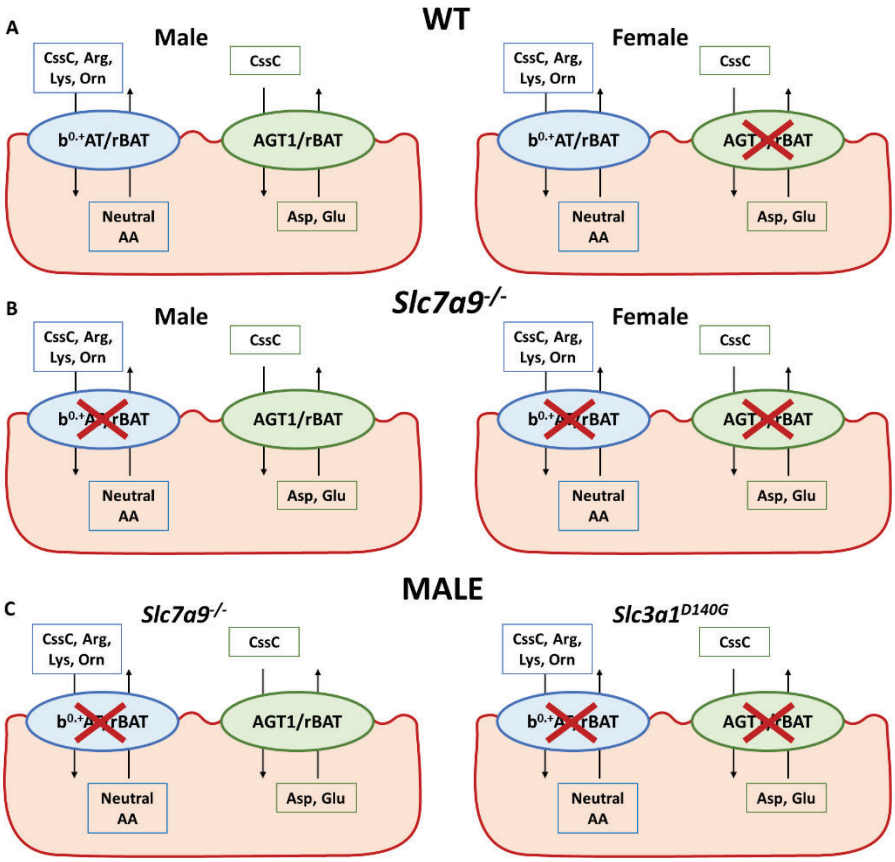

Figure 13. Schematic representation of cystine transporters in the models used to evaluate AGT1 role in cystinuria

Cystine transporters expression in ***(A)*** *WT male and female,* ***(B)*** *Slc7a9$^{-/-}$ male and female and* ***(C)*** *Slc7a9$^{-/-}$ and Slc3a1^{D140G} male mice. CssC = Cystine, Arg = Arginine, Lys = Lysine, Orn = Ornithine, Asp = Aspartate, Glu = Glutamate and AA = amino acids.*

to its respective male mice, but excreted cystine levels were also lower (**Figure 14B**). However, to further study cystine excretion variations, male/female ratio of cystine excretion levels was calculated in WT and *Slc7a9$^{-/-}$* stone former and non-stone former mice. Results showed that sex differences in cystine excretion were more evident in WT than in *Slc7a9$^{-/-}$* mice (3.70-fold vs. 1.71-fold and 1.36-fold) (**Table 26**), suggesting an increase in AGT1/rBAT reabsorption in *Slc7a9$^{-/-}$* male mice. In addition, male/female ratios of aspartate and glutamate excretion were higher in *Slc7a9$^{-/-}$* mice than in WT, above all in non-stone former mice (3.16-fold vs. 24.88-fold and 1.85-fold vs. 6.02-

fold) (**Table 26**). These results suggest an increased impact of AGT1/rBAT transport in *Slc7a9*$^{-/-}$ male mice compared to WT ones, probably due to the amount of cystine in the urine of cystinuric mice. In addition, their revealed differences in amino acid excretion between non-stone and stone former mice.

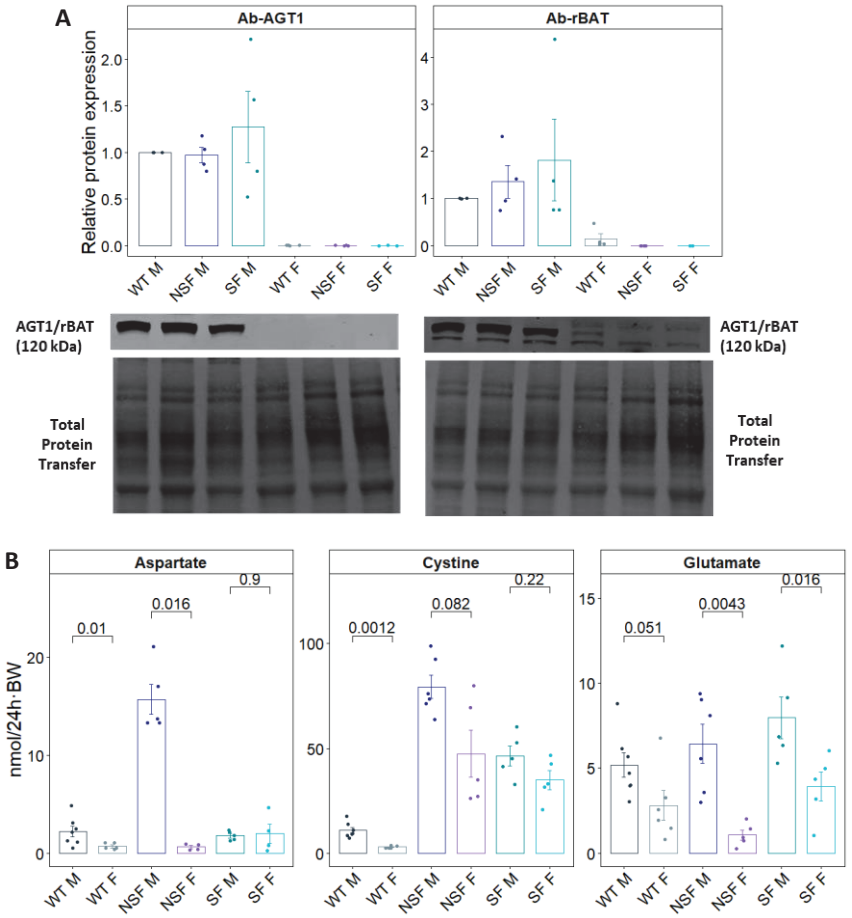

Figure 14. Study of AGT1 function comparing male and female Slc7a9$^{-/-}$ mice

(A) *AGT1/rBAT heterodimer expression in WT and Slc7a9$^{-/-}$ mice assessed using both AGT1 and rBAT antibodies. Representative immunoblots showing AGT1/rBAT heterodimer protein levels and their corresponding total transfer line used to normalize data obtained.* ***(B)*** *Aspartate, cystine and glutamate excretion by genotype (WT and Slc7a9$^{-/-}$), phenotype (stone and non-stone formers) and sex (male and female). Data are expressed as mean ± SEM and p-value is showed at the top after Mann-Whitney-Wilcoxon test. Ab = Antibody, NSF= Non-stone formers, SF = Stone formers, M = Male, F = Female, BW = Body weight.*

Table 26. Male/female cystine excretion ratio by genotype and phenotype in Slc7a9$^{-/-}$ mice

Genotype-phenotype	AA	Mean excretion in **Male** (nmol/24h·BW)	Mean excretion in **Female** (nmol/24h·BW)	Ratio
WT	Asp	2.21 (±1.45)	0.70 (±0.33)	3.16
NSF	Asp	15.68 (±3.40)	0.63 (±0.31)	24.88
SF	Asp	1.78 (±0.47)	1.98 (±1.97)	0.90
WT	CssC	10.93 (±3.59)	2.96 (±0.52)	3.70
NSF	CssC	79.35 (±13.52)	46.49 (±10.62)	1.71
SF	CssC	47.46 (±25.31)	34.92 (±10.12)	1.36
WT	Glu	5.18 (±1.91)	2.80 (±2.12)	1.85
NSF	Glu	6.43 (±2.78)	1.07 (±0.67)	6.02
SF	Glu	7.96 (±2.74)	3.92 (±1.9)	2.03

Data are expressed as mean ± SEM. AA = amino acid. NSF= Non-stone formers, SF = Stone formers, Asp = Aspartate, CssC = Cystine, Glu = Glutamate.

To further study AGT1 role in cystinuria, cystine, aspartate and glutamate excretion patterns of *Slc7a9*$^{-/-}$ and *Slc3a1*^{D140G} male mice were analyzed. *Slc3a1*^{D140G} male mice showed higher levels of cystine, and lower levels of aspartate and glutamate excretion compared to *Slc7a9*$^{-/-}$ male mice, in both stone and non-stone former groups (**Figure 15**). However, concerning cystine excretion, significant differences were only observed in stone former mice as non-stone former showed high variability. These results together with the ones described above comparing male and female excretion, indicate that AGT1/rBAT decreases cystine excretion in *Slc7a9*$^{-/-}$ mice by increasing aspartate and glutamate excretion.

Finally, to determine the impact of AGT1/rBAT in cystine lithiasis, a 6-month follow-up of the rate of stone formation in *Slc7a9*$^{-/-}$ and *Slc3a1*^{D140G} male and female mice was performed. *Slc7a9*$^{-/-}$ mice showed significant differences in stone formation rate according to sex while in *Slc3a1*^{D140G} mice similar rates were observed during the whole follow-up (**Figure 16A-B**). In addition, *Slc7a9*$^{-/-}$ female mice and both genders for

Slc3a1^{D140G} mice showed a similar rate of stone formers at six-months of age suggesting that AGT1/rBAT cystine reabsorption delays and reduce cystine lithiasis *Slc7a9*$^{-/-}$ male mice.

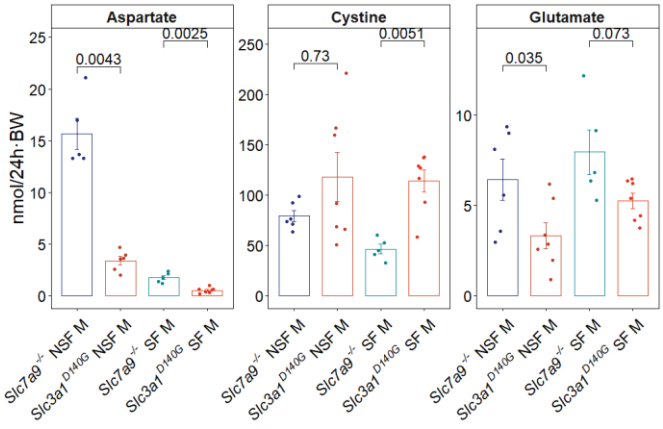

Figure 15. Comparison of aspartate, cystine and glutamate excretion between Slc7a9$^{-/-}$ and Slc3a1^{D140G} male mice

Aspartate, cystine and glutamate excretion by genotype (Slc7a9$^{-/-}$ and Slc3a1^{D140G}) and phenotype (stone and non-stone formers). Data are expressed as mean ± SEM and p-value is showed at the top after Mann-Whitney-Wilcoxon test. NSF = Non-stone formers, SF = Stone formers, M = Male, F = Female, BW = Body weight.

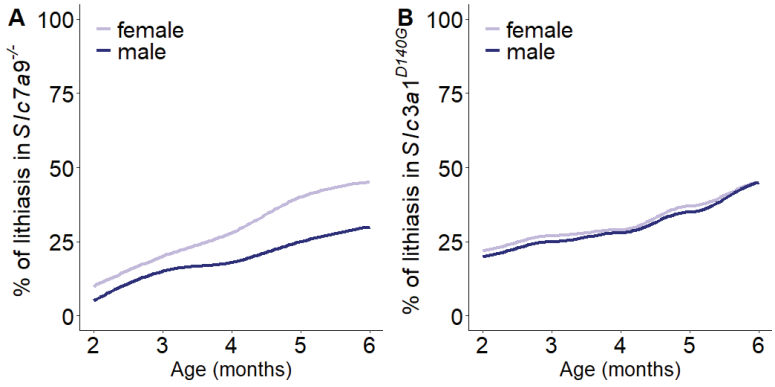

Figure 16. 6-month follow-up of the rate of stone formation in Slc7a9$^{-/-}$ and Slc3a1^{D140G} mouse models

(A) *Slc7a9$^{-/-}$ and* ***(B)*** *Slc3a1^{D140G} male and female stone formation rate monthly assessed up to 6-months of age.*

4.1.2. *SLC7A13* genetic analysis in cystinuric patients

It is well known that about 10 % of cystinuric patients remain genetically uncharacterized for one or both alleles after *SLC3A1* and *SLC7A9* gene analysis (Olschok et al., 2018), and no genotype-phenotype correlation related to cystine lithiasis have been described so far, as even brothers with the same mutation show differences in lithiasis onset and recurrence (Dello Strologo et al., 2002). For these reasons, it has been suggested that alterations in other genes could take part in the cystinuria phenotype. Since it was described as a second cystine transporter, AGT1 (*SLC7A13*) has been proposed as a candidate to be the third cystinuria gene or to modulate this disease. In addition, the dominant with incomplete penetrance pattern observed in type B cystinuria patients (*SLC7A9* gene affected) increases the reasons to study the role of AGT1 in this disease. In contrast to gender expression differences reported in mice, AGT1 is expressed in the kidneys of both human male and female (https://www.proteinatlas.org/ENSG00000164893-SLC7A13/tissue/kidney). Thus, after the promising results obtained in the study of AGT1 role in cystinuric mice, next steps were focused on searching *SLC7A13* genetic variants in cystinuric patients.

As AGT1 heterodimerizes with rBAT, the first approach was to analyze cystinuric patients with only one *SLC7A9* allele explained or without any genetic variant described. Of our lab cohort, *SLC7A13* was sequenced in 8 unexplained patients and their respective families. *SLC7A13* missense variants were found in all families, but in heterozygosis. Five families carried the c.745G>A (p.Val249Met) variant, two the c.1112G>A (p.Arg380Lys) variant and one the c.1355T>C (p.Met452Thr) variant (**Table 27**). The c.745G>A variant was the only predicted by Polyphen2 (Adzhubei et al., 2010) as probably damaging.

To determine the impact of the c.745G>A variant, the urinary excretion values of cystine, aspartate and glutamate of patients were explored. Unfortunately, as these families were recruited years ago from different hospitals and traditionally only urinary levels of cystine or the 4 cystinuria-related amino acids were recorded, just partial aminograms could be obtained and not from all relatives.

Table 27. SLC7A13 variants found in 8 families of cystinuric patients

SLC7A13 variant	AGT1 change	Location	Nº of alleles found	Polyphen2 score	gnomAD allele frequency
c.745G>A	p.Val249Met	Exon 1	5	Damaging	0.112
c.1139G>A	p.Arg380Lys	Exon 3	2	Benign	0.181
c.1355T>C	p.Met452Thr	Exon 4	1	Benign	0.140

Thus, cystine was the only amino acid related to AGT1 function that could be analyzed in those patients (**Table 28**). Non-cystinuric patients heterozygous for the c.745G>A variant (F3 I.2 and II.2, and F5 I.2) showed physiological levels of cystine excretion while uncharacterized patients in which only the c.745G>A variant was detected (also in heterozygous) (F2 II.2 and F3 II.1), presented cystine hyperexcretion. This finding indicates that the c.745G>A variant in the *SLC7A13* gene was not responsible for their cystine hyperexcretion phenotype. In addition, in F5, both children have the same *SLC7A9* variation and similar levels of cystine hyperexcretion, although the II.2 has the additional c.745G>A variant in heterozygosis. Collectively, these data pointed to no observable effect of c.745G>A variant, in heterozygosis, on cystine excretion.

To further explore the role of AGT1 in cystinuric patients, 18 new patients without genetic diagnosis were recruited during this thesis, in which *SLC3A1*, *SLC7A9* and *SLC7A13* genes were deeply examined by sanger sequencing and MLPA techniques. The **Table 29** summarizes variants found in *SLC3A1*, *SLC7A9* and *SLC7A13* genes per patient. Unfortunately, in 16 out of 18 patients both cystinuria causing mutations were found in the *SLC3A1* gene which reduced the possibilities of studying the impact of *SLC7A13* gene variants. The **Table 30** summarizes the main clinical aspects of each patient related to interventions needed to remove the cystine calculi, the average of interventions and lithiasis episodes per year during the follow-up, and the urinary amino acid excretion levels when the genetic analysis was performed. Although it is not shown, all patients were taken potassium citrate as treatment at the analysis, and when needed, D-penicillamine.

Table 28. Genetic description of families with the c.745G>A variant in the SLC7A13 gene and their cystine excretion levels

Family ID	Patient/ parents	*SLC7A9* variant	$b^{0,+}$AT change	*SLC7A13* variant	AGT1 change	[CssC]
F1	I.1	c.730_732delGAA	p.Glu244del			
F1	I.2			c.745G>A	p.Val249Met	
F1	**II.1**	c.730_732delGAA	p.Glu244del	c.745G>A	p.Val249Met	
F1	II.2			c.745G>A	p.Val249Met	
F2	I.1			c.745G>A	p.Val249Met	
F2	I.2	c.368C>A	p.Thr123Met			
F2	II.1	c.368C>A	p.Thr123Met	c.745G>A	p.Val249Met	144
F2	**II.2**			c.745G>A	p.Val249Met	700
F3	I.1					
F3	I.2			c.745G>A	p.Val249Met	61
F3	**II.1**			c.745G>A	p.Val249Met	483
F3	II.2			c.745G>A	p.Val249Met	36
F4	I.1	c.578_580dupCAT	p.Ile193dup	c.745G>A	p.Val249Met	995
F4	I.2					185
F4	**II.1**	c.578_580dupCAT	p.Ile193dup	c.745G>A	p.Val249Met	1331
F4	II.2					710
F5	I.1	c.614dupA	p.Asn206Glufs*3			372
F5	I.2			c.745G>A	p.Val249Met	38
F5	II.1	c.614dupA	p.Asn206Glufs*3			698
F5	**II.2**	c.614dupA	p.Asn206Glufs*3	c.745G>A	p.Val249Met	697

Cystinuria patients are in bold. Amino acid concentration is given in µmol/g Creatinine. CssC = Cystine.

Table 29. Variants detected in SLC3A1, SLC7A9 and SLC7A13 genes in the 18 new cystinuric patients after sanger sequencing and MLPA analysis

ID	Gen	Gene variant	Gen	Gene variant
372	*SLC3A1*	c.1093C>T/ c.1400T>C	*SLC7A13*	-
373	*SLC3A1*	c.1093C>T/ c.1400T>C	*SLC7A13*	-
374	*SLC3A1*	c.1400T>C/ c.1400T>C	*SLC7A13*	c.745G>A
376	*SLC3A1*	c.1400T>C/ c.1400T>C	*SLC7A13*	c.745G>A
415	*SLC3A1*	c.1354C>T/DupE5-E9	*SLC7A13*	c.658+2C>T /c.1139G>A/ c.1413_*7delGATGTCGG
416	*SLC3A1*	c.266T>C/c.266T>C	*SLC7A13*	c.745G>A /c.988C>T
417	*SLC3A1*	DelE1-E6/DelE1-E6	*SLC7A13*	c.658+2C>T /c.1139G>A/ c.1413_*7delGATGTCGG
418	*SLC3A1*	c.1400T>C/DupE5-E9	*SLC7A13*	c.745G>A
420	*SLC7A9*	c.368C>T/-	*SLC7A13*	c.658+2C>T / c.745G>A /c.1139G>A/ c.1413_*7delGATGTCGG
421	*SLC3A1*	c.1354C>T/DupE5-E9	*SLC7A13*	c.658+2C>T /c.1139G>A/ c.1413_*7delGATGTCGG
422	*SLC3A1*	c.431G>C/c.431G>C	*SLC7A13*	c.658+2C>T /c.1139G>A/ c.1413_*7delGATGTCGG
423	*SLC3A1*	c.1400T>C/DupE5-E9	*SLC7A13*	c.745G>A
424	*SLC3A1*	c.647C>T/c.647C>T	*SLC7A13*	-
425	*SLC3A1*	c.1400T>C/DupE5-E9	*SLC7A13*	c.658+2C>T / c.745G>A / c.1355T>C
426	*SLC3A1* & *SLC7A9*	c.1139delT/c.1354C>T c.368C>T/c.578_580delTCA	*SLC7A13*	c.745G>A
427	*SLC7A9*	c.368C>T/c.997C>T	*SLC7A13*	c.658+2C>T/c.1355T>C
428	*SLC3A1*	c.1400T>C/ c.1400T>C	*SLC7A13*	c.658+2C>T /c.1139G>A/ c.1413_*7delGATGTCGG
429	*SLC3A1*	c.754C>T/c.754C>T	*SLC7A13*	c.745G>A

Table 30. Clinical parameters and amino acid excretion in the 18 new cystinuric patients

ID	Sex	Age at analysis	Y. of follow-up	Number of			Interventions per year	Lithiasic episodes	Affected gene	Variants in *SLC7A13*	Cystine (µmol/g Cre)	Aspartate (µmol /g Cre)	Glutamate (µmol /g Cre)
				ESWL	URS	PCNL							
372	male	38	24	25	4	5	1.42	4 times per year	*SLC3A1*	-	2446.6	17.2	24.1
373	male	35	24	1	-	2	0.13	every year	*SLC3A1*	-	2441.0	20.6	30.6
374	male	70	42	25	1	2	0.67	4 times per year	*SLC3A1*	c.745G>A	1338.3	8.3	15.6
376	female	64	46	0	0	1	0.02	unique	*SLC3A1*	c.745G>A	2003.9	8.0	30.7
415	male	63	10	1	1	1	0.30	every 2 years	*SLC3A1*	c.658+2C>T /c.1139G>A/ c.1413_*7delGATGTCGG	1671.0	9.5	33.8
416	female	46	11	-	-	1	0.09	unique	*SLC3A1*	c.745G>A /c.988C>T	925.7	62.4	45.1
417	female	67	10	-	-	-	-	unique	*SLC3A1*	c.658+2C>T /c.1139G>A/ c.1413_*7delGATGTCGG	3180.1	13.5	41.5
418	female	55	6	-	-	-	-	unique	*SLC3A1*	c.745G>A	3297.8	5.1	12.3
420	female	35	8	-	-	-	-	unique	*SLC7A9* het	c.658+2C>T / c.745G>A /c.1139G>A/ c.1413_*7delGATGTCGG	1243.0	4.8	13.9
421	female	53	12	1	-	1	0.17	every 5 years	*SLC3A1*	c.658+2C>T /c.1139G>A/ c.1413_*7delGATGTCGG	3186.9	9.7	21.6

ID	Sex	Age at analysis	Y. of follow-up	Number of			Interventions per year	Lithiasic episodes	Affected gene	Variants in AGT1	Cystine (µmol/g Cre)	Aspartate (µmol /g Cre)	Glutamate (µmol /g Cre)
				ESWL	URS	PCNL							
422	male	41	7	6	-	4	1.38	every year	*SLC3A1*	c.658+2C>T /c.1139G>A/ c.1413_*7delGATGTCGG	2216.0	5.5	9.9
423	male	22	5	1	-	3	0.83	every year	*SLC3A1*	c.745G>A	2078.2	4.5	9.1
424	female	62	12	2	-	0	0.16	every 5 years	*SLC3A1*	-	2617.1	11.4	14.4
425	male	79	3	-	-	-	-	unique	*SLC3A1*	c.658+2C>T /c.1139G>A/ c.1413_*7delGATGTCGG	1532.6	8.5	13.5
426	male	40	5	-	-	3	0.61	every 2 years	*SLC3A1 & SLC7A9*	c.745G>A	3229.1	10.6	20.6
427	female	39	8	-	2	1	0.37	every 2 years	*SLC7A9*	c.658+2C>T/c.1355T>C	1689.2	2.0	8.7
428	male	48	5	-	-	-	-	unique	*SLC3A1*	c.658+2C>T /c.1139G>A/ c.1413_*7delGATGTCGG	2470.3	2.4	11.2
429	male	52	6	-	-	1	0.16	every 2 years	*SLC3A1*	c.745G>A	2233.4	5.3	14.2

Reference levels of amino acid excretion obtained in healthy subjects are: Cystine ≈ 15-150 µmol/g Cre, Asp ≈ 0-100 µmol/g Cre and Glutamate ≈ 0-100 µmol/g Cre. Interventions per year is an average of the sum of interventions per year of follow-up. In lithiasis episodes, unique means than a single lithiasis episode was detected during the follow-up. Y= years, ESWL = extracorporeal shockwave lithotripsy, URS = ureteroscopy, PCNL = percutaneous nephrolithotomy, Cre = creatinine.

Regarding the *SLC7A13* gene analysis, 6 variants were found in heterozygosis: the three already described above (c.745G>A, c.1139G>A and c.1355T>C), two with high gnomAD (Karczewski et al., 2020) allele frequency and unknown impact, and one, with low gnomAD allele frequency and classified by Polyphen2 as probably damaging (**Table 31**). As the c.1413_*7delGATGTCGG deletion starts at the last nucleotide of the last exon of *SLC7A13* and it has been considered as a nonpathological polymorphism (Olschok et al., 2018), and high allele frequency was observed in the intronic variant c.658+2C>T, both variants were considered as non-damaging. The already studied variant, c.745G>A, was the most frequent in our cohort being found in 9 patients. Its allele frequency in normal population is high but it was higher in our new cystinuric patient's cohort (0.117 vs. 0.25). However, in all cases the c.745G>A variant was found in heterozygosis.

Table 31. SLC7A13 variants detected by sanger sequencing in the 18 new cystinuric patients

***SLC7A13* variant**	**AGT1 change**	**Location**	**Nº of alleles found**	**Polyphen2 score**	**gnomAD Allele Frequency**
c.658+2C>T		intronic	8		0.351
c.745G>A	p.Val249Met	Exon 1	9	Damaging	0.112
c.988C>T	p.Leu330Phe	Exon 3	1	Damaging	0.021
c.1139G>A	p.Arg380Lys	Exon 3	6	Benign	0.181
c.1355T>C	p.Met452Thr	Exon 4	2	Benign	0.140
c.1413_*7delGATGTCGG	p.Ter471fs	Exon 4	5		0.181

All variants were found in heterozygosis.

As mentioned above, only 2 patients did not presented mutations in *SLC3A1*: the 420 and the 427, in which *SLC7A13* variations could be evaluated. The patient 420 had an unexplained cystinuria allele as only a missense mutation was detected in *SLC7A9* in heterozygosis (**Table 29**). When analyzing her *SLC7A13* gene, four variants were detected: the predicted as damaging c.745G>A and three predicted as non-damaging

(c.658+2C>T, c.1139G>A and c.1413_*7delGATGTCGG) (**Table 29**). Her clinical history revealed that only suffered one episode of cystine lithiasis during 8 years of follow-up and no clinical interventions were needed (**Table 30**). In addition, her urinary levels of aspartate and glutamate did not show significant differences comparing to the other patients (**Table 30**). The patient 427, with the two *SLC7A9* alleles affected and carrying two non-damaging variants in *SLC7A13* (c.658+2C>T and c.1355T>C), showed a slightly lower levels of aspartate and glutamate excretion compared to the cohort average, although her cystine levels and stone episodes recurrence did not differ from the cohort average (**Table 30**). As only in two additional patients *SLC7A13* variations could be analyzed, which showed a mild progression of the disease during the follow-up and similar levels of cystine, aspartate and glutamate excretion, no evidence of the role of *SLC7A13* variants in cystinuria could be inferred.

As *SLC3A1* mutations induce the impairment of AGT1/rBAT transporter assembly and function, a deeper study of *SLC7A13* variants on type A cystinuric patients was not performed. In addition, the different variants were observed in patients with high recurrence rate and unique stone episode during the follow-up (**Table 30**). However, because of its particularity, the patient 416 should be mentioned. This patient showed the lowest urinary cystine levels and the highest of aspartate and glutamate (**Table 30**). Besides to a homozygous mutation in *SLC3A1*, this patient has both pathological *SLC7A13* variants (c.745G>A and c.988C>T) but the results suggest a gain of function of the transporter, probably related to c.988C>T variant, as no such increased was observed in other c.745G>A carriers. In addition, this patient showed a unique lithiasis episode and a unique clinical intervention during the 11 years of follow-up, indicating a good disease progression. This finding will be further discussed in the discussion section.

In summary, after screening *SLC7A13* gene in 26 cystinuria patients, 9 of them with only one *SLC7A9* allele explained or without any genetic variant found related to cystinuria, no strong evidence of its causal effect on cystinuria or disease progression could be inferred. However, the lack of enough samples of type B cystinuric patients

and the absence of patients with homozygous variants in *SLC7A13* gene, made these results preliminary.

4.2. CHAPTER II: Transcriptome analysis to identify cystinuria modulating factors. Description of mitochondrial dysfunction in the *Slc7a9*$^{-/-}$ cystinuria mouse model.

It has been more than two decades since it was described that cystinuria is caused by mutations in *SLC3A1* and *SLC7A9* genes. During these years, cystinuria animal models have been generated to study the molecular bases of the diseases and to propose new therapeutic approaches to improve patients quality of life. It is well known, that the hyperexcretion of cystine is the main condition for cystine stone formation, but although the severity of *SLC3A1* and *SLC7A9* mutations correlates with the level of amino acids hyperexcretion, it does not correlate to cystine lithiasis episodes (Dello Strologo et al., 2002; Font et al., 2001). In this chapter, a kidney gene expression analysis of the *Slc7a9*$^{-/-}$ mouse model is presented with the aim to identify new genes and pathways that could contribute to understand differences in the progression and severity of this disease.

4.2.1. RNA-seq analysis revealed an impairment in oxidative phosphorylation and focal adhesion pathways in the kidneys of the *Slc7a9*$^{-/-}$ mouse model

An RNA-seq analysis was performed on kidneys from 4-month-old WT and *Slc7a9*$^{-/-}$ mice of both sexes. The Principal Component Analysis (PCA) revealed the importance of sex in kidney gene expression (**Figure 17A-B**). For this reason, two comparisons were performed according to sex and genotype: WT vs. *Slc7a9*$^{-/-}$ in both male and female mice, and then, common differentially expressed genes (DEGs) obtained from both comparisons were crossed to obtain the final list of DEGs. Out of 26,390 transcripts detected, 31 were upregulated and 109 were downregulated in both *Slc7a9*$^{-/-}$ male and female mice (Log2 FC ±0.20 and adjusted p-value ≤ 0.05) (**Figure 18 and Supp Table 1**). As expected, the most downregulated gene observed in both male and female was *Slc7a9* (**Supp Table 1**). For the functional annotation of the DEGs, an enrichment analysis of the biological pathways (based on KEGG Database) related to the 140 DEGs found was performed using the DAVID (v6.8) online server. The KEGG enrichment analysis revealed an impairment in oxidative phosphorylation

and focal adhesion processes among others (**Table 32**). In both pathways, all the DEGs detected were significantly downregulated (**Supp Table 1**).

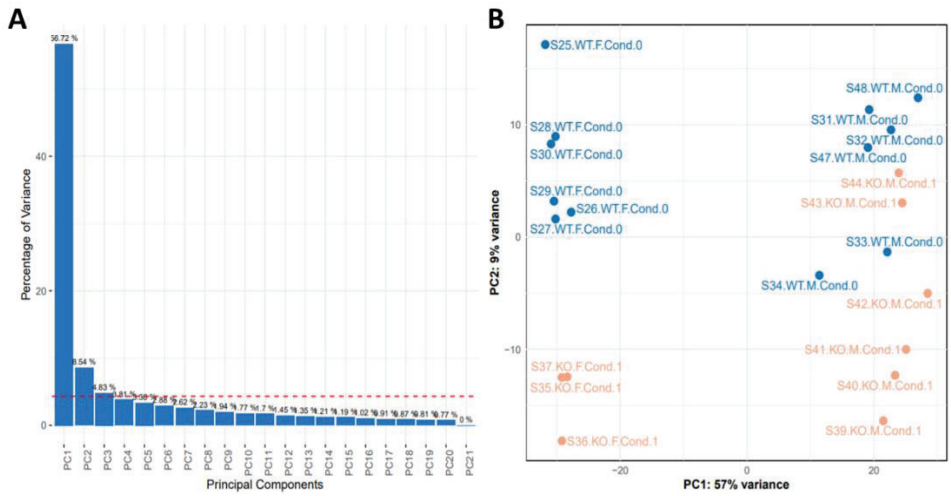

Figure 17. Graphic representation of the Principal Component Analysis (PCA)

(A) *Percentage of variance attributed to each component.* ***(B)*** *Distribution of samples according to PC1 (x axis) and PC2 (y axis). WT F Cond 0 = WT female, WT M Cond 0 = WT male, KO F Cond 1 = Slc7a9$^{-/-}$ female, KO M Cond 1 = Slc7a9$^{-/-}$ male.*

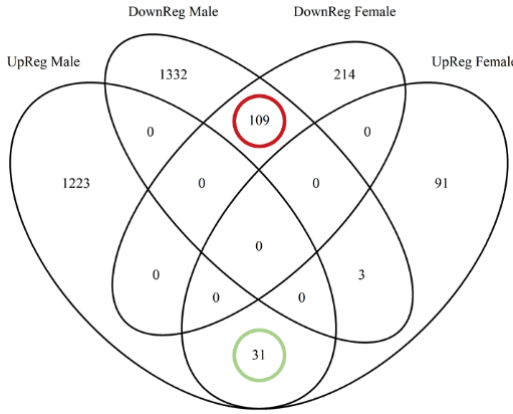

Figure 18. Venn Diagram of common DEGs detected in both male and female Slc7a9$^{-/-}$ mice

The red circle includes the number of genes downregulated in both male and female mice, and the green circle, the genes upregulated in both groups. UpReg = genes upregulated in Slc7a9$^{-/-}$ mice, DownReg = genes downregulated in Slc7a9$^{-/-}$ mice.

Table 32. Pathway enrichment analysis

KEGG PATHWAY	Nº of genes	p-value	Benjamini Test	Genes
Oxidative phosphorylation	12	2.70E-09	3.70E-07	*mt-Atp6, Ndufa6, Ndufb11, mt-Nd1, mt-Nd2, mt-Nd3, mt-Nd4, mt-Nd4l, mt-Nd5, mt-Cytb, mt-Cox2, mt-Cox3*
Parkinson's disease	12	5.70E-09	3.90E-07	*mt-Atp6, Ndufa6, Ndufb11, mt-Nd1, mt-Nd2, mt-Nd3, mt-Nd4, mt-Nd4l, mt-Nd5, mt-Cytb, mt-Cox2, mt-Cox3*
Focal adhesion	13	1.70E-08	7.50E-07	*Col1a2, Col3a1, Col5a1, Col6a1, Col6a2, Itga9, Itgb3, Kdr, Mylk, Pik3cd, Pdgfrb, Tnxb, Thbs*
ECM-receptor interaction	9	1.70E-07	5.60E-06	*Col1a2, Col3a1, Col5a1, Col6a1, Col6a2, Itga9, Itgb3, Tnxb, Thbs*
PI3K-Akt signaling pathway	13	5.00E-06	1.40E-04	*Col1a2, Col3a1, Col5a1, Col6a1, Col6a2, Itga9, Itgb3, Kdr, Mylk, Pik3cd, Pdgfrb, Tnxb, Thbs*
Alzheimer's disease	8	2.40E-04	5.50E-03	*mt-Atp6, Ndufa6, Ndufb11, mt-Cytb, mt-Cox2, mt-Cox3, Lrp1, Ppp3ca*
Platelet activation	7	3.20E-04	6.10E-03	*Col1a2, Col3a1, Col5a1, Gucy1a3, Itgb3, Mylk, Pik3cd*
Protein digestion and absorption	6	3.90E-04	6.50E-03	*Col1a2, Col3a1, Col5a1, Slc7a9*

Nº of genes means number of DEGs detected related to each pathway.

4.2.2. Oxidative phosphorylation impairment in the kidneys of the *Slc7a9*$^{-/-}$ mouse model

As oxidative phosphorylation (OXPHOS) was the main DEG enriched pathway, further analyses were performed to evaluate the gene expression of the whole pathway, validate RNA-seq results and to study its physiological consequences in cystinuria.

4.2.2.1. OXPHOS gene expression analysis in the Slc7a9$^{-/-}$ mouse model

RNA-seq analysis showed that about 9 % (12 out of 139 genes annotated in the KEGG Pathway Database) of genes related to OXPHOS were downregulated in both *Slc7a9*$^{-/-}$ male and female mice. Next steps were focused on identifying the role of those genes in the pathway and to analyze the expression of the other genes annotated in the pathway.

Of the 12 DEGs detected, 10 corresponded to mtDNA encoded structural subunit genes of the electron transport chain (ETC) (*mt-Atp6, mt-Nd1, mt-Nd2, mt-Nd3, mt-Nd4, mt-Nd4l, mt-Nd5, mt-Cytb, mt-Cox2, mt-Cox3*) and 2, to nuclear encoded structural subunit genes (*Ndufa6* and *Ndufb11*). Thus, each ETC complex had at least the 50 % of its mtDNA encoded structural subunit genes downregulated (**Table 33**), suggesting the impairment of the whole system as mtDNA encoded subunits are essential for its function. In addition, above 70 % of all mtDNA encoded structural subunit genes were downregulated in both *Slc7a9*$^{-/-}$ male and female mice. To discard that these results could be a consequence of mtDNA disruption, the expression of other genes encoded by the mtDNA and key genes that regulate mtDNA expression were compared between WT and *Slc7a9*$^{-/-}$ mice. No differences were observed in mt-tRNA and mt-rRNA either in male or in female (**Table 34**). Concerning mtDNA regulation by nuclear encoded genes, expression of the key genes of mtDNA replication (*Twnk*), maintenance (*Tfam*), transcription (*Polrmt*), RNA stability (*Lrpprc*) and translation (*Mterf4*) was evaluated and not significant differences were found (**Table 35**). In addition, mitochondrial content in *Slc7a9*$^{-/-}$ mice was assessed by quantifying the activity of the mitochondrial enzyme Citrate Synthase (CS) (**Figure 19**). In summary, no differences were observed in mtDNA expression and regulation, and mitochondrial content, suggesting a particular impairment of the ETC gene expression.

Table 33. Gene expression of ETC mtDNA encoded structural subunits in Slc7a9$^{-/-}$ mice expressed as a Log2 Fold Change to WT mice expression

Symbol	Gene name	Log2FC M	padj M	Log2FC F	padj F
mt-Nd1	NADH dehydrogenase subunit 1	**-0.41**	**0.00**	**-0.49**	**0.00**
mt-Nd2	NADH dehydrogenase subunit 2	**-0.27**	**0.03**	**-0.56**	**0.00**
mt-Nd3	NADH dehydrogenase subunit 3	**-0.44**	**0.00**	**-0.62**	**0.00**
mt-Nd4	NADH dehydrogenase subunit 4	**-0.36**	**0.00**	**-0.56**	**0.00**
mt-Nd4l	NADH dehydrogenase subunit 4L	**-0.27**	**0.01**	**-0.39**	**0.01**
mt-Nd5	NADH dehydrogenase subunit 5	**-0.29**	**0.02**	**-0.56**	**0.00**
mt-Nd6	NADH dehydrogenase subunit 6	0.04	0.71	-0.02	0.55
mt-Cyba	cytochrome b-245, alpha polypeptide	-**0.22**	**0.01**	-0.03	0.85
mt-Cybb	cytochrome b-245, beta polypeptide	0.00	0.97	**-0.51**	**0.06**
mt-Cox1	cytochrome c oxidase subunit I	-0.08	0.44	**-0.4**	**0.01**
mt-Cox2	cytochrome c oxidase subunit II	-**0.43**	**0.00**	**-0.38**	**0.04**
mt-Cox3	cytochrome c oxidase subunit III	-**0.35**	**0.00**	**-0.4**	**0.01**
mt-Atp6	ATP synthase F0 subunit 6	-**0.49**	**0.00**	-**0.48**	**0.00**
mt-Atp8	ATP synthase F0 subunit 8	-0.06	0.44	-0.02	0.5

M = male, F = females, padj = p-value adjusted.

Table 34. Gene expression of mt-tRNA and mt-rRNA in Slc7a9$^{-/-}$ mice expressed as a Log2 Fold Change to WT mice expression

Symbol	Gene name	Log2FC M	padj M	Log2FC F	padj F
mt-Aars2	alanyl-tRNA synthetase 2 mitochondrial	-**0.32**	**0.00**	0.00	0.99
mt-Cars2	cysteinyl-tRNA synthetase 2 mitochondrial	-0.18	0.00	-0.06	0.48
mt-Dars2	aspartyl-tRNA synthetase 2 mitochondrial	0.12	0.09	0.04	0.77
mt-Ears2	glutamyl-tRNA synthetase 2 mitochondrial	0.08	0.31	-0.01	0.97
mt-Fars2	phenylalanine-tRNA synthetase 2 mitochondrial	-0.04	0.66	-0.02	0.90

Symbol	Gene name	Log2FC M	padj M	Log2FC F	padj F
mt-Hars2	histidyl-tRNA synthetase 2 mitochondrial	0.03	0.77	0.02	0.88
mt-Iars2	isoleucine-tRNA synthetase 2 mitochondrial	0.14	0.06	0.04	0.74
mt-Lars2	leucyl-tRNA synthetase 2 mitochondrial	0.00	0.95	**1.37**	0.06
mt-Mars2	methionine-tRNA synthetase 2 mitochondrial	0.06	0.52	0.05	0.62
mt-Nars2	asparaginyl-tRNA synthetase 2 mitochondrial	0.17	0.08	0.00	1.00
mt-Pars2	prolyl-tRNA synthetase 2 mitochondrial	-0.12	0.25	0.02	0.88
mt-Rars2	arginyl-tRNA synthetase 2 mitochondrial	0.01	0.91	0.00	0.99
mt-Tars2	threonyl-tRNA synthetase 2 mitochondrial	-0.16	0.01	-0.03	0.78
mt-Vars2	valyl-tRNA synthetase 2 mitochondrial	-0.10	0.25	0.04	0.77
mt-Yars2	tyrosyl-tRNA synthetase 2 mitochondrial	0.12	0.18	0.06	0.54
mt-Wars2	tryptophanyl tRNA synthetase 2 mitochondrial	0.07	0.42	0.03	0.80
mt-Rnr1	Mitochondrially encoded 12S ribosomal RNA	-0.03	0.78	-0.01	0.80
mt-Rnr2	Mitochondrially encoded 16S ribosomal RNA	0.00	0.97	-0.02	0.73

M = male, F = females, padj = p-value adjusted.

Table 35. Gene expression of nuclear encoded mtDNA regulators in Slc7a9$^{-/-}$ mice expressed as a Log2 Fold Change to WT mice expression

Symbol	Gene name	Log2FC M	padj M	Log2FC F	padj F
Twnk	twinkle mtDNA helicase	0.04	0.69	0.00	1.00
Tfam	transcription factor A, mitochondrial	0.14	0.05	-0.01	0.97
Polrmt	polymerase (RNA) mitochondrial	-0.11	0.24	0.10	0.34
Lrpprc	leucine-rich PPR-motif containing	0.04	0.61	0.02	0.91
Mterf4	mitochondrial transcription termination factor 4	0.04	0.54	-0.03	0.78

M = male, F = females, padj = p-value adjusted.

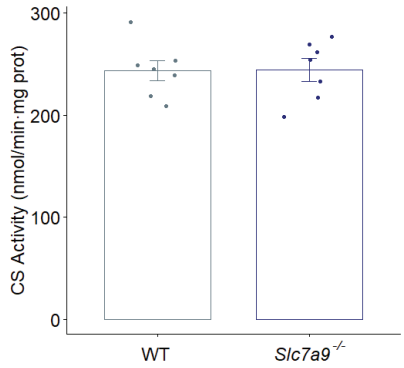

Figure 19. Assessment of kidney citrate synthase activity in WT and Slc7a9$^{-/-}$ mice to determine mitochondrial content

Determination of kidney mitochondrial citrate synthase (CS) activity (nmol/min per mg of protein) in WT and Slc7a9$^{-/-}$ mice. Data are expressed as mean ± SEM.

Once analyzed the gene expression of ETC mtDNA encoded structural subunits, gene expression of ETC nuclear encoded structural subunits and assembly factors was assessed. **Table 36** summarizes the percentage of DEGs detected in each complex by sex in the RNA-seq (raw data is available in the **Supp Table 2**). Complexes I, III and IV showed a higher number of DEGs in both male and female mice. Complex II subunits, fully encoded by nuclear DNA, showed no impairment of its structural subunit expression. Most DEGs detected were found downregulated and the only 2 upregulated, *Ndufaf4* in males and *Cox15,* in both males and females, correspond to assembly factors of complex I and complex IV, respectively (**Supp Table 2**). The increase in assembly factors expression as *Cox15* has been described as a compensatory response to the decrease in ETC expression (Kühl et al., 2017). The nuclear encoded structural subunits *Ndufa6* and *Ndufb11,* and the assembly factor Cep89, were the only ones found downregulated in both male and female mice.

Table 36. Percentage of differentially expressed ETC nuclear encoded structural subunits and assembly factors of each complex by sex

ETC Complex	Ratio of DEGs of ETC Nuclear encoded structural subunits				Ratio of DEGs of ETC assembly factors				Total % of DEGs	
	Male	%	Female	%	Male	%	Female	%	Male	Female
CI	10/37	**27%**	4/37	**11%**	3/14	**21%**	0/14	**0%**	**25%**	**8%**
CII	0/4	**0%**	0/4	**0%**	1/4	**25%**	0/4	**0%**	**13%**	**0%**
CIII	2/9	**22%**	1/9	**11%**	1/7	**14%**	0/7	**0%**	**19%**	**6%**
CIV	4/15	**27%**	3/5	**20%**	4/25	**15%**	2/25	**7%**	**20%**	**13%**
ATP synthase	2/13	**15%**	0/13	**0%**	0/3	**0%**	0/3	**0%**	**13%**	**0%**

4.2.2.2. Mitochondrial function defects in the Slc7a9$^{-/-}$ mouse model

To evaluate the physiologic effect of the genetic downregulation of the ETC subunits, four approaches were performed. First, as complex I subunits were the main downregulated at mitochondrial and nuclear level, the NAD^+/NADH ratio was determined in the kidneys of WT and *Slc7a9*$^{-/-}$ mice. A decrease in the NAD^+/NADH ratio was detected in *Slc7a9*$^{-/-}$ mice, caused by an increase in intracellular NADH content (**Figure 20A**). Then, mitochondrial enzymatic activity of complex II and IV was assessed in kidney homogenates and confirmed the results obtained in the transcriptomic analysis. While no differences were observed regarding the activity of complex II, complex IV activity was significantly lower in *Slc7a9*$^{-/-}$ mice compared to WT ones (**Figure 20B**). As NADH is the substrate of complex I and its accumulation could be attributed to a chronic impairment of this complex, and a 25 % reduction of complex IV activity was observed in *Slc7a9*$^{-/-}$ mice, these data demonstrate an ETC impairment in the cystinuric mouse model. To further study the ETC defect, a high-resolution respirometry experiment was performed with fresh kidney tissue using the Oroboros technology. No differences were observed in leak state (Malate + Pyruvate),

complex I activation (ADP + Glutamate) and complex II activation (Succinate) (**Figure 20C**). However, when inducing uncoupled respiration adding FCCP, a tendency on lower maximal mitochondrial respiration capacity was observed in *Slc7a9*$^{-/-}$ mice. And then, when rotenone was added to inhibit complex I, a significant lower respiration was detected in *Slc7a9*$^{-/-}$ mice suggesting the dependence on complex I on maintaining the maximal mitochondrial respiration in the cystinuric mouse model. Collectively, these data evidence an impairment on mitochondrial ETC that although at basal level does not alter physiological respiration, it does affect the maximal mitochondrial respiration capacity in kidneys from 4-month-old *Slc7a9*$^{-/-}$ mice.

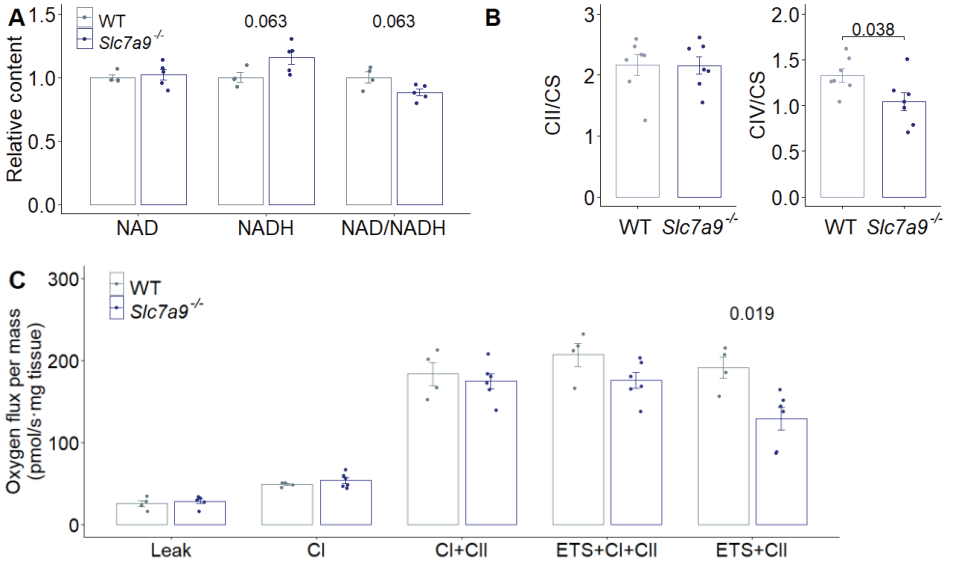

Figure 20. Validation of mitochondrial defect in the kidneys of Slc7a9$^{-/-}$ mice

(A) *NAD^+ and NADH levels, and their ratio NAD^+/NADH, in kidneys of WT and Slc7a9$^{-/-}$ mice. NAD^+ and NADH levels were normalized by total kidney protein content and data are represented as fold-change to WT mice.* ***(B)*** *Determination of kidney mitochondrial succinate dehydrogenase (CII) and cytochrome c oxidase (CIV) activity (nmol/min per mg of protein) in WT and Slc7a9$^{-/-}$ mice. Data is shown as a ratio to citrate synthase (CS) activity.* ***(C)*** *Ex vivo mitochondrial respiration of saponin permeabilized kidneys of WT and Slc7a9$^{-/-}$ mice (CI = Complex I, CII = Complex II, ETS = Electronic Transfer System). Oxygen flux was normalized by mg of kidney tissue. Data are expressed as mean ± SEM and p-value is showed at the top after Mann-Whitney-Wilcoxon test.*

Finally, intracellular metabolites of the TCA cycle were assessed as this cycle provides essential substrates for the ETC. A depletion of intracellular citrate content and lower levels of fumarate were observed in *Slc7a9*$^{-/-}$ mice kidneys (**Figure 21A**). To further understand these intracellular variations, gene expression of the enzymes related to the citrate and fumarate synthesis were analyzed in the RNA-seq and validated by qPCR (**Figure 21B-C**). Pyruvate carboxylase (*Pcx*) was found downregulated in *Slc7a9*$^{-/-}$ male mice which implies a lower repletion of oxalacetate to the TCA cycle that could partially explain the depletion found in citrate, as no differences in expression in pyruvate dehydrogenase (*Pdha*) and *Cs* were observed. In addition, the mitochondrial phosphoenolpyruvate carboxykinase (*Pck2* or *Pepck*), which converts oxalacetate to phosphenolpyruvate, was also found downregulated in the RNA-seq analysis (Log2FC -0.28 and p-adj 0.002) suggesting an impairment in oxalacetate levels. Nevertheless, oxalacetate and pyruvate levels must be assessed to infer the impact of *Pcx* downregulation on citrate depletion.

In summary, these data indicate an impairment on mitochondrial function in *Slc7a9*$^{-/-}$ mice as in both OXPHOS system and TCA cycle genetic and functional alterations have been observed.

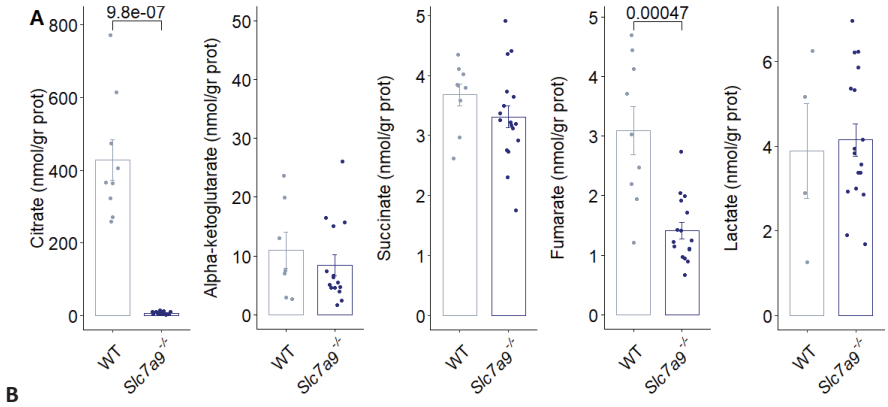

Symbol	Description	Log2FC Male	padj Male	Log2FC Female	padj Female
Pcx	pyruvate carboxylase	**-0.41**	**0.00**	-0.1	0.04
Pdha1	pyruvate dehydrogenase E1 alpha 1	0.12	0.03	-0.02	0.52
Cs	citrate synthase	0.02	0.78	0.04	0.31
Sdha	succinate dehydrogenase complex, subunit A, flavoprotein	0.01	0.93	-0.03	0.82
Sdhb	succinate dehydrogenase complex, subunit B, iron sulfur (Ip)	-0.19	0.01	-0.19	0.07
Sdhc	succinate dehydrogenase complex, subunit C	-0.08	0.21	-0.04	0.71
Sdhd	succinate dehydrogenase complex, subunit D	-0.04	0.56	-0.11	0.20

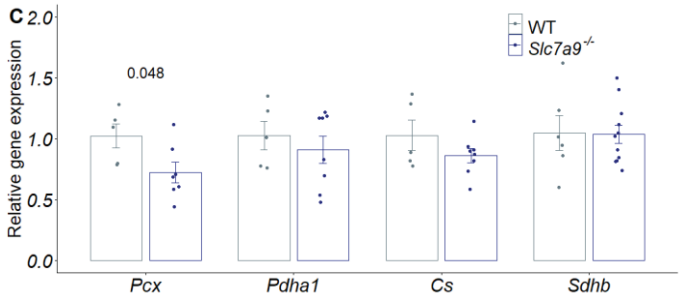

Figure 21. TCA cycle metabolite levels and enzyme gene expression in kidneys of WT and Slc7a9$^{-/-}$ mice

(A) *Intracellular kidney content of metabolites related to TCA cycle in WT and Slc7a9$^{-/-}$ mice. Metabolite levels were normalized by total kidney protein content.* ***(B)*** *Log2 Fold Change of Slc7a9$^{-/-}$ to WT gene expression of citrate and fumarate related enzymes in both male and female mice obtained in the RNA-seq analysis.* ***(C)*** *Validation of gene expression differences observed in the RNA-seq analysis by qPCR. Gene expression levels were normalized relative to Actb and data are represented as fold-change to WT mice. Data are expressed as mean ± SEM and p-value is showed at the top after Mann-Whitney-Wilcoxon test.*

4.3. CHAPTER III: Study of L-Ergothioneine, the main substrate of OCTN1, as a therapeutical target for cystinuria.

4.3.1. Preliminary studies

4.3.1.1. OCTN1 and L-Ergothioneine as candidates

Previous analysis of whole genome microsatellites and mRNA expression comparing *Slc7a9*$^{-/-}$ non-stone and stone former mice in mixed background, lead to identify *Slc22a4* as a possible modulating gene of cystine lithiasis. In her thesis, Dr. Espino described that *Slc22a4* mRNA expression was decreased by 50 % in lithiasic mice when comparing to non-lithiasic ones, at 3 months of age (Espino, 2012). This gene encodes an organic cation and zwitterion transporter, OCTN1, highly expressed in kidney BBM. As its main substrate, L-Ergothioneine (L-Erg), is a thiol compound with antioxidant capacities, and thiol-agents are used as treatment of cystine lithiasis, L-Erg was suggested as a candidate molecule for the treatment of cystinuria. In this thesis chapter, the results obtained after treating cystinuria mouse models with L-Erg and the attempt to understand its mechanism of action are presented. Before starting to describe the main results obtained in this thesis, two preliminary and yet not published experiments are briefly explained: the generation and lithiasis characterization of the *Slc7a9*$^{-/-}$*Slc22a4*$^{-/-}$ mouse model and a one-month treatment with L-Erg to determine the dose to administrate in further experiments.

4.3.1.2. Slc7a9$^{-/-}$*Slc22a4*$^{-/-}$ *mouse model generation and lithiasis characterization*

Before the start of this thesis, *Slc7a9*$^{-/-}$ and *Slc22a4*$^{-/-}$ mouse models were crossed to obtain the *Slc7a9*$^{-/-}$*Slc22a4*$^{-/-}$ double mutant mouse (dKO), which is a cystinuria type B mouse model lacking the L-Erg transporter. An 8-month follow-up of the rate of stone formation in *Slc7a9*$^{-/-}$*Slc22a4*$^{-/-}$ mice revealed that, when the L-Erg transporter is not expressed in cystinuria type B model, an increase in the rate stone former mice is observed (**Figure 22A-B**). Differences were more evident in 3-month-old than in 8-month-old mice, in both male and female, indicating an earlier onset of the disease

in the double mutant. These data evidenced the role of OCTN1, or its substrate L-Erg, modulating the lithiasic phenotype in the cystinuria type B model.

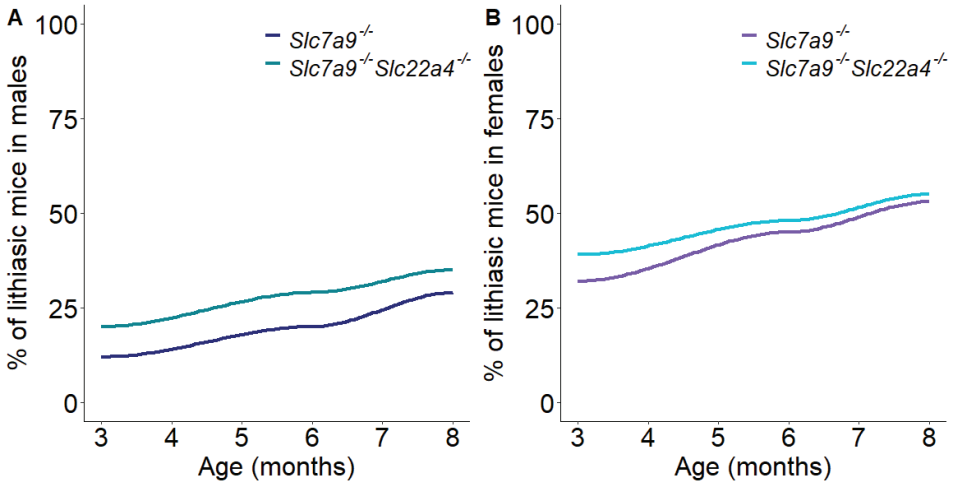

Figure 22. 8-month follow-up of the rate of stone formation in Slc7a9$^{-/-}$ and Slc7a9$^{-/-}$ Slc22a4$^{-/-}$ mouse models

*Comparison of **(A)** male and **(B)** female rates of stone formation between Slc7a9$^{-/-}$ and Slc7a9$^{-/-}$ Slc22a4$^{-/-}$ mouse models up to 8-months of age. N= 57-75 per group.*

4.3.1.3. Treatment dose determination

Also prior to this thesis, a 1-month L-Erg treatment was performed in 3-month-old mice to evaluate the intake and excretion of two different L-Erg doses. Thus, drinking water of treated mice were prepared containing a L-Erg concentration of 15 or 60 mg/L. After 1-month treatment, in none of the tested concentrations side-effects or significant variations of metabolic parameters were observed, and L-Erg concentration in urine increased 3-fold and 175-fold after administering 15 mg/L and 60 mg/L, respectively. As after administering L-Erg at 60 mg/L a higher urinary L-Erg concentration was detected and no side-effects were reported, this was the dose selected to perform further experiments. The concentration of 60 mg/mL of L-Erg in the drinking water corresponded to a dose of 13.6 ± 1.6 mg/kg/day which Human Equivalent Dose (HED) is 66 ± 8 mg/day for a 60 kg adult (Nair & Jacob, 2016).

4.3.2. Effect of L-Erg treatment in lithiasis

4.3.2.1. Long-term L-Erg administration prevents cystine lithiasis events and delays its onset

Slc7a9$^{-/-}$ mouse model was chosen to evaluate the effect of L-Erg administration in cystine lithiasis as it has been described as a valid cystinuria model for antilithiasic pharmacological studies (Font-Llitjós et al., 2007). As cystinuric patients have an early onset of stone episodes (75 % at childhood-adolescence), the first approach was the administration of L-Erg as a preventive treatment since weaning (prior to any stone formation) and up to 7-month-old. Stone onset and progression were examined monthly by X-ray imaging in both treated and control groups (**Figure 23A**). As mice weight significantly increases from weaning to 7-months of age and to have a better control of the L-Erg dose administrated, L-Erg concentration in the drinking water of treated mice was weekly adjusted per cage according to its mice weight and water intake means.

During the 6-month L-Erg treatment, the treated group showed a reduction of above 50 % in the rate of stone former mice (**Figure 23B**). In addition, through the monthly X-ray follow-up a 2-month delay on stone onset and growth evolution were observed in the treated group (**Figure 23C**). Moreover, at the end of the treatment, the post-mortem stone weight of the treated group was significantly lower (**Figure 23D**). As these results indicate that L-Erg could be a good preventive treatment for cystine lithiasis, further studies to understand its mechanism of action were performed.

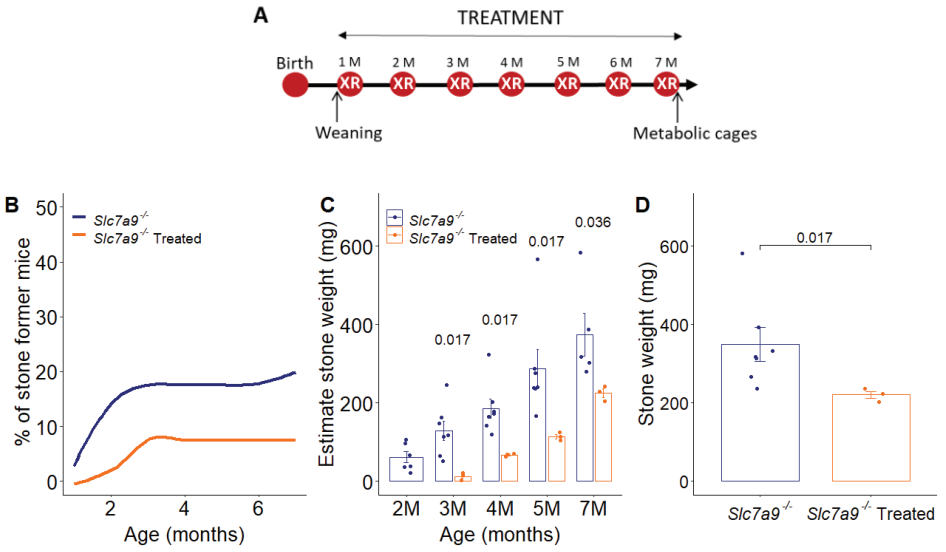

Figure 23. Long-term L-Erg treatment reduces and delays stone formation in the Slc7a9$^{-/-}$ mouse model

(A) *Timeline of L-Erg (16 mg/kg/day) preventing treatment since weaning and up to four months of age in Slc7a9$^{-/-}$ mice.* ***(B)*** *Evolution of stone former mice percentage in Slc7a9$^{-/-}$ groups. N = 40 per group.* ***(C)*** *Comparison of monthly stone weight evolution of Slc7a9$^{-/-}$ control and treated stone former mice. The stone weight follow-up was estimated by X-ray images.* ***(D)*** *Post-mortem stone weight of Slc7a9$^{-/-}$ control and treated stone former mice after L-Erg treatment. Data are expressed as mean ± SEM and p-value is showed at the top after Mann-Whitney-Wilcoxon test. M = Month of age, XR= X-ray.*

4.3.2.2. L-Erg has no effect on cystine stone growth rate

To further investigated the potential effect of L-Erg on cystine lithiasis, 3-month-old mice with an already formed stone were treated during 3 months by supplementing its drinking water with L-Erg to achieve a dose of 16 mg/kg/day. Stone progression was examined monthly by X-ray imaging in both treated and control group (**Figure 24A**). No differences neither in the post-mortem stone dry weight (**Figure 24B**) nor in the stone growth rate (**Figure 24C**) were observed after the 3-month treatment, indicating that L-Erg has no effect once the stone is formed.

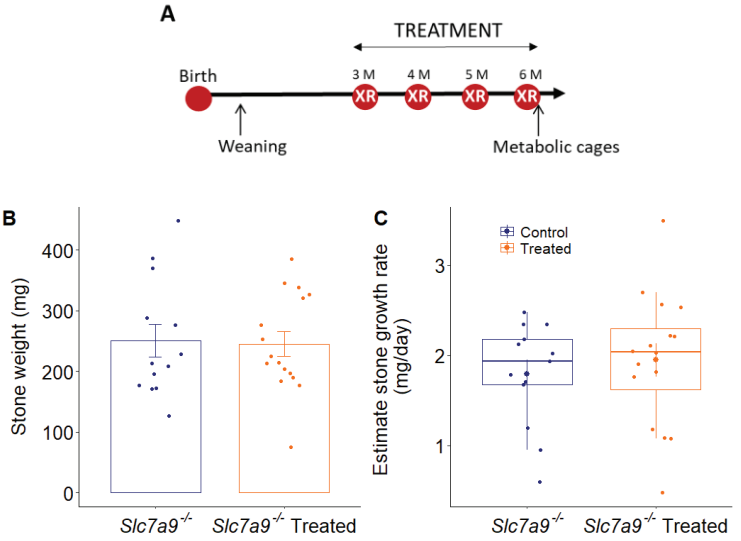

Figure 24. L-Erg treatment has no effect on cystine stone growth in adult lithiasic mice

(A) *Timeline of L-Erg (16 mg/kg/day) treatment in 3-month-old Slc7a9$^{-/-}$ mice lithiasic mice.* ***(B)*** *Post-mortem stone weight of Slc7a9$^{-/-}$control and treated mice at the end of the treatment.* ***(C)*** *Estimate stone growth rate during the 3-month follow-up of Slc7a9$^{-/-}$control and treated mice was calculated as the difference of the estimate stone weight at the first (3-month-old) and the last (6-month-old) X-ray images per days of follow-up. Data are expressed as mean ± SEM. M = Month of age, XR= X-ray.*

4.3.3. Approaches to understand long-term L-Erg treatment mechanism of action

4.3.3.1. Metabolic parameters are not affected after long-term L-Erg treatment

The first approach to study L-Erg mechanism of action was to evaluate metabolic parameters in treated mice. The last week of the 6-month treatment, mice were placed individually and for one week in metabolic cages to register its weigh, water intake and urine excretion. No significant changes were detected in mouse body weight and water intake (**Figure 25A-B**). However, treated male mice showed lower levels of urine excretion (**Figure 25C**). In addition, as cystine solubility is highly dependent on urinary pH, pH was measured in urine samples obtained from the metabolic cages. Urinary

pH was not significantly different in treated mice compared to untreated ones (**Figure 25D**). These results reveal that L-Erg is not acting as a diuretic or urinary alkalinization drug.

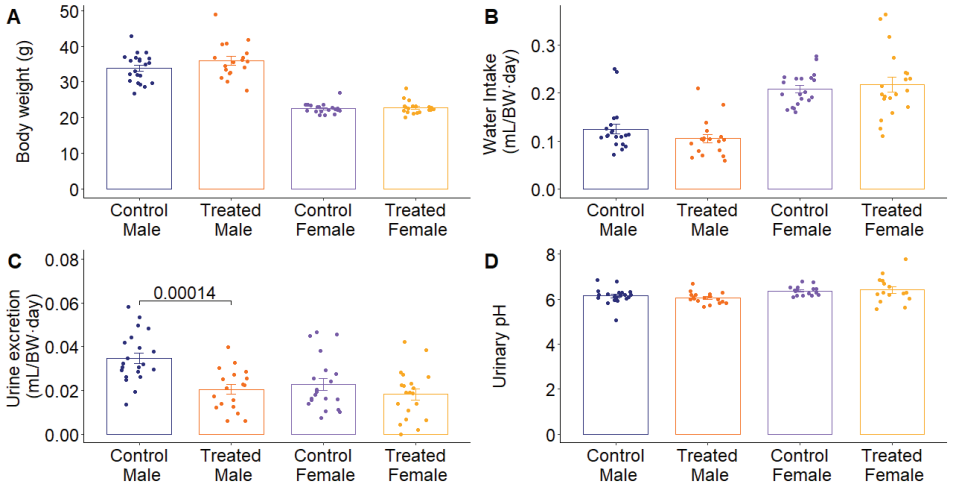

Figure 25. Long-term L-Erg treatment has no effect on physiological parameters

(A) *Mice body weight,* ***(B)*** *water intake,* ***(C)*** *urine excretion and* ***(D)*** *urinary pH by sex in control and L-Erg (16 mg/kg/day) treated groups. Values are expressed as mean ± SEM. p-value is shown at the top after Mann-Whitney-Wilcoxon test. BW = body weight.*

4.3.3.2. L-Erg does not act as a thiol-binding molecule

L-Erg is a thiol molecule that could act chelating cysteine in the urine. However, an *in vitro* assay combining different concentrations of L-Erg and cysteine at pH 7.2 showed that no L-Erg-cysteine heterodimers were formed at those conditions as were not detected by LC/MS-MS (previous thesis work in Dr. Nunes' group). But this assay was not performed reproducing urine conditions. However, after long-term L-Erg treatment, no differences in urinary cystine concentration were observed between treated and untreated mice, and both were highly increased when compared to WT mice (**Figure 26**). Thus, cystine supersaturation levels in treated urines indicate that L-Erg is not reducing cystine concentration and therefore, not binding cysteine.

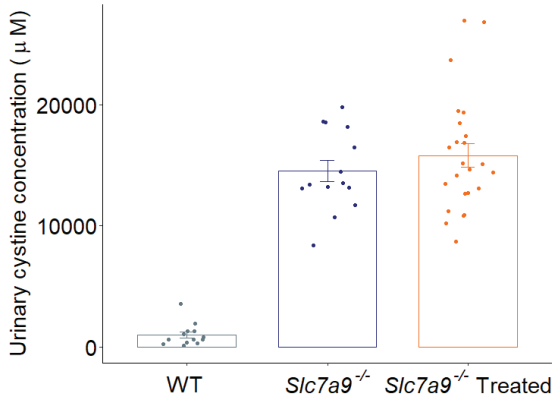

Figure 26. Long-term L-Erg treatment does not reduce urinary cystine concentration

Comparison of urinary cystine concentration (µM) in WT, Slc7a9$^{-/-}$ and Slc7a9$^{-/-}$ L-Erg (16 mg/kg/day) treated mice. Values are expressed as mean ± SEM.

4.3.3.3. Long-term L-Erg treatment increases cystine solubility in urine

As no differences in urinary cystine concentration were detected when compared treated and untreated mice but a lower stone formation rate was observed after preventive L-Erg treatment, the urinary cystine solubility was assessed both *ex vivo* and *in vitro* by a cystine precipitation assay. After adding a cystine supersaturated solution to untreated, treated and untreated *in vitro* supplemented with L-Erg (240 µM final urinary concentration) urines, cystine precipitation was found significantly lower in treated mice compared to both untreated and untreated L-Erg supplemented group (**Figure 27**). These results suggest that although treated mouse urines contained high amounts of cystine, the L-Erg treatment is reducing its precipitation which could explain the effect observed in stone formation. In addition, in the L-Erg *in vitro* supplemented urines no effect on cystine precipitation was observed, revealing an indirect effect of the L-Erg treatment.

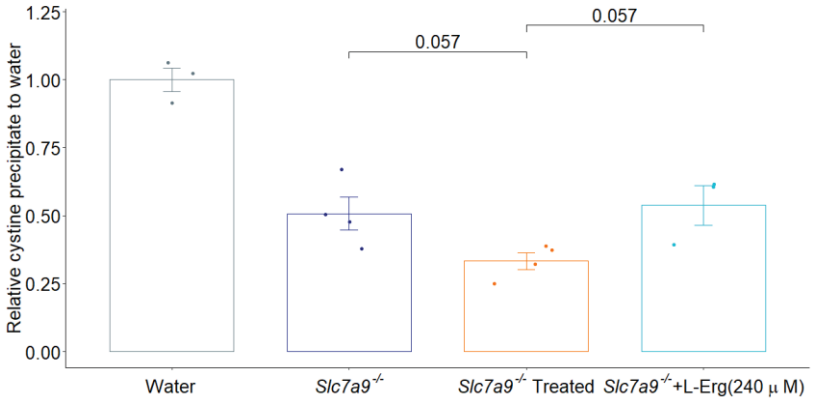

Figure 27. L-Erg treatment reduces cystine precipitation in urine

Cystine precipitate obtained after adding a supersaturated cystine solution. Experimental conditions were water, urine of Slc7a9$^{-/-}$ mice, urine of Slc7a9$^{-/-}$ L-Erg (16 mg/kg/day) treated mice and urine of Slc7a9$^{-/-}$ mice in vitro supplemented with L-Erg to obtain a final concentration of 240 μM. Values are expressed as mean ± SEM. p-value is shown at the top after Mann-Whitney-Wilcoxon test.

4.3.3.4. Stone morphology and elemental composition are not affected after L-Erg treatment

After observing that L-Erg treatment reduced cystine precipitation in urine, cystine stones removed during the necropsies were analyzed using a SEM coupled with an EDS detector. High resolution images obtained by SEM allowed to observe that the crystal hexagonal structure of cystine was not affected by L-Erg treatment, neither in the stone surface nor in the internal core of the stone (**Figure 28**). In the surface images, the hexagonal prismatic crystals were conserved as no corrosion signs were found (**Figure 28A-C**). In the core, the same pattern of stone cleavage (thin sheets) was observed in stones from untreated and treated mice after manually splitting the stone in two halves (**Figure 28B-D**). In addition, when analyzing elemental composition of both surface and core, stones from untreated and treated mice showed the same spectrum (**Figure 28E-H**). Cystine representative spectrum is composed by carbon, nitrogen, oxygen and sulfur, but in both treated and untreated mice aluminum was detected. To date, the presence of aluminum is cystine stones has

not been described. However, as aluminum was observed in all samples and there is no evidence that L-Erg can chelate aluminum, its detection does not seem relevant for this work. In summary, as neither stone morphology nor elemental composition was affected by L-Erg treatment, these results together with the reduction of cystine precipitation suggest that L-Erg is affecting cystine stone nucleation rather than aggregation or growth.

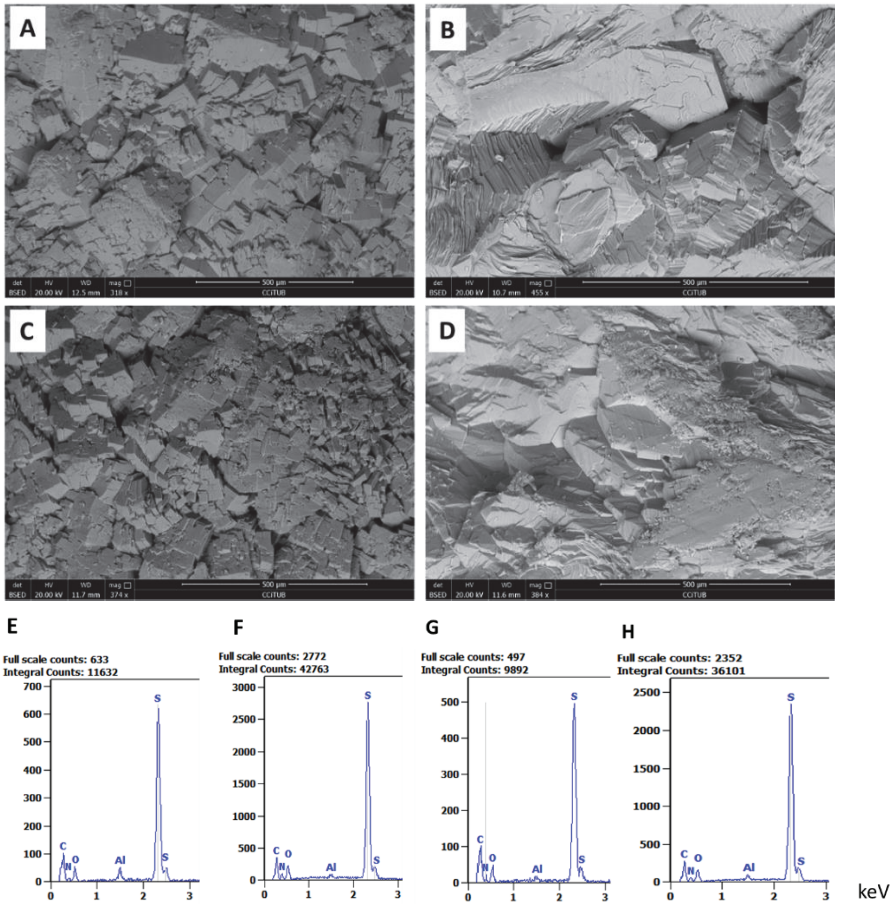

Figure 28. SEM images and elemental composition of cystine stones removed from the bladder of Slc7a9$^{-/-}$ and Slc7a9$^{-/-}$ treated mice

*A representative SEM image of **(A)** the surface and **(B)** the core of a cystine stone of Slc7a9$^{-/-}$ mice and of **(C)** the surface and **(D)** the core of a cystine stone of Slc7a9$^{-/-}$ L-Erg (16 mg/kg/day) treated mice. The magnification is indicated by the scale bar. A representative EDS spectrum of **(E)** the surface and **(F)** the core of a cystine stone of Slc7a9$^{-/-}$ mice, and of **(G)** the surface and **(H)** the core of a cystine stone of Slc7a9$^{-/-}$ L-Erg (16 mg/kg/day) treated mice. C = Carbon, N = Nitrogen, O = Oxygen, Al = Aluminum, S =Sulfur.*

4.3.4. L-Erg treatment effect in the *Slc7a9*$^{-/-}$*Slc22a4*$^{-/-}$ dKO mouse model

Considering the results of the cystine precipitation assay (4.3.3.3), it seems that L-Erg derived metabolism is needed to prevent the stone formation process. To validate this hypothesis, L-Erg (16 mg/kg/day) was administered to the *Slc7a9*$^{-/-}$*Slc22a4*$^{-/-}$ dKO mouse model (cystinuria type B model lacking L-Erg transporter). *Slc22a4*$^{-/-}$ mice can absorb L-Erg at intestinal level, but cannot retained this molecule in the body showing a higher L-Erg urine excretion compared to WT mice (Kato et al., 2010). Thus, theoretically, dKO treated mice should have a higher amount of urinary L-Erg concentration but no L-Erg internalization and metabolism.

L-Erg (16 mg/kg/day) was administered as a preventive treatment since weaning (prior to stone formation) and up to 4-month-old. Stone onset and progression were examined monthly by X-ray imaging in both treated and control groups (**Figure 29A**). L-Erg concentration in the drinking water of treated mice was adjusted per cage according to its mouse weight and water intake means. No L-Erg effect in weight evolution was detected during the follow-up (**Figure 29B**) and the mean dose administrated during the whole treatment was maintained around 16 mg/kg/day (**Figure 29C**).

After the 4-month follow-up of L-Erg treatment, both control and treated groups showed a similar percentages of stone former mice (**Figure 29D**). In addition, no significant differences were observed either in stone growth evolution during the follow-up (**Figure 29E**) or post-mortem stone weight at the end of the treatment (**Figure 29F**). These results confirmed that L-Erg derived metabolism is needed for treatment effectiveness.

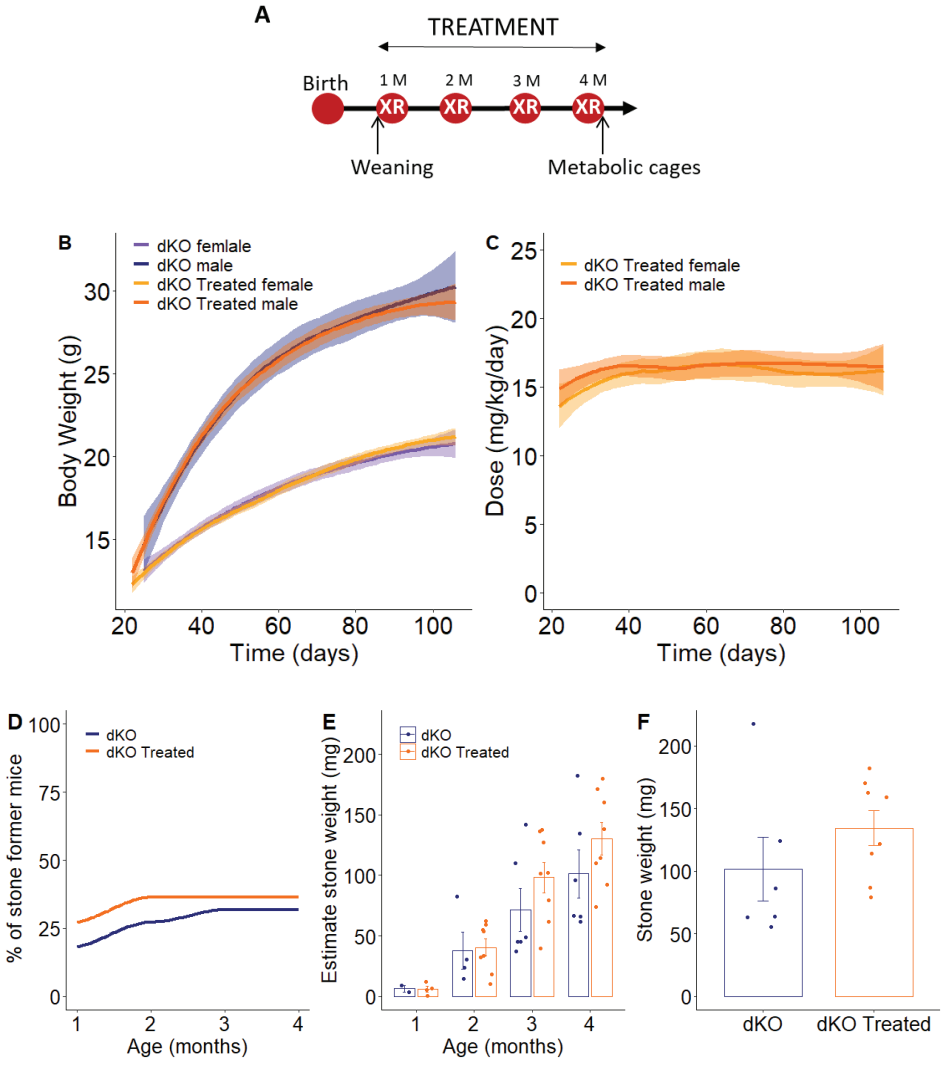

Figure 29. Long-term L-Erg treatment in Slc7a9$^{-/-}$Slc22a4$^{-/-}$ mice

(A) *Timeline of L-Erg (16 mg/kg/day) preventing treatment since weaning and up to 4-months of age in Slc7a9$^{-/-}$Slc22a4$^{-/-}$ mice.* ***(B)*** *Body weight evolution during the treatment in both Slc7a9$^{-/-}$ Slc22a4$^{-/-}$ male and female, control and treated mice.* ***(C)*** *Mean of estimate L-Erg dose intake per cage weekly calculated in Slc7a9$^{-/-}$Slc22a4$^{-/-}$male and female treated mice.* ***(D)*** *Evolution of stone former mice percentage in Slc7a9$^{-/-}$Slc22a4$^{-/-}$ control and treated groups. N= 22 per group.* ***(E)*** *Comparison of monthly stone weight evolution of Slc7a9$^{-/-}$Slc22a4$^{-/-}$ control and treated stone former mice. The stone weight follow-up was estimated by X-ray images.* ***(F)*** *Post-mortem stone weight of Slc7a9$^{-/-}$Slc22a4$^{-/-}$ control and treated stone former mice after L-Erg treatment. M = month of age, XR= X-ray, dKO = Slc7a9$^{-/-}$Slc22a4$^{-/-}$ mice.*

4.3.4. Long-term L-Erg treatment improves kidney oxidative damage in *Slc7a9*$^{-/-}$ mice

As above results showed that L-Erg does not work as a thiol-binding drug and the treatment in dKO mice confirmed the need of L-Erg derived metabolism to prevent cystine lithiasis, next steps were focused on understanding L-Erg intracellular effect in the kidneys. L-Erg is accumulated in damaged tissues and its properties described so far are related to its condition of antioxidant and metal chelating molecule (Halliwell et al., 2016). These evidence together with cysteine being the limiting precursor of GSH induced the study of the oxidative status in the kidneys of treated mice.

4.3.4.1. Kidney total GSH content is severely decreased in Slc7a9$^{-/-}$ *mice and increases after L-Erg treatment*

It has been described that cystinuric patients have lower levels of GSH in leukocytes (Mårtensson et al., 1990) and the *Slc3a1*$^{-/-}$ mouse model showed a reduced content of total GSH in liver (Woodard et al., 2019), but as far as we know, no data have been published about kidney GSH levels in cystinuria. Thus, to assess GSH content in the kidneys of the *Slc7a9*$^{-/-}$ mouse model and the effect of L-Erg treatment in this antioxidant molecule, metabolites related to GSH were quantified by UPLC-MS/MS.

Kidney GSH and GSSG intracellular pools in *Slc7a9*$^{-/-}$ mice were about 10-fold lower when compared to WT mice (**Figure 30A-B**). Long term L-Erg (16 mg/kg/day) treatment significantly increased GSH content (1.55-fold increase) although not to recover WT levels. These results were also observed in the kidney total GSH content (**Figure 30C**). Regarding GSH/GSSG ratio, *Slc7a9*$^{-/-}$ mice showed a more reduced state compared to WT mice, with no significant effect after L-Erg treatment (**Figure 30D**). These results revealed an impairment on GSH content in the kidneys of cystinuric mice as both reduced and oxidized pools were severely decreased. To assess the origin of the lower amount of GSH and the partial recovery after L-Erg treatment, further experiments were performed to study: GSH content in liver and urine, GSH precursor levels in kidney and GSH synthesis enzyme expression in both kidneys and livers.

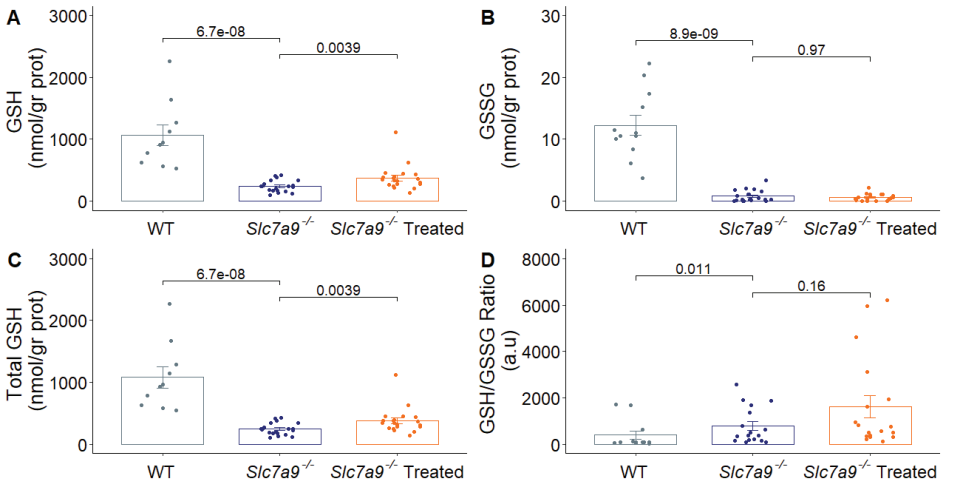

Figure 30. GSH levels increased in the kidneys of Slc7a9$^{-/-}$ mice after L-Erg treatment although not to recovered WT levels

(A) *Reduced (GSH),* ***(B)*** *oxidized (GSSG) and* ***(C)*** *total (GSH+GSSG) GSH content in the kidneys of WT, Slc7a9$^{-/-}$ and Slc7a9$^{-/-}$ L-Erg (16 mg/kg/day) treated mice. Levels were normalized by kidney total protein content (grams of proteins).* ***(D)*** *Kidney intracellular ratio of reduced and oxidized GSH forms (GSH/GSSG). Data are expressed as mean ± SEM. p-value is shown at the top after Mann-Whitney-Wilcoxon test.*

4.3.4.2. Liver total GSH content is reduced in Slc7a9$^{-/-}$ mice and L-Erg treatment improves GSH/GSSG ratio

As liver is the organ that has the highest capacity to synthesize GSH and it is its main reservoir, the first approach was to assess if the lower levels of kidney GSH observed were due to an impairment of GSH synthesis in liver and a consequent alteration of liver-kidney interorgan GSH metabolism. As the liver GSH pool in *Slc7a9$^{-/-}$* mice were significantly lower when compared to WT mice (**Figure 31A**) and no differences were observed concerning the GSSG pool (**Figure 31B**), the liver total GSH content was about 20 % reduced in *Slc7a9$^{-/-}$* mice (**Figure 31C**). After L-Erg treatment, no recovery in the liver GSH content was observed, but significantly lower GSSG levels were found in treated mice. In addition, this reduction in the GSSG content led to a significant increase in the GSH/GSSG ratio compared to untreated mice (**Figure 31D**). Thus, these

findings illustrate that GSH impairment is also observed in the livers of cystinuric mice, and although no recovery of the GSH content is observed after L-Erg treatment, an improvement of oxidative stress status is induced in the livers of L-Erg treated mice.

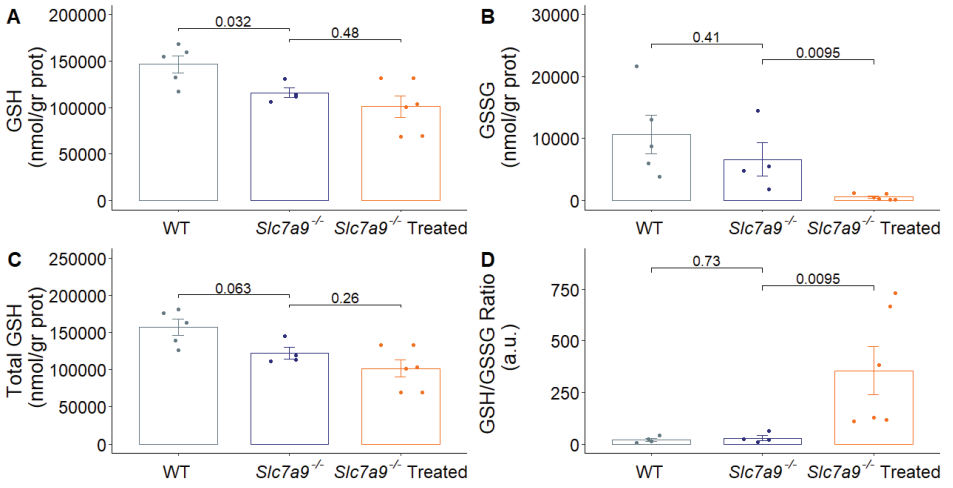

Figure 31. L-Erg treatment does not increase GSH levels in the livers of Slc7a9$^{-/-}$ mice but improves the GSH/GSSG ratio

(A) *Reduced (GSH),* ***(B)*** *oxidized (GSSG) and* ***(C)*** *total (GSH+GSSG) GSH content in the livers of WT, Slc7a9$^{-/-}$ and Slc7a9$^{-/-}$ L-Erg (16 mg/kg/day) treated mice. Levels were normalized by liver total protein content (grams of proteins).* ***(D)*** *Liver intracellular ratio of reduced and oxidized GSH forms (GSH/GSSG). Data are expressed as mean ± SEM. p-value is shown at the top after Mann-Whitney-Wilcoxon test.*

4.3.4.3. Slc7a9$^{-/-}$ mice show an impaired GSH turnover in the BBM of proximal tubules

Pathways of synthesis, degradation, uptake and efflux of GSH coexist in proximal tubules. Kidney function is essential for GSH metabolism as they are the primary organ that extracts GSH from blood being responsible for its degradation and resynthesis having the highest GGT enzyme activity. As GGT is an ectoenzyme, located on the kidney BBM, GSH cleavage takes place in the luminal space of proximal tubules. Thus, the second approach to elucidate the origin of the GSH deficiency in *Slc7a9$^{-/-}$* mice was to study GSH urine excretion and GGT protein expression.

Slc7a9$^{-/-}$ mice showed a significant increase in GSH and GSSG excretion compared to WT mice, resulting in a higher excretion level of total GSH content (**Figure 32A-C**). In addition, *Slc7a9*$^{-/-}$ mice showed a 2-fold reduction in the urinary GSH/GSSG ratio indicating the more oxidized status of the urine of cystinuric mice (**Figure 32D**). No effect of L-Erg treatment was observed in GSH and GSSG content and even a lower GSH/GSSG ratio was obtained compared to untreated mice. Regarding GGT1 protein expression, significantly lower levels were found in *Slc7a9*$^{-/-}$ mice with no effect after L-Erg treatment (**Figure 32E**). Thus, the higher GSH excretion detected in both *Slc7a9*$^{-/-}$ untreated and treated mice could be related to a decrease in GGT1 activity in the BBM. Additionally, urine redox potential status was assessed using an ORP electrode. *Slc7a9*$^{-/-}$ mice showed a significant increase in ORP confirming the oxidate status of cystinuric mice urines. However, although a decrease in GSH/GSSG ratio was observed after L-Erg treatment, when evaluating the urinary ORP status, treated mice showed significantly lower ORP levels (**Figure 32F**) indicating that treated urines were more reduced.

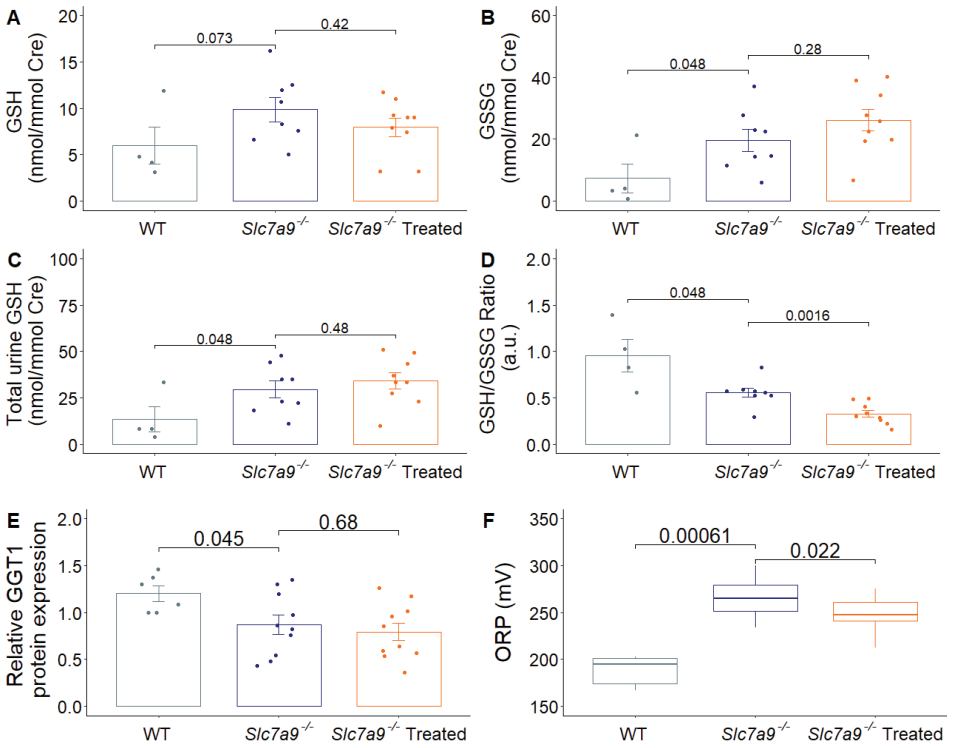

Figure 32. Differences in GSH excretion and GGT1 enzyme expression in Slc7a9$^{-/-}$ mice

(A) *Reduced (GSH),* ***(B)*** *oxidized (GSSG) and* ***(C)*** *total (GSH+GSSG) urinary GSH excretion of WT, Slc7a9$^{-/-}$ and Slc7a9$^{-/-}$ L-Erg (16 mg/kg/day) treated mice. Levels were normalized by mmol of creatinine.* ***(D)*** *Urinary ratio of reduced and oxidized GSH forms (GSH/GSSG).* ***(E)*** *GGT1 protein expression in the BBM of kidneys of WT, Slc7a9$^{-/-}$ and Slc7a9$^{-/-}$ L-Erg treated mice. Protein levels were normalized by total protein lane transferred and data are represented as fold-change to WT mice.* ***(F)*** *ORP measured in urines collected every 24 h in individual metabolic cages. Values are expressed as mean ± SEM. p-value is shown at the top after Mann-Whitney-Wilcoxon test.*

4.3.4.4. L-Erg treatment increases GSH synthesis in kidneys by inducing GCLM-GCLC expression via NRF2 pathway activation

Finally, the whole GSH synthesis pathway was assessed in the kidney in terms of precursor metabolite levels and enzyme expression. In the kidneys of L-Erg treated mice an increase in all GSH precursors was observed compared to untreated mice (**Figure 33A**). As intracellular cysteine levels were found significatively increased after

L-Erg treatment, transsulfuration pathway metabolites were also evaluated as participate in the intracellular biosynthesis of cysteine. L-Erg treated mice showed increased levels of methionine and cystathionine (**Figure 33B**).

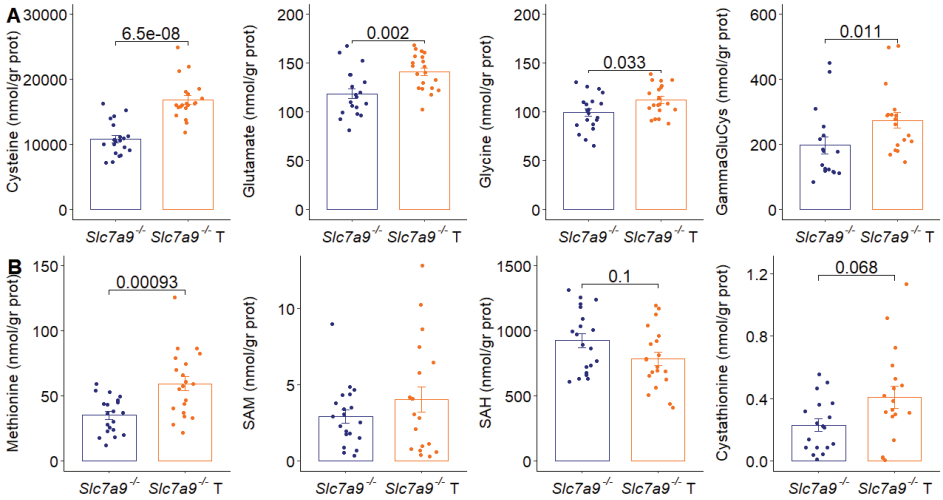

Figure 33. L-Erg treated kidneys showed an increase in transsulfuration pathway and GSH synthesis metabolites

Comparison of kidney intracellular content of ***(A)*** *GSH precursors and* ***(B)*** *transsulfuration pathway metabolites in Slc7a9$^{-/-}$ untreated and L-Erg (16 mg/kg/day) treated mice. Levels were normalized by total kidney protein content. Values are expressed as mean ± SEM. p-value is shown at the top after Mann-Whitney-Wilcoxon test. SAM = S-adenosylmethionine, SAH= S-adenosylhomocysteine. T= Treated.*

However, the expression analysis of the key enzymes of GSH synthesis in kidney showed non-significantly differences between treated and untreated mice (**Figure 34A**). Nevertheless, when samples were analyzed according to its stone phenotype, L-Erg treated stone formers showed a lower expression of *Gsr*, *Gclm* and *Nfe2l2* genes compared to L-Erg treated non-stone former mice (**Figure 34B**), suggesting an association between a lower NRF2 pathway activation and stone formation. Differences in *Nfe2l2* gene expression were also observed in untreated mice, as non-stone formers showed a higher expression when compared to stone formers. Finally, protein analysis confirmed that L-Erg treatment increases the expression of GCLC-

GCLM heterodimer and NRF2 protein in the kidneys of *Slc7a9*$^{-/-}$ non-stone former mice (**Figure 34C**).

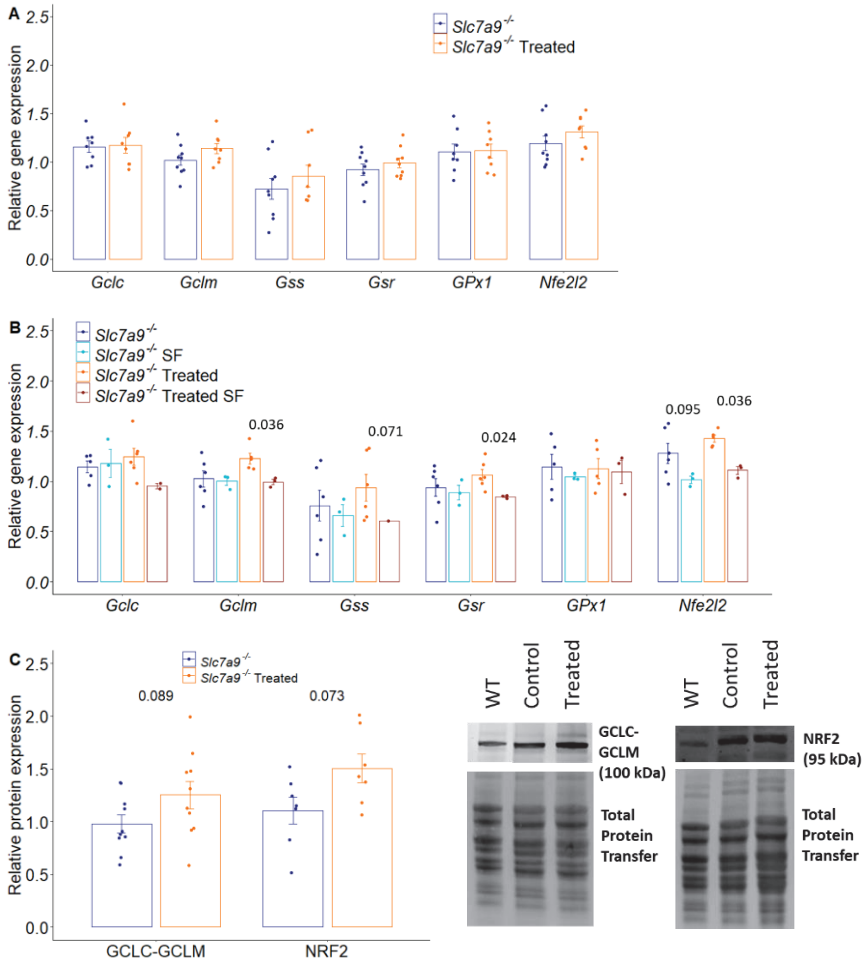

Figure 34. GSH synthesis is induced in Slc7a9$^{-/-}$ kidneys via NRF2 after L-Erg treatment

*Kidney gene expression of GSH synthesis enzymes after L-Erg treatment in **(A)** Slc7a9$^{-/-}$ untreated and treated mice and **(B)** in Slc7a9$^{-/-}$ mice grouped by treatment and stone phenotype (non-stone (NSF) and stone former (SF)). Gene expression levels were normalized relative to Actb and data are represented as fold-change to WT mice. **(C)** GCLC-GCLM heterodimer and NRF2 protein expression in the kidneys of L-Erg untreated and treated mice. Representative immunoblots showing the GCLC-GCLM heterodimer and NRF2 protein levels and their corresponding total transfer line used to normalize data obtained. Data are represented as fold-change to WT mice. Values are expressed as mean ± SEM. p-value is shown at the top after Mann-Whitney-Wilcoxon test.*

Moreover, in the livers, an increase in *Gclm* and *GPx* expression was detected in treated mice but without *Nfe2l2* significant induction (**Figure 35A**). However, when analyzing by stone condition, non-stone formers of both untreated and tread mice groups showed an increased *Nfe2l2* expression compared to stone formers mice (**Figure 35B),** although significance was not achieved due to the low number of samples analyzed. In addition, regarding *Gclm* expression by stone phenotype, a higher expression in non-stone formers was also observed in both untreated and treated mice. Thus, similar results to those obtained in the kidney regarding *Gclm* and *Nfe2l2* gene expression were found in the liver.

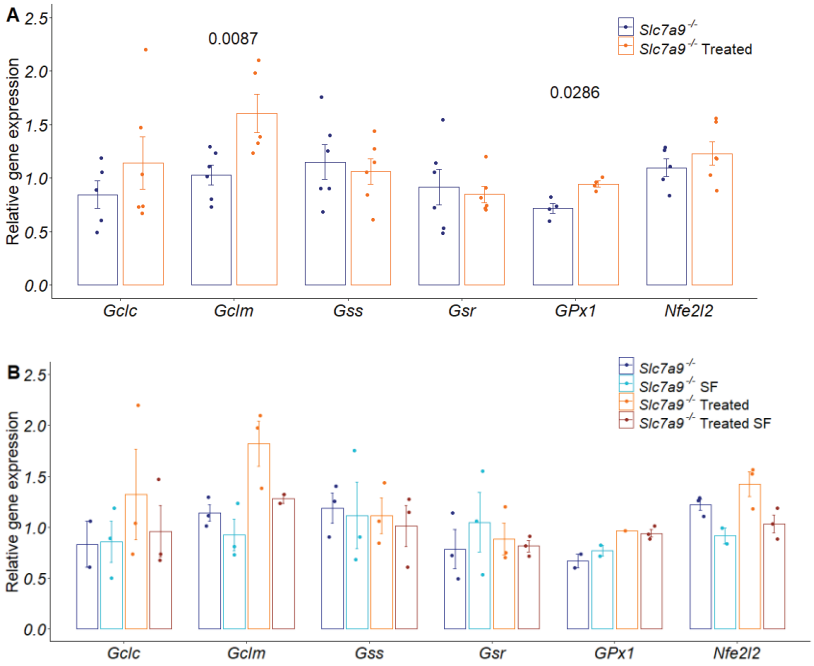

Figure 35. Gclm and GPx1 gene expression is induced in Slc7a9$^{-/-}$ livers after L-Erg treatment

(A) *Liver gene expression of GSH synthesis enzymes after L-Erg (16 mg/kg/day) treatment. Gene expression levels were normalized relative to Actb and data are represented as fold-change to WT mice.* ***(B)*** *Liver gene expression of GSH synthesis enzymes comparing non-stone and stone former (SF) mice after L-Erg treatment. Gene expression levels were normalized relative to Actb and data are represented as fold-change to WT mice. Values are expressed as mean ± SEM. p-value is shown at the top after Mann-Whitney-Wilcoxon test.*

Collectively, these data evidence an induction of GSH synthesis in *Slc7a9*$^{-/-}$ mice kidneys by L-Erg (16 mg/kg/day) treatment mediated by an increase in GCLC-GCLM heterodimer expression via NRF2 pathway activation. In addition, a differential expression of GSH synthesis enzymes were observed in stone former mice in both untreated and treated groups. Similar results were observed in livers as *Gclm* was also induced after L-Erg treatment above all in non-stone former mice.

4.3.5. Long-term L-Erg treatment improves kidney mitochondrial damage in *Slc7a9*$^{-/-}$ mice

As in the second chapter of this thesis we described the kidney mitochondrial dysfunction related to cystinuria and L-Erg is suggested to preserve mitochondrial function (Williamson et al., 2020), next steps were focused on determine if L-Erg treatment has any beneficial effect in mitochondrial function in our cystinuria model. First, the kidney content of TCA cycle metabolites was analyzed in *Slc7a9*$^{-/-}$ and *Slc7a9*$^{-/-}$ treated mice. After describing a depletion in citrate levels in *Slc7a9*$^{-/-}$ mice, L-Erg treatment showed to significantly increase intracellular citrate content (3-fold increase) although not to restore WT levels (**Figure 36A**). In addition, lower levels of fumarate and lactate were found compared to untreated mice. Then, NAD^+/NADH content was determined showing that L-Erg treatment restored NAD^+/NADH ratio in *Slc7a9*$^{-/-}$ treated mice (**Figure 36B**). These results suggest an improve in mitochondrial function in the kidneys of L-Erg treated mice.

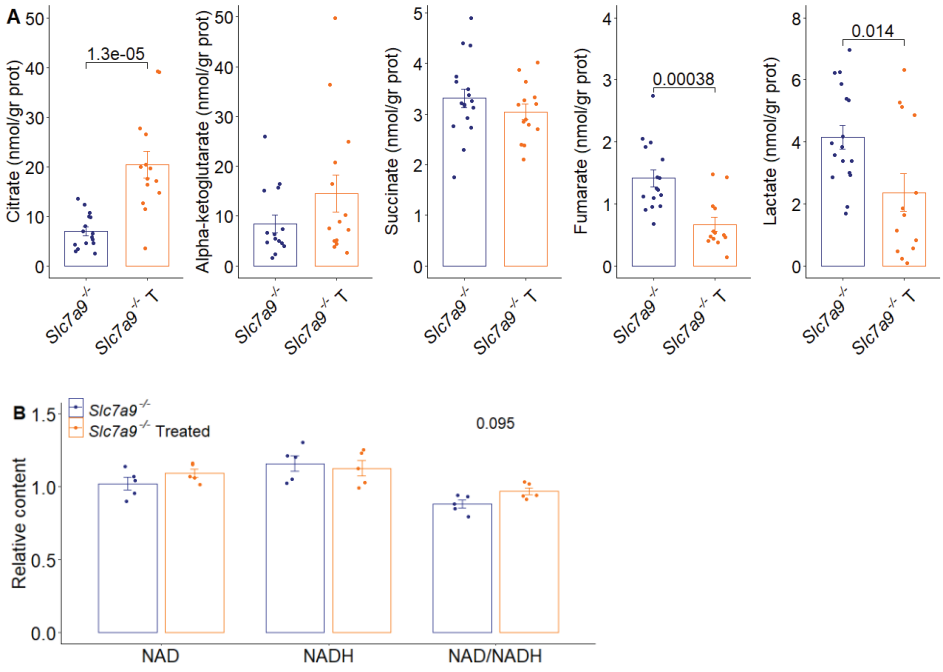

Figure 36. L-Erg treatment increases intracellular citrate and restores NAD⁺/NADH ratio in Slc7a9$^{-/-}$ mice

(A) *Intracellular kidney content of metabolites related to the TCA cycle in Slc7a9$^{-/-}$ and Slc7a9$^{-/-}$ L-Erg (16 mg/kg/day) treated mice. Metabolite levels were normalized by total kidney protein content.* ***(B)*** *NAD⁺ and NADH levels, and their ratio NAD⁺/NADH, in the kidneys of Slc7a9$^{-/-}$ and Slc7a9$^{-/-}$ L-Erg treated mice. NAD⁺ and NADH levels were normalized by total kidney protein content and data are represented as fold-change respect to WT mice. Values are expressed as mean ± SEM. p-value is shown at the top after Mann-Whitney-Wilcoxon test. T= Treated*

4.3.6. High dose L-Erg administration prevents cystine lithiasis in *Slc7a9$^{-/-}$* mice.

Finally, to determine if the effect observed after L-Erg treatment could be improved increasing the dose administered, a high dose long-term L-Erg treatment was performed from weaning and up-to 4-month-old. In this case, the dose administered was 200 mg/kg/day which corresponds to a Human Equivalent Dose (HED) of 1 g/day for a 60 kg adult. As in the other experiments, stone onset and progression were examined monthly by X-ray imaging in both treated and control group (**Figure 37A**).

In addition, L-Erg concentration in the drinking water of treated mice was weekly adjusted per cage according to its mice weight and water intake means. High dose L-Erg treatment did not induced changes in body weight during mice development either in male or in female (**Figure 37B**). The mean dose administrated during the whole treatment was maintained around 200 mg/kg/day (**Figure 37C**).

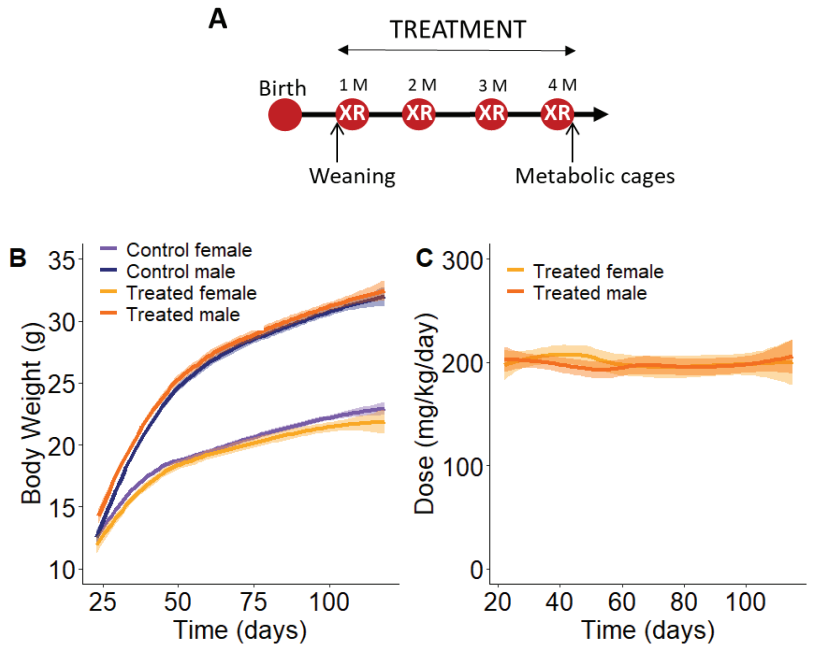

Figure 37. High dose L-Erg treatment follow-up in Slc7a9$^{-/-}$ mice

(A) *Timeline of L-Erg (200 mg/kg/day) preventing treatment since weaning and up to four months of age in Slc7a9$^{-/-}$ mice.* ***(B)*** *Body weight evolution during the treatment in both Slc7a9$^{-/-}$ male and female, control and treated mice.* ***(C)*** *Mean of estimate L-Erg dose intake per cage weekly calculated in Slc7a9$^{-/-}$ male and female treated mice. M = month of age, XR= X-ray.*

At the end of the 4-month high dose L-Erg treatment, the treated group showed a reduction in the rate of stone former mice (**Figure 38A**). In addition, during the follow-up a delay on stone formation was observed in the treated group (**Figure 38B**) and, at the end of the treatment, treated mice showed a lower post-mortem stone dry weight (**Figure 38C**). In the control group, a stone former mouse naturally died at the

third month of the follow-up, which has been taken into consideration for calculating the rate of stone former mice in the control group, but it has been excluded from the estimate and post-mortem stone weight data. These results confirmed the potential of L-Erg as a preventive treatment for cystinuria. In addition, administrating a higher dose of L-Erg increased the effect detected, reducing the rate of stone formation 3.52 times vs the 2.3 times observed in the L-Erg 16 mg/kg/day treatment.

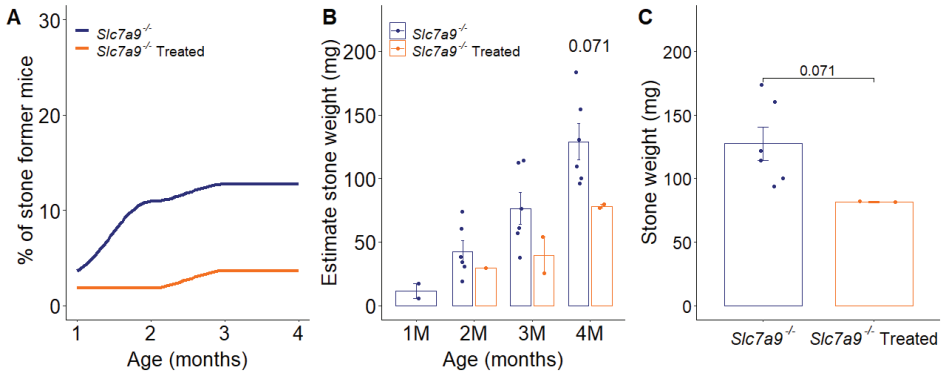

Figure 38. High dose L-Erg treatment reduces stone formation in Slc7a9$^{-/-}$ mice

(A) *Evolution of the rate of stone former mice in Slc7a9$^{-/-}$ control and treated groups after L-Erg (200 mg/kg/day) treatment. N=55 per group.* ***(B)*** *Comparison of monthly stone weight evolution of Slc7a9$^{-/-}$ control and treated stone former mice. The stone weight follow-up was estimated by X-ray images.* ***(C)*** *Post-mortem stone weight of Slc7a9$^{-/-}$ control and treated stone former mice after L-Erg treatment. Data are expressed as mean ± SEM and p-value is showed at the top after Mann-Whitney-Wilcoxon test. M = month of age.*

Further analyses are still needed to study the intracellular effect of the high dose L-Erg administration and to validate the cystine solubility results obtained with the 16 mg/kg/day dose. However, mitochondrial function could be assessed in the high dose L-Erg treated mice as fresh tissue was needed. Concerning enzymatic activity, while non significantly differences were observed in complex II activity, an activity increase was induced in complex IV by L-Erg treatment that could restored WT levels (**Figure 39A**). Then, in the high-resolution respirometry assay, a tendency in higher oxygen consumption was observed in treated mice after inducing complex II by succinate and

differences were maintained after uncoupled respiration adding FCCP (**Figure 39B**). In addition, when rotenone was added to inhibit complex I, significantly higher respiration was detected in treated mice that reached the same levels observed in WT mice (**Figure 39B**). These findings indicate that high dose L-Erg treatment restored ETC mitochondrial defects observed in the kidneys of *Slc7a9*$^{-/-}$ mice to WT levels.

Together, these data evidence that L-Erg treatment not only prevents cystine stone formation, but it also normalizes kidney mitochondrial function in *Slc7a9*$^{-/-}$ mice.

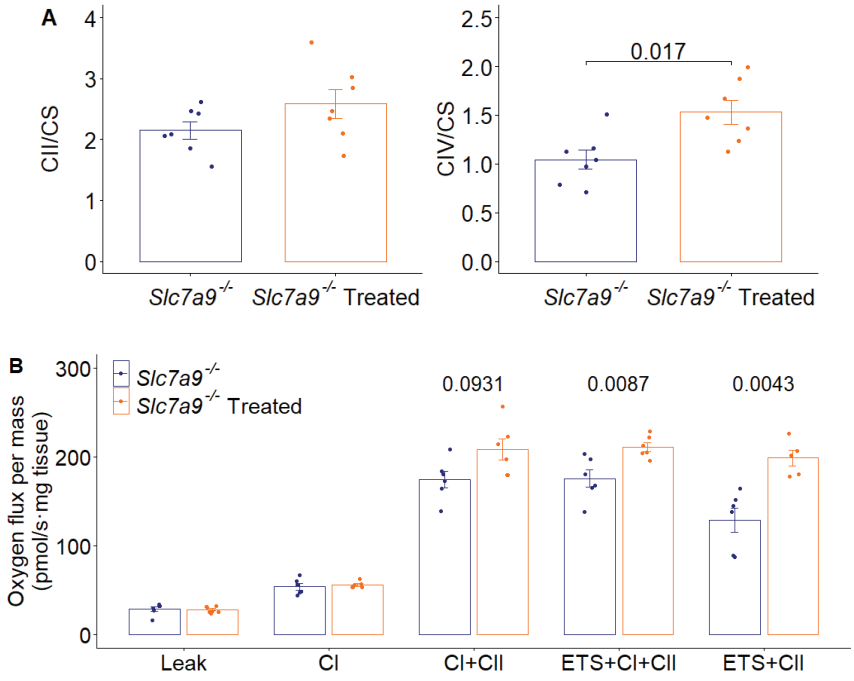

Figure 39. High dose L-Erg treatment improves OXPHOS activity and mitochondrial respiration in Slc7a9$^{-/-}$ mice

(A) *Determination of kidney mitochondrial succinate dehydrogenase (CII) and cytochrome c oxidase (CIV) activity (nmol/min per mg of protein) in Slc7a9$^{-/-}$ and Slc7a9$^{-/-}$ L-Erg high dose treated mice. Data is shown as a ratio to citrate synthase activity (CS).* ***(B)*** *Ex vivo mitochondrial respiration of saponin permeabilized kidneys of Slc7a9$^{-/-}$ and Slc7a9$^{-/-}$ L-Erg high dose treated mice (CI = Complex I, CII = Complex II, ETS = Electronic Transfer System). Oxygen flux was normalized by mg of tissue. Values are expressed as mean ± SEM. p-value is shown at the top after Mann-Whitney-Wilcoxon test.*

DISCUSSION

5. DISCUSSION

The hallmark of cystinuria is the hyperexcretion of cystine that led to calculi formation as cystine is not soluble in the urine. However, although all cystinuric patients present a cystine excretion above its saturation point, differences in stone onset and recurrence are observed, and even around 6 % of patients do not form stones during their entire life (Eggermann et al., 2012). Similar findings are observed in cystinuria mouse models as even mice with the same mutation, siblings and with controlled environmental factors show differences in lithiasis phenotype. Together, these data suggest the presence of modulating factors affecting the aggregation of cystine crystals that promotes stone formation.

Each chapter of this thesis attempts to provide new evidence about the molecular bases of cystinuria and the modulation of cystine lithiasis. First, as AGT1 was recently described as a second cystine transporter in the BBM of proximal tubules, the role of this protein in amino acid reabsorption and cystine lithiasis has been studied in both cystinuria mouse models and patients, showing its influence in the lithiasis process and amino acid reabsorption in mouse models, although no such evidence was observed in patients. Second, an RNA-seq analysis was performed to identify differentially expressed genes in the kidneys of the *Slc7a9*$^{-/-}$ mouse model, and results uncovered a defect in the mitochondrial ETC in this disease. Third, L-Erg was evaluated in *Slc7a9*$^{-/-}$ mouse model as potential treatment for cystinuria, and promising results preventing and delaying stone formation were obtained when administered as a chronic preventive treatment due to an increase in cystine solubility in the urine of cystinuric mice.

5.1. Chapter I

At physiological conditions, more than 90 % of cystine is reabsorbed by $b^{0,+}$AT/rBAT in the S1 segment of proximal tubules and the contribution of AGT1/rBAT in the S3 segment is about the remaining 10 % (Giacopo et al., 2013). However, little is known about the relevance of AGT1/rBAT in cystinuria when $b^{0,+}$AT/rBAT transporter is disrupted and the amount of cystine in urine is severely increased. Since Nagamori *et al.,* described AGT1/rBAT as the second cystine transporter in the BBM of proximal tubules, only one work attempted to study AGT1 role in cystinuria patients (Olschok et al., 2018). In addition, in their work, Nagamori *et al.,* performed the functional characterization of AGT1 using proteoliposomes and localized AGT1 expression in the BBM of mouse kidneys, but no further *in vivo* studies were described (Nagamori et al., 2016). Thus, in this thesis, it is described the role of AGT1 in amino acid reabsorption and excretion in physiological and cystinuria conditions using mouse models.

Taking advantage of the biological sex differences related to AGT1 expression in mice (Nagamori et al., 2016), using females as a functional KO, cystine, aspartate and glutamate excretion was compared according to sex and genotype in the *Slc7a9*$^{-/-}$ mouse model. When comparing the male to female ratio of excretion between WT and *Slc7a9*$^{-/-}$ mice, the results showed that cystine excretion ratio was higher while aspartate and glutamate excretion ratios were lower in WT mice. These results indicate that, in the pathological condition of cystinuria, AGT1/rBAT facilitates cystine reabsorption and aspartate and glutamate excretion in males. In addition, this finding was confirmed comparing AGT1-related amino acid excretion between *Slc7a9*$^{-/-}$ and *Slc3a1*^{D140G} male mice, as in *Slc3a1*^{D140G} mice (which has no AGT1/rBAT expression) higher levels of cystine excretion and lower of aspartate and glutamate were observed. Taking a deeper look, differences in aspartate excretion were higher than those in the glutamate excretion in most comparisons. This observation could be explained by the EAAC1 (*Slc1a1*) transporter which colocalize with AGT1/rBAT in the apical membrane of the S3 segment of proximal tubules and reabsorbs aspartate and glutamate from the luminal fluid (Shayakul et al., 1997). Mutations in this gene are responsible for

dicarboxylic aminoaciduria, and both patients and mouse models present hyperexcretion of aspartate and glutamate, being more severe in the case of glutamate, suggesting a higher affinity for this amino acid (Bailey et al., 2011; Peghini et al., 1997). Thus, EAAC1 could be partially reabsorbing the amount of aspartate and glutamate released by AGT1/rBAT with preferential uptake of glutamate and confirming the increased cystine reabsorption capacity by AGT1/rBAT.

Apart from characterizing the role of AGT1/rBAT in amino acid reabsorption in cystinuria, its impact in stone formation was described in this work for the first time. While no sex differences were observed in the rate of stone formation in our *Slc3a1*^{D140G} colony during 6-month follow-up, in our *Slc7a9*$^{-/-}$ colony, males showed a significantly lower stone formation rate during the whole follow-up. In fact, the same percentages of stone formation were observed in both male and female *Slc3a1*^{D140G} mice and female *Slc7a9*$^{-/-}$, indicating the protective role of AGT1/rBAT expression in *Slc7a9*$^{-/-}$ male mice. However, in the other cystinuria type A and B mouse models, sex differences observed were the opposite, with female mice showing a significantly lower rate of stone formation compared to male mice (Beckermann et al., 2020; Peters et al., 2003) or even not forming stones (Bai et al., 2021; Livrozet et al., 2014). In addition, when our cystinuria type B model was described, no sex differences in stone formation were reported (Feliubadaló et al., 2003), and in the description of *Slc3a1*^{D140G} mice, a lower rate of stone formation was observed in females (Peters et al., 2003). These differences in the stone formation rate could be related to the genetic background of mice, as most cystinuria mouse models were generated and described in a mixed background, and all colonies available in our lab are currently in a pure C57Bl/6J background. Previous studies in male mice comparing lithiasic phenotype of cystinuria type B mouse model between pure C57Bl/6J and mixed C57Bl/6J-129 and C57Bl/6J-C3H backgrounds showed 2-time higher stone formation rate in mixed background mice, uncovering the impact of background in lithiasis phenotype (Espino, 2012). Even tough further studies are needed to elucidate the influence of C57Bl/6J background in the results obtained, in this thesis AGT1/rBAT amino acid transport has been

characterized in cystinuria mouse models and its presence has been related to a lower rate of cystine lithiasis formation.

As mentioned before, only one work has been published searching *SLC7A13* mutations in uncharacterized cystinuria patients (Olschok et al., 2018). In their cohort of 103 cystinuria patients, Olschok *et al.,* detected 17 individuals with no mutations either in *SLC3A1* or in *SLC7A9*. However, when screening the *SLC7A13* gene on those patients only nonpathogenic polymorphisms were found and they excluded *SLC7A13* as the third cystinuria gene (Olschok et al., 2018). Nevertheless, no additional clinical parameters as cystine excretion levels or stone progression were provided to infer the impact of those nonpathogenic polymorphisms in cystinuria pathology. In our case, *SLC7A13* gene was sequenced in 8 patients and their families with only one *SLC7A9* allele explained or without any genetic variant described in *SLC3A1* and *SLC7A9* genes. The predicted as pathogenic c.745G>A (p.Val249Met) variant was found in heterozygous in 5 of those families while in the others only nonpathogenic variants were observed. Unfortunately, only partial aminograms were recorded from those families and, with the data available, no influence of c.745G>A variant on cystine excretion was observed as, when comparing healthy subjects and cystinuric patients both heterozygous for the variant, cystinuric patients showed a significantly higher levels of cystine in urine. These results suggest that we are missing something on those patients that induces cystine hyperexcretion as it cannot be attributed to the c.745G>A variant in *SLC7A13* gene.

Additionally, in 18 new cystinuria patients without genetic diagnose a screening analysis of *SLC3A1, SLC7A9* and *SLC7A13* genes was performed. Most patients presented homozygous pathogenic variants in *SLC3A1* gene which difficult the study of the hypothetic impact of *SLC7A13* variants as the assembly of the AGT1/rBAT transporter is impaired. Nevertheless, 6 *SLC7A13* variants were detected in this cohort: 4 of them predicted as benign and with high allele frequency, and two predicted as damaging, c.745G>A (p.Val249Met) and c.988C>T (p.Leu330Phe), all of them in heterozygosis. The c.745G>A variant was the most frequent as it was detected in

heterozygosis in 50 % of studied patients. Its impact was studied in the patient 420 as only one *SLC7A9* allele was found affected by the c.266C>T (p.Thr123Met) mutation but, no significant differences were observed in her aspartate and glutamate urinary levels compared to other patients. In addition, the p.Thr123Met mutation in the *SLC7A9* gene has been described to already caused isolated cystine hyperexcretion in heterozygous (Font-Llitjós et al., 2005). These findings together with the previous results obtained, indicate that the c.745G>A variant in heterozygous has no obvious effect on amino acid reabsorption in patients.

The other predicted as damaging variant detected in *SLC7A13* gene, c.988C>T (p.Leu330Phe), was observed in the 416 patient in heterozygous, together with the c.745G>A variation. This patient presented the highest urinary levels of aspartate and glutamate together with the lowest levels of cystine observed in our cohort, suggesting an induction of AGT1/rBAT function. However, genotypically, this patient has a homozygous mutation affecting *SLC3A1* gene (c.266C>T, pLeu89Pro). Nevertheless, previous studies in $b^{0,+}$AT/rBAT transporter showed a small amount of p.Leu89Pro mutated heterodimers reaching the membrane being functional for amino acid transport while other mutated heterodimers as p.Met467Thr, p.Arg365Trp and p.Thr216Met showed no transport function at all (Bartoccioni et al., 2008). Thus, small amounts of AGT1/rBAT transporter could be functional in the patient 416. This finding suggests that the c.998C>T variant in *SLC7A13* could result in a gain of function of AGT1/rBAT transport as no such increase was observed in other c.745G>A carriers, but functional mutational analyses are needed to confirm this hypothesis. In addition, *SLC1A1* gene should be analyzed to discard its implication.

In summary, data described in this first chapter confirmed the role of AGT1/rBAT transporter in cystine, aspartate and glutamate excretion and cystine lithiasis in cystinuria mouse models. However, no cystinuria causative or modulating effect could be associated to AGT1 after screening *SLC7A13* in 9 uncharacterized cystinuric patients. The lack of evidence of AGT1 role in cystinuria patients in this work, together with the similar results observed by Olschok *et al* in the 17 uncharacterized patients of

their cohort, reduces the probability of the expected relevance of AGT1 in cystinuria. Nevertheless, further studies analyzing cystinuric patients with mutations in *SLC7A9* gene should be performed to evaluate AGT1 role modulating cystine reabsorption, and lithiasis onset and recurrence.

5.2. Chapter II

In the second chapter of this thesis, an impairment of the mitochondrial ETC in the kidneys of the cystinuria *Slc7a9*$^{-/-}$ mouse model is described for the first time. The RNA-seq analysis performed in the kidneys of WT and *Slc7a9*$^{-/-}$ mice uncovered the downregulation of most mtDNA encoded ETC subunits in both male and female cystinuric mice, with neither dysregulation of the other mtDNA encoded genes nor alteration in the mitochondria content. Although mtDNA encoded subunits are a small proportion of the ETC subunits, they are essential for the OXPHOS system as have catalytic roles or are core subunits for complexes assembly (Signes & Fernandez-Vizarra, 2018; Vartak et al., 2015). In addition, mutations in mtDNA encoded subunits have been related to several diseases as myopathies, neuropathies and encephalopathies (Taylor & Turnbull, 2005; Wallace, 1992).

Regarding nuclear DNA encoded subunits and assembly factors, a downregulation of about 20-25 % of complex I, III and IV subunits was observed in *Slc7a9*$^{-/-}$ male mice while in females those percentages were between 6-13 %. Few or any nuclear encoded components of complex II and ATP synthase were found downregulated in male and female mice, respectively. In contrast to the robust results obtained in mtDNA encoded subunits, showing a highly concordance in downregulated genes in male and female mice, only two nuclear DNA encoded ETC subunits were downregulated in both male and female (*Ndufa6* and *Ndufb11*) and one assembly factor (*Cep89*). These results suggest a mayor defect in mtDNA expression, although no genetic alterations in mtDNA replication, transcription or translation were observed. However, it has been described that mtDNA is damaged under oxidative stress and can accumulate point mutations and deletions that may alter its transcription (Cha et al., 2015; Yakes & Van Houten, 1997). As example, in humans, a 4,977 bp deletion affecting *MT-ND3*, *MT-ND4*, *MT-ND4L*, *MT-ND5*, *MT-COX3*, *MT-ATP6* and *MT-ATP8* genes has been commonly found and related to oxidative stress and aging processes (Lee et al., 1994; Li et al., 2016). mtDNA is more susceptible than nuclear DNA to oxidative stress as it is easily affected by ROS generation and mitochondria has limited mtDNA repair

enzymes (Fontana & Gahlon, 2020). In addition, as mt-RNAs are transcribed as long polycistronic precursor transcripts that need to be further processed to obtained mature mRNAs and rRNAs, mechanisms that regulate these processes may contribute to mtDNA subunits downregulation (Bonawitz et al., 2006; Ojala et al., 1981). Alterations of the *Tfam* gene have been related to depletion of mitochondrial transcripts and respiratory chain deficiencies (Silva et al., 2000; Wang et al., 1999) and when knocking down the *Tefm* gene, reduced transcript levels are observed leading to a severe respiratory chain defect (Minczuk et al., 2011). However, defects in *Tfam* and *Tefm* genes would also affect tRNA and rRNA transcription and this was not observed in *Slc7a9*$^{-/-}$ mice. Specifically, depletion of OXPHOS mRNAs with no effect in rRNAs and tRNAs transcription has been observed in *Lrpprc* inactivation which induces an impairment on OXPHOS subunits assembly (Gohil et al., 2010; Sasarman et al., 2010). LRPPRC protein is found associated with SLIRP (LRPPRC-SLIRP) which function is essential for mitochondrial mRNA maintenance and stability (Sasarman et al., 2010). Inactivation of either LRPPRC or SLIRP proteins induces a lower expression of the other protein and a reduction in mitochondrial mRNAs polyadenylation and an increase in mRNAs degradation (Chujo et al., 2012; Ruzzenente et al., 2012). LRPPRC regulatory pathways described until now are related to mTOR complex 1, as its inhibition decreases LRPPRC expression (Mukaneza et al., 2019), and SIRT3 activity (Liu et al., 2014). Further studies regarding mtDNA damage by oxidative stress, and LRPPRC function and regulation in *Slc7a9*$^{-/-}$ mice are needed to infer their role in ETC mitochondrially encoded mRNAs downregulation in cystinuria.

The observed consequences of the downregulation of OXPHOS gene expression in *Slc7a9*$^{-/-}$ mice were a decrease in NAD^+/NADH ratio, lower complex IV enzymatic activity and a reduction in the maximal mitochondrial respiration. Increased NADH levels in *Slc7a9*$^{-/-}$ mice suggests an impairment of complex I activity that led to its substrate accumulation. However, *ex vivo* mitochondrial respiration assay showed no differences in complex I functional activity in *Slc7a9*$^{-/-}$ mice compared to WT mice indicating that, although genetic alterations were found, physiological activity of

complex I can be stimulated by malate, pyruvate and glutamate in *Slc7a9*$^{-/-}$ mice to WT mice levels. Accordingly with gene expression results, no differences were found between WT and *Slc7a9*$^{-/-}$ mice in complex II neither in enzymatic activity nor in its physiological activity when stimulated by succinate. Regarding complex III, no direct evidence was further studied. Finally, concerning complex IV, lower levels of its enzymatic activity were observed in *Slc7a9*$^{-/-}$ mice providing evidence of its impairment in this cystinuria mouse model. Interestingly, in addition of common complex IV downregulated mtDNA encoded subunits in male and female *Slc7a9*$^{-/-}$ mice, the expression of the complex IV assembly factor *Cep89* was also found downregulated in both sexes. In humans, *CEP89* gene is located next to *SLC7A9* gene in the chromosome 19q13 and a deletion affecting both genes has been described in one patient affected by cystinuria and isolated complex IV deficiency (Van Bon et al., 2013). In the mouse genome, both genes are also located together in the chromosome 7. The *Slc7a9*$^{-/-}$ mouse model was generated replacing exons 3 to 9 by homologous recombination (Feliubadaló et al., 2003), but, as the *Slc7a9* gene has 13 exons, no alteration on *Cep89* gene sequence should be observed. However, further studies analyzing *Cep89* gene sequence and gene expression in other tissues should be performed in order to discard direct or indirect genetic defects related to mouse model generation.

Complex IV is the last component of the ETC being responsible for the electron transfer to O_2 and is highly regulated by mitochondrial electric membrane potential and allosterically inhibition by ATP (Dalmonte et al., 2009; Ramzan et al., 2010). Thus, complex IV regulates oxidative phosphorylation and determines the maximal, basal and reserve respiratory capacity of the mitochondria. In the *Slc7a9*$^{-/-}$ mouse model a decreased maximal respiration capacity was observed compared to WT, above all when complex I was inhibited. Maximal respiratory capacity plays a pivotal role during acute or chronic stress and in high demanding energy conditions, and several cardiovascular (Gong et al., 2003), neurological (Bell et al., 2020) and metabolic (Mali et al., 2016) pathologies results in lower maximal respiratory capacity. Additionally, these findings have been described in aging and connected to age and oxidative-related mtDNA

mutations (Boffoli et al., 1994; Short et al., 2005). The kidney is a high energy-demanding organ and proximal tubules are highly dependent on ATP production by OXPHOS system to maintain active reabsorption of glucose, ions and essential nutrients (Hall et al., 2009; Weinberg et al., 2000), and maximal respiratory could be essential in stressful conditions. As example, lower levels of maximal respiratory capacity have been observed in renal cells under hyperglycemia conditions (Czajka & Malik, 2016). In cystinuria, the loss of cystine in urine and/or the presence of cystine crystals in the luminal fluid may produce oxidative stress in the kidneys that could induce mutations in mtDNA and dysfunction of the OXPHOS system. However, further studies are needed to understand if mitochondrial dysfunction is a consequence of cystine crystal induced stress or has a role in the stone formation process.

The relation between the OXPHOS system and the TCA cycle is obvious as both share the succinate dehydrogenase enzymatic complex and the TCA cycle supplies essential substrates to the OXPHOS system. When the ETC is impaired, NADH is accumulated and can inhibit regulatory enzymes of TCA as *PDHA*, iso-citrate dehydrogenase (*IDH*) and oxoglutarate dehydrogenase (*OGDH*) (Donnelly et al., 2012; Harris et al., 2002; Martínez-Reyes & Chandel, 2020). Downregulation of these genes was not observed in the RNA-seq analysis, but this could be explained as ATP and acetyl-CoA levels also regulated their gene expression (Donnelly et al., 2012; Martínez-Reyes & Chandel, 2020). In contrast, we observed a depletion on citrate and lower fumarate levels in the kidneys of the *Slc7a9*$^{-/-}$ mouse model. A possible explanation for the citrate depletion observed could be the impairment of the anaplerotic TCA cycle mechanism by pyruvate as *Pcx* gene was downregulated in cystinuric mice. The other anaplerotic TCA cycle mechanism, glutaminolysis, that use glutamine to regenerate α-Ketoglutarate, could restored the α-Ketoglutarate levels in *Slc7a9*$^{-/-}$ mice as no differences were observed when compared to WT, but it has also been described to maintained citrate levels in cells with defective transport of pyruvate (Yang et al., 2014). Thus, *Pcx* downregulation seems not enough to deplete kidney intracellular citrate levels.

In renal cells, apart from its synthesis by the TCA cycle, high amounts of citrate are reabsorbed through proximal tubules and used for renal oxidative metabolism. The apical Na^+-dependent dicarboxylate cotransporter (*Slc13a2*, NaDC-1) is the main responsible for citrate reabsorption (Pajor, 1996), and it was found downregulated in *Slc7a9*$^{-/-}$ male mice (LogFC -0.40 and padj 0.003, data not shown), although depletion of citrate levels were observed in both male and female cystinuric mice kidneys. NaDC-1 expression is mainly regulated by acid-base homeostasis and an increase in alkali load inhibit citrate reabsorption whereas acid load induces hypocitraturia (Aruga et al., 2000; Kaufman et al., 1985). In addition, hypercitraturia can be caused by divalent cations that retain citrate in the urine and the oxalate transporter (*Slc26a6*) that inhibits NaDC-1 activity (Ohana et al., 2013). Citrate is a deeply studied molecule in stone formation processes as inhibits calcium stone growth by chelating free calcium ions and binding CaOx or CaP crystals preventing its aggregation (Krieger et al., 2015). However, it has not been described that citrate could bind cystine and potassium citrate is administered to cystinuria patients not as crystal growth inhibitor but as an alkalinizing agent (Fjellsted et al., 2001).

Collectively, these chapter uncover a genetic defect in the ETC that lead to an impaired maximal respiratory capacity in the kidneys of the *Slc7a9*$^{-/-}$ cystinuria mouse model. In addition, a TCA cycle alteration was also observed in cystinuric mice as kidneys intracellular levels of citrate were severely reduced. The mechanism by which these defects are produced and its consequence to stone formation need further investigation.

5.3. Chapter III

After finding that the *Slc22a4* gene expression was downregulated in *Slc7a9*$^{-/-}$ stone former mice compared to non-stone former ones, OCTN1 was suggested as a modulating factor of cystinuria (Espino, 2012). In fact, it was its main substrate, L-Erg, that for its thione/thiol structure was thought to has a protecting role in cystine lithiasis. Then, when a double mutant *Slc7a9*$^{-/-}$*Slc22a4*$^{-/-}$ mouse was generated in our group, an increase in the rate of stone formation was observed in both male and female double mutant mice compared to *Slc7a9*$^{-/-}$ mice. This finding supported the hypothesis of OCTN1 and/or L-Erg modulating cystine lithiasis. Now, in the third chapter of this thesis, it has been demonstrated the potential therapeutical effect of L-Erg preventing cystine lithiasis in the *Slc7a9*$^{-/-}$ cystinuria mouse model by increasing cystine solubility in the urine. In addition, an improve in oxidative stress status and mitochondrial function in the kidneys of cystinuric mice was also observed after L-Erg treatment.

The preventive (before any stone event) and long-term administration (6 months) of 16 mg/kg/day of L-Erg decreased the rate of stone formation and delayed the lithiasis onset in *Slc7a9*$^{-/-}$ mice. No adverse effects were observed regarding mice weight and development, water and food intake. When attempting to understand the mechanism by which L-Erg reduced stone formation, the first approach was to study if L-Erg could bind cysteine and act as a thiol-binding molecule. But, in an *in vitro* assay combining different concentration gradients of cysteine and L-Erg in a pH 7.2 water solution no cysteine-L-Erg heterodimers were detected by LC/MS-MS. In addition, when cystine concentration was measured in urines of treated and untreated mice no differences were observed, confirming that L-Erg was not chelating cysteine in treated urines. Moreover, other authors attempt to study L-Erg-cysteine dimerization in physiological conditions and obtained the same results, and only in strongly acid solutions cysteine-L-Erg disulfides were formed (Heath & Toennies, 1958). This could be explained as although L-Erg exist as a tautomer between the thione and the thiol form, at physiological pH, the thione is the predominant form (Heath & Toennies, 1958).

In this work, it is shown that L-Erg (16 mg/kg/day) treatment increased cystine solubility in urines of treated mice independently of urinary pH or hydration and diuretic induction. The increase in cystine solubility was not observed when L-Erg was *in vitro* added to urines of cystinuric mice suggesting the needed of intracellular kidney metabolism of L-Erg, being reabsorbed by OCTN1, to induce treatment effectiveness. The relevance of L-Erg metabolism in preventing stone formation was confirmed when double mutant *Slc7a9*$^{-/-}$*Slc22a4*$^{-/-}$ mice were treated with L-Erg (16 mg/kg/day) as no differences were observed in stone formation rate or onset between untreated and treated mice. Intracellular mechanisms attributed to L-Erg are related to its antioxidant and metal chelating properties (reviewed in the **Table 6** of the introduction). Interestingly, the antioxidant α-Lipoic Acid, also increases cystine solubility in the urine of cystinuria patients and mouse models via its derived metabolism, although the specific pathway or metabolite(s) have not been yet identify (Cil & Perwad, 2020; Zee et al., 2017). In addition, Salvianolic Acid B and Selenium, other antioxidant molecules described as a potential treatment for cystinuria, reduced cystine crystal formation when administered to cystinuric mice and patients, respectively (Mohammadi et al., 2018; Yifan et al., 2019). Thus, common pathways of these molecules could clarify the effect of antioxidants in cystinuria.

Alterations in oxidative stress status have been observed in both cystinuria patients and mouse models. To date, the evidence described in patients related to oxidative stress are lower levels of GSH in leukocytes (Mårtensson et al., 1990), a decreased activity of SOD, GPx and iNOS antioxidant enzymes and an accumulation of lipid peroxidation in blood samples (Al-Shehabat et al., 2017; Yifan et al., 2019). Studies using the *Slc7a9*$^{-/-}$ mouse model allowed to analyze oxidative status in the kidneys where similar results were observed: a decrease in SOD and GPx antioxidant enzymes and an increase in lipid peroxidation (Yifan et al., 2019). In addition, total liver GSH content was found diminished in the *Slc3a1*$^{-/-}$ mouse model (Woodard et al., 2019). In this thesis, kidney, liver and urinary GSH levels were determined in the *Slc7a9*$^{-/-}$ mouse model for the first time. In the kidney, severely lower GSH and GSSG levels were

observed in cystinuric mice confirming the alteration of oxidative stress status related to cystinuria. In the liver, as previously observed in the *Slc3a1*$^{-/-}$ mouse model (Woodard et al., 2019), GSH content was significantly diminished in *Slc7a9*$^{-/-}$ mice compared to WT ones indicating the oxidative impairment in the whole organism. Finally, higher GSH and GSSG excretion was detected in the urine of cystinuric mice probably due to the lower GGT1 protein expression detected in these mice that diminish GSH turnover. These three findings reinforce the evidence of a compromised antioxidant capacity in cystinuria that could improve with antioxidant treatments.

L-Erg (16 mg/kg/day) treatment significatively increased GSH levels in the kidneys of cystinuric mice, although not to restored WT levels. This increase in GSH content was not observed in the livers of treated mice, but lower levels of GSSG were detected reflecting an improvement of the oxidative status after L-Erg treatment. The interorgan metabolism could explain that GSH levels were not increased in livers as, under oxidative stress conditions, large amounts of GSH are released from the liver to blood to supply other organs (Anderson et al., 1980; Griffith & Meister, 1979). Exogenous GSH is vital to increase the kidney GSH content to protect cells from oxidative stress or toxicological conditions, even above renal resynthesis of GSH from its precursors, which can be limited under these conditions (Visarius et al., 1996). As after L-Erg treatment GSH turnover could not be restored in the kidneys of *Slc7a9*$^{-/-}$ mice (no changes in GGT activity and total GSH excretion were observed when compared to untreated mice), the induction of the interorgan metabolism could be responsible for the increase in kidney GSH levels in treated mice. In addition, when analyzing the gene expression of enzymes related to GSH synthesis in the livers of treated mice, an increase in *Gclm* and *GPx* expression was observed compared to untreated ones, demonstrating the induction of GSH synthesis by L-Erg treatment. Although GCLM is the modifier subunit of GCL enzyme, *Gclm* up-regulation directly correlates with GCL activity facilitating the heterodimer formation and improving its efficiency by lowering substrates K_m (Chen et al., 2005; Lee et al., 2006). Regarding GSH synthesis in the kidneys, differences in *Gclm*, *Gss* and *Gsr* gene expression were only observed between

non-stone and stone former treated mice uncovering a differential GSH synthesis induction by L-Erg according to mice lithiasic phenotype. Nevertheless, concerning GCLC-GCLM heterodimer protein expression in the kidneys, an increased expression in treated compared to untreated mice was detected together with higher levels of its product γ-glutamyl-L-cysteine, indicating that GSH synthesis was also induced in the kidneys of treated mice. These findings related to the improvement of oxidative stress status in both kidneys and livers of L-Erg treated mice could be mediated by NRF2 pathway activation as NRF2 protein expression was found increased in treated kidneys.

Previous studies have also described the L-Erg modulation of oxidative stress in kidneys and livers of animal models (Dare et al., 2021; Deiana et al., 2004; Shinozaki et al., 2017). In addition, the induction of NRF2 pathway by L-Erg has been observed in the kidneys of rat models of type 2 diabetes and cisplatin-evoked nephrotoxicity after the orally administration of 35 or 70 mg/kg/day of L-Erg, respectively (Dare et al., 2021; Salama et al., 2021). In both studies, NRF2 induction led to a recovery of GSH levels, an increase in antioxidant defenses (SOD and GPx) and a reduction in lipid peroxidation that improve renal function. Moreover, a downregulation of NF-kβ expression and reduced concentrations of its downstream inflammatory cytokines were also observed, probably due to NRF2 inhibition of IkB degradation (Cuadrado et al., 2014; Wardyn et al., 2015). These additional properties reported in the literature to L-Erg treatment could recover the antioxidant defect observed in cystinuria patients and mouse models: lower levels of GSH, a decrease activity in SOD and GPx enzymes, and an accumulation of lipid peroxidation (Al-Shehabat et al., 2017; Mårtensson et al., 1990; Woodard et al., 2019; Yifan et al., 2019). Although antioxidant enzymes activity and lipid peroxidation have still to be determined in our cystinuric model to completely assess L-Erg beneficial effect in cystinuria, in this work, NRF2 induction and an increase in GSH levels in *Slc7a9*$^{-/-}$ mice kidneys after L-Erg treatment was demonstrated indicating the improvement of the oxidative status in cystinuria by L-Erg.

However, the α-Lipoic Acid effect in cystine lithiasis was showed to be independently of NFR2 action as the reduction in stone growth rate was also observed in double

mutant *Slc3a1*$^{-/-}$*Nrf2*$^{-/-}$ treated mice (Zee et al., 2017). α-Lipoic Acid shares other common biological functions with L-Erg as scavenging reactive oxygen species (Li et al., 2004), chelation of divalent metal ions (Ou et al., 1995) and inhibition of NF-kβ activation independently of its antioxidant effect (Ying et al., 2011). In addition, several studies have described the improvement of mitochondrial function after α-Lipoic Acid supplementation (Chang et al., 2021; El-Beshbishy et al., 2013; Mozaffarian et al., 2021; Zeng et al., 2021). In this thesis, an impaired mitochondrial activity related to OXPHOS and TCA cycle was described for the first time in cystinuria, and, after L-Erg treatment, a recovery in NAD^+/NADH levels, complex IV enzymatic activity and maximal respiratory capacity was achieved. Only *in vitro* studies have described the localization of OCTN1 in the mitochondrial membrane (Lamhonwah & Tein, 2006, 2020; Shitara et al., 2012), but, L-Erg has also been found accumulated inside the mitochondria (Kawano et al., 1982) demonstrating that targets this organelle. In addition, L-Erg administration was showed to reduce mitochondrial ROS production *in vitro* (D'onofrio et al., 2016; Markova et al., 2009; Obayashi et al., 2005) and in the kidneys of a preeclampsia mouse model (Williamson et al., 2020). The protective role of L-Erg to mitochondrial components affected by ROS is supported as in cells with OCTN1 silenced, an increased mtDNA damage by H_2O_2 is observed (Paul & Snyder, 2010). In addition, several works have described the reduction in lipid peroxidation in the presence of L-Erg (Deiana et al., 2004; Kawano et al., 1983; Markova et al., 2009; Paul & Snyder, 2010). Collectively, these findings together with the results presented in this thesis suggest the potential beneficial effect of L-Erg treatment improving the mitochondrial function and the mitochondrial oxidative derived damage in cystinuria.

Oxidative stress and mitochondrial dysfunction have been proposed to be involved in the pathophysiology of kidney stone disease, mainly studied in CaOx stones (Cao et al., 2004; Farooq et al., 2014; Niimi et al., 2012). Moreover, several antioxidants targeting mitochondrial defects showed beneficial effects in nephrolithiasis mouse models reducing crystals depositions by lowering ROS and lipid peroxidation, and restoring antioxidant defenses and respiratory chain activity (Hirose et al., 2010; Li et

al., 2009; Marhoume et al., 2021; Niimi et al., 2014; Sharma et al., 2015, 2016). Crystal interaction with renal epithelial cells induces cytotoxicity leading to membrane disruption, stimulation of ROS production and the subsequent impairment of mitochondria (Hirose et al., 2010; Peerapen et al., 2018; Sun et al., 2016). Then, ROS induction of cell membrane lipid peroxidation allow crystal deposition on the surface of injured renal tubular cells and its aggregation promoting the stone formation (Cao et al., 2016; Fong-Ngern et al., 2017; Huang et al., 2003). However, CaOx crystals can also be internalized into renal cells by macropinocytosis to be degraded by the endolysosomes (Chaiyarit & Thongboonkerd, 2012; Kanlaya et al., 2013), and the intracellular overload of calcium and oxalate ions could also contributed to ROS production and mitochondrial dysfunction (Calvo-Rodriguez et al., 2020; Peng & Jou, 2010). Cyst(e)ine cytotoxicity has been demonstrated in renal epithelial cells *in vitro* studies and is mainly related to lipid peroxidation and necrosis induction (Mulay et al., 2016; Nakanishi et al., 2005; Nishiuch et al., 1976). Thus, lipid peroxidation could promote cystine stone formation as does with CaOx stones. However, although cystine plugs can be observed in the tubules of cystinuria patients, those are not strongly attached to the tissue (Evan et al., 2006) and, in mouse models, cystine stones are mainly observed in the bladder rather than in the kidney. Nevertheless, lipid peroxidation could induce initial cystine crystals nucleation and aggregation although further stone growth take place freely in solution. This hypothesis could explain why L-Erg treatment prevents and delays stone onset but has no effect once the stone is already formed.

Finally, high dose (200 mg/kg/day) L-Erg treatment confirmed the preventive effect of this molecule in cystinuria reducing the stone formation rate and the post-mortem stone weight in *Slc7a9*$^{-/-}$ treated mice. In addition, an increased effect was observed compared to the previous dose administered. This finding suggests a dose dependent L-Erg effect in the prevention of cystine lithiasis. The 200 mg/kg/day dose administered to mice corresponds approximately to a HED of 1 g/day for a 60 kg adult (or 16.2 mg/kg/day) (Nair & Jacob, 2016). The L-Erg NOAEL stablished for adults,

pregnant women and infants is 800 mg/kg/day which led to a 49.4 times (800/16.2) margin of exposure to our highest dose (FDA, 2017). However, a pharmacokinetic study of L-Erg distribution and accumulation in mouse tissues showed no differences in kidney L-Erg accumulation comparing the administration of two different doses: 35 and 70 mg/kg/day, suggesting the saturation of L-Erg transporter at 35 mg/kg/day (Tang et al., 2018). Further studies are needed to determine L-Erg metabolism after high dose administration and its impact in cystine solubility, which results could lead to narrow the optimal dose. In addition, the evaluation of L-Erg metabolism in treated mice could shed a light on those mice in which the treatment was not fully effective as the urinary S-Methyl-L-Ergothioneine to L-Erg ratio showed to be a robust biomarker of cystine lithiasis in the *Slc7a9*$^{-/-}$ mouse model, associating a higher L-Erg metabolism with no stone formation (Lopez de Heredia et al., 2021). Moreover, as *SLC22A4* variants with high allele frequency have been related to an increase (p.Leu503Phe, Taubert et al., 2005) or to an impaired transport of L-Erg (Toh et al., 2013), the *SLC22A4* gene should be analyzed in cystinuric patients to assess its possible role in stone formation and to better control the L-Erg dose to administered as a preventing treatment for cystine lithiasis.

In summary, L-Erg treatment has showed a potential preventive effect in cystine lithiasis by increasing cystine solubility in urine. L-Erg internalization by OCTN1 was essential for its effectiveness indicating the importance of the intracellular mechanism of L-Erg or its derived metabolism. In addition, L-Erg treatment overcame kidney mitochondrial functional impairment described in chapter II and ameliorated the oxidative stress defect related to cystinuria. Collectively, these data and the safety profile of L-Erg indicates that its administration to cystinuria patients should be tested as a preventive treatment in combination with the conservative therapies described in the introduction.

CONCLUSIONS

6. CONCLUSIONS

1. AGT1/rBAT expression modulates cystine lithiasis and aspartate, glutamate and cystine excretion in cystinuria mouse models.
2. No evidence of cystinuria causative or modulating *SLC7A13* variants was observed in 9 uncharacterized cystinuria patients (with only one *SLC7A9* allele affected or without any genetic variant described in *SLC3A1* and *SLC7A9* genes).
3. The RNA-seq analysis performed in the kidneys of WT and *Slc7a9*$^{-/-}$ mice uncovered the downregulation of the oxidative phosphorylation pathway.
4. Most electron transport chain mtDNA encoded subunits are downregulated in the kidneys of the *Slc7a9*$^{-/-}$ cystinuria mouse model, leading to impaired maximal respiratory capacity.
5. Long-term L-Ergothioneine administration prevents cystine lithiasis events and delays its onset in the *Slc7a9*$^{-/-}$ cystinuria mouse model by increasing cystine solubility in the urine.
6. L-Ergothioneine internalization by OCTN1 is essential for treatment effectiveness.
7. Long-term L-Ergothioneine treatment recovers cystinuria mitochondrial defects and improves oxidative damage in the kidneys of the *Slc7a9*$^{-/-}$ cystinuria mouse model.

ANNEXES

7. ANNEXES

7.1. DIFFERENTIALLY EXPRESSED GENES FROM RNA-SEQ ANALYSIS

Supplementary Table 1. Transcripts downregulated and upregulated in both Slc7a9$^{-/-}$ mice expressed as a Log2FC to WT mice gene expression

Symbol	Description	Log2FC M	padj M	Log2FC F	padj F
Slc7a9	solute carrier family 7 (cationic amino acid transporter, y+ system), member 9	-2.30	0.00	-2.18	0.00
Nudt19	nudix (nucleoside diphosphate linked moiety X)-type motif 19	-1.35	0.00	-1.56	0.00
AW822252	expressed sequence AW822252	-0.98	0.00	-1.24	0.00
Mogat2	monoacylglycerol O-acyltransferase 2	-0.95	0.00	-0.78	0.00
Dzip1	DAZ interacting protein 1	-0.86	0.00	-0.61	0.01
Pou2f2	POU domain, class 2, transcription factor 2	-0.83	0.00	-1.02	0.01
Pxdn	peroxidasin	-0.72	0.00	-0.60	0.00
Pdlim2	PDZ and LIM domain 2	-0.69	0.00	-0.49	0.00
Slc34a3	solute carrier family 34 (sodium phosphate), member 3	-0.68	0.00	-0.48	0.04
Islr	immunoglobulin superfamily containing leucine-rich repeat	-0.67	0.00	-0.61	0.02
Sectm1b	secreted and transmembrane 1B	-0.65	0.00	-0.48	0,04
A730008H23Rik	RIKEN cDNA A730008H23 gene///Holliday junction recognition protein	-0.65	0.00	-0.51	0.00
Dpep1	dipeptidase 1	-0.64	0.00	-0.63	0.00
Gpc3	glypican 3	-0.62	0.00	-0.88	0.00
Ntng2	netrin G2	-0.60	0.00	-0.61	0.01
Adamts5	a disintegrin-like and metallopeptidase (reprolysin type) with thrombospondin type 1 motif, 5 (aggrecanase-2)	-0.60	0.00	-1.39	0.00
Loxl1	lysyl oxidase-like 1	-0.58	0.00	-0.60	0.00
Wdr86	WD repeat domain 86	-0.56	0.00	-0.83	0.00
Cep89	centrosomal protein 89	-0.55	0.00	-0.28	0.00
Tm7sf2	transmembrane 7 superfamily member 2	-0.53	0.00	-0.39	0.02
Prr15	proline rich 15	-0.52	0.00	-0.52	0.01
Egflam	EGF-like, fibronectin type III and laminin G domains	-0.51	0.00	-0.73	0.00
Dcn	decorin	-0.50	0.01	-0.75	0.01
BC049352	cDNA sequence BC049352	-0.49	0.02	-0.87	0.04
Ltbp4	latent transforming growth factor beta binding protein 4	-0.49	0.00	-0.42	0.02
ATP6	ATP synthase F0 subunit 6	-0.49	0.00	-0.48	0.00
Mgst3	microsomal glutathione S-transferase 3	-0.48	0.00	-0.28	0.03
Mmp14	matrix metallopeptidase 14 (membrane-inserted)	-0.47	0.00	-0.64	0.01
Pvalb	parvalbumin	-0.47	0.01	-0.59	0.02

Abca8a	ATP-binding cassette, sub-family A (ABC1), member 8a	-0.47	0.00	-0.61	0.01
ND3	NADH dehydrogenase subunit 3	-0.44	0.00	-0.62	0.00
D430019H16Rik	RIKEN cDNA D430019H16 gene	-0.43	0.00	-0.62	0.01
COX2	cytochrome c oxidase subunit II	-0.43	0.00	-0.38	0.04
Col6a1	collagen type VI, alpha 1	-0.42	0.01	-0.53	0.02
Ak5	adenylate kinase 5	-0.41	0.02	-0.84	0.01
Col3a1	collagen, type III, alpha 1	-0.41	0.02	-1.00	0.00
ND1	NADH dehydrogenase subunit 1	-0.41	0.00	-0.49	0.00
Gpx3	glutathione peroxidase 3	-0.40	0.00	-0.27	0.04
Pdcd5	programmed cell death 5	-0.40	0.00	-0.48	0.00
Gdf10	growth differentiation factor 10	-0.40	0.01	-0.57	0.02
Pdgfrb	platelet derived growth factor receptor, beta polypeptide	-0.39	0.00	-0.44	0.00
Flt3l	FMS-like tyrosine kinase 3 ligand	-0.39	0.00	-0.46	0.03
C1qtnf2	C1q and tumor necrosis factor related protein 2	-0.39	0.01	-0.67	0.00
Tgfbi	transforming growth factor, beta induced	-0.39	0.00	-0.80	0.00
Il11ra1	interleukin 11 receptor, alpha chain 1	-0.39	0.00	-0.29	0.02
Clec2h	C-type lectin domain family 2, member h	-0.38	0.01	-0.71	0.00
Scarf2	scavenger receptor class F, member 2	-0.38	0.00	-0.30	0.04
Gpatch1	G patch domain containing 1	-0.38	0.00	-0.24	0.05
E230016K23Rik	RIKEN cDNA E230016K23 gene	-0.38	0.00	-0.45	0.04
Hebp1	heme binding protein 1	-0.37	0.00	-0.30	0.03
Mettl1	methyltransferase like 1	-0.36	0.00	-0.36	0.02
ND4	NADH dehydrogenase subunit 4	-0.36	0.00	-0.56	0.00
Tnxb	tenascin XB	-0.36	0.01	-0.41	0.04
Col6a2	collagen, type VI, alpha 2	-0.36	0.03	-0.63	0.02
Thbs3	thrombospondin 3	-0.35	0.01	-0.60	0.01
COX3	cytochrome c oxidase subunit III	-0.35	0.00	-0.40	0.01
Igfbp3	insulin-like growth factor binding protein 3	-0.35	0.01	-0.62	0.00
Rasa3	RAS p21 protein activator 3	-0.34	0.00	-0.39	0.03
Mrc2	mannose receptor, C type 2	-0.34	0.00	-0.71	0.00
Kdr	kinase insert domain protein receptor	-0.34	0.01	-0.48	0.01
P2rx4	purinergic receptor P2X, ligand-gated ion channel 4	-0.34	0.00	-0.22	0.03
Itgb3	integrin beta 3	-0.33	0.04	-0.77	0.03
Gucy1a1	guanylate cyclase 1, soluble, alpha 1	-0.33	0.02	-0.57	0.01
Svep1	sushi. von Willebrand factor type A, EGF and pentraxin domain containing 1	-0.33	0.02	-0.82	0.00
Emp3	epithelial membrane protein 3	-0.32	0.01	-0.37	0.04
Ccn4	cellular communication network factor 4	-0.32	0.04	-1.07	0.00
Col1a2	collagen, type I, alpha 2	-0.32	0.02	-0.60	0.01
Nes	nestin	-0.32	0.00	-0.41	0.01
Ext1	exostosin glycosyltransferase 1	-0.32	0.00	-0.36	0.02
Angptl2	angiopoietin-like 2	-0.31	0.02	-0.55	0.01
Col5a1	collagen, type V, alpha 1	-0.31	0.00	-0.46	0.00
Ripor3	RIPOR family member 3	-0.30	0.03	-0.40	0.05

Rell1	RELT-like 1	-0.30	0.00	-0.31	0.03
Pik3cd	phosphatidylinositol-4,5-bisphosphate 3-kinase catalytic subunit delta	-0.30	0.02	-0.57	0.01
Rcn3	reticulocalbin 3, EF-hand calcium binding domain	-0.30	0.01	-0.52	0.00
ND5	NADH dehydrogenase subunit 5	-0.29	0.02	-0.56	0.00
Cdh13	cadherin 13	-0.29	0.01	-0.74	0.00
Lrp1	low density lipoprotein receptor-related protein 1	-0.29	0.01	-0.58	0.00
Lpar1	lysophosphatidic acid receptor 1	-0.29	0.02	-0.48	0.02
Esm1	endothelial cell-specific molecule 1	-0.29	0.04	-0.78	0.00
CYTB	cytochrome b	-0.29	0.01	-0.50	0.00
Ndufa6	NADH:ubiquinone oxidoreductase subunit A6	-0.28	0.00	-0.22	0.03
Ndufb11	NADH:ubiquinone oxidoreductase subunit B11	-0.28	0.00	-0.26	0.02
Daam2	dishevelled associated activator of morphogenesis 2	-0.27	0.02	-0.64	0.00
Galnt10	polypeptide N-acetylgalactosaminyltransferase 10	-0.27	0.00	-0.31	0.03
Cd300lg	CD300 molecule like family member G	-0.27	0.03	-0.40	0.04
ND2	NADH dehydrogenase subunit 2	-0,27	0.03	-0.56	0.00
Hnf4aos	hepatic nuclear factor 4 alpha. opposite strand	-0.27	0.03	-0.46	0.02
Fbln5	fibulin 5	-0.27	0.05	-0.82	0.00
Rpl26	ribosomal protein L26	-0.27	0.00	-0.33	0.01
Mxra7	matrix-remodelling associated 7	-0.27	0.00	-0.33	0.03
ND4L	NADH dehydrogenase subunit 4L	-0.27	0.01	-0.39	0.01
Mgp	matrix Gla protein	-0.26	0.04	-0.76	0.00
P3h3	prolyl 3-hydroxylase 3	-0.26	0.01	-0.37	0.01
Ybx1	Y box protein 1	-0.26	0.00	-0.33	0.01
Pfdn1	prefoldin 1	-0.26	0.00	-0.25	0.04
Mylk	myosin, light polypeptide kinase	-0.26	0.01	-0.30	0.02
Camk2n1	calcium/calmodulin-dependent protein kinase II inhibitor 1	-0.25	0.00	-0.27	0.00
Zranb1	zinc finger, RAN-binding domain containing 1	-0.25	0.00	-0.45	0.00
Fbn1	fibrillin 1	-0.25	0.04	-0.52	0.01
Tmem256	transmembrane protein 256	-0.24	0.01	-0.29	0.03
Cxcl16	chemokine (C-X-C motif) ligand 16	-0.24	0.01	-0.40	0.00
Eif5b	eukaryotic translation initiation factor 5B	-0.24	0.02	-0.69	0.00
Itga9	integrin alpha 9	-0.24	0.03	-0.52	0.00
C1s1	complement component 1, s subcomponent 1	-0.23	0.04	-0.58	0.00
Ppp3ca	protein phosphatase 3, catalytic subunit, alpha isoform	-0.23	0.01	-0.56	0.00
Fhl2	four and a half LIM domains 2	-0.22	0.03	-0.36	0.02
Dnajc19	DnaJ heat shock protein family (Hsp40) member C19	-0.22	0.02	-0.32	0.02
Irf8	interferon regulatory factor 8	-0.20	0.03	-0.39	0.01
Lmtk2	lemur tyrosine kinase 2	0.21	0.01	0.36	0.00

Fn3krp	fructosamine 3 kinase related protein	0.22	0.02	0.38	0.01
Gm11992	predicted gene 11992	0.23	0.02	0.33	0.03
Gpc4	glypican 4	0.25	0.01	0.45	0.00
Plscr1	phospholipid scramblase 1	0.25	0.00	0.23	0.02
Spats2	spermatogenesis associated, serine-rich 2	0.26	0.01	0.38	0.01
Hoxb9	homeobox B9	0.26	0.00	0.32	0.01
Btg1	BTG anti-proliferation factor 1	0.27	0.00	0.32	0.01
Nucks1	nuclear casein kinase and cyclin-dependent kinase substrate 1	0.29	0.00	0.37	0.01
Marveld2	MARVEL (membrane-associating) domain containing 2	0.30	0.00	0.28	0.02
Cobll1	Cobl-like 1	0.31	0.00	0.30	0.04
Esrp1	epithelial splicing regulatory protein 1	0.31	0.00	0.44	0.00
Slc41a2	solute carrier family 41. member 2	0.31	0.01	0.39	0.04
Apoa4	apolipoprotein A-IV	0.33	0.02	0.89	0.00
Aqp7	aquaporin 7	0.34	0.00	0.61	0.00
Ugt3a1	UDP glycosyltransferases 3 family, polypeptide A1	0.38	0.01	0.58	0.00
Bbx	bobby sox HMG box containing	0.39	0.00	0.24	0.05
Scin	scinderin	0.40	0.00	0.35	0.04
Slc7a13	solute carrier family 7, (cationic amino acid transporter, y+ system) member 13	0.40	0.04	1.53	0.00
Mdk	midkine	0.44	0.01	0.78	0.00
Plekhb1	pleckstrin homology domain containing, family B (evectins) member 1	0.48	0.00	0.42	0.02
Cdh6	cadherin 6	0.51	0.00	0.38	0.04
Wasf1	WAS protein family, member 1	0.51	0.00	0.56	0.05
Stc1	stanniocalcin 1	0.54	0.02	1.31	0.00
Cyp4a12b	cytochrome P450, family 4, subfamily a, polypeptide 12B	0.57	0.02	1.65	0.00
Ugt8a	UDP galactosyltransferase 8A	0.69	0.00	0.49	0.02
Cftr	cystic fibrosis transmembrane conductance regulator	0.69	0.00	0.50	0.05
Adm2	adrenomedullin 2	0.70	0.00	1.06	0.00
Nnt	nicotinamide nucleotide transhydrogenase	0.72	0.00	0.78	0.00
Cck	cholecystokinin	0.76	0.00	0.71	0.04
Slco4c1	solute carrier organic anion transporter family, member 4C1	0.79	0.00	0.63	0.00

The dashed line separates downregulated and upregulated transcripts. M = male, F = females, padj = p-value adjusted.

7.2. GENE EXPRESSION OF ETC NUCLEAR ENCODED SUBUNITS

Supplementary Table 2. Gene expression of ETC nuclear encoded subunits in Slc7a9$^{-/-}$ male and female mice expressed as a Log2FC of WT mice expression

Symbol	Log2FC M	padj M	Log2FC F	padj F
Complex I				
Ndufa1	-0.23	0.00	-0.14	0.20
Ndufa10	-0.02	0.81	0.02	0.88
Ndufa11	-0.24	0.00	-0.02	0.91
Ndufa12	-0.12	0.07	-0.04	0.73
Ndufa13	-0.35	0.00	-0.16	0.19
Ndufa2	-0.37	0.00	-0.25	0.08
Ndufa3	-0.02	0.86	0.01	0.96
Ndufa5	-0.16	0.02	-0.16	0.08
Ndufa6	-0.28	0.00	-0.22	0.03
Ndufa7	-0.09	0.26	-0.01	0.96
Ndufa8	-0.11	0.02	0.06	0.58
Ndufa9	-0.18	0.00	-0.10	0.14
Ndufab1	-0.05	0.42	0.00	1.00
Ndufb10	-0.15	0.02	-0.02	0.86
Ndufb11	-0.28	0.00	-0.26	0.02
Ndufb1-ps	-0.03	0.81	-0.14	0.21
Ndufb2	-0.04	0.71	-0.02	0.88
Ndufb3	-0.14	0.02	-0.20	0.03
Ndufb4	-0.11	0.25	-0.06	0.56
Ndufb5	-0.01	0.94	-0.09	0.38
Ndufb6	-0.04	0.65	-0.06	0.63
Ndufb7	-0.33	0.00	-0.08	0.41
Ndufb8	-0.20	0.04	-0.06	0.60
Ndufb9	-0.18	0.02	-0.05	0.66
Ndufc1	-0.03	0.77	-0.04	0.77
Ndufc2	-0.06	0.45	-0.01	0.93
Ndufs1	0.14	0.06	-0.02	0.92
Ndufs2	-0.09	0.08	-0.04	0.71
Ndufs3	-0.05	0.32	-0.04	0.75
Ndufs4	-0.05	0.63	-0.08	0.43
Ndufs5	-0.12	0.12	-0.17	0.12
Ndufs6	-0.25	0.00	-0.13	0.25
Ndufs7	-0.30	0.00	0.01	0.96
Ndufs8	-0.19	0.01	-0.07	0.53
Ndufv1	-0.12	0.14	-0.01	0.96
Ndufv2	-0.01	0.97	-0.05	0.70
Ndufv3	-0.03	0.80	0.15	0.19
Ndufaf1	0.11	0.15	0.02	0.88
Ndufaf2	0.00	0.97	-0.03	0.84
Ndufaf3	-0.12	0.09	0.03	0.82
Ndufaf4	0.33	0.01	0.02	0.84
Ndufaf5	-0.04	0.65	-0.03	0.84
Ndufaf6	0.00	1.00	-0.01	0.97
Ndufaf7	0.03	0.69	-0.01	0.96
Ndufaf8	-0.31	0.01	-0.06	0.46

Acad9	0.01	0.91	0.00	0.97
Ecsit	-0.26	0.00	-0.05	0.69
Foxred1	-0.07	0.34	-0.02	0.88
Nubpl	0.07	0.49	-0.04	0.65
Timmdc1	-0.12	0.12	-0.06	0.59
Tmem126b	0.08	0.39	-0.02	0.86
Complex II				
Sdha	0.01	0.93	-0.03	0.82
Sdhb	-0.19	0.01	-0.19	0.07
Sdhc	-0.08	0.21	-0.04	0.71
Sdhd	-0.04	0.56	-0.11	0.20
Sdhaf1	-0.25	0.02	0.01	0.97
Sdhaf2	0.14	0.03	0.00	0.99
Sdhaf3	0.03	0.81	-0.03	0.69
Sdhaf4	0.03	0.75	0.00	1.00
Complex III				
Uqcr10	-0.19	0.01	-0.08	0.45
Uqcr11	-0.25	0.01	-0.09	0.42
Uqcrb	0.01	0.92	-0.03	0.83
Cyc1	-0.17	0.01	-0.03	0.86
Uqcrc1	-0.13	0.05	0.00	0.99
Uqcrc2	0.06	0.26	-0.06	0.45
Uqcrfs1	-0.03	0.71	-0.01	0.97
Uqcrh	-0.14	0.04	-0.26	0.01
Uqcrq	-0.30	0.00	-0.09	0.40
Bcs1l	0.00	0.98	0.02	0.87
Lyrm7	-0.01	0.97	-0.02	0.90
Ptcd2	0.06	0.42	0.08	0.44
Ttc19	0.03	0.71	-0.01	0.96
Uqcc1	0.02	0.79	0.00	0.99
Uqcc2	-0.07	0.48	-0.02	0.87
Uqcc3	-0.30	0.00	-0.01	0.97
Complex IV				
Cox4i1	-0.16	0.05	-0.03	0.78
Cox4i2	-0.04	0.70	-0.04	0.30
Cox5a	-0.08	0.15	0.09	0.26
Cox5b	-0.21	0.00	-0.02	0.91
Cox6a1	-0.26	0.00	-0.02	0.89
Cox6a2	-0.83	0.01	-0.01	0.90
Cox6b1	-0.04	0.57	0.00	1.00
Cox6b2	-0.05	0.68	0.07	0.47
Cox6c	-0.18	0.04	-0.26	0.04
Cox7a1	0.12	0.28	0.00	0.97
Cox7a2	-0.12	0.17	-0.09	0.38
Cox7b	-0.15	0.09	-0.23	0.04
Cox7c	-0.14	0.09	-0.21	0.09
Cox8a	-0.29	0.00	-0.10	0.35
Cox8b	0.04	0.30	0.00	0.99
Apopt1	-0.13	0.13	-0.05	0.68
Cep89	-0.55	0.00	-0.28	0.00
Coa3	-0.04	0.65	0.02	0.87

Coa4	-0.03	0.75	-0.11	0.30
Coa5	0.11	0.09	0.00	1.00
Coa6	-0.11	0.24	-0.04	0.71
Coa7	-0.05	0.57	0.01	0.97
Cox10	-0.14	0.10	0.02	0.90
Cox11	0.10	0.22	0.03	0.77
Cox14	-0.28	0.00	-0.05	0.65
Cox15	0.23	0.01	0.21	0.08
Cox16	-0.14	0.16	-0.13	0.25
Cox17	-0.01	0.94	-0.05	0.47
Cox18	0.13	0.09	0.10	0.38
Cox19	-0.03	0.74	0.01	0.95
Cox20	0.10	0.30	-0.01	0.97
Fastkd2	0.06	0.53	-0.01	0.97
Lrpprc	0.04	0.61	0.02	0.91
Ndufa4	-0.05	0.59	-0.09	0.39
Ndufa4l2	-0.24	0.04	-0.06	0.42
Oxa1l	-0.08	0.29	0.04	0.73
Pet100	-0.05	0.62	-0.08	0.41
Sco2	-0.07	0.50	0.00	0.99
Surf1	-0.08	0.15	-0.08	0.40
Taco1	0.11	0.29	0.00	0.98
ATP Synthase				
Atp5a1	-0.05	0.57	-0.01	0.94
Atp5b	0.00	1.00	0.03	0.93
Atp5c1	-0.04	0.61	-0.11	0.20
Atp5d	-0.27	0.00	0.02	0.90
Atp5e	0.00	0.99	-0.02	0.90
Atp5g1	-0.21	0.00	0.01	0.97
Atp5g2	-0.09	0.21	0.00	0.99
Atp5g3	-0.16	0.00	-0.02	0.86
Atp5h	-0.15	0.01	-0.09	0.32
Atp5j	-0.02	0.86	-0.05	0.71
Atp5j2	-0.14	0.13	-0.10	0.34
Atp5l	-0.11	0.21	-0.19	0.12
Atp5o	-0.08	0.17	-0.06	0.51
Atpaf1	0.04	0.60	0.00	1.00
Atpaf2	0.06	0.41	0.06	0.58
Tmem70	0.12	0.19	0.00	0.99

Dashed lines separate ETC nuclear encoded structural subunits from assembly factors.
M = male, F = females, padj = p-value adjusted.

REFERENCES

8. REFERENCES

Adzhubei, I. A., Schmidt, S., Peshkin, L., Ramensky, V. E., Gerasimova, A., Bork, P., Kondrashov, A. S., & Sunyaev, S. R. (2010). A method and server for predicting damaging missense mutations. *Nature Methods*, *7*(4), 248–249. https://doi.org/10.1038/nmeth0410-248

Akanmu, D., Cecchini, R., Aruoma, O. I., & Halliwell, B. (1991). The antioxidant action of ergothioneine. *Archives of Biochemistry and Biophysics*, *288*(1), 10–16. https://doi.org/10.1016/0003-9861(91)90158-F

Al-Shehabat, M. A., Hani, I. B., Jaradat, S., & Hunaiti, A. A. (2017). Evaluation and comparison of a set of oxidative and antioxidative biomarkers in cystinuric patients with age- and sex-matched healthy subjects. *Comparative Clinical Pathology*, *26*(2), 411–416. https://doi.org/10.1007/s00580-016-2393-z

Alelign, T., & Petros, B. (2018). *Kidney Stone Disease: An Update on Current Concepts*. https://doi.org/10.1155/2018/3068365

Anderson, M. E., & Meister, A. (1980). Dynamic state of glutathione in blood plasma. *Journal of Biological Chemistry*, *255*(20), 9530–9533. https://doi.org/10.1016/s0021-9258(18)43421-7

Anderson, Mary E., Bridges, R. J., & Meister, A. (1980). Direct evidence for inter-organ transport of glutathione and that the non-filtration renal mechanism for glutathione utilization involves γ-glutamyl transpeptidase. *Topics in Catalysis*, *96*(2), 848–853. https://doi.org/10.1016/0006-291X(80)91433-3

Andries, A., Daenen, K., Jouret, F., Bammens, B., Mekahli, D., & Van Schepdael, A. (2019). Oxidative stress in autosomal dominant polycystic kidney disease: player and/or early predictor for disease progression? *Pediatric Nephrology*, *34*(6), 993–1008. https://doi.org/10.1007/s00467-018-4004-5

Aruga, S., Wehrli, S., Kaissling, B., Moe, O. W., Preisig, P. A., Pajor, A. M., & Alpern, R. J. (2000). Chronic metabolic acidosis increases NaDC-1 mRNA and protein abundance in rat kidney. *Kidney International*, *58*(1), 206–215. https://doi.org/10.1046/j.1523-1755.2000.00155.x

Aruoma, O. I., Whiteman, M., England, T. G., & Halliwell, B. (1997). Antioxidant action of ergothioneine: Assessment of its ability to scavenge peroxynitrite. *Biochemical and Biophysical Research Communications*, *231*(2), 389–391. https://doi.org/10.1006/bbrc.1997.6109

Asatoor, A., Freedman, P., Gabriel, J., MD, M., Prosser, D. I., Roberts, J. T., & Willoughby, C. P. (1974). Amino acid imbalance in Cystinuria. *J Clin Path*, *27*, 500–504.

Bai, Y., Tang, Y., Han, P., & Wang, J. (2019). Gene therapy for cystinuria. *Urolithiasis*, *47*(3), 309–310. https://doi.org/10.1007/s00240-019-01111-7

Bai, Y., Tang, Y., Wang, J., Wang, X., Wang, Z., Cao, D., Han, P., & Wang, J. (2021). Tolvaptan treatment of cystine urolithiasis in a mouse model of cystinuria. *World Journal of Urology*, *39*(1), 263–269. https://doi.org/10.1007/s00345-020-03166-3

Bailey, C. G., Ryan, R. M., Thoeng, A. D., Ng, C., King, K., Vanslambrouck, J. M., Auray-Blais, C., Vandenberg, R. J., Bröer, S., & Rasko, J. E. J. (2011). Loss-of-function mutations in the glutamate transporter SLC1A1 cause human dicarboxylic aminoaciduria. *The Journal of Clinical Investigation*, *121*. https://doi.org/10.1172/JCI44474

Bannai, S., & Tateishi, N. (1986). Role of membrane transport in metabolism and function of glutathione in mammals. *The Journal of Membrane Biology*, *89*(1), 1–8. https://doi.org/10.1007/BF01870891

Barbey, F., Joly, D., Rieu, P., Méjean, A., & Daudon, M. (2000). Medical Treatment of cystinuria: critical Reappraisal of long-term results. *The Journal of Urology*, *163*(May), 1419–1423.

Bartoccioni, P., Rius, M., Zorzano, A., Palacín, M., & Chillarón, J. (2008). Distinct classes of trafficking rBAT mutants cause the type I cystinuria phenotype. *Human Molecular Genetics*, *17*(12), 1845–1854. https://doi.org/10.1093/hmg/ddn080

Bauch, C., Forster, N., Loffing-Cueni, D., Summa, V., & Verrey, F. (2003). Functional cooperation of epithelial heteromeric amino acid transporters expressed in Madin-Darby canine kidney cells. *Journal of Biological Chemistry*, *278*(2), 1316–1322. https://doi.org/10.1074/jbc.M210449200

Beckermann, T. M., Welch, R. C., Williams, F. M., Mortlock, D. P., Sha, F., Ikizler, T. A., Woodard, L. E., &

Wilson, M. H. (2020). CRISPR/Cas9 engineering of albino cystinuria Type A mice. *Genesis*, *58*(5), e23357. https://doi.org/10.1002/dvg.23357

Bedirli, A., Sakrak, O., Muhtaroglu, S., Soyuer, I., Guler, I., Riza Erdogan, A., & Sozuer, E. M. (2004). Ergothioneine pretreatment protects the liver from ischemia-reperfusion injury caused by increasing hepatic heat shock protein 70. *Journal of Surgical Research*, *122*(1), 96–102. https://doi.org/10.1016/j.jss.2004.06.016

Bell, S. M., De Marco, M., Barnes, K., Shaw, P. J., Ferraiuolo, L., Blackburn, D. J., Mortiboys, H., & Venneri, A. (2020). Deficits in mitochondrial spare respiratory capacity contribute to the neuropsychological changes of Alzheimer's disease. *Journal of Personalized Medicine*, *10*(2). https://doi.org/10.3390/jpm10020032

Benjamini, Y., & Hochberg, Y. (1995). Controlling the False Discovery Rate: A Practical and Powerful Approach to Multiple Testing. *Journal of the Royal Statistical Society. Series B (Methodological)*, *57*(1), 289–300. http://www.stat.purdue.edu/~doerge/BIOINFORM.D/FALL06/Benjamini and Y FDR.pdf%5Cnhttp://engr.case.edu/ray_soumya/mlrg/controlling_fdr_benjamini95.pdf

Bertran, J., Werner, A., Moore, M. L., Stange, G., Markovich, D., Biber, J., Testart, X., Zorzanot, A., Palacin, M., & Murer, H. (1992). Expression cloning of a cDNA from rabbit kidney cortex that induces a single transport system for cystine and dibasic and neutral amino acids. *Proceedings of the National Academy of Sciences of the United States of America*, *89*(June), 5601–5605.

Berzelius, J. (1833). Calculus urinaries. *Traite Chemistrie*, *7*, 424–428. https://doi.org/10.1177/095952871200300117

Bhargava, P., & Schnellmann, R. G. (2017). Mitochondrial energetics in the kidney. *Nature Publishing Group*, *13*. https://doi.org/10.1038/nrneph.2017.107

Biber, J., Stieger, B., Stange, G., & Murer, H. (2007). Isolation of renal proximal tubular brush-border membranes. *Nature Protocols*, *2*(6), 1356–1359. https://doi.org/10.1038/nprot.2007.156

Bisceglia, L., Calonge, M. J., Totaro, A., Feliubadalo, L., Melchionda, S., Garcia, J., Testar, X., Gallucci, M., Ponzone, A., Zelante, L., Zorzano, A., Estivill, X., Gasparini, P., Nunes, V., & Palacfn, M. (1997). Localization , by Linkage Analysis , of the Cystinuria Type. *American Journal of Human Genetics*, *60*, 611–616.

Boffoli, D., Scacco, S. C., Vergari, R., Solarino, G., Santacroce, G., & Papa, S. (1994). Decline with age of the respiratory chain activity in human skeletal muscle. *BBA - Molecular Basis of Disease*, *1226*(1), 73–82. https://doi.org/10.1016/0925-4439(94)90061-2

Bonawitz, N. D., Clayton, D. A., & Shadel, G. S. (2006). Initiation and Beyond: Multiple Functions of the Human Mitochondrial Transcription Machinery. *Molecular Cell*, *24*(6), 813–825. https://doi.org/10.1016/j.molcel.2006.11.024

Bostroem, H., & Hambraeus, L. (1964). Cistinuria in sweden Sweden. VII. Clinical, histopathological, and medico-social aspects of the disease. *Acta Med Scand*, *175*. https://pubmed.ncbi.nlm.nih.gov/14131787/

Bourderioux, M., Nguyen-Khoa, T., Chhuon, C., Jeanson, L., Tondelier, D., Walczak, M., Ollero, M., Bekri, S., Knebelmann, B., Escudier, E., Escudier, B., Edelman, A., & Guerrera, I. C. (2015). A new workflow for proteomic analysis of urinary exosomes and assessment in cystinuria patients. *Journal of Proteome Research*, *14*(1), 567–577. https://doi.org/10.1021/pr501003q

Bröer, S., & Wagner, C. A. (2002). Structure-function relationships of heterodimeric amino acid transporters. *Cell Biochemistry and Biophysics*, *36*(2–3), 155–168. https://doi.org/10.1385/CBB:36:2-3:155

Budisavljevic, M. N., Hodge, L. A., Barber, K., Fulmer, J. R., Durazo-Arvizu, R. A., Self, S. E., Kuhlmann, M., Raymond, J. R., & Greene, E. L. (2003). Oxidative stress in the pathogenesis of experimental mesangial proliferative glomerulonephritis. *American Journal of Physiology - Renal Physiology*, *285*(6 54-6), 1138–1148. https://doi.org/10.1152/ajprenal.00397.2002

Calonge, M. J., Gasparini, P., Chillaron, J., Chillon, M., Rousaud, G. F., Zelante, L., Testar, X., Dallapiccola, B., Silverio, F. Di, Barcel, P., Estivill, X., Zorzano, A., Nunes, V., & Paladn, M. (1994). rBAT , a gene involved in the transport of cystine. *Nature Genetics*, *6*, 420–425. https://doi.org/10.1038/ng0494-420

Calvo-Rodriguez, M., Hou, S. S., Snyder, A. C., Kharitonova, E. K., Russ, A. N., Das, S., Fan, Z., Muzikansky, A., Garcia-Alloza, M., Serrano-Pozo, A., Hudry, E., & Bacskai, B. J. (2020). Increased mitochondrial calcium levels associated with neuronal death in a mouse model of Alzheimer's disease. *Nature Communications*, *11*(1), 1–17. https://doi.org/10.1038/s41467-020-16074-2

Cantó, C., & Garcia-Roves, P. M. (2015). High-Resolution Respirometry for Mitochondrial Characterization of Ex Vivo Mouse Tissues. *Current Protocols in Mouse Biology*, *5*(2), 135–153. https://doi.org/10.1002/9780470942390.mo140061

Cao, L. C., Honeyman, T. W., Cooney, R., Kennington, L., Scheid, C. R., & Jonassen, J. A. (2004). Mitochondrial dysfunction is a primary event in renal cell oxalate toxicity. *Kidney International*, *66*(5), 1890–1900. https://doi.org/10.1111/j.1523-1755.2004.00963.x

Cao, Y., Liu, W., Hui, L., Zhao, J., Yang, X., Wang, Y., & Niu, H. (2016). Renal tubular injury induced by ischemia promotes the formation of calcium oxalate crystals in rats with hyperoxaluria. *Urolithiasis*, *44*(5), 389–397. https://doi.org/10.1007/s00240-016-0876-7

Casado, M., Sierra, C., Batllori, M., Artuch, R., & Ormazabal, A. (2018). A targeted metabolomic procedure for amino acid analysis in different biological specimens by ultra-high-performance liquid chromatography–tandem mass spectrometry. *Metabolomics*, *14*(6), 1–12. https://doi.org/10.1007/s11306-018-1374-4

Ceban, E., Banov, P., Galescu, A., & Botnari, V. (2016). Oxidative stress and antioxidant status in patients with complicated urolithiasis. In *Journal of Medicine and Life* (Vol. 9).

Cha, M.-Y., Kim, D. K., & Mook-Jung, I. (2015). The role of mitochondrial DNA mutation on neurodegenerative diseases. *Experimental & Molecular Medicine*, *47*, 47. https://doi.org/10.1038/emm.2014.122

Chaiyarit, S., & Thongboonkerd, V. (2012). Changes in mitochondrial proteome of renal tubular cells induced by calcium oxalate monohydrate crystal adhesion and internalization are related to mitochondrial dysfunction. *Journal of Proteome Research*, *11*(6), 3269–3280. https://doi.org/10.1021/pr300018c

Chang, M., Xu, G., Xiong, C., Yang, X., Yan, S., Tao, Y., Li, H., Li, Y., Yao, S., & Zhao, Y. (2021). Alpha-lipoic acid attenuates silica-induced pulmonary fibrosis by improving mitochondrial function via AMPK/PGC1α pathway activation in C57BL/6J mice. *Toxicology Letters*, *350*. https://doi.org/10.1016/j.toxlet.2021.07.003

Cheah, I. K., Ong, R. L. S., Gruber, J., Yew, T. S. K., Ng, L. F., Chen, C. B., & Halliwell, B. (2013). Knockout of a putative ergothioneine transporter in Caenorhabditis elegans decreases lifespan and increases susceptibility to oxidative damage. *Free Radical Research*, *47*(12), 1036–1045. https://doi.org/10.3109/10715762.2013.848354

Cheah, I., Tang, R., Yew, T., Li, K., & Halliwell, B. (2017). Administration of Pure Ergothioneine to Healthy Human Subjects: Uptake, Metabolism, and Effects on Biomarkers of Oxidative Damage and Inflammation. *Antioxidants & Redox Signaling*, *26*(5), 193–206. https://doi.org/10.1089/ars.2016.6778

Cheah, Irwin K., Ng, L. T., Ng, L. F., Lam, V. Y., Gruber, J., Huang, C. Y. W., Goh, F. Q., Lim, K. H. C., & Halliwell, B. (2019). Inhibition of amyloid-induced toxicity by ergothioneine in a transgenic Caenorhabditis elegans model. *FEBS Letters*, *593*(16), 2139–2150. https://doi.org/10.1002/1873-3468.13497

Cheah, Irwin K, Feng, L., Tang, R. M. Y., Lim, K. H. C., & Halliwell, B. (2016). *Ergothioneine levels in an elderly population decrease with age and incidence of cognitive decline; a risk factor for neurodegeneration?* https://doi.org/10.1016/j.bbrc.2016.07.074

Chen, Y., Shertzer, H. G., Schneider, S. N., Nebert, D. W., & Dalton, T. P. (2005). Glutamate cysteine ligase catalysis: Dependence on ATP and modifier subunit for regulation of tissue glutathione levels. *Journal of Biological Chemistry*, *280*(40), 33766–33774. https://doi.org/10.1074/jbc.M504604200

Chen, Z., Putt, D. A., & Lash, L. H. (2000). Enrichment and functional reconstitution of glutathione transport activity from rabbit kidney mitochondria. Further evidence for the role of the dicarboxylate and 2-oxoglutarate carriers in mitochondrial glutathione transport. *Archives of Biochemistry and Biophysics*, *373*(1), 193–202. https://doi.org/10.1006/abbi.1999.1527

Chillarón, J., Estévez, R., Mora, C., Wagner, C. A., Suessbrich, H., Lang, F., Gelpí, J. L., Testar, X., Busch, A. E., Zorzano, A., & Palacín, M. (1996). Obligatory amino acid exchange via systems b(o,+)-like and y+L-like. A tertiary active transport mechanism for renal reabsorption of cystine and dibasic amino acids. *Journal of Biological Chemistry*, *271*(30), 17761–17770. https://doi.org/10.1074/jbc.271.30.17761

Chillarón, J., Font-Llitjós, M., Fort, J., Zorzano, A., Goldfarb, D. S., Nunes, V., & Palacín, M. (2010). Pathophysiology and treatment of cystinuria. *Nature Reviews Nephrology*, *6*(7), 424–434. https://doi.org/10.1038/nrneph.2010.69

Chrzan, D., Ramaswamy, K., Killilea, D., Zee, T., Chi, T., Kapahi, P., Kahn, A., & Stoller, M. (2015). Inhibition of Nucleation and Growth of Cystine Crystals in Urine. *Journal of Urology*, *193*(4S), e412. https://doi.org/10.1016/j.juro.2015.02.1302

Chujo, T., Ohira, T., Sakaguchi, Y., Goshima, N., Nomura, N., Nagao, A., & Suzuki, T. (2012). LRPPRC/SLIRP suppresses PNPase-mediated mRNA decay and promotes polyadenylation in human mitochondria. *Nucleic Acids Reasearch*, *40*, 8033–8047. https://doi.org/10.1093/nar/gks506

Cil, O., & Perwad, F. (2020). a -Lipoic Acid (ALA) Improves Cystine Solubility in Cystinuria : Report of 2 Cases. *Pediatrics*, *145*(5).

Claes, D. J., & Jackson, E. (2012). Cystinuria : mechanisms and management. *Pediatr Nephrol*, 2031–2038. https://doi.org/10.1007/s00467-011-2092-6

Coe, F. L., Evan, A. P., Lingeman, J. E., & Worcester, E. M. (2010). Plaque and Deposits in Nine Human Stone Diseases. *Urol Res*, *38*(4), 239–247. https://doi.org/10.1007/s00240-010-0296-z

Cross, C. E., Halliwell, B., Borish, E. T., Pryor, W. A., Ames, B. N., Saul, R. L., McCord, J. M., & Harman, D. (1987). Oxygen radicals and human disease. *Annals of Internal Medicine*, *107*(4), 526–545. https://doi.org/10.7326/0003-4819-107-4-526

Cuadrado, A., Martín-Moldes, Z., Ye, J., & Lastres-Becker, I. (2014). Transcription factors NRF2 and NF-κB are coordinated effectors of the rho family, GTP-binding protein RAC1 during Inflammation. *Journal of Biological Chemistry*, *289*(22), 15244–15258. https://doi.org/10.1074/jbc.M113.540633

Cumming, B. M., Chinta, K. C., Reddy, V. P., & Steyn, A. J. C. (2018). Role of Ergothioneine in Microbial Physiology and Pathogenesis. *Antioxidants & Redox Signaling*, *28*(431–444). https://doi.org/10.1089/ars.2017.7300

Czajka, A., & Malik, A. N. (2016). Hyperglycemia induced damage to mitochondrial respiration in renal mesangial and tubular cells: Implications for diabetic nephropathy. *Redox Biology*, *10*(September), 100–107. https://doi.org/10.1016/j.redox.2016.09.007

D'onofrio, N., Servillo, L., Giovane, A., Casale, R., Vitiello, M., Marfella, R., Paolisso, G., & Balestrieri, M. L. (2016). *Ergothioneine oxidation in the protection against high-glucose induced endothelial senescence: Involvement of SIRT1 and SIRT6*. https://doi.org/10.1016/j.freeradbiomed.2016.04.013

Dalton, T. P., Chen, Y., Schneider, S. N., Nebert, D. W., & Shertzer, H. G. (2004). Genetically altered mice to evaluate glutathione homeostasis in health and disease. *Free Radical Biology and Medicine*, *37*(10), 1511–1526. https://doi.org/10.1016/j.freeradbiomed.2004.06.040

Dare, A., Channa, M. L., & Nadar, A. (2021). L-ergothioneine and its combination with metformin attenuates renal dysfunction in type-2 diabetic rat model by activating Nrf2 antioxidant pathway. *Biomedicine & Pharmacotherapy*, *141*, 111921. https://doi.org/10.1016/j.biopha.2021.111921

Deberardinis, R. J., Coughlin, C. R., & Kaplan, P. (2008). Penicillamine therapy in pediatric cystinuria: experience from a cohort of American children. *J Urol*, *180*(6), 2620–2623. https://doi.org/10.1016/j.juro.2008.08.057

Deiana, M., Rosa, A., Casu, V., Piga, R., Dess, M. A., Aruoma, O. I., Sperimentale, B., & Sperimentale, S. P. (2004). L -Ergothioneine modulates oxidative damage in the kidney and liver of rats in vivo : studies upon the profile of polyunsaturated fatty acids. *Clinical Nutrition*, *5614*, 183–193. https://doi.org/10.1016/S0261-5614(03)00108-0

Dello Strologo, L., Pras, E., Pontesilli, C., Beccia, E., Ricci-Barbini, V., De Sanctis, L., Ponzone, A., Gallucci,

M., Bisceglia, L., Leopoldo, Z., Jimenez-Vidal, M., Font, M., Zorzano, A., Rousaud, F., Nunes, V., Gasparini, P., Palacín, M., & Rizzoni, G. (2002). Comparison between SLC3A1 and SLC7A9 Cystinuria Patients and Carriers: A Need for a New Classification. *Journal of the American Society of Nephrology*, *13*(10), 2547–2553. https://doi.org/10.1097/01.ASN.0000029586.17680.E5

Dent, C. E., Senior, B., & Walshe, J. M. (1954). The pathogenesis of cystinuria. I. Chromatographic and microbiological studies of the metabolism of sulphur-containing amino-acids. *The Journal of Clinical Investigation*, *33*(9), 1210–1215. https://doi.org/10.1172/JCI102995

Dent, C., & Rose, G. (1949). Amino acid metabolism in cystinuria. *I Int. Congr. Biochem*, 196–198. https://doi.org/10.3181/00379727-78-19189

Donnelly, P. S., Liddell, J. R., Lim, S. C., Paterson, B. M., Cater, M. A., Savva, M. S., Mot, A. I., James, J. L., Trounce, I. A., White, A. R., & Crouch, P. J. (2012). An impaired mitochondrial electron transport chain increases retention of the hypoxia imaging agent diacetylbis(4-methylthiosemicarbazonato)copper II. *Proceedings of the National Academy of Sciences of the United States of America*, *109*(1), 47–52. https://doi.org/10.1073/pnas.1116227108

Drenberg, C. D., Gibson, A. A., Pounds, S. B., Shi, L., Rhinehart, D. P., Li, L., Hu, S., Du, G., Nies, A. T., Schwab, M., Pabla, N., Blum, W., Gruber, T. A., Baker, S. D., & Sparreboom, A. (2017). OCTN1 is a high-affinity carrier of nucleoside analogues. *Cancer Research*, *77*(8), 2102–2111. https://doi.org/10.1158/0008-5472.CAN-16-2548

Eggermann, T., Venghaus, A., & Zerres, K. (2012). Cystinuria : an inborn cause of urolithiasis. *Orphanet Journal of Rare Diseases*, *7*, 1–11.

Eggermann, T., Zerres, K., Nunes, V., Font-llitjo, M., Bisceglia, L., Chatzikyriakidou, A., dello Strologo, L., Pras, E., Creemers, J., & Palacin, M. (2012). Clinical utility gene card for : Cystinuria. *European Journal of Human Genetics*, *20*, 8–11. https://doi.org/10.1038/ejhg.2011.163

El-Beshbishy, H. A., Aly, H. A. A., & El-Shafey, M. (2013). Lipoic acid mitigates bisphenol A-induced testicular mitochondrial toxicity in rats. *Toxicology and Industrial Health*, *29*(10), 875–887. https://doi.org/10.1177/0748233712446728

Elena Dalmonte, M., Forte, E., Luisa Genova, M., Giuffrè, A., Sarti, P., & Lenaz, G. (2009). Control of Respiration by Cytochrome c Oxidase in Intact Cells. *Journal of Biological Chemistry*, *284*(47), 32331–32335. https://doi.org/10.1074/jbc.M109.050146

Erbagci, A., Ergbagci, A., Yilmaz, M., Yagci, F., Tarakcloglu, M., Yurtseven, C., Koyluoglu, O., & Sarica, K. (2003). Pediatric Urolithiasis. *Scand J Urol Nephrol*, *37*, 129–133.

Escobar, J., Sánchez-illana, Á., Kuligowski, J., Torres-cuevas, I., Solberg, R., Garberg, H. T., Huun, M. U., Saugstad, O. D., Vento, M., & Cháfer-pericás, C. (2016). Analysis Development of a reliable method based on ultra-performance liquid chromatography coupled to tandem mass spectrometry to measure thiol-associated oxidative stress in whole blood samples. *Journal of Pharmaceutical and Biomedical Analysis*, *123*, 104–112. https://doi.org/10.1016/j.jpba.2016.02.007

Espino, M. (2012). Mouse models of heteromeric amino acid transporters : cystinuria and LAT2 protein. *Thesis*, 354.

Espino, M., Font-Llitjos, M., Vilches, C., Salido, E., Prat, E., De Heredia, M. L., Palacin, M., & Nunes, V. (2015). Digenic inheritance in cystinuria mouse model. *PLoS ONE*, *10*(9), 1–12. https://doi.org/10.1371/journal.pone.0137277

Evan, A. P., Coe, F. L., Lingeman, J. E., Shao, Y., Matlaga, B. R., Kim, S. C., Bledsoe, S. B., Sommer, A. J., Grynpas, M., Phillips, C. L., & Worcester, E. M. (2006). Renal crystal deposits and histopathology in patients with cystine stones. *Kidney International*, *69*(12), 2227–2235. https://doi.org/10.1038/sj.ki.5000268

Farooq, S. M., Boppana, N. B., Asokan, D., Sekaran, S. D., & Shankar, E. M. (2014). C-Phycocyanin Confers Protection against Oxalate-Mediated Oxidative Stress and Mitochondrial Dysfunctions in MDCK Cells. *PLoS ONE*, *9*(4), 93056. https://doi.org/10.1371/journal.pone.0093056

FDA, U. (2017). *GRAS Notification of Ergothioneine*.

Feliubadaló, L., Arbonés, M., Mañas, S., Chillarón, J., Visa, J., Rodés, M., Rousaud, F., Zorzano, A., Palacín, M., & Nunes, V. (2003). Slc7a9-deficient mice develop cystinuria non-l and cystine urolithiasis.

Human Molecular Genetics, *12*(17), 2097–2108. https://doi.org/10.1093/hmg/ddg228

Feliubadaló, L., Font, M., Purroy, J., Rousaud, F., Estivill, X., Nunes, V., Golomb, E., Centola, M., Aksentijevich, I., Kreiss, Y., Goldman, B., Pras, M., Kastner, D. L., Pras, E., Gasparini, P., Bisceglia, L., Beccia, E., Gallucci, M., de Sanctis, L., … Palacín, M. (1999). Non-type I cystinuria caused by mutations in SLC7A9, encoding a subunit (bo,+AT) of rBAT. *Nature Genetics*, *23*(1), 52–57. https://doi.org/10.1038/12652

Fjellsted, E., Denneberg, T., Jeppsson, J.-O., & Tiselius, H.-G. (2001). A comparison of the effects of potassium citrate and sodium bicarbonate in the alkalinization of urine in homozygous cystinuria. *Urological Research*, *29*(5), 295–302. https://doi.org/10.1007/s002400100200

Fong-Ngern, K., Vinaiphat, A., & Thongboonkerd, V. (2017). Microvillar injury in renal tubular epithelial cells induced by calcium oxalate crystal and the protective role of epigallocatechin-3-gallate. *FASEB Journal*, *31*(1), 120–131. https://doi.org/10.1096/fj.201600543R

Font-Llitjós, M., Feliubadaló, L., Espino, M., Clèries, R., Mañas, S., Frey, I., Puertas, S., Colell, G., Palomo, S., Aranda, J., Visa, J., Palacín, M., & Nunes, V. (2007). Slc7a9 knockout mouse is a good cystinuria model for antilithiasic pharmacological studies. *American Journal of Physiology - Renal Physiology*, *293*(3), 732–740. https://doi.org/10.1152/ajprenal.00121.2007

Font-Llitjós, M., Jiménez-Vidal, M., Bisceglia, L., Di Perna, M., de Sanctis, L., Rousaud, F., Zelante, L., Palacín, M., & Nunes, V. (2005). New insights into cystinuria: 40 new mutations, genotype-phenotype correlation, and digenic inheritance causing partial phenotype. *Journal of Medical Genetics*, *42*(1), 58–68. https://doi.org/10.1136/jmg.2004.022244

Font, M. a, Feliubadaló, L., Estivill, X., Nunes, V., Golomb, E., Kreiss, Y., Pras, E., Bisceglia, L., d'Adamo, a P., Zelante, L., Gasparini, P., Bassi, M. T., George, a L., Manzoni, M., Riboni, M., Ballabio, a, Borsani, G., Reig, N., Fernández, E., … Palacín, M. (2001). Functional analysis of mutations in SLC7A9, and genotype-phenotype correlation in non-Type I cystinuria. *Human Molecular Genetics*, *10*(4), 305–316. http://www.ncbi.nlm.nih.gov/pubmed/11157794

Fontana, G. A., & Gahlon, H. L. (2020). Mechanisms of replication and repair in mitochondrial DNA deletion formation. *Nucleic Acids Research*, *48*(20), 11244–11258. https://doi.org/10.1093/nar/gkaa804

Forster, R., Spézia, F., Papineau, D., Sabadie, C., Erdelmeier, I., Moutet, M., & Yadan, J. C. (2015). Reproductive safety evaluation of L-Ergothioneine. *Food and Chemical Toxicology*, *80*, 85–91. https://doi.org/10.1016/j.fct.2015.02.019

Fotiadis, D., Kanai, Y., & Palacin, M. (2013). The SLC3 and SLC7 families of amino acid transporters. *Molecular Aspects of Medicine*, *34*(2–3), 139–158. https://doi.org/10.1016/j.mam.2012.10.007

Furriols, M., Chillarón, J., Mora, C., Castelló, A., Bertran, J., Camps, M., Testar, X., Vilaró, S., Zorzano, A., & Palacín, M. (1993). rBAT, related to L-cystine transport, is localized to the microvilli of proximal straight tubules, and its expression is regulated in kidney by development. *Journal of Biological Chemistry*, *268*(36), 27060–27068.

Garrod, A. (1908). The Croonian Lectures on Inborn Errors of Metabolism. *The Lancet*, *172*(4427), 1–7.

Genghof, D. S. (1964). Biosynthesis of ergothioneine and hercynine by mycobacteria. *Journal of Bacteriology*, *103*(2), 475–478. https://doi.org/10.1128/jb.103.2.475-478.1970

Giacopo, A. Di, Rubio-Aliaga, I., Cantone, A., Artunc, F., Rexhepaj, R., Frey-Wagner, I., Font-Llitjós, M., Gehring, N., Stange, G., Jaenecke, I., Mohebbi, N., Closs, E. I., Palacín, M., Nunes, V., Daniel, H., Lang, F., Capasso, G., & Wagner, C. A. (2013). Differential cystine and dibasic amino acid handling after loss of function of the amino acid transporter b 0,+ AT (Slc7a9) in mice . *American Journal of Physiology-Renal Physiology*, *305*(12), F1645–F1655. https://doi.org/10.1152/ajprenal.00221.2013

Gohil, V. M., Nilsson, R., Belcher-Timme, C. A., Luo, B., Root, D. E., & Mootha, V. K. (2010). Mitochondrial and nuclear genomic responses to loss of LRPPRC expression. *Journal of Biological Chemistry*, *285*(18), 13742–13747. https://doi.org/10.1074/jbc.M109.098400

Gong, G., Liu, J., Liang, P., Guo, T., Hu, Q., Ochiai, K., Hou, M., Ye, Y., Wu, X., Mansoor, A., From, A. H. L., Ugurbil, K., Bache, R. J., & Zhang, J. (2003). Oxidative capacity in failing hearts. *American Journal of Physiology - Heart and Circulatory Physiology*, *285*(2 54-2), 541–548.

https://doi.org/10.1152/ajpheart.01142.2002

Govindaraj, A., & Selvam, R. (2001). Increased calcium oxalate crystal nucleation and aggregation by peroxidized protein of human kidney stone matrix and renal cells. *Urological Research*, *29*(3), 194–198. https://doi.org/10.1007/s002400100177

Griffith, O., & Meister, A. (1979). Glutathione: Interorgan translocation, turnover, and metabolism. *Proceedings of the National Academy of Sciences of the United States of America*, *76*(11), 5606–5610. https://doi.org/10.1073/pnas.76.11.5606

Gross, H., Reitner, J., & König, G. M. (2004). Isolation and structure elucidation of azoricasterol, a new sterol of the deepwater sponge Macandrewia azorica. *Naturwissenschaften*, *91*(9), 441–446. https://doi.org/10.1007/s00114-004-0552-6

Gründemann, D., Harlfinger, S., Golz, S., Geerts, A., Lazar, A., Berkels, R., Jung, N., Rubbert, A., & Schömig, E. (2005). Discovery of the ergothioneine transporter. *Proceedings of the National Academy of Sciences of the United States of America*, *102*(14), 5256–5261. https://doi.org/10.1073/pnas.0408624102

Guijarro, M. V, Indart, A., Aruoma, O. I., Viana, M., & Bonet, B. (2002). *Effects of ergothioneine on diabetic embryopathy in pregnant rats*. www.elsevier.com/locate/foodchemtox

Hagos, Y., Burckhardt, G., & Burckhardt, B. C. (2013). Human organic anion transporter OAT1 is not responsible for glutathione transport but mediates transport of glutamate derivatives. *Am J Physiol Renal Physiol*, *304*, 403–409. https://doi.org/10.1152/ajprenal.00412.2012.-Due

Hahn, R., Wendel, A., & Flohé, L. (1978). The fate of extracellular glutathione in the rat. *BBA - General Subjects*, *539*(3), 324–337. https://doi.org/10.1016/0304-4165(78)90037-5

Hall, A. M., Unwin, R. J., Parker, N., & Duchen, M. R. (2009). Multiphoton imaging reveals differences in mitochondrial function between nephron segments. *Journal of the American Society of Nephrology*, *20*(6), 1293–1302. https://doi.org/10.1681/ASN.2008070759

Halliwell, B., Cheah, I. K., & Drum, C. L. (2016). Ergothioneine, an adaptive antioxidant for the protection of injured tissues? A hypothesis. *Biochemical and Biophysical Research Communications*, *470*(2), 245–250. https://doi.org/10.1016/j.bbrc.2015.12.124

Halperin, E. C., Thier, S. O., & Rosenberg, L. E. (1981). The use of D-penicillamine in cystinuria: Efficacy and untoward reactions. *Yale Journal of Biology and Medicine*, *54*(6), 439–446.

Handy, D. E., Lubos, E., Yang, Y., Galbraith, J. D., Kelly, N., Zhang, Y. Y., Leopold, J. A., & Loscalzo, J. (2009). Glutathione peroxidase-1 regulates mitochondrial function to modulate redox-dependent cellular responses. *Journal of Biological Chemistry*, *284*(18), 11913–11921. https://doi.org/10.1074/jbc.M900392200

Hanigan, M. H., & Frierson, H. F. (1996). Immunohistochemical detection of γ-glutamyl transpeptidase in normal human tissue. *Journal of Histochemistry and Cytochemistry*, *44*(10), 1101–1108. https://doi.org/10.1177/44.10.8813074

Hanlox, P. (1971). *Interaction of Ergothioneine with Metal Ions and Metalloenzymes*. *14*(11), 1084–1087.

Harding, C. O., Williams, P., Wagner, E., Chang, D. S., Wild, K., Colwell, R. E., & Wolff, J. A. (1997). Mice with genetic γ-glutamyl transpeptidase deficiency exhibit glutathionuria, severe growth failure, reduced life spans, and infertility. *Journal of Biological Chemistry*, *272*(19), 12560–12567. https://doi.org/10.1074/jbc.272.19.12560

Harris, B., Mittwoch, U., Robson, E., & Warren, F. (1955). Pheotypes and Genotypes in Cytinuria. *Ann Hum Genet*, *20*, 57–91.

Harris, R. A., Bowker-Kinley, M. M., Huang, B., & Wu, P. (2002). Regulation of the activity of the pyruvate dehydrogenase complex. *Advances in Enzyme Regulation*, *42*, 249–259. https://doi.org/10.1016/S0065-2571(01)00061-9

Heath, H., & Toennies, G. (1958). The Preparation and Properties of Ergothioneine Disulphide. *Biochemical Journal*, *68*, 204–210. https://doi.org/10.1042/bj0680204

Hinchman, C. A., & Ballatori, N. (1990). Glutathione-degrading capacities of liver and kidney in different species. *Biochemical Pharmacology*, *40*(5), 1131–1135. https://doi.org/10.1016/0006-2952(90)90503-D

Hirose, M., Tozawa, K., Okada, A., Hamamoto, S., Higashibata, Y., Gao, B., Hayashi, Y., Shimizu, H.,

Kubota, Y., Yasui, T., & Kohri, K. (2012). Role of osteopontin in early phase of renal crystal formation: Immunohistochemical and microstructural comparisons with osteopontin knock-out mice. *Urological Research*, *40*(2), 121–129. https://doi.org/10.1007/s00240-011-0400-z

Hirose, M., Yasui, T., Okada, A., Hamamoto, S., Shimizu, H., Itoh, Y., Tozawa, K., & Kohri, K. (2010). Renal tubular epithelial cell injury and oxidative stress induce calcium oxalate crystal formation in mouse kidney. *International Journal of Urology*, *17*(1), 83–92. https://doi.org/10.1111/j.1442-2042.2009.02410.x

House, J. D., Brosnan, M. E., & Brosnan, J. T. (1997). Characterization of homocysteine metabolism in the rat kidney. *Biochemical Journal*, *328*(1), 287–292. https://doi.org/10.1042/bj3280287

Hovgaard, K., Katja, A., Pedersen, V., & Sloth, S. (2015). How should patients with cystine stone disease be evaluated and treated in the twenty - first century? *Urolithiasis*, *44*, 65–76. https://doi.org/10.1007/s00240-015-0841-x

Hseu, Y. C., Vudhya Gowrisankar, Y., Chen, X. Z., Yang, Y. C., & Yang, H. L. (2020). The Antiaging Activity of Ergothioneine in UVA-Irradiated Human Dermal Fibroblasts via the Inhibition of the AP-1 Pathway and the Activation of Nrf2-Mediated Antioxidant Genes. *Oxidative Medicine and Cellular Longevity*, *2020*. https://doi.org/10.1155/2020/2576823

Hseu, Y., Lo, H., Korivi, M., Tsai, Y., Tang, M., & Yang, H. (2015). Dermato-protective Propertoies of Ergothioneine through Induction of Nrf2/ARE-mediated Antioxidant Genes in UVA-irradiated Human Keratinocytes. *Free Radical Biology and Medicine*. https://doi.org/10.1016/j.freeradbiomed.2015.05.026

Hu, L., Yang, Y., Sloysius, H., Albanyan, H., Yang, M., Liang, J., Yu, A., Shtukenberg, A., Poloni, L., Kholodovych, V., Tischfield, J., Goldfard, D., Ward, M., & Sahota, A. (2016). L-Cystine Diamides as L-Cystine Crystallization Inhibitors for Cystinuria. *Physiology & Behavior*, *176*(1), 139–148. https://doi.org/10.1021/acs.jmedchem.6b00647.L-Cystine

Huang, C. S., Anderson, M. E., & Meister, A. (1993). Amino acid sequence and function of the light subunit of rat kidney γ- glutamylcysteine synthetase. *Journal of Biological Chemistry*, *268*(27), 20578–20583. https://doi.org/10.1016/s0021-9258(20)80764-9

Huang, C. S., Chang, L. S., Anderson, M. E., & Meister, A. (1993). Catalytic and regulatory properties of the heavy subunit of rat kidney γ- glutamylcysteine synthetase. *Journal of Biological Chemistry*, *268*(26), 19675–19680. https://doi.org/10.1016/s0021-9258(19)36569-x

Huang, D. W., Sherman, B. T., & Lempicki, R. A. (2009). Systematic and integrative analysis of large gene lists using DAVID bioinformatics resources. *Nature Protocols*, *4*(1), 44–57. https://doi.org/10.1038/nprot.2008.211

Huang, H. S., Ma, M. C., Chen, C. F., & Chen, J. (2003). Lipid peroxidation and its correlations with urinary levels of oxalate, citric acid, and osteopontin in patients with renal calcium oxalate stones. *Urology*, *62*(6), 1123–1128. https://doi.org/10.1016/S0090-4295(03)00764-7

Ishii, I., Akahoshi, N., Yu, X.-N., Kobayashi, Y., Namekata, K., Komaki, G., & Kimura, H. (2004). Murine cystathionine γ-lyase: complete cDNA and genomic sequences, promoter activity, tissue distribution and developmental expression. In *Biochem. J* (Vol. 381).

Ishimoto, T., Nakamichi, N., Hosotani, H., Masuo, Y., Sugiura, T., Kato, Y., & Strack, S. (2014). Organic Cation Transporter-Mediated Ergothioneine Uptake in Mouse Neural Progenitor Cells Suppresses Proliferation and Promotes Differentiation into Neurons. *PLoS ONE*, *9*(2). https://doi.org/10.1371/journal.pone.0089434

Jackson, R. C. (1969). Studies in the enzymology of glutathione metabolism in human erythrocytes. *The Biochemical Journal*, *111*(3), 309–315. https://doi.org/10.1042/bj1110309

Jaeken, J., Martens, K., François, I., Eyskens, F., Lecointre, C., Derua, R., Meulemans, S., Slootstra, J. W., Waelkens, E., De Zegher, F., Creemers, J. W. M., & Matthijs, G. (2006). Deletion of PREPL, a gene encoding a putative serine oligopeptidase, in patients with hypotonia-cystinuria syndrome. *American Journal of Human Genetics*, *78*(1), 38–51. https://doi.org/10.1086/498852

Jones, H. (1840). The presence of Sulphur in Cystic Oxyde and a Account of a Cystic Oxyde Calculus. *Med Chir Trans*, *23*, 192–198.

Jung, K. J., Jang, H. S., Kim, J. I., Han, S. J., Park, J. W., & Park, K. M. (2013). Involvement of hydrogen

sulfide and homocysteine transsulfuration pathway in the progression of kidney fibrosis after ureteral obstruction. *Biochimica et Biophysica Acta - Molecular Basis of Disease*, *1832*(12), 1989–1997. https://doi.org/10.1016/j.bbadis.2013.06.015

Kandasamy, P., Gyimesi, G., Kanai, Y., & Hediger, M. A. (2018). Amino acid transporters revisited: New views in health and disease. *Trends in Biochemical Sciences*, *43*(10), 752–789. https://doi.org/10.1016/j.tibs.2018.05.003

Kanlaya, R., Sintiprungrat, K., Chaiyarit, S., & Thongboonkerd, V. (2013). Macropinocytosis is the Major Mechanism for Endocytosis of Calcium Oxalate Crystals into Renal Tubular Cells. *Cell Biochemistry and Biophysics*, *67*(3), 1171–1179. https://doi.org/10.1007/s12013-013-9630-8

Karczewski, K. J., Francioli, L. C., Tiao, G., Cummings, B. B., Alföldi, J., Wang, Q., Collins, R. L., Laricchia, K. M., Ganna, A., Birnbaum, D. P., Gauthier, L. D., Brand, H., Solomonson, M., Watts, N. A., Rhodes, D., Singer-Berk, M., England, E. M., Seaby, E. G., Kosmicki, J. A., … MacArthur, D. G. (2020). The mutational constraint spectrum quantified from variation in 141,456 humans. *Nature*, *581*(7809), 434–443. https://doi.org/10.1038/s41586-020-2308-7

Kato, Y., Kubo, Y., Iwata, D., Kato, S., Sudo, T., Sugiura, T., Kagaya, T., Wakayama, T., Hirayama, A., Sugimoto, M., Sugihara, K., Kaneko, S., Soga, T., Asano, M., Tonuta, M., Matsui, T., Wada, M., & Tsuji, A. (2010). Gene knockout and metabolome analysis of carnitine/organic cation transporter OCTN1. *Pharmaceutical Research*, *27*(5), 832–840. https://doi.org/10.1007/s11095-010-0076-z

Kaufman, A. M., Brod-Miller, C., & Kahn, T. (1985). Role of citrate excretion in acid-base balance in diuretic-induced alkalosis in the rat. *American Journal of Physiology - Renal Fluid and Electrolyte Physiology*, *17*(6). https://doi.org/10.1152/ajprenal.1985.248.6.f796

Kawano, H., Murata, H., Iriguchi, S., Mayumi, T., & Hama, T. (1983). Studies on Ergothioneine. XI. Inhibitory Effect of Lipid Peroxide Formation in Mouse Liver. *Chem. Pharm. Bull.*, *31*(5), 1682–1687.

Kawano, H., Otani, M., Takeyama, K., Kawai, Y., Mayumi, T., & Hama, T. (1982). Studies on Ergothioneine. Distribution and Fluctuations of Ergothioneine in Rats. *Chem. Pharm. Bull.*, *30*(5), 1760–1765.

Khan, S. R. (1995). Calcium oxalate crystal interaction with renal tubular epithelium, mechanism of crystal adhesion and its impact on stone development. *Urological Research*, *23*(2), 71–79. https://doi.org/10.1007/BF00307936

Khan, Saeed R. (2014). Reactive oxygen species, inflammation and calcium oxalate nephrolithiasis. *Translational Andrology and Urology*, *3*(3), 256–276. https://doi.org/10.3978/j.issn.2223-4683.2014.06.04

Khaskhali, M. H., Byer, K. J., & Khan, S. R. (2009). The effect of calcium on calcium oxalate monohydrate crystal-induced renal epithelial injury. *Urological Research*, *37*(1), 1–6. https://doi.org/10.1007/s00240-008-0160-6

Knoll, T., Zöllner, A., Maurice, G. W., & Michel, S. (2005). Cystinuria in childhood and adolescence: recommendations for diagnosis , treatment , and follow-up. *Pediatr Nephrol*, *20*, 19–24. https://doi.org/10.1007/s00467-004-1663-1

Koepsell, H. (2020). Organic cation transporters in health and disease. *Pharmacological Reviews*, *72*(1), 253–319. https://doi.org/10.1124/pr.118.015578

Königsberger, E., Wang, Z., & Königsberger, L.-C. (2000). Solubility of L-Cystine in NaCl and Artifcial Urine Solutions. *Chemical Monthly*, *131*, 39–45. https://doi.org/10.1007/s007060050004

Kornberg, H. L., & Krebs, H. A. (1957). Biosynthesis of Ergothioneine. *Group Nature Publishing*, *180*, 756–757.

Kovacevic, L., Caruso, J. A., Lu, H., Kovacevic, N., Lakshmanan, Y., Carruthers, N. J., & Goldfarb, D. S. (2019). Urine proteomic profiling in patients with nephrolithiasis and cystinuria. *International Urology and Nephrology*, *51*(4), 593–599. https://doi.org/10.1007/s11255-018-2044-1

Kovacevic, L., Lu, H., Goldfarb, D. S., Lakshmanan, Y., & Caruso, J. A. (2015). Urine proteomic analysis in cystinuric children with renal stones. *Journal of Pediatric Urology*, *11*(4), 217.e1-217.e6. https://doi.org/10.1016/j.jpurol.2015.04.020

Krieger, N. S., Asplin, J. R., Frick, K. K., Granja, I., Culbertson, C. D., Ng, A., Grynpas, M. D., & Bushinsky, D. A. (2015). Effect of potassium citrate on calcium phosphate stones in a model of

hypercalciuria. *Journal of the American Society of Nephrology*, *26*(12), 3001–3008. https://doi.org/10.1681/ASN.2014121223

Kühl, I., Miranda, M., Atanassov, I., Kuznetsova, I., Hinze, Y., Mourier, A., Filipovska, A., & Larsson, N. G. (2017). Transcriptomic and proteomic landscape of mitochondrial dysfunction reveals secondary coenzyme Q deficiency in mammals. *ELife*, *6*, 1–33. https://doi.org/10.7554/eLife.30952

Kum, F., Wong, K., Game, D., Bultitude, M., & Thomas, K. (2019). Hypertension and renal impairment in patients with cystinuria : findings from a specialist cystinuria centre. *Urolithiasis*, *47*(4), 357–363. https://doi.org/10.1007/s00240-019-01110-8

Lamhonwah, A.-M., & Tein, I. (2006). Novel localization of OCTN1, an organic cation/carnitine transporter, to mammalian mitochondria q. *Biochemical and Biophysical Research Communications*, *345*, 1315–1325. https://doi.org/10.1016/j.bbrc.2006.05.026

Lamhonwah, A.-M., & Tein, I. (2020). Expression of the organic cation/carnitine transporter family (Octn1,-2 and-3) in mdx muscle and heart: Implications for early carnitine therapy in Duchenne muscular dystrophy to improve cellular carnitine homeostasis. *Clinica Chimica Acta*, *505*, 92–97. https://doi.org/10.1016/j.cca.2020.02.015

Lash, L. H., Putt, D. A., Xu, F., & Matherly, L. H. (2007). Role of rat organic anion transporter 3 (Oat3) in the renal basolateral transport of glutathione. *Chemico-Biological Interactions*, *170*(2), 124–134. https://doi.org/10.1016/j.cbi.2007.07.004

Lee, H. C., Pang, C. Y., Hsu, H. S., & Wei, Y. H. (1994). Differential accumulations of 4,977 bp deletion in mitochondrial DNA of various tissues in human ageing. *BBA - Molecular Basis of Disease*, *1226*(1), 37–43. https://doi.org/10.1016/0925-4439(94)90056-6

Lee, J.-I., Kang, J., & Stipanuk, M. H. (2006). Differential regulation of glutamate-cysteine ligase subunit expression and increased holoenzyme formation in response to cysteine deprivation. *Biochem. J*, *393*, 181–190. https://doi.org/10.1042/BJ20051111

Lee, M. H., Sahota, A., Ward, M. D., & Goldfarb, D. S. (2015). Cystine growth inhibition through molecular mimicry: A new paradigm for the prevention of crystal diseases. *Current Rheumatology Reports*, *17*(5), 1–6. https://doi.org/10.1007/s11926-015-0510-7

Leusmann, D. B., Blaschke, R., & Schmandt, W. (1990). Results of 5035 stone analyses: a contribution to epidemiology of urinary stone disease. *Scand J Urol Neprhol*, *24*, 205–210.

Li, C. Y., Deng, Y. L., & Sun, B. H. (2009). Taurine protected kidney from oxidative injury through mitochondrial-linked pathway in a rat model of nephrolithiasis. *Urological Research*, *37*(4), 211–220. https://doi.org/10.1007/s00240-009-0197-1

Li, C., Yang, Y., Zheng, Y., Shen, F., Liu, L., Li, Y., Li, L., & Zhao, Y. (2020). Genetic and Clinical Analyses of 13 Chinese Families With Cystine Urolithiasis and Identification of 15 Novel Pathogenic Variants in SLC3A1 and SLC7A9. *Frontiers in Genetics*, *11*(February), 1–10. https://doi.org/10.3389/fgene.2020.00074

Li, L., Lee, T. K., Meier, P. J., & Ballatori, N. (1998). Identification of glutathione as a driving force and leukotriene C4 as a substrate for oatp1, the hepatic sinusoidal organic solute transporter. *Journal of Biological Chemistry*, *273*(26), 16184–16191. https://doi.org/10.1074/jbc.273.26.16184

Li, N., Chen, L., Muh, R. W., & Li, P.-L. (2006). Hyperhomocysteinemia Associated With Decreased Renal Transsulfuration Activity in Dahl S Rats. *Hypertension*, *47*, 1094–1100. https://doi.org/10.1161/01.HYP.0000219634.83928.6e

Li, T., Chen, G. L., Lan, H., Mao, L., & Zeng, B. (2016). Prevalence of the 4977-bp and 4408-bp mitochondrial DNA deletions in mesenteric arteries from patients with colorectal cancer. *Mitochondrial DNA*, *27*(5), 3774–3776. https://doi.org/10.3109/19401736.2015.1079900

Li, Y., Zhao, Y., Yu, W., & Jiang, S. (2004). Scavenging ability on ROS of alpha-lipoic acid (ALA). *Food Chemistry*, *84*(4), 563–567. https://doi.org/10.1016/S0308-8146(03)00279-6

Lieske, J. C., Huang, E., & Toback, F. G. (2000). Regulation of renal epithelial cell endocytosi of calcium oxalate monohydrate crystals. *American Journal of Physiology - Renal Physiology*, *278*(1 47-1). https://doi.org/10.1152/ajprenal.2000.278.1.f130

Liguori, I., Russo, G., Curcio, F., Bulli, G., Aran, L., Della-Morte, D., Gargiulo, G., Testa, G., Cacciatore, F.,

Bonaduce, D., & Abete, P. (2018). Oxidative stress, aging, and diseases. *Clinical Interventions in Aging*, *13*, 757–772. https://doi.org/10.2147/CIA.S158513

Ling, X. C., & Kuo, K. L. (2018). Oxidative stress in chronic kidney disease. *Renal Replacement Therapy*, *4*(1). https://doi.org/10.1186/s41100-018-0195-2

Liu, L., Nam, M., Fan, W., Akie, T. E., Hoaglin, D. C., Gao, G., Keaney, J. F., & Cooper, M. P. (2014). Nutrient sensing by the mitochondrial transcription machinery dictates oxidative phosphorylation. *The Journal of Clinical Investigation*, *124*. https://doi.org/10.1172/JCI69413

Livak, K. J., & Schmittgen, T. D. (2001). *Analysis of Relative Gene Expression Data Using Real-Time Quantitative PCR and the 2-ΔΔCT Method* (pp. 402–408).

Livrozet, M., Vandermeersch, S., Mesnard, L., Thioulouse, E., Jaubert, J., Boffa, J. J., Haymann, J. P., Baud, L., Bazin, D., Daudon, M., & Letavernier, E. (2014). An animal model of type a cystinuria due to spontaneous mutation in 129S2/SvPasCrl mice. *PLoS ONE*, *9*(7), 3–10. https://doi.org/10.1371/journal.pone.0102700

Lopez de Heredia, M., Muñoz, L., Carru, C., Sotgia, S., Zinellu, A., Serra, C., Llebaria, A., Kato, Y., & Nunes, V. (2021). S-Methyl-L-Ergothioneine to L-Ergothioneine Ratio in Urine Is a Marker of Cystine Lithiasis in a Cystinuria Mouse Model. *Antioxidants*, *10*, 1–14.

Lou, H., Ookhtens, M., Stolz, A., & Kaplowitz, N. (2003). *Chelerythrine stimulates GSH transport by rat Mrp2 (Abcc2) expressed in canine kidney cells*. https://doi.org/10.1152/ajpgi.00271.2003.-Rat

Love, M. I., Huber, W., & Anders, S. (2014). Moderated estimation of fold change and dispersion for RNA-seq data with DESeq2. *Genome Biology*, *15*(12), 1–21. https://doi.org/10.1186/s13059-014-0550-8

Makiishi, S., Furuichi, K., Yamamura, Y., Sako, K., Shinozaki, Y., Toyama, T., Kitajima, S., Iwata, Y., Sakai, N., Shimizu, M., Hirose-Sugiura, T., Kaneko, S., Kato, Y., & Wada, T. (2021). Carnitine/organic cation transporter 1 precipitates the progression of interstitial fibrosis through oxidative stress in diabetic nephropathy in mice. *Scientific Reports* |, *11*, 9093. https://doi.org/10.1038/s41598-021-88724-4

Makrides, V., Camargo, S. M. R., & Verrey, F. (2014). Transport of amino acids in the kidney. *Comprehensive Physiology*, *4*(1), 367–403. https://doi.org/10.1002/cphy.c130028

Mali, V. R., Pan, G., Deshpande, M., Thandavarayan, R. A., Xu, J., Yang, X.-P., & Palaniyandi, S. S. (2016). Cardiac Mitochondrial Respiratory Dysfunction and Tissue Damage in Chronic Hyperglycemia Correlate with Reduced Aldehyde Dehydrogenase-2 Activity. *PLoS ONE*, *11*(10), 163158. https://doi.org/10.1371/journal.pone.0163158

Marcet, A. (1817). An Essay on the Chemical History and Medical Treatment of Calculous Disorders. *London: Longman, Hurst, Rees, Orme and Brown*, 79–88.

Marhoume, F. Z., Aboufatima, R., Zaid, Y., Limami, Y., Duval, R. E., Laadraoui, J., Belbachir, A., Chait, A., & Bagri, A. (2021). Antioxidant and polyphenol-rich ethanolic extract of Rubia Tinctorum l. Prevents urolithiasis in an ethylene glycol experimental model in rats. *Molecules*, *26*(4), 1–17. https://doi.org/10.3390/molecules26041005

Markova, N. G., Karaman-Jurukovska, N., Dong, K. K., Damaghi, N., Smiles, K. A., & Yarosh, D. B. (2009). Skin cells and tissue are capable of using l-ergothioneine as an integral component of their antioxidant defense system. In *Free Radical Biology and Medicine* (Vol. 46, Issue 8, pp. 1168–1176). https://doi.org/10.1016/j.freeradbiomed.2009.01.021

Mårtensson, J., Denneberg, T., Lindell, Å., & Textorius, O. (1990). Sulfur amino acid metabolism in cystinuria: A biochemical and clinical study of patients. *Kidney International*, *37*(1), 143–149. https://doi.org/10.1038/ki.1990.20

Martin, K. R. (2010). The bioactive agent ergothioneine, a key component of dietary mushrooms, inhibits monocyte binding to endothelial cells characteristic of early cardiovascular disease. *Journal of Medicinal Food*, *13*(6), 1340–1346. https://doi.org/10.1089/jmf.2009.0194

Martínez-Reyes, I., & Chandel, N. S. (2020). Mitochondrial TCA cycle metabolites control physiology and disease. *Nature Communications*, *11*, 1–11. https://doi.org/10.1038/s41467-019-13668-3

Mastroberardino, L., Spindler, B., Pfeiffer, R., Skelly, P. J., Loffing, J., Shoemaker, C. B., & Verrey, F. (1998). Amino-acid transport by heterodimers of 4F2hc/CD98 and members of a permease family.

Nature, *395*(6699), 288–291. https://doi.org/10.1038/26246

Matta, C. F., & Massa, L. (2017). Information Theory and the Thermodynamic Efficiency of Biological Sorting Systems: Case Studies of the Kidney and of Mitochondrial ATP-Synthase. Case Studies of the Kidney and of Mitochondrial ATP-Synthase. In *Sustained Energy for Enhanced Human Functions and Activity* (Issue 1965). Elsevier Inc. https://doi.org/10.1016/B978-0-12-805413-0.00001-6

Mcintyre, T. M. (1980). The Interorgan Metabolism of Glutathione. *Int J Biochem*, *12*, 545–551.

Méchin, V., Damerval, C., & Zivy, M. (2007). Total protein extraction with TCA-acetone. *Methods in Molecular Biology (Clifton, N.J.)*, *355*(2), 1–8. https://doi.org/10.1385/1-59745-227-0:1

Milliner, D., Mary, E., & R, M. (1993). Urolithiasis in Pediatric Patients. *Mayo Clinic Proceedings*, *68*(3), 241–248. https://doi.org/10.1016/S0025-6196(12)60043-3

Milne, M. D., Asatoor, A. M., Edwards, K. D. G., & Loughridge, L. W. (1961). The intestinal absorption defect in cystinuria. *Gut*, *2*, 323–337.

Minczuk, M., He, J., Duch, A. M., Ettema, T. J., Chlebowski, A., Dzionek, K., Nijtmans, L. G. J., Huynen, M. A., & Holt, I. J. (2011). TEFM (c17orf42) is necessary for transcription of human mtDNA. *Nucleic Acids Reasearch*, *39*, 4284–4299. https://doi.org/10.1093/nar/gkq1224

Mohammadi, M., Shohani, A., Khorami, H., Mahdavi, K. N., Izad Panahi, M. H., Alizadeh, F., & Azizi, M. (2018). The effect of selenium supplementation on cystine crystal volume in patients with cystinuria. *BioMedicine (France)*, *8*(4), 28–32. https://doi.org/10.1051/bmdcn/2018080426

Moore, S. L., Somani, B. K., & Cook, P. (2019). Journey of a cystinuric patient with a long-term follow-up from a medical stone clinic : necessity to be SaFER (stone and fragments entirely removed). *Urolithiasis*, *47*(2), 165–170. https://doi.org/10.1007/s00240-018-1059-5

Morillon, A.-C., Williamson, R. D., Baker, P. N., Kell, D. B., Kenny, L. C., English, J. A., McCarthy, F. P., & McCarthy, C. (2020). Effect of L-Ergothioneine on the metabolic plasma profile of the RUPP rat model of pre-eclampsia. *Plos One*, *15*(3), e0230977. https://doi.org/10.1371/journal.pone.0230977

Morin, C. L., Thompson, M. W., Jackson, S. H., & Sass-Kortsak, A. (1971). Biochemical and genetic studies in cystinuria: observations on double heterozygotes of genotype I-II. *The Journal of Clinical Investigation*, *50*(9), 1961–1976. https://doi.org/10.1172/JCI106688

Motohashi, N., Mori, I., & Sugiura, Y. (1976). Complexing of Copper Ion by Ergothioneine. *Chem. Pharm. Bull.*, *24*(10), 2364–2368.

Moussa, M., Papatsoris, A. G., Chakra, M. A., & Moussa, Y. (2020). Update on cystine stones : current and future concepts in treatment. *Intractable & Rare Diseases Research*, *9*(2), 71–78. https://doi.org/10.5582/irdr.2020.03006

Mozaffarian, F., Dehghani, M. A., Vanani, A. R., & Mahdavinia, M. (2021). Protective Effects of Alpha Lipoic Acid Against Arsenic Induced Oxidative Stress in Isolated Rat Liver Mitochondria. *Biological Trace Element Research*. https://doi.org/10.1007/s12011-021-02712-3

Mukaneza, Y., Cohen, A., Rivard, M.-È., Tardif, J., Deschênes, S., Ruiz, M., Consortium, L., Laprise, C., Rosiers, C. Des, & Coderre, L. (2019). mTORC1 is required for expression of LRPPRC and cytochrome-c oxidase but not HIF-1 in Leigh syndrome French Canadian type patient fibroblasts. *Am J Physiol Cell Physiol*, *317*, 58–67. https://doi.org/10.1152/ajpcell.00160.2017

Mulay, S. R., Desai, J., Kumar, S. V, Eberhard, J. N., Thomasova, D., Romoli, S., Grigorescu, M., Kulkarni, O. P., Popper, B., Vielhauer, V., Zuchtriegel, G., Reichel, C., Bräsen, J. H., Romagnani, P., Bilyy, R., Munoz, L. E., Herrmann, M., Liapis, H., Krautwald, S., … Anders, H.-J. (2016). Cytotoxicity of crystals involves RIPK3-MLKL-mediated necroptosis. *Nature Communications*, *7*. https://doi.org/10.1038/ncomms10274

Nagamori, S., Wiriyasermkul, P., Guarch, M. E., Okuyama, H., Nakagomi, S., Tadagaki, K., Nishinaka, Y., Bodoy, S., Takafuji, K., Okuda, S., Kurokawa, J., Ohgaki, R., Nunes, V., Palacín, M., & Kanai, Y. (2016). Novel cystine transporter in renal proximal tubule identified as a missing partner of cystinuria-related plasma membrane protein rBAT/SLC3A1. *Proceedings of the National Academy of Sciences of the United States of America*, *113*(3), 775–780. https://doi.org/10.1073/pnas.1519959113

Nair, A. B., & Jacob, S. (2016). *A simple practice guide for dose conversion between animals and human*. Journal of Basic and Clinical Pharmacy. https://doi.org/10.4103/0976-0105.177703

Nakagawa, Y., & Coe, F. L. (1999). A modified cyanide-nitroprusside method for quantifying urinary cystine concentration that corrects for creatinine interference. *Clin Chim Acta*, *289*, 57–68.

Nakamichi, N, Nakao, S., Nishiyama, M., Takeda, Y., Ishimoto, T., Masuo, Y., Matsumoto, S., Suzuki, M., & Kato, Y. (2021). Oral Administration of the Food-Derived Hydrophilic Antioxidant Ergothioneine Enhances Object Recognition Memory in Mice. *Current Molecular Pharmacology*, *14*(2), 220–233. https://doi.org/10.2174/1874467213666200212102710

Nakamichi, Noritaka, Nakayama, K., Ishimoto, T., Masuo, Y., Wakayama, T., Sekiguchi, H., Sutoh, K., Usumi, K., Iseki, S., & Kato, Y. (2016). Food-derived hydrophilic antioxidant ergothioneine is distributed to the brain and exerts antidepressant effect in mice. *Brain and Behavior*, *6*(6). https://doi.org/10.1002/brb3.477

Nakamichi, Noritaka, Shima, H., Asano, S., Ishimoto, T., Sugiura, T., Matsubara, K., Kusuhara, H., Sugiyama, Y., Sai, Y., Miyamoto, K. I., Tsuji, A., & Kato, Y. (2013). Involvement of carnitine/organic cation transporter OCTN1/SLC22A4 in gastrointestinal absorption of metformin. *Journal of Pharmaceutical Sciences*, *102*(9), 3407–3417. https://doi.org/10.1002/jps.23595

Nakanishi, T., Akabane, E. R., Nanami, M., Kiyobayashi, Y., Moriguchi, R., Hasuike, Y., Otaki, Y., Miyagawa, K., Itahana, R., & Izumi, M. (2005). Comparison of cytotoxicity of cysteine and homocysteine for renal epithelial cells. *Nephron. Experimental Nephrology*, *100*(1), 11–21. https://doi.org/10.1159/000084108

Narrea, P. I. ˜, Moini, H., Han, D., Rettori, D., Aguil´o, I., Aguil´o, A., Alava, M. A., Iturralde, M., & Cadenas, E. (2007). Mitochondrial respiratory chain and thioredoxin reductase regulate intermembrane Cu,Zn-superoxide dismutase activity: implications for mitochondrial energy metabolism and apoptosis. *Biochem. J*, *405*, 173–179. https://doi.org/10.1042/BJ20061809

Nelson, C. P., Kurtz, M. P., Venna, A., Jr, B. G. C., & Baum, M. A. (2020). Pharmacological dilutional therapy using the vasopressin antagonist tolvaptan for young patients with cystinuria: a pilot investigation. *Urology*, *144*, 65–70. https://doi.org/10.1016/j.urology.2020.07.002

Niimi, K., Yasui, T., Hirose, M., Hamamoto, S., Itoh, Y., Okada, A., Kubota, Y., Kojima, Y., Tozawa, K., Sasaki, S., Hayashi, Y., & Kohri, K. (2012). Contribution Mitochondrial permeability transition pore opening induces the initial process of renal calcium crystallization. *Free Radical Biology & Medicine*, *52*, 1207–1217. https://doi.org/10.1016/j.freeradbiomed.2012.01.005

Niimi, K., Yasui, T., Okada, A., Hirose, Y., Kubota, Y., Umemoto, Y., Kawai, N., Tozawa, K., & Kohri, K. (2014). Novel effect of the inhibitor of mitochondrial cyclophilinD activation, N-methyl-4-isoleucine cyclosporin, on renal calcium crystallization. *International Journal of Urology*, *21*(7), 707–713. https://doi.org/10.1111/iju.12425

Nishida, K., Takeuchi, K., Hosoda, A., Sugano, S., Morisaki, E., Ohishi, A., & Nagasawa, K. (2018). *Ergothioneine ameliorates oxaliplatin-induced peripheral neuropathy in rats*. https://doi.org/10.1016/j.lfs.2018.07.006

Nishiuch, Y., Sasaki, M., Nakayasu, M., & Oikawa, A. (1976). Cytotoxicity of cysteine in culture media. *In Vitro*, *12*(9), 635–638.

Obayashi, K., Kurihara, K., Okano, Y., Masaki, H., & Yarosh, D. (2005). L-Ergothioneine scavenges superoxide and singlet oxygen and suppresses TNF-a and MMP-1 expression in UV-irradiated human dermal fibroblasts. *International Journal of Cosmetic Science*, *27*, 191–192. https://doi.org/10.1046/j.1467-2494.2001.00096.x

Ohana, E., Shcheynikov, N., Moe, O. W., & Muallem, S. (2013). SLC26A6 and NaDC-1 transporters interact to regulate oxalate and citrate homeostasis. *Journal of the American Society of Nephrology*, *24*(10), 1617–1626. https://doi.org/10.1681/ASN.2013010080

Ojala, D., Montoya, J., & Attardi, G. (1981). tRNA punctuation model of RNA processing in human mitochondria. *Nature*, *290*(5806), 470–474. https://doi.org/10.1038/290470a0

Olschok, K., Vester, U., Lahme, S., Kurth, I., & Eggermann, T. (2018). No evidence for point mutations in the novel renal cystine transporter AGT1 / SLC7A13 contributing to the etiology of cystinuria. *BMC Neprhology*, *19:278*, 5–8.

Ou, P., Tritschler, H. J., & Wolff, S. P. (1995). Thioctic (lipoic) acid: a therapeutic metal-chelating antioxidant? *Biochemical Pharmacology*, *50*(1), 123–126. https://doi.org/10.1016/0006-2952(95)00116-H

Pajor, A. M. (1996). Molecular cloning and functional expression of a sodium-dicarboxylate cotransporter from human kidney. *American Journal of Physiology*, *270*(4 PART 2). https://doi.org/10.1152/ajprenal.1996.270.4.f642

Pak, C. Y. C., & Fuller, C. J. (1983). Assessment of cystine solubility in urine and of heterogeneous nucleation. *Journal of Urology*, *129*(5), 1066–1070. https://doi.org/10.1016/S0022-5347(17)52543-4

Pak, C. Y. C., Fuller, C., Sakhaee, K., Zerwekh, J. E., & Adams, B. V. (1986). Management of cystine nephrolithiasis with alpha-mercaptopropionylglycine. *Journal of Urology*, *136*(5), 1003–1008. https://doi.org/10.1016/S0022-5347(17)45188-3

Palacín, M., & Kanai, Y. (2004). The ancillary proteins of HATs: SLC3 family of amino acid transporters. *Pflugers Archiv European Journal of Physiology*, *447*(5), 490–494. https://doi.org/10.1007/s00424-003-1062-7

Palacín, M., Nunes, V., Font-llitjós, M., Jiménez-vidal, M., Fort, J., Pineda, M., Feliubadaló, L., Chillarón, J., Zorzano, A., Bartoccioni, P., Rio, C., Ratera, M., Kowalczyk, L., Baldwin, J. M., Zorzano, A., Quick, M., Baldwin, S. A., Vázquez-ibar, J. L., Palacín, M., … Zorzano, A. (2011). *The Genetics of Heteromeric Amino Acid Transporters*. 112–124. https://doi.org/10.1152/physiol.00051.2004

Palipoch, S. (2013). A review of oxidative stress in acute kidney injury: protective role of medicinal plants-derived antioxidants. *Palipoch Afr J Tradit Complement Altern Med*, *10*(4), 88–93. https://doi.org/10.4314/ajtcam.v10i4.15

Patel, M., Yarlagadda, V., Adedoyin, O., Saini, V., Assimos, D. G., Holmes, R. P., & Mitchell, T. (2018). Oxalate induces mitochondrial dysfunction and disrupts redox homeostasis in a human monocyte derived cell line. *Redox Biology*, *15*(October 2017), 207–215. https://doi.org/10.1016/j.redox.2017.12.003

Paul, B. D., & Snyder, S. H. (2010). The unusual amino acid L-ergothioneine is a physiologic cytoprotectant. *Cell Death and Differentiation*, *17*, 1134–1140. https://doi.org/10.1038/cdd.2009.163

Pearle, M. S., Goldfarb, D. S., Assimos, D. G., Curhan, G., Denu-Ciocca, C. J., Matlaga, B. R., Monga, M., Penniston, K. L., Preminger, G. M., Turk, T. M. T., & White, J. R. (2014). Medical management of kidney stones: AUA guideline. *Journal of Urology*, *192*(2), 316–324. https://doi.org/10.1016/j.juro.2014.05.006

Peerapen, P., Chaiyarit, S., & Thongboonkerd, V. (2018). Protein Network Analysis and Functional Studies of Calcium Oxalate Crystal-Induced Cytotoxicity in Renal Tubular Epithelial Cells. *Proteomics*, *18*(8), 1–23. https://doi.org/10.1002/pmic.201800008

Peghini, P., Janzen, J., & Stoffel, W. (1997). Glutamate transporter EAAC-1-deficient mice develop dicarboxylic aminoaciduria and behavioral abnormalities but no neurodegeneration Pietro. *The EMBO Journal Pines et Al*, *16*(13), 3822–3832.

Peng, T. I., & Jou, M. J. (2010). Oxidative stress caused by mitochondrial calcium overload. *Annals of the New York Academy of Sciences*, *1201*, 183–188. https://doi.org/10.1111/j.1749-6632.2010.05634.x

Perazella, M. A., & Buller, G. K. (1993). Successful Treatment of Cystinuria With Captopril. *American Journal of Kidney Diseases*, *21*(5), 504–507. https://doi.org/10.1016/S0272-6386(12)80396-9

Peters, T., Thaete, C., Wolf, S., Popp, a., Sedlmeier, R., Grosse, J., Nehls, M. C., Russ, a., & Schlueter, V. (2003). A mouse model for cystinuria type I. *Human Molecular Genetics*, *12*(17), 2109–2120. https://doi.org/10.1093/hmg/ddg189

Pfeiffer, C., Bach, M., Bauer, T., Campos Da Ponte, J., Schömig, E., & Gründemann, D. (2015). Knockout of the ergothioneine transporter ETT in zebrafish results in increased 8-oxoguanine levels. *Free Radical Biology and Medicine*, *83*, 178–185. https://doi.org/10.1016/j.freeradbiomed.2015.02.026

Pfeiffer, C., Bauer, T., Surek, B., Schömig, E., & Gründemann, D. (2011). Cyanobacteria produce high

levels of ergothioneine. *Food Chemistry*, *129*(4), 1766–1769. https://doi.org/10.1016/j.foodchem.2011.06.047

Pfeiffer, R., Loffing, J., Bauch, C., Meier, C., Eggermann, T., Loffing-cueni, D., Ku, L. C., & Zu, C.-. (1999). Luminal HEterodimeric Amino Acid Transporter Defective in Cystinuria. *Molecular Biology of the Cell*, *10*(December), 4135–4147.

Pickel, V. M., Nirenberg, M. J., Chan, J., Mosckovitz, R., Udenfriend, S., & Tate, S. S. (1993). Ultrastructural localization of a neutral and basic amino acid transporter in rat kidney and intestine. *Proceedings of the National Academy of Sciences of the United States of America*, *90*(16), 7779–7783. https://doi.org/10.1073/pnas.90.16.7779

Plotnikov, E., Palmeira, C., Grases, F., Sayer, J. A., Thongboonkerd, V., & Chaiyarit, S. (2020). Mitochondrial Dysfunction and Kidney Stone Disease. *Frontiers in Physiology | Www.Frontiersin.Org*, *11*, 566506. https://doi.org/10.3389/fphys.2020.566506

Pochini, L., Scalise, M., Di Silvestre, S., Belviso, S., Pandolfi, A., Arduini, A., Bonomini, M., & Indiveri, C. (2016). Acetylcholine and acetylcarnitine transport in peritoneum: Role of the SLC22A4 (OCTN1) transporter. *Biochimica et Biophysica Acta - Biomembranes*, *1858*(4), 653–660. https://doi.org/10.1016/j.bbamem.2015.12.026

Poon, I., Morioka, S., Kurts, C., Thongboonkerd, V., Singhto, N., Kanlaya, R., & Nilnumkhum, A. (2018). Roles of Macrophage exosomes in immune response to calcium Oxalate Monohydrate crystals. *Frontiers in Immunology*, *9*, 27. https://doi.org/10.3389/fimmu.2018.00316

Prathapasinghe, G. A., Siow, Y. L., Xu, Z., & Karmin, O. (2008). Inhibition of cystathionine-β-synthase activity during renal ischemia-reperfusion: Role of pH and nitric oxide. *American Journal of Physiology - Renal Physiology*, *295*(4), 912–922. https://doi.org/10.1152/ajprenal.00040.2008

Prot-Bertoye, C., Lebbah, S., Daudon, M., Tostivint, I., Bataille, P., Bridoux, F., Brignon, P., Choquenet, C., Cochat, P., Combe, C., Conort, P., Decramer, S., Doré, B., Dussol, B., Essig, M., Gaunez, N., Joly, D., Le Toquin-Bernard, S., Méjean, A., … Courbebaisse, M. (2015). CKD and its risk factors among patients with cystinuria. *Clinical Journal of the American Society of Nephrology*, *10*(5), 842–851. https://doi.org/10.2215/CJN.06680714

Prot-Bertoye, C., Lebbah, S., Daudon, M., Tostivint, I., Jais, J. P., Lillo-Le Louët, A., Pontoizeau, C., Cochat, P., Bataille, P., Bridoux, F., Brignon, P., Choquenet, C., Combe, C., Conort, P., Decramer, S., Doré, B., Dussol, B., Essig, M., Frimat, M., … Courbebaisse, M. (2019). Adverse events associated with currently used medical treatments for cystinuria and treatment goals: results from a series of 442 patients in France. *BJU International*, *124*(5), 849–861. https://doi.org/10.1111/bju.14721

Ramzan, R., Staniek, K., Kadenbach, B., & Vogt, S. (2010). Mitochondrial respiration and membrane potential are regulated by the allosteric ATP-inhibition of cytochrome c oxidase. *Biochimica et Biophysica Acta - Bioenergetics*, *1797*(9), 1672–1680. https://doi.org/10.1016/j.bbabio.2010.06.005

Rech, V. C., Feksa, L. R., Do Amaral, M. F. A., Koch, G. W., Wajner, M., Dutra-Filho, C. S., De Souza Wyse, A. T., & Wannmacher, C. M. D. (2007). Promotion of oxidative stress in kidney of rats loaded with cystine dimethyl ester. *Pediatric Nephrology*, *22*(8), 1121–1128. https://doi.org/10.1007/s00467-007-0494-2

Repine ∗, J. E., & Elkins, N. D. (2011). *Effect of ergothioneine on acute lung injury and inflammation in cytokine insufflated rats*. https://doi.org/10.1016/j.ypmed.2011.12.006

Richman, P. G., & Meister, A. (1975). Regulation of γ glutamyl cysteine synthetase by nonallosteric feedback inhibition by glutathione. *Journal of Biological Chemistry*, *250*(4), 1422–1426. https://doi.org/10.1016/s0021-9258(19)41830-9

Richter, C., Park, J. W., & Ames, B. N. (1988). Normal oxidative damage to mitochondrial and nuclear DNA is extensive. *Proceedings of the National Academy of Sciences of the United States of America*, *85*(17), 6465–6467. https://doi.org/10.1073/pnas.85.17.6465

Rius, M., Hummel-Eisenbeiss, J., Hofmann, A. F., & Keppler, D. (2006). Substrate specificity of human ABCC4 (MRP4)-mediated cotransport of bile acids and reduced glutathione. *American Journal of Physiology - Gastrointestinal and Liver Physiology*, *290*(4), 640–647. https://doi.org/10.1152/ajpgi.00354.2005

Rodman, J., Williams, J., & Peterson, C. (1984). Dissolution of uric acid calculi. *The Journal of Urology*, *131*(6), 1039–1044. https://doi.org/10.1016/S0022-5347(17)50798-3

Rosenberg, L. E., Downing, S., Durant, J. L., & Segal, S. (1966). Cystinuria: biochemical evidence for three genetically distinct diseases. *Journal of Clinical Investigation*, *45*(3), 365–371. https://doi.org/10.1172/JCI105351

Ruzzenente, B., Metodiev, M. D., Wredenberg, A., Bratic, A., Park, C. B., Cámara, Y., Milenkovic, D., Zickermann, V., Wibom, R., Hultenby, K., Erdjument-Bromage, H., Tempst, P., Brandt, U., Stewart, J. B., Gustafsson, C. M., & Larsson, N. G. (2012). LRPPRC is necessary for polyadenylation and coordination of translation of mitochondrial mRNAs. *EMBO Journal*, *31*(2), 443–456. https://doi.org/10.1038/emboj.2011.392

Sahota, A., Tischfield, J. A., Goldfarb, D. S., Ward, M. D., & Hu, L. (2020). Cystinuria : Genetic aspects, mouse models, and a new approach to therapy. *Urolithiasis*, *47*(1), 57–66. https://doi.org/10.1007/s00240-018-1101-7.Cystinuria

Sakly, R., Chaouch, A., El Hani, A., & Najjar, M. F. (2003). Effects of intraperitoneally administered vitamin E and selenium on calcium oxalate renal stone formation: Experimental study in rat. *Annales d'Urologie*, *37*(2), 47–50. https://doi.org/10.1016/S0003-4401(03)00007-X

Salama, S. A., Abd-Allah, G. M., Mohamadin, A. M., Elshafey, M. M., & Gad, H. S. (2021). Ergothioneine mitigates cisplatin-evoked nephrotoxicity via targeting Nrf2, NF-κB, and apoptotic signaling and inhibiting γ-glutamyl transpeptidase. *Life Sciences*, *278*(March), 119572. https://doi.org/10.1016/j.lfs.2021.119572

Sasarman, F., Brunel-Guitton, C., Antonicka, H., Wai, T., & Shoubridge, E. A. (2010). LRPPRC and SLIRP Interact in a Ribonucleoprotein Complex That Regulates Posttranscriptional Gene Expression in Mitochondria. *Molecular Biology of the Cell*, *21*, 1315–1323. https://doi.org/10.1091/mbc.E10

Schorbach, L., Krick, W., Burckhardt, G., & Burckhardt, B. C. (2013). Glutathione is a low-affinity substrate of the human sodium-dependent dicarboxylate transporter. *Nephron - Physiology*, *124*(1–2), 1–5. https://doi.org/10.1159/000356419

Schulman, J. D., Goodman, S. I., Mace, J. W., Patrick, A. D., Tietze, F., & Butler, E. J. (1975). Glutathionuria: Inborn error of metabolism due to tissue deficiency of gamma-glutamyl transpeptidase. *Biochemical and Biophysical Research Communications*, *65*(1), 68–74. https://doi.org/10.1016/S0006-291X(75)80062-3

Seebeck, F. P. (2010). In vitro reconstitution of mycobacterial ergothioneine biosynthesis. *Journal of the American Chemical Society*, *132*(19), 6632–6633. https://doi.org/10.1021/ja101721e

Servais, A., Thomas, K., Dello Strologo, L., Sayer, J. A., Bekri, S., Bertholet-Thomas, A., Bultitude, M., Capolongo, G., Cerkauskiene, R., Daudon, M., Doizi, S., Gillion, V., Gràcia-Garcia, S., Halbritter, J., Heidet, L., van den Heijkant, M., Lemoine, S., Knebelmann, B., Emma, F., & Levtchenko, E. (2021). Cystinuria: clinical practice recommendation. *Kidney International*, *99*(1), 48–58. https://doi.org/10.1016/j.kint.2020.06.035

Servillo, L., D'Onofrio, N., Casale, R., Cautela, D., Giovane, A., Castaldo, D., & Balestrieri, M. L. (2017). Ergothioneine products derived by superoxide oxidation in endothelial cells exposed to high-glucose. *Free Radical Biology and Medicine*, *108*(March), 8–18. https://doi.org/10.1016/j.freeradbiomed.2017.03.009

Sharma, M., Kaur, T., & Singla, S. K. (2015). Protective effects of N-acetylcysteine against hyperoxaluria induced mitochondrial dysfunction in male wistar rats. *Molecular and Cellular Biochemistry*, *405*(1–2), 105–114. https://doi.org/10.1007/s11010-015-2402-6

Sharma, M., Kaur, T., & Singla, S. K. (2016). Role of mitochondria and NADPH oxidase derived reactive oxygen species in hyperoxaluria induced nephrolithiasis: Therapeutic intervention with combinatorial therapy of N-acetyl cysteine and Apocynin. *Mitochondrion*, *27*, 15–24. https://doi.org/10.1016/j.mito.2016.01.002

Shayakul, C., Kanai, Y., Lee, W. S., Brown, D., Rothstein, J. D., & Hediger, M. A. (1997). Localization of the high-affinity glutamate transporter EAAC1 in rat kidney. *The American Journal of Physiology*, *273*(6 Pt 2), F1023–F1029. http://www.ncbi.nlm.nih.gov/pubmed/9435692

Shinozaki, Y., Furuichi, K., Toyama, T., Kitajima, S., Hara, A., Iwata, Y., Sakai, N., Shimizu, M., Kaneko, S.,

Isozumi, N., Nagamori, S., Kanai, Y., Sugiura, T., Kato, Y., & Wada, T. (2017). Impairment of the carnitine/organic cation transporter 1–ergothioneine axis is mediated by intestinal transporter dysfunction in chronic kidney disease. *Kidney International*, *92*(6), 1356–1369. https://doi.org/10.1016/j.kint.2017.04.032

Shitara, Y., Nakamichi, N., Norioka, M., Shima, H., Kato, Y., & Horie, T. (2012). Role of Organic Cation/Carnitine Transporter 1 in Uptake of Phenformin and Inhibitory Effect on Complex I Respiration in Mitochondria. *Toxicological Sciences*, *132*(1), 32–42. https://doi.org/10.1093/toxsci/kfs330

Short, K. R., Bigelow, M. L., Kahl, J., Singh, R., Coenen-Schimke, J., Raghavakaimal, S., & Sreekumaran Nair, K. (2005). *Decline in skeletal muscle mitochondrial function with aging in humans*. www.pnas.orgcgidoi10.1073pnas.0501559102

Siener, R., Bitterlich, N., Birwé, H., & Hesse, A. (2021). The impact of diet on urinary risk factors for cystine stone formation. *Nutrients*, *13*(2), 1–10. https://doi.org/10.3390/nu13020528

Signes, A., & Fernandez-Vizarra, E. (2018). Assembly of mammalian oxidative phosphorylation complexes I-V and supercomplexes. *Essays in Biochemistry*, *62*, 255–270. https://doi.org/10.1042/EBC20170098

Silbernagl, S. (1988). The renal handling of amino acids and oligopeptides. *Physiological Reviews*, *68*(3), 911–1007. https://doi.org/10.1152/physrev.1988.68.3.911

Silva, J. P., Köhler, M., Graff, C., Oldfors, A., Magnuson, M. A., Berggren, P. O., & Larsson, N. G. (2000). Impaired insulin secretion and β-cell loss in tissue-specific knockout mice with mitochondrial diabetes. *Nature Genetics*, *26*(3), 336–340. https://doi.org/10.1038/81649

Smith, E., Ottosson, F., Hellstrand, S., Ericson, U., Orho-Melander, M., Fernandez, C., & Melander, O. (2019). *Ergothioneine is associated with reduced mortality and decreased risk of cardiovascular disease | Enhanced Reader*. BMJ. https://doi.org/(http:// dx. doi. org/ 10. 1136/ heartjnl- 2019-315485)

Song, T.-Y., Yang, N.-C., Chen, C.-L., Lan, T., & Thi, V. (2017). *Protective Effects and Possible Mechanisms of Ergothioneine and Hispidin against Methylglyoxal-Induced Injuries in Rat Pheochromocytoma Cells*. https://doi.org/10.1155/2017/4824371

Stein, W. H. (1951). Excretion of Amino Acids in Cystinuria. *Proceedings of the Society for Experimental Biology and Medicine*, *78*(3), 705–708. https://doi.org/10.3181/00379727-78-19189

Stephens, A. D. (1989). Richard Watts Symposium Cystinuria and its Treatment : 25 years Experience at St . Bartholomew ' s Hospital. *J Inher Metab Dis*, *12*, 197–209.

Stoffels, C., Oumari, M., Perrou, A., Termath, A., Schlundt, W., Schmalz, H. G., Schäfer, M., Wewer, V., Metzger, S., Schömig, E., & Gründemann, D. (2017). Ergothioneine stands out from hercynine in the reaction with singlet oxygen: Resistance to glutathione and TRIS in the generation of specific products indicates high reactivity. *Free Radical Biology and Medicine*, *113*(July), 385–394. https://doi.org/10.1016/j.freeradbiomed.2017.10.372

Sugioka, K., Nakano, M., Totsune-Nakano, H., Minakami, H., Tero-Kubota, S., & Ikegami, Y. (1988). Mechanism of O-2 generation in reduction and oxidation cycle of ubiquinones in a model of mitochondrial electron transport systems. *BBA - Bioenergetics*, *936*(3), 377–385. https://doi.org/10.1016/0005-2728(88)90014-X

Sun, X. Y., Ouyang, J. M., Gan, Q. Z., & Liu, A. J. (2016). Renal epithelial cell injury induced by calcium oxalate monohydrate depends on their structural features: Size, surface, and crystalline structure. *Journal of Biomedical Nanotechnology*, *12*(11), 2001–2014. https://doi.org/10.1166/jbn.2016.2289

Suzuki, R., & Shimodaira, H. (2006). Pvclust: An R package for assessing the uncertainty in hierarchical clustering. *Bioinformatics*, *22*(12), 1540–1542. https://doi.org/10.1093/bioinformatics/btl117

Tamai, I., Ohashi, R., Nezu, J. I., Sai, Y., Kobayashi, D., Oku, A., Shimane, M., & Tsuji, A. (2000). Molecular and functional characterization of organic cation/carnitine transporter family in mice. *Journal of Biological Chemistry*, *275*(51), 40064–40072. https://doi.org/10.1074/jbc.M005340200

Tamai, I., Yabuuchi, H., Nezu, J. I., Sai, Y., Oku, A., Shimane, M., & Tsuji, A. (1997). Cloning and characterization of a novel human pH-dependent organic cation transporter, OCTN1. *FEBS*

Letters, *419*(1), 107–111. https://doi.org/10.1016/S0014-5793(97)01441-5

Tang, R., Cheah, I., Yew, T., & Halliwell, B. (2018). Distribution and accumulation of dietary ergothioneine and its metabolites in mouse tissues. *Scientific Reports*, *8*(1), 1–15. https://doi.org/10.1038/s41598-018-20021-z

Tang, Y., Masuo, Y., Sakai, Y., Wakayama, T., Sugiura, T., Harada, R., Futatsugi, A., Komura, T., Nakamichi, N., Sekiguchi, H., Sutoh, K., Usumi, K., Iseki, S., Kaneko, S., & Kato, Y. (2016). Localization of Xenobiotic Transporter OCTN1/SLC22A4 in Hepatic Stellate Cells and Its Protective Role in Liver Fibrosis. *Journal of Pharmaceutical Sciences*, *105*(5), 1779–1789. https://doi.org/10.1016/j.xphs.2016.02.023

Tate, S., Yant, N., & Udenfriendtt, S. (1992). Expression cloning of a Na + -independent neutral amino acid transporter from rat kidney. *Proceedings of the National Academy of Sciences of the United States of America*, *89*, 1–5.

Taubert, D., Grimberg, G., Jung, N., Rubbert, A., & Schömig, E. (2005). Functional role of the 503F variant of the organic cation transporter OCTN1 in Crohn's disease. *Gut*, *54*(10), 1505–1506. https://doi.org/10.1136/gut.2005.075820

Taylor, R. W., & Turnbull, D. M. (2005). *MITOCHONDRIAL DNA MUTATIONS IN HUMAN DISEASE*. https://doi.org/10.1038/nrg1606

Thomas, K., Wong, K., Withington, J., Bultitude, M., & Doherty, A. (2014). Cystinuria — a urologist ' s perspective. *Nature Reviews Urology*, *11*, 270–277. https://doi.org/10.1038/nrurol.2014.51

Toel, F. (1855). Beobachtungen iiber Cystinbildung. *EurJOC*, 247–251. https://doi.org/https://doi.org/10.1002/jlac.18550960215

Toh, D. S. L., Cheung, F. S. G., Murray, M., Pern, T. K., Lee, E. J. D., & Zhou, F. (2013). Functional analysis of novel variants in the organic cation/ergothioneine transporter 1 identified in singapore populations. *Molecular Pharmaceutics*, *10*(7), 2509–2516. https://doi.org/10.1021/mp400193r

Tucker, R. A. J., Cheah, I. K., & Halliwell, B. (2019). Specificity of the ergothioneine transporter natively expressed in HeLa cells. *Biochemical and Biophysical Research Communications*, *513*(1), 22–27. https://doi.org/10.1016/j.bbrc.2019.02.122

Tungsanga, K., Sriboonlue, Æ. P., & Futrakul, Æ. P. (2005). Renal tubular cell damage and oxidative stress in renal stone patients and the effect of potassium citrate treatment. *Urol Res*, *33*, 65–69. https://doi.org/10.1007/s00240-004-0444-4

Turck, D., Bresson, J., Burlingame, B., Dean, T., Fairweather-Tait, S., Heinonen, M., Hirsch-Ernst, K. I., Mangelsdorf, I., McArdle, H. J., Naska, A., Neuhäuser-Berthold, M., Nowicka, G., Pentieva, K., Sanz, Y., Siani, A., Sjödin, A., Stern, M., Tomé, D., Vinceti, M., … van Loveren, H. (2016). Safety of synthetic l-ergothioneine (Ergoneine®) as a novel food pursuant to Regulation (EC) No 258/97. *EFSA Journal*, *14*(11). https://doi.org/10.2903/j.efsa.2016.4629

Turck, D., Bresson, J., Burlingame, B., Dean, T., Fairweather-Tait, S., Heinonen, M., Hirsch-Ernst, K. I., Mangelsdorf, I., McArdle, H. J., Naska, A., Neuhäuser-Berthold, M., Nowicka, G., Pentieva, K., Sanz, Y., Siani, A., Sjödin, A., Stern, M., Tomé, D., Vinceti, M., … van Loveren, H. (2017). Statement on the safety of synthetic l-ergothioneine as a novel food – supplementary dietary exposure and safety assessment for infants and young children, pregnant and breastfeeding women. *EFSA Journal*, *15*(11). https://doi.org/10.2903/j.efsa.2017.5060

Turrens, J. F., Alexandre, A., & Lehninger, A. L. (1985). Ubisemiquinone is the electron donor for superoxide formation by complex III of heart mitochondria. *Archives of Biochemistry and Biophysics*, *237*(2), 408–414. https://doi.org/10.1016/0003-9861(85)90293-0

Vaisbich, M. H., Pache de Faria Guimaraes, L., Shimizu, M. H. M., & Seguro, A. C. (2011). Oxidative Stress in Cystinosis Patients. *Nephron Extra*, *1*(1), 73–77. https://doi.org/10.1159/000331445

Van Bon, B. W. M., Oortveld, M. A. W., Nijtmans, L. G., Fenckova, M., Nijhof, B., Besseling, J., Vos, M., Kramer, J. M., De Leeuw, N., Castells-Nobau, A., Asztalos, L., Viragh, E., Ruiter, M., Hofmann, F., Eshuis, L., Collavin, L., Huynen, M. A., Asztalos, Z., Verstreken, P., … Schenck, A. (2013). CEP89 is required for mitochondrial metabolism and neuronal function in man and fly. *Human Molecular Genetics*, *22*(15), 3138–3151. https://doi.org/10.1093/hmg/ddt170

Vartak, R., Deng, J., Fang, H., & Bai, Y. (2015). Redefining the roles of mitochondrial DNA-encoded

subunits in respiratory Complex I assembly. *Biochimica et Biophysica Acta - Molecular Basis of Disease*, *1852*(7), 1531–1539. https://doi.org/10.1016/j.bbadis.2015.04.008

Veena, C. K., Josephine, A., Preetha, S. P., Rajesh, N. G., & Varalakshmi, P. (2008). Mitochondrial dysfunction in an animal model of hyperoxaluria: A prophylactic approach with fucoidan. *European Journal of Pharmacology*, *579*(1–3), 330–336. https://doi.org/10.1016/j.ejphar.2007.09.044

Veena, C. K., Josephine, A., Preetha, S. P., Varalakshmi, P., & Sundarapandiyan, R. (2006). Renal peroxidative changes mediated by oxalate: The protective role of fucoidan. *Life Sciences*, *79*(19), 1789–1795. https://doi.org/10.1016/j.lfs.2006.06.014

Verrey, F., Singer, D., Ramadan, T., Vuille-dit-Bille, R., Mariotta, L., & Camargo, S. (2009). Kidney amino acid transport. *European Journal of Physiology*, *458*(1), 53–60. https://doi.org/10.1007/S00424-009-0638-2

Visarius, T. M., Putt, D. A., Schure, J. M., Pegouske, D. M., & Lasht, L. H. (1996). Pathways of Glutathione Metabolism a & d Transport in Isolated Proximal Tubular Cells from Rat Kidney. *Biochemical Pharmacology*, *52*(April 1995), 259–272.

Wallace, D. (1992). Diseases of the mitochondrial DNA. *Annu Rev Biochem*, *61*, 1175–1212. https://doi.org/10.33588/rn.3104.2000236

Wang, J., Wilhelmsson, H., Graff, C., Li, H., Oldfors, A., Rustin, P., Brüning, J. C., Kahn, C. R., Clayton, D. A., Barsh, G. S., Thorén, P., & Larsson, N.-G. (1999). *Dilated cardiomyopathy and atrioventricular conduction blocks induced by heart-specific inactivation of mitochondrial DNA gene expression*. http://genetics.nature.com

Wang, Z., Ying, Z., Bosy-Westphal, A., Zhang, J., Schautz, B., Later, W., Heymsfield, S., & Müller, M. (2010). Specific metabolic rates of major organs and tissues across adulthood: Evaluation by mechanistic model of resting energy expenditure. *American Journal of Clinical Nutrition*, *92*(6), 1369–1377. https://doi.org/10.3945/ajcn.2010.29885

Wardyn, J. D., Ponsford, A. H., & Sanderson, C. M. (2015). Dissecting molecular cross-talk between Nrf2 and NF-κB response pathways. *Biochemical Society Transactions*, *43*, 621–626. https://doi.org/10.1042/BST20150014

Wartenfeld, R., Golomb, E., Katz, G., Bale, S. J., Goldman, B., Pras, M., Kastner, D. L., & Pras, E. (1997). Molecular Analysis of Cystinuria in Libyan Jews : Exclusion of the SLC3A1 Gene and Mapping of a New Locus on 19q. *American Journal of Human Genetics*, *60*, 617–624.

Weinberg, J. M., Venkatachalam, M. A., Roeser, N. F., Saikumar, P., Dong, Z., Senter, R. A., & Nissim, I. (2000). Anaerobic and aerobic pathways for salvage of proximal tubules from hypoxia-induced mitochondrial injury. *American Journal of Physiology - Renal Physiology*, *279*(5 48-5), 927–943. https://doi.org/10.1152/ajprenal.2000.279.5.f927

Wells, R. G., & Hediger, M. A. (1992). Cloning of a rat kidney cDNA that stimulates dibasic and neutral amino acid transport and has sequence similarity to glucosidases. *Proceedings of the National Academy of Sciences of the United States of America*, *89*, 5596–5600.

Williamson, R. D., McCarthy, F. P., Manna, S., Groarke, E., Kell, D. B., Kenny, L. C., & McCarthy, C. M. (2020). L-(+)-Ergothioneine Significantly Improves the Clinical Characteristics of Preeclampsia in the Reduced Uterine Perfusion Pressure Rat Model. *Hypertension*, 561–568. https://doi.org/10.1161/HYPERTENSIONAHA.119.13929

Wilmer, M. J., Willems, P. H., Verkaart, S., Visch, H. J., De Graaf-Hess, A., Blom, H. J., Monnens, L. A., Van Den Heuvel, L. P., & Levtchenko, E. N. (2007). Cystine dimethylester model of cystinosis: Still reliable? *Pediatric Research*, *62*(2), 151–155. https://doi.org/10.1203/PDR.0b013e31809fd9a7

Wilson, G. J., Gois, P. H. F., Zhang, A., Wang, X., Law, B. M. P., Kassianos, A. J., & Healy, H. G. (2018). The Role of Oxidative Stress and Inflammation in Acute Oxalate Nephropathy Associated With Ethylene Glycol Intoxication. *Kidney International Reports*, *3*(5), 1217–1221. https://doi.org/10.1016/j.ekir.2018.05.005

Wollaston, W. (1810). Cystic Oxide, a new species of Urinary Calculus. *Phil. Trans. Roy. Soc. London B Biol. Sci*, *100*, 223–224.

Wong, K. A., Mein, R., Wass, M., Flinter, F., Pardy, C., Bultitude, M., & Thomas, K. (2015). The genetic

diversity of cystinuria in a UK population of patients. *BJU International*, *116*(1), 109–116. https://doi.org/10.1111/bju.12894

Woodard, L. E., Welch, R. C., Veach, R. A., Beckermann, T. M., Sha, F., Weinman, E. J., Ikizler, T. A., Tischfield, J. A., Sahota, A., & Wilson, M. H. (2019). Metabolic consequences of cystinuria. *BMC Nephrology*, *20*(1), 1–9. https://doi.org/10.1186/s12882-019-1417-8

Yahyaoui, R., & Pérez-Frías, J. (2020). Amino acid transport defects in human inherited metabolic disorders. *International Journal of Molecular Sciences*, *21*(1). https://doi.org/10.3390/ijms21010119

Yakes, F. M., & Van Houten, B. (1997). Mitochondrial DNA damage is more extensive and persists longer than nuclear DNA damage in human cells following oxidative stress. *Proceedings of the National Academy of Sciences of the United States of America*, *94*(2), 514–519. https://doi.org/10.1073/pnas.94.2.514

Yan, R., Li, Y., Shi, Y., Zhou, J., Lei, J., Huang, J., & Zhou, Q. (2020). Cryo-EM structure of the human heteromeric amino acid transporter b 0,+ AT-rBAT. *Science Advances*, *6*. http://advances.sciencemag.org/

Yang, C., Ko, B., Hensley, C. T., Jiang, L., Wasti, A. T., Kim, J., Sudderth, J., Calvaruso, M. A., Lumata, L., Mitsche, M., Rutter, J., Merritt, M. E., & DeBerardinis, R. J. (2014). Glutamine oxidation maintains the TCA cycle and cell survival during impaired mitochondrial pyruvate transport. *Molecular Cell*, *56*(3), 414–424. https://doi.org/10.1016/j.molcel.2014.09.025

Yang, N.-C., Lin, H.-C., Wu, J.-H., Ou, H.-C., Chai, Y.-C., Tseng, C.-Y., Liao, J.-W., & Song, T.-Y. (2012). *Ergothioneine protects against neuronal injury induced by b-amyloid in mice*. https://doi.org/10.1016/j.fct.2012.08.021

Yang, Y., Albanyan, H., Lee, S., Aloysius, H., Liang, J., Kholodovych, V., Sahota, A., & Hu, L. (2018). Bioorganic & Medicinal Chemistry Letters Design , synthesis , and evaluation of L -cystine diamides as L -cystine crystallization inhibitors for cystinuria. *Bioorganic & Medicinal Chemistry Letters*, *28*, 1303–1308. https://doi.org/10.1016/j.bmcl.2018.03.024

Yifan, Z., Luwei, X., Kai, L., Liuhua, Z., Yuzheng, G., & Ruipeng, J. (2019). Protective effect of salvianolic acid B against oxidative injury associated with cystine stone formation. *Urolithiasis*, *47*(6), 503–510. https://doi.org/10.1007/s00240-019-01114-4

Ying, Z., Kampfrath, T., Sun, Q., Parthasarathy, S., & Rajagopalan, S. (2011). Evidence that α-lipoic acid inhibits NF-κB activation independent of its antioxidant function. *Inflam Res*, *60*(3), 219–255. https://doi.org/10.1007/s00011-010-0256-7.Evidence

Zee, T., Bose, N., Zee, J., Beck, J. N., Yang, S., Parihar, J., Yang, M., Damodar, S., Hall, D., O'Leary, M. N., Ramanathan, A., Gerona, R. R., Killilea, D. W., Chi, T., Tischfield, J., Sahota, A., Kahn, A., Stoller, M. L., & Kapahi, P. (2017). α-Lipoic acid treatment prevents cystine urolithiasis in a mouse model of cystinuria. *Nature Medicine*, *23*(3), 288–290. https://doi.org/10.1038/nm.4280

Zeng, M., Xu, J., Zhang, Z., Zou, X., Wang, X., Cao, K., Lv, W., Cui, Y., Long, J., Feng, Z., & Liu, J. (2021). Htd2 deficiency-associated suppression of α-lipoic acid production provokes mitochondrial dysfunction and insulin resistance in adipocytes. *Redox Biology*, *41*, 101948. https://doi.org/10.1016/j.redox.2021.101948

Zhu, A., Ibrahim, J. G., & Love, M. I. (2019). Heavy-Tailed prior distributions for sequence count data: Removing the noise and preserving large differences. *Bioinformatics*, *35*(12), 2084–2092. https://doi.org/10.1093/bioinformatics/bty895

Zhuo, J. L., & Li, X. C. (2013). Proximal Nephron. *Comprehensive Physiology*, *3*(3), 1079–1123. https://doi.org/10.1002/cphy.c110061